ornl

OAK RIDGE NATIONAL LABORATORY

LOCKHEED MARTIN

ORNL/TM-13467

Heavy Vehicle Propulsion System Materials Program Semiannual Progress Report for October 1996 Through March 1997

Prepared for
U.S. Department of Energy
Assistant Secretary for
Energy Efficiency and Renewable Energy
Office of Transportation Technologies

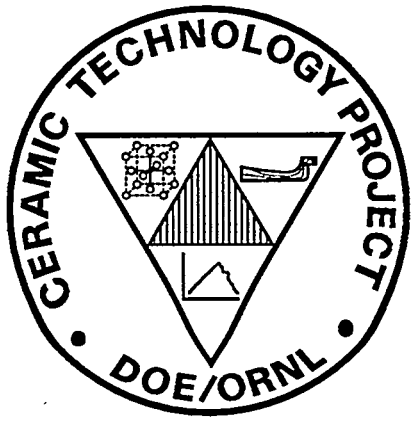

MANAGED AND OPERATED BY
LOCKHEED MARTIN ENERGY RESEARCH CORPORATION
FOR THE UNITED STATES
DEPARTMENT OF ENERGY

ORNL-27 (3-96)

ORNL/TM-13467

Metals and Ceramics Division

HEAVY VEHICLE PROPULSION SYSTEM MATERIALS PROGRAM SEMIANNUAL PROGRESS REPORT FOR OCTOBER 1996 THROUGH MARCH 1997

D. R. Johnson
Program Manager

Date Published: July 1997

Prepared for
U.S. Department of Energy
Assistant Secretary for Energy Efficiency and Renewable Energy
Office of Transportation Technologies
EE 07 01 00 0

Prepared by the
OAK RIDGE NATIONAL LABORATORY
Oak Ridge, Tennessee 37831-6285
managed by
LOCKHEED MARTIN ENERGY RESEARCH CORP.
for the
U.S. DEPARTMENT OF ENERGY
under Contract DE-AC05-96OR22464

REPORTS PREVIOUSLY ISSUED

ORNL/TM-9325	Period March 1983-September 1983
ORNL/TM-9466	Period October 1983-March 1984
ORNL/TM-9497	Period April 1984-September 1984
ORNL/TM-9673	Period October 1984-March 1985
ORNL/IM-9947	Period April 1985-September 1985
ORNL/TM-10079	Period October 1985-March 1986
ORNL/TM-10308	Period April 1986-September 1986
ORNL/TM-10469	Period October 1986-March 1987
ORNL/TM-10705	Period April 1987-September 1987
ORNL/TM-10838	Period October 1987-March 1988
ORNL/TM-11116	Period April 1988-September 1988
ORNL/TM-11239	Period October 1988-March 1989
ORNL/TM-11489	Period April 1989-September 1989
ORNL/TM-11586	Period October 1989-March 1990
ORNL/TM-11719	Period April 1990-September 1990
ORNL/TM-11859	Period October 1990-March 1991
ORNL/TM-11984	Period April 1991-September 1991
ORNL/TM-12133	Period October 1991-March 1992
ORNL/TM-12363	Period April 1992-September 1992
ORNL/TM-12428	Period October 1992-March 1993
ORNL/TM-12674	Period April 1993-September 1993
ORNL/TM-12778	Period October 1993-March 1994
ORNL/TM-12924	Period April 1994-September 1994
ORNL/TM-13046	Period October 1994-March 1995
ORNL/TM-13219	Period April 1995-September 1995
ORNL/TM-13262	Period October 1995-March 1996
ORNL/TM-13395	Period April 1996-September 1996

Research sponsored by the U.S. Department of Energy, Assistant Secretary for Energy Efficiency and Renewable Energy, Office of Transportation Technologies, as part of the Heavy Vehicle Propulsion System Materials Program, under contract DE-AC05-96OR22464 with Lockheed Martin Energy Research Corporation.

CONTENTS

HEAVY VEHICLE PROPULSION SYSTEM MATERIALS PROGRAM
SEMIANNUAL PROGRESS REPORT
FOR OCTOBER 1996 THROUGH MARCH 1997

SUMMARY AND INTRODUCTION

The purpose of the Heavy Vehicle Propulsion System Materials Program is the development of materials: ceramics, intermetallics, metal alloys, and metal and ceramic coatings, to support the dieselization of class 1-3 trucks to realize a 35% fuel-economy improvement over current gasoline-fueled trucks and to support commercialization of fuel-flexible LE-55 low-emissions, high-efficiency diesel engines for class 7-8 trucks.

The Office of Transportation Technologies, Office of Heavy Vehicle Technologies (OTT OHVT) has an active program to develop the technology for advanced LE-55 diesel engines with 55% efficiency and low emissions levels of 2.0 g/bhp-h NOx and 0.05 g/bhp-h particulates. The goal is also for the LE-55 engine to run on natural gas with efficiency approaching that of diesel fuel. The LE-55 program is being completed in FY 1997 and, after approximately 10 years of effort, has largely met the program goals of 55% efficiency and low emissions. However, the commercialization of the LE-55 technology requires more durable materials than those that have been used to demonstrate the goals. Heavy Vehicle Propulsion System Materials will, in concert with the heavy duty diesel engine companies, develop the durable materials required to commercialize the LE-55 technologies.

OTT OHVT also recognizes a significant opportunity for reduction in petroleum consumption by dieselization of pickup trucks, vans, and sport utility vehicles. Application of the diesel engine to class 1, 2, and 3 trucks is expected to yield a 35% increase in fuel economy per vehicle. The foremost barrier to diesel use in this market is emission control. Once an engine is made certifiable, subsequent challenges will be in cost; noise, vibration, and harshness (NVH); and performance.

The design of advanced components for high-efficiency diesel engines has, in some cases, pushed the performance envelope for materials of construction past the point of reliable operation. Higher mechanical and tribological stresses and higher temperatures of advanced designs limit the engine designer; advanced materials allow the design of components that may operate reliably at higher stresses and temperatures, thus enabling more efficient engine designs. Advanced materials also offer the opportunity to improve the emissions, NVH, and performance of diesel engines for pickup trucks, vans, and sport utility vehicles.

The principal areas of research are:

Cost Effective High Performance Materials and Processing
Advanced Manufacturing Technology
Testing and Characterization
Materials and Testing Standards

COST EFFECTIVE HIGH PERFORMANCE MATERIALS AND PROCESSING

COST-EFFECTIVE SINTERED REACTION-BONDED SILICON NITRIDE AND MICROWAVE ANNEALING OF SILICON NITRIDE

J. O. Kiggans, Jr., T. N. Tiegs, F. C. Montgomery, H. T. Lin
M. K. Ferber, C. C. Davisson, and A. M. Williams
Oak Ridge National Laboratory
Oak Ridge, TN 37831

Objective / Scope

There are two major objectives of this research element: the first objective is the development of new sintered reaction-bonded silicon nitride materials; the second objective of this element is the investigation of properties of dense silicon nitride materials annealed in the microwave furnace.

Technical Highlights

Study 1: Improved SRBSN Materials

The purpose of the present study is to further examine the current state of SRBSN materials and to determine the effect of different silicon precursor powders, sintering additives, Si_3N_4 seed materials, and powder processing methods on the final mechanical and chemical properties.

The activities in this work period involved the sintering of various SRBSN die-pressed and gelcast preforms prepared in the previous reporting period, and the determination of the mechanical properties of the sintered materials. All SRBSN materials were sintered at 1800° C. Table 1 is a listing of the gelcast and die pressed preforms, along with their final composition after sintering, the temperature and dwell time used for sintering, and the mechanical properties (the modulus, strength, and toughness values). Of particular interest in this study was to determine whether the "cost-effective" Dow silicon nitride powder (described in previous reports) could be used as the α-seed material in the powders used for forming the "green" silicon preforms. The first two samples analyzed were SRB-1 materials from the Feb. 1996 powder batch. These preforms were nitrided and then sintered for 2 h and 10 h, respectively. The data show that there was a clear improvement in both the strength and toughness for the longer sintering time. The third sample, the SRB-1 AM May 1996, was a sample made from powders milled using an attritor mill, versus the turbomill used for most of our batches. This sample was nitrided and then sintered at for 10 h. There was a slightly lower strength for this sample; however, the toughness value was extremely good. These results indicate that attritor mills may be slightly less effective for processing these silicon materials, when strength is the determinant factor. The next sample, SRB-1 July 1995, was a batch milled using a turbomill. Once again the silicon preform was nitrided and sintered for 10 h. The strength for this batch was higher than the previously discussed attritor batch and the toughness was identical. The fifth SRB-1 batch, SRB-1 Mar. 1996, was also a turbomill powder blend. The preform was nitrided and sintered for 10 h. The strength of this material was lower than all the first 4 batches of SRB-1 materials. The reason for the low strength was not understood, but it was possible that the gelcast may have introduced microscopic pore flaws in this particular sample.

In addition to the five batches of SRB-1 materials which were studied, a number of other compositions were characterized. The first sample studied, TM-154, was a variant of the SRB-1, with a Cr_2O_3 addition (as low temperature nitridation stimulant). Once again, a comparison was made of mechanical properties of materials prepared from turbomilled

powders, which were then gelcast, nitrided and then sintered for 2 or 10h. Good strength and toughness values were obtained for the 2 h material, with higher strength and very high toughness obtained for the 10h sample. It is though that the Cr_2O_3 addition is responsible for the higher toughness. The next set of samples, SRB-27 B1 and B2, were made from gelcast powders containing a cheap Starck S1 α-seed and a Globe silicon powder (particle size range discussed in previous reports). Disappointing results were obtained for the 2 and 10 h samples. Although the gelcast parts looked good, the properties looked to be a result of poor sample quality. This sample preparation may be repeated in the future. The next set of gelcast samples, SRB-29 and SRB-29 B1, were made from turbomilled powders containing Dow α- Si_3N_4 as the seed material together with the standard Elkem silicon. The strength was good for the 2 and 10 h materials, but the toughness values were lower than that for the SRB-1 materials (which contained either LC-10 or LC-10N seed). The next sample type, SRB-30 A and B, were similar to SRB-29, except a lower yittria and higher alumina content were used. This material could not be gelcast, possibly due to some inhibitor in the powder mix, so samples were made by the standard die press, isopress procedure. Acceptable strength and toughness was obtained, especially with the 10 h sample. The last gelcast samples analyzed in this study, SRB-31 A, B, and C, contained the Dow α- seed along with a different sintering aid, a mixture of yittria and spinel. A very good strength was obtained for both the 2 and 10 h samples, and good toughness obtained for the 10h sample.

Several conclusions were reached for this study of several SRBSN material types: The gelcast procedure developed for the silicon preform preparation is reliable in most cases, and can produce SRBSN materials with good properties. Silicon types, α- seed types, and nitridation stimulants all play roles in producing the highest quality SRBSN materials. Sintering times are of utmost importance for producing SRBSN materials with high toughness properties. Several compositions have been identified for further SRBSN development work. And last, the Dow α- seed appeared to result in lower toughness values in the final sintered materials.

The next activity in this work period involved: 1) The SEM analysis of SRBSN materials sintered for 2 and 10 h at 1800° C; 2) The measurement of the high temperature creep properties of SRBSN materials sintered for 2 and 10 h at 1800° C.

Data have been given in previous bimonthly reports concerning the differences in the room temperature and the high temperature mechanical properties of SRBSN materials that were sintered for either 2 or 10 h at 1800° C. Table 2 is a compilation of some of these data. In order to determine the effect of the sintering time on the microstructures of the various materials listed in Table 2, bend bar fragments from the various samples were polished, etched, and examined at a magnification of 8000 X on the SEM. Figures 1, 2, 3, and 4 are photographs of the SEM images at 8000 X magnification of all the samples listed in Table 2.

One general observation upon examination of all of the images of the SRBSN batches sintered for 2 and 10 h is that a significant increase in the sizes of the grains resulted from the longer sintering times. Samples containing the LC10N and LC-10 alpha-Si_3N_4 seed additions, such as the SRB 1 material (Fig. 1), the SRB 14 material (Fig. 2), and the SRB 21 material (Fig. 4). showed the most striking grain elongation, and these batches also exhibited the highest toughness values (Table 2). Batches containing the Dow alpha-Si_3N_4 seed additions, SRB 29 and SRB 30 (Fig. 3), and SRB 31 (Fig. 4), exhibited less grain elongation; these materials also exhibited lower toughness values. Batch TM154 (Fig. 1), which had the LC10N alpha-Si_3N_4 seed and the chrome oxide addition, achieved a very high toughness increase for the 10 h sintering, but the microstructure did not show significant grain elongation. A more quantitative analysis of the microstructures of all of these images may reveal the exact differences of the grain structures.

The second activity was the analysis, by H. T. Lin, of the high temperature creep properties of flexural bars prepared from several batches of SRBSN materials. This work

was valuable in identifying the temperature regimes for use of the different SRBSN materials. The methods for performing the high temperature creep properties of SRBSN materials have been reported in previous bi-monthly reports. The samples studied were prepared from sintered samples made from die-pressed, isopressed discs. Figure 5 shows creep data for the SRB 11 sample composition (Si_3N_4-9% Y_2O_3-3% Al_2O_3) and the SRB 21 composition (Si_3N_4-8% Y_2O_3-4% Al_2O_3). Figure 6 shows creep data for the TM154 SRBSN (Si_3N_4-9% Y_2O_3-3% Al_2O_3 -0.2% Cr_2O_3) material, as compared to data from the SRB 11 material. Data in both Figures 5 and 6 show that the creep values for SRBSN materials sintered for 10 h were far superior to creep for the materials sintered for 2 h. This was due to at least two changes that occurred as result of the longer sintering time; the increased densification which occurs (typical densities for these samples increased from 98 to 99.5% with the increased sintering time), and the increased acicular grain growth. A second observation about the data, in both Figures 5 and 6, was that all of these SRBSN moved from the creep regime to the creep-slow crack growth regime at similar loads. This was positive, since it indicated that the yittria content (an expensive component) could be lowered from 9 wt % (Si_3N_4-9% Y_2O_3-3% Al_2O_3) to 8 wt % (Si_3N_4-8% Y_2O_3-4% Al_2O_3) with little loss in creep properties, and also that the Cr_2O_3 addition (a nitridation aide) in the TM154 batch (Si_3N_4-9% Y_2O_3-3% Al_2O_3 -0.2% Cr_2O_3) could be used to increase room temperature properties, without harming the high temperature properties.

Study 2: Improved Gas Pressure Sintered Silicon Nitride (GPS-SN) and SRBSN through Microwave Annealing

The present study was designed to expand the data base for microwave annealing of silicon nitride materials. In the present study, microwave heating was compared to conventional heating for thermal annealing of both GPS-SN and SRBSN. Up to this time, there have been no studies devoted to the effects of microwave annealing on dense SRBSN materials. Since SRBSN represents a class of silicon nitride materials that is more cost-effective than SSN, it is hoped that microwave annealing would significantly improve the creep properties of these materials, thus making them more attractive for automotive applications.

The dense silicon nitride materials used for the annealing study were prepared from "green" ceramic preforms. Two types of preforms were prepared: 1) silicon nitride compacts fabricated from spray dried powder mixtures using standard die-press and isopress techniques and 2) silicon-based preforms fabricated using gelcast plus isopress techniques. Details for preparing samples using these methods has been discussed in previous publications.[1,2] The silicon nitride preforms (designated AY6) consisted of appropriate amounts of α-Si_3N_4 (Ube E-10 grade), Al_2O_3, and Y_2O_3 to give a final composition of Si_3N_4-6% Y_2O_3-2% Al_2O_3. The silicon preforms (designated SRB-1) consisted of appropriate amounts of silicon (Elkem metallurgical grade), Al_2O_3, and Y_2O_3 to give a final composition of Si_3N_4-9% Y_2O_3-3% Al_2O_3).

After preparing the preforms, the organic binders were removed by heating the silicon nitride green compacts at 1° C per minute in air to 600°C with a 1 h dwell, and the silicon preforms at 1° C per minute in air to 550°C with a 1 h dwell.

The silicon nitride parts were sintered at a final condition of 1950°C for 3 h in N_2 gas at a pressure of 1.3 MPa. The silicon preforms were nitrided in flowing N_2 in a graphite furnace in an approximately 24 h heating cycle to a final temperature of 1450 °C, and they were then cooled and re-packed in a silicon nitride powder mix and sintered in flowing N_2 gas at a final condition of 1800°C for 5 h. Further details for the sintering of GPS-SN, and the nitridation and sintering of SRBSN materials have been discussed in previous publications.[3,1] After the densification, the density of each sample was measured by the Archimedes method.

The dense GPS-SN and SRBSN samples were then annealed at 1150°C or 1600°C for either 5 or 20 h in a graphite element furnace or a microwave furnace. A schematic showing

how samples were arranged in the annealing experiments is shown ion Figure 7. For conventional anneal treatments, samples were surrounded on all sides by a 1.5 cm layer of Si_3N_4-4% Y_2O_3 10% BN powder bed inside a pre-conditioned graphite crucible (crucible fired to 1800°C for 10 h with a Si_3N_4 paint on all inner surfaces to convert the graphite to SiC). Microwave treatments were performed by placing the dense parts inside a BN crucible surrounded by a 3 cm bed of the Si_3N_4-4% Y_2O_3 10% BN powder, all inside an alumina fiber box. Temperature measurements for both the conventional and microwave anneals were made with "Type" C thermocouples. A BN sheath was place over the last 5 cm of the metallic sheath for the microwave anneals to allow direct contact with the heated parts. Ballast machined AY6 and the TM-145 SRBSN parts were also placed around the BN tip during microwave anneals to help assure that a proper mass was available for accurate temperature measurement. In addition to recording the temperature during the anneal treatments, the microwave power input into the furnace cavity was also continuously monitored. Further details concerning conditions for microwave annealing have been discussed in previous papers. [4,5] In addition, unheated samples were used as control samples.

Mechanical testing was done using 3 by 4 by 45 mm flexural bars prepared from each annealed sample. Flexural testing was done in four point bending with inner and outer spans of 20 and 40 mm, respectively. Fracture toughness was determined by the Chantikul method using a 20 kg load.[6] High temperature fast fracture and creep tests were performed in air at 1200°C. Stress levels used for the various high temperature creep tests are indicated within the figures. The creep was calculated from the load and load point displacement data using the procedures described by Hollenberg.[7] Details of the room temperature and high temperature mechanical properties tests have also been discussed in earlier publications.[8,9,10]

Bend bar fragments from the room temperature fracture toughness tests were polished, etched, and analyzed by SEM to determine the microstructures of the annealed and the control materials.

The average sintered densities (g/cm^3) obtained for the SRB-1 and the AY6 parts were 3.27 +/- 0.003 and 3.24 +/- 0.01, respectively, which corresponded to 99.2 % and 98.3% of the theoretical density for each

Figures 8 and 9, show graphs of the microwave power and temperature for the anneal treatments of the dense TM-145 SRBSN samples and the dense AY6 samples at 1150°C and 1600°C for 5 h. These figures show that power ranging from approximately 1 to 2 kW are required to heat the silicon nitride pellets to the annealing soak temperature of 1150°C or 1600°C, but very minimal levels of microwave power (approximately 400 to 500 W) were required to maintain the samples at the soak temperature. Almost identical plots were obtained for the 20h anneals (data not shown). The low power requirements for microwave annealing were due to very efficient insulation provided by the powder bed and the outer fiber board box.

Figure 10 shows the room temperature strength and toughness values of the control bend bar specimens prepared from the control and the annealed SRB-1 and AY6 materials. These data show that both the conventional and the microwave annealing of the SRB-1 at 1150°C for both 5 and 20 h caused an approximately 20% reduction in strength and toughness. Similar results were obtained for the AY6 materials. These reductions in strength and toughness values, when compared to the untreated controls have been observed previously in our laboratory for silicon nitride materials containing yittria, alumina, and silica as sintering additives. We believe that these reductions in the strength and the toughness values are caused by the development of undesirable thermal expansion coefficient (CTE) mismatches between the host silicon nitride materials and the crystalline phases that form during the annealing treatments. These thermal expansion mismatches may lead to altered crack growth phenomena, which is made evident during the application of a stress (as mechanical testing). Figure 10 also shows that there were no significant differences in the room temperature strength and toughness values between the SRB-1

control and the materials annealed at 1600°C by conventional or microwave heating. We believe this finding was due to the fact that these materials were annealed above the glass melting point (1280°C), where crystallization is not favored. Similar results were observed with the AY6 materials.

The high temperature fracture strengths of conventional and microwave annealed SRB-1 and AY6 samples were measured at 1200°C in air, in order to determine strength properties expected under severe service conditions. Figure 11 shows that the high temperature strengths for both SRB-1 and AY6 annealed by either type of heat treatment were lower than the room temperature counterparts. No differences were seen between samples annealed under different conditions. The lower fast fracture strengths were expected, since at high temperatures, the viscosity of the intergranular glasses that bond together the silicon nitride particles is lower, and this in turn lowers the strengths.

The high temperature creep properties of SRB-1 and AY6 materials were also measured. Figure 12 shows the creep strain versus time curves for SRB-1 material annealed under different conditions and tested at 1200°C at a 150 MPa stress. The control sample (data not shown) and samples annealed at 1600°C for 20 h by either heating method failed within 5 h hours of the test start. Of the two remaining test samples, the SRB-1 material annealed at 1150°C for 20 h by microwave heating showed a lower creep than did the SRB-1 material annealed by conventional heating at 1150° C for 20 h. The secondary creep rates for the samples annealed by conventional and microwave heating at 1150°C were not determined.

Figure 13 shows creep strain versus time curves for AY6 in a stepped-stress experiment. The AY6 samples which were annealed at 1600 °C by conventional heating showed the highest creep for a given set of conditions. The AY6 material annealed at 1600° C by microwave heating performed slightly better. The control sample and the AY6 sample annealed by conventional heating at 1150°C showed almost identical creep, and both failed immediately when the stress was raised to 350 MPa. The AY6 material which was annealed by microwave heating at 1150°C for 20 h showed the lowest initial creep, and thus had the best performance. Further tests are required to verify the creep results for both the SRB-1 and AY6 materials, since the creep data in Figures 12 and 13 represent data collected from tests involving only one or two samples for each test treatment.

Status of Milestones

On schedule

Problems Encountered

None

Publications

None

REFERENCES

[1]Kiggans, J. O., Nunn, S. D., Tiegs, T. N., Davisson, C. C., Coffey, D.W., and Maria, J-P., "Gelcasting of Preforms for the Production of Sintered Reaction-Bonded Silicon Nitride," MPIF 4th International Conference on Powder Metallurgy in Aerospace, Defense, and Demanding Applications Proceedings, Metal Powder Industries Federation, Princeton, NJ, pp. 157-164 (1995).

[2]Walker, W. J., Jr., and Reed, J. S., "Organic Additive Systems for Spray-Drying and Dry Pressing Silicon Nitride," Ceram. Trans. Vol. 62, pp. 141-148

(1996).

[3]Tiegs, T. N., Nunn, S. D., Beavers, T. M., Menchhofer, P. A., Barker, D. L., and Coffey, D. W., "Gas Pressure Sintering of Silicon Nitride to Optimize Fracture Toughness," Ceram. Eng. Sci. Proc., Vol. 16, No. 4, pp. 467-473 (1995).

[4]Tiegs, T. N., Ploetz, K. L., Kiggans, J. O., and Yeckley, R. L., "Crystallization of Grain Boundary Phases in Silicon Nitride with Low Additive Contents By Microwave Annealing" in Ceramic Transactions, Microwaves: Theory And Applications In Materials Processing II, edited by D. E. Clark, W. R. Tinga, and J. R. Laia, Jr. (Am. Cer. Soc., Westerville, Ohio) 259-267 (1993).

[5]Tiegs, T. N., Ferber, M. K., Kiggans, J. O., More, K. L., Hubbard, C. M., and Coffey, D. W., "Microstructure Development During Microwave Annealing of Dense Silicon Nitride," Proc. 93rd Annual Meeting / Expo. Am. Ceram. Soc., Cincinnati, OH., Cincinnati, OH. (1991).

[6]Chantikul, P., Anstis, G. R., Lawn, B. R., and Marshal, D. B., "A Critical Evaluation of Indentation Techniques for Measuring Fracture Toughness: II Strength Method," J. of the Amer. Ceram. Soc., Vol. 64 (9) pp. 539-543 (1981).

[7]Hollenberg, G. R., Terwillinger, G. R., and Gordon, R. S., "Calculation of Stresses and Strains in Four Point Bending Creep Tests," J. Amer. Cer. Soc., Vol. 54 (4) pp. 196-199 (1971).

[8]Kiggans, J. O., Jr. and Tiegs, T. N., "Characterization of Sintered Reaction-Bonded Silicon Nitride Processed by Microwave Heating," Proc. Spring Meeting Mater. Res. Soc., San Francisco, CA. (1992).

[9]Tiegs, T. N., Kiggans, J. O., Jr., Lin, H. T., and Wilkens, C. A., "Comparison Of The Properties Of Sintered And Sintered Reaction-Bonded Silicon Nitride Fabricated By Microwave And Conventional Heating," Materials Research Society Proceedings , San Francisco, CA. (1994).

[10]Ferber, M. K., Tiegs, T. N., and Jenkins, M. G., "Effect of Post-Sintering Microwave Treatments Upon the Mechanical Performance of Silicon Nitride," Ceram. Eng. Proc., Vol. 12, No. 9-10, pp. 1993-2004 (1991).

Table 1. Mechanical properties of die-pressed and gelcast SRBSN materials

Sample #	Composition	α-Seed Type	Treatment	Youngs Modulus		Strength (MPa)		Toughness (20kg) GPa	
				Avg.	Std. Dev.	Avg.	Std. Dev.	Avg.	Std. Dev.
SRB-1 Feb. 1996	Si_3N_4-9% Y_2O_3-3% Al_2O_3	Starck LC-10	TM[2], GC[3], Conv. Nit.Sint. 1800°C 2h	289	0.4	542	129	6.1	0.1
SRB-1 Feb. 1996	Si_3N_4-9% Y_2O_3-3% Al_2O_3	Starck LC-10	TM, GC, Conv.Nit. Sint. 1800°C 10h	292	0.7	747	58	6.8	0.3
SRB-1 AM[1] May 1996	Si_3N_4-9% Y_2O_3-3% Al_2O_3	Starck LC-10N	AM, GC, Conv.Nit. Sint. 1800°C 10h	293	1.8	639	92	7.3	0.2
SRB-1 July 1995	Si_3N_4-9% Y_2O_3-3% Al_2O_3	Starck LC-10N	TM, GC, Conv. Nit.Sint. 1800°C 10h	293	2.6	721	106	7.3	0.1
SRB-1 Mar. 1996	Si_3N_4-9% Y_2O_3-3% Al_2O_3	Starck LC-10N LC-10	TM, GC, Conv. Nit.Sint. 1800°C 10h	295	1.5	451	71	7.3	0.1
TM-154 B2	Si_3N_4-9% Y_2O_3-3% Al_2O_3 - 0.5% Cr_2O_3	Starck LC-10N	TM, GC, Conv.Nit. Sint. 1800°C 2h	279	1.2	611	57	6.7	0.2
TM-154 B1	Si_3N_4-9% Y_2O_3-3% Al_2O_3 - 0.4% Cr_2O_3	Starck LC-10N	TM, GC, Conv.Nit. Sint. 1800°C 10h	293	1.0	659	48	7.7	0.4
SRB-27 B1	Si_3N_4-9% Y_2O_3-3% Al_2O_3	Starck S1	TM, GC, Conv.Nit. Sint. 1800°C 2h	270	0.7	353	15	5.3	0.2
SRB-27 B2	Si_3N_4-9% Y_2O_3-3% Al_2O_3	Starck S1	TM, GC, Conv.Nit. Sint. 1800°C 10h	283	0.9	397	30	6.1	0.6
SRB-29 B1	Si_3N_4-9% Y_2O_3-3% Al_2O_3	Dow XU3556	TM, GC, Conv.Nit. Sint. 1800°C 2h	283	0.9	603	142	6.3	0.2
SRB-29	Si_3N_4-9% Y_2O_3-3% Al_2O_3	Dow XU3556	TM, GC, Conv.Nit. Sint. 1800°C 10h	291	5.6	725	96	6.4	0.5
SRB-30 C	Si_3N_4-8% Y_2O_3-4% Al_2O_3	Dow XU3556	TM, DP-IP[4], Conv.Nit. Sint. 1800°C 2h	280	1.9	635	80	6.0	0.0
SRB-30 A&B	Si_3N_4-8% Y_2O_3-4% Al_2O_3	Dow XU3556	TM, DP-IP, Conv.Nit. Sint. 1800°C 10h	291	0.6	678	38	6.8	0.1
SRB-31 B&C	Si_3N_4-% Y_2O_3-6% Spinel	Dow XU3556	TM, GC, Conv.Nit. Sint. 1800°C 2h	284	0.9	801	33	6.0	0.1
SRB-31 A	Si_3N_4-% Y_2O_3-6% Spinel	Dow XU3556	TM, GC, Conv.Nit. Sint. 1800°C 10h	291	0.4	817	29	6.6	0.01

[1]AM Attritor milled powders
[2]TM Turbomilled powders
[3]GC Green body Gelcast
[4]DP-IP Die pressed and then isopressed

Table 2. Summary of the mechanical properties of SRBSN materials fabricated in-house and sintered for
2 and 10 h at 1800°C.

	S 2h	S 10h	S 2h	S 10h	S 2h	S 10h
Sample ID (Description)	Density (g/cm^3)	Density (g/cm^3)	Strength (MPa)	Strength (MPa)	Toughness ($MPa\sqrt{m}$)	Toughness ($MPa\sqrt{m}$)
SRB 1 (9Y3A, 10% LC10N seed)	98.0	99.4	759	721	6.8	7.3
TM154 (9Y3ACr, 10% LC10N seed)	97.8	99.5	676	665	5.8	7.8
SRB 14 (9Y3A, 10% LC10 seed)	96.2	99.0	526	582	6.0	8.4
SRB 15 (9Y3A, 20% LC10 seed)	95.4	100.4	475	594	6.5	8.4
SRB 21 (8Y4A, 10% LC10 seed)	97.1	99.8	647	766	5.6	8.2
SRB 29 (9Y3A, 10% Dow seed)	98.4	99.4	603	725	6.3	6.4
SRB 30 (8Y4A, 10% Dow seed)	98.2	99.1	635	678	6.0	6.8
SRB 31 (6Y4 Spinel, 10% Dow seed)	97.6	97.9	801	817	6.0	6.6

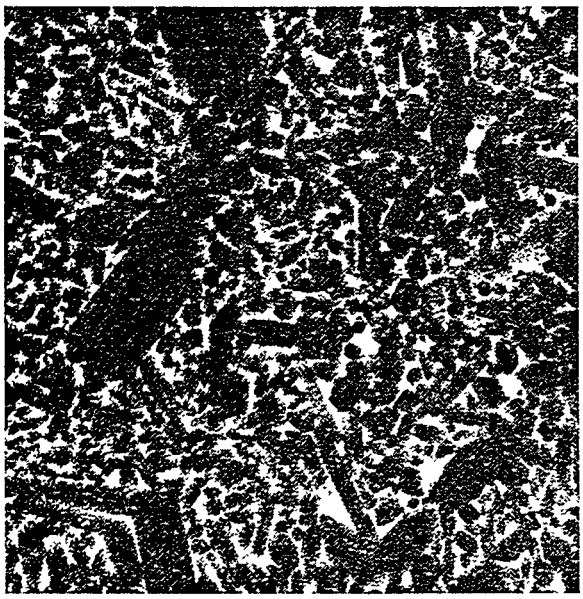

SRB-1, Run 3
1800°C 2 h

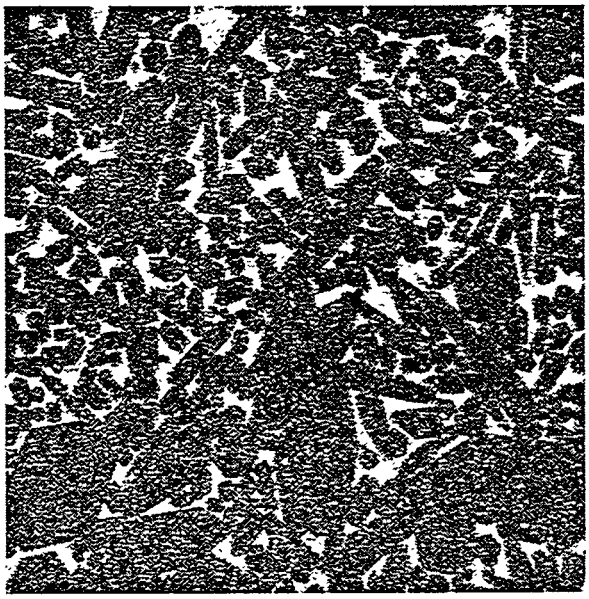

SRB-1, July 1996
1800°C 10 h

10.7 micron

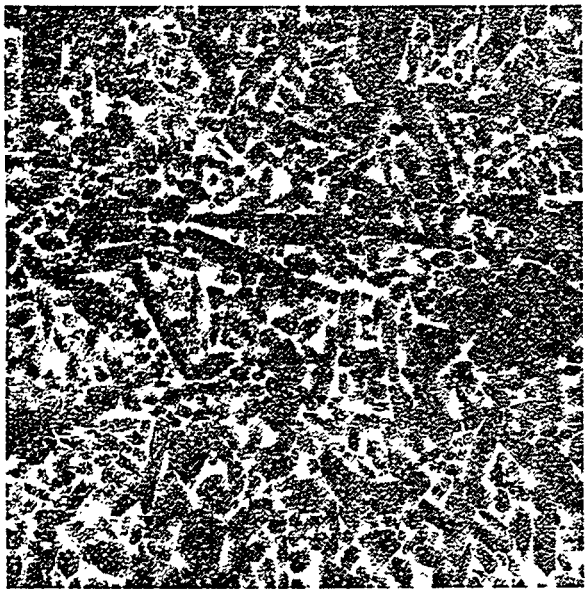

TM-154, 1800°C 2 h

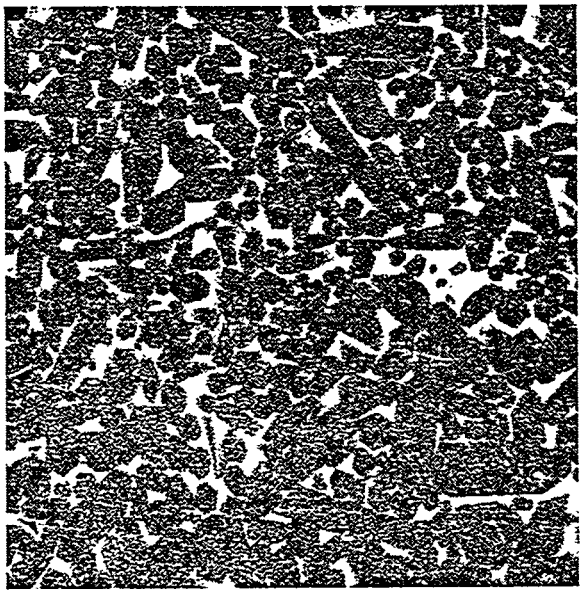

TM-154 B1, 1800°C 10 h

Figure 1. Photographs of SEM images (8000X magnification) of SRBSN materials sintered for 2 and 10h at 1800°C.

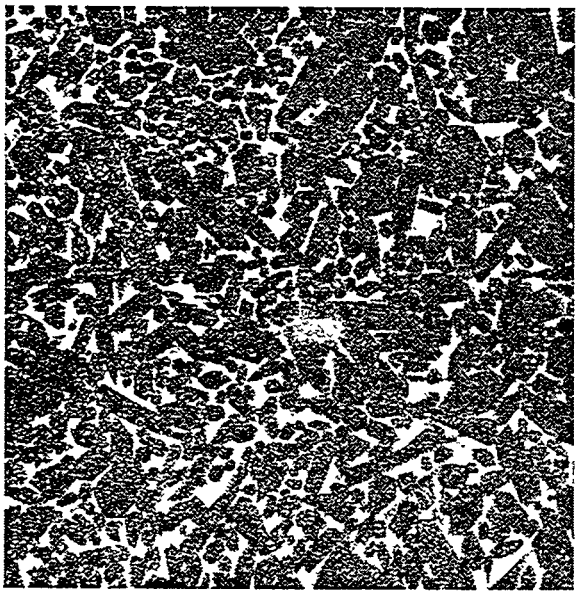

SRB-14, 1800°C 2 h

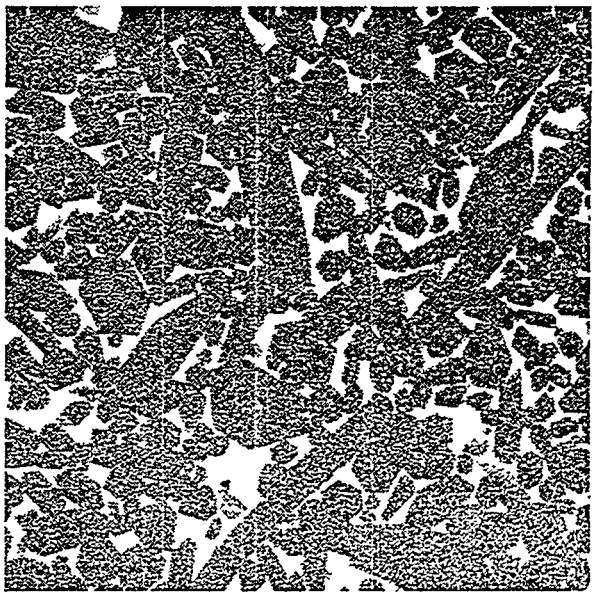

SRB 14-2, 1800°C 10 h

10.7 micron

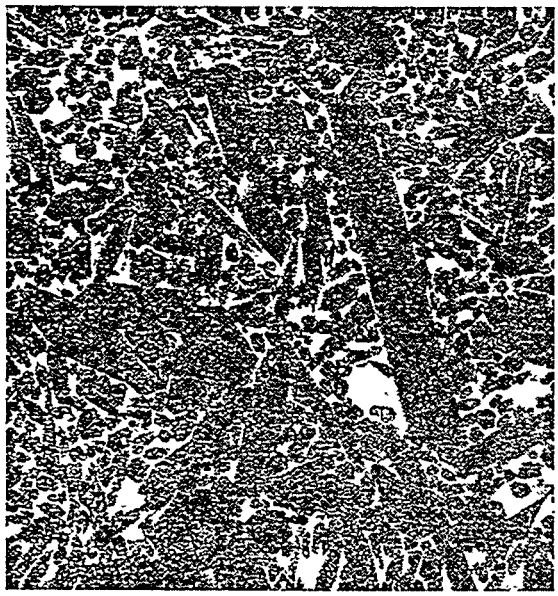

SRB 15/1, 1800°C 2 h

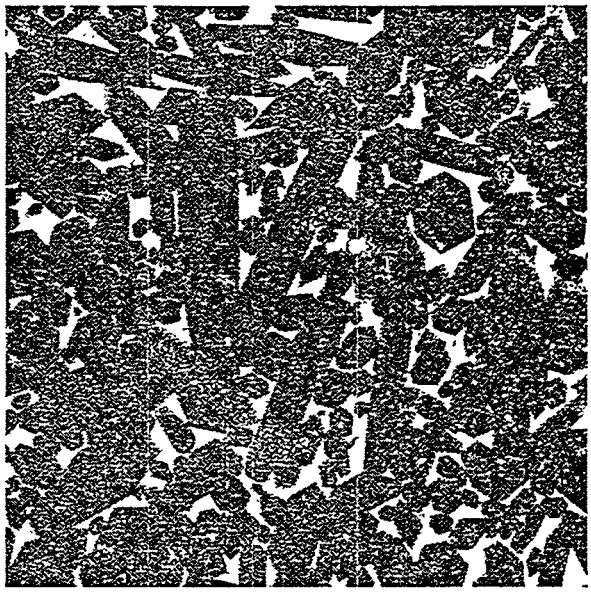

SRB15/2, 1800°C 10 h

Figure 2. Photographs of SEM images (8000X magnification) of SRBSN materials sintered for 2 and 10 h at 1800°C.

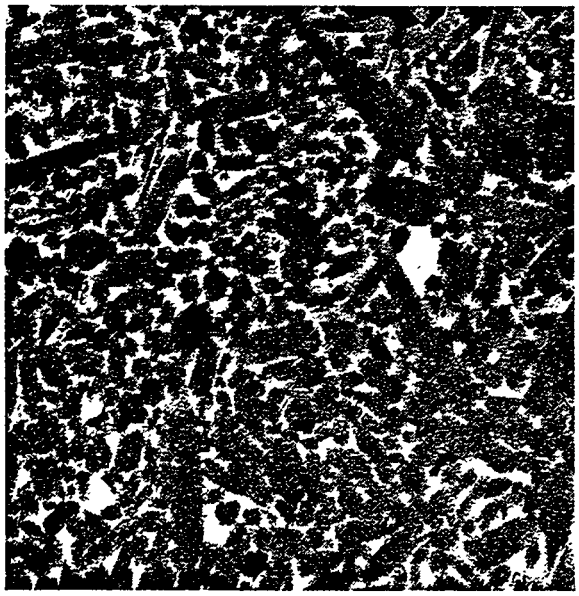

SRB 29B1, 1800°C 2 h

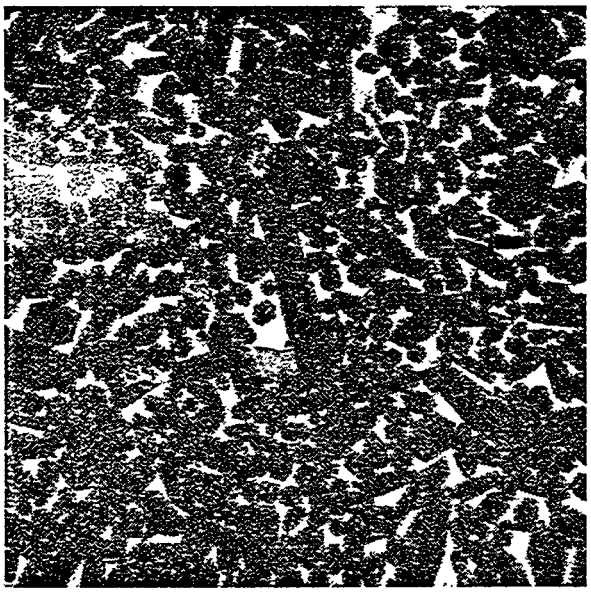

SRB29, 1800C 10 h

10.7 micron

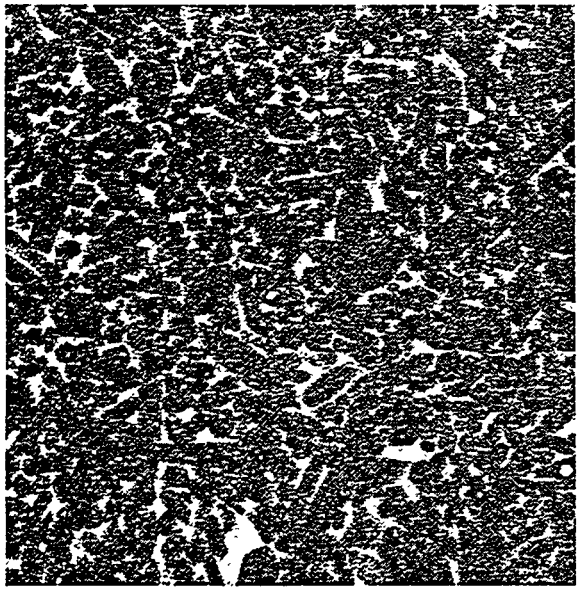

SRB 30C, 1800°C 2 h

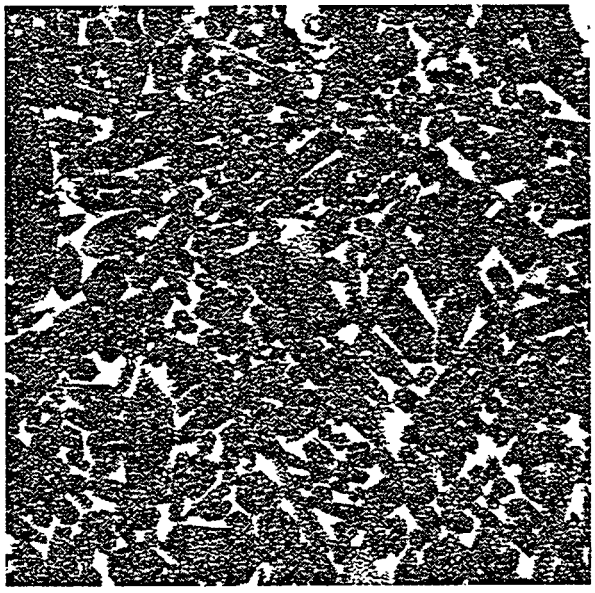

SRB 30 A&B, 1800°C 10 h

Figure 3. Photographs of SEM images (8000X magnification) of SRBSN materials sintered for 2 and 10 h at 1800°C.

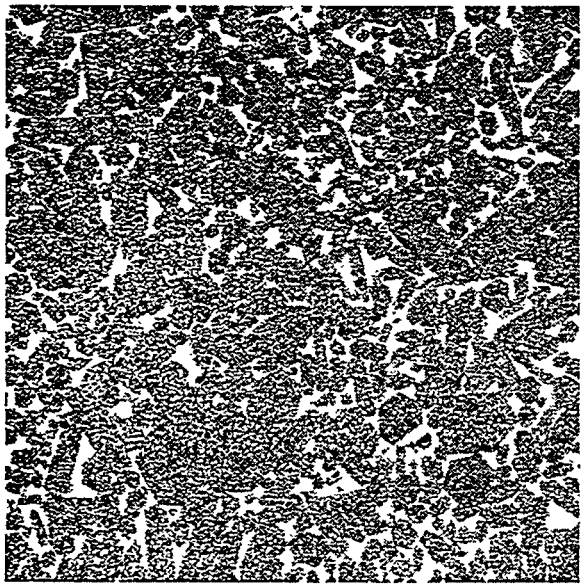

SRB 21, 1800°C 2 h

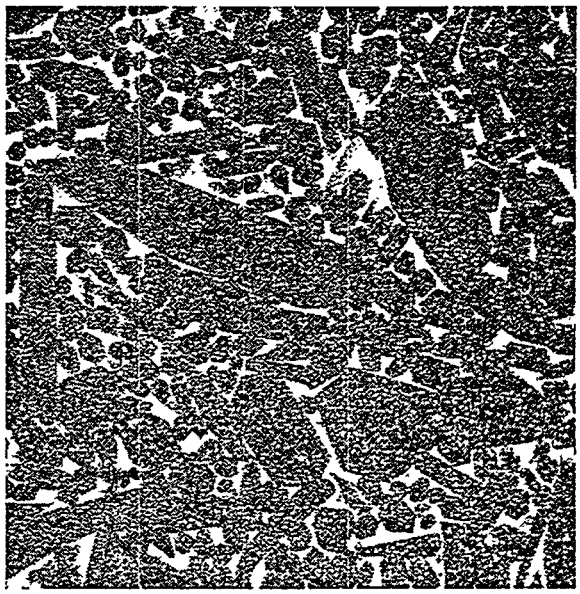

SRB 21b, 1800°C 10 h

10.7 micron

SRB31B&C, 1800°C 2 h

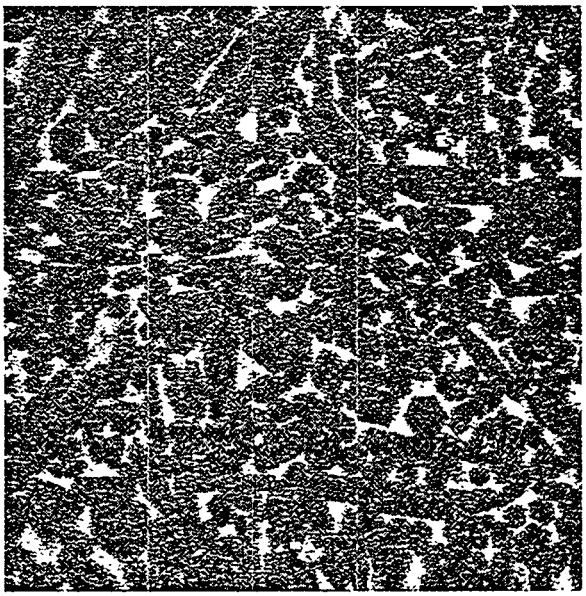

SRB31A, 1800°C 10 h

Figure 4. Photographs of SEM images (8000X magnification) of SRBSN materials sintered for 2 and 10 h at 1800°C.

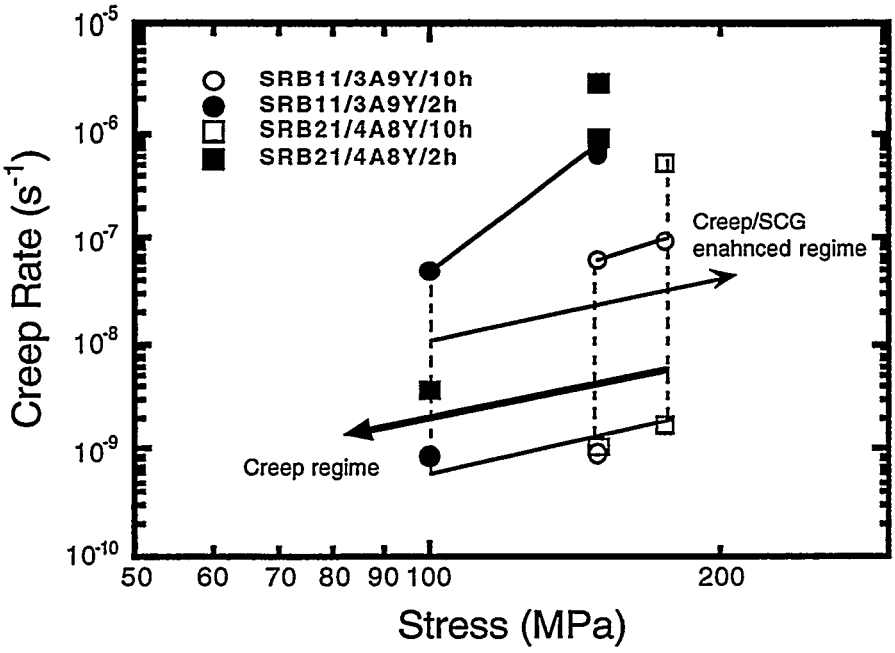

Figure 5. Creep Rate versus stress curve for SRB 11 and SRB 21 compositions sintered for both 2 h. and 10 h at 1800°C.

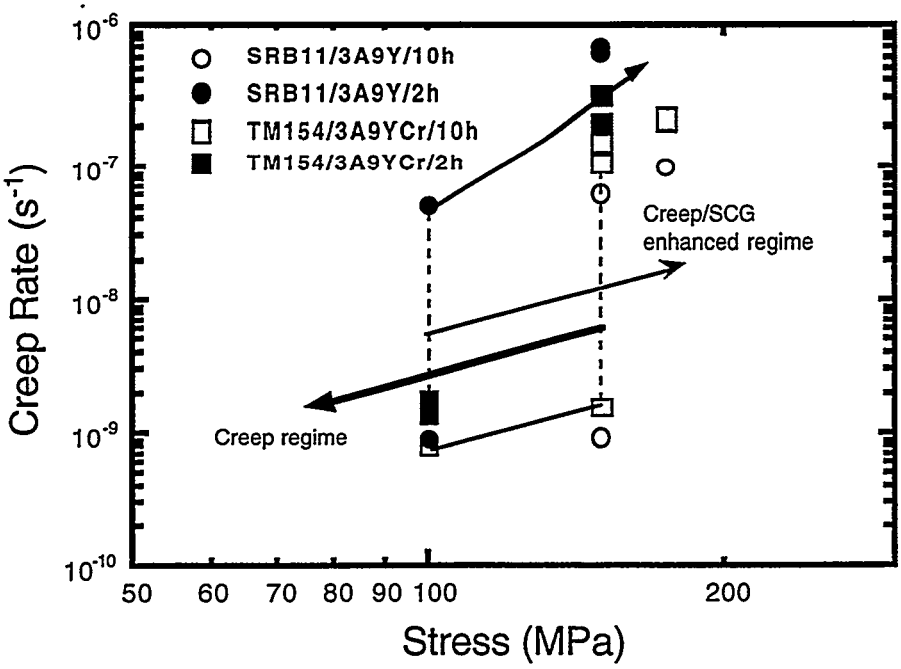

Figure 6. Creep Rate versus stress curve for SRB 11 and TM154 compositions sintered for both 2 h and 10 h at 1800°C.

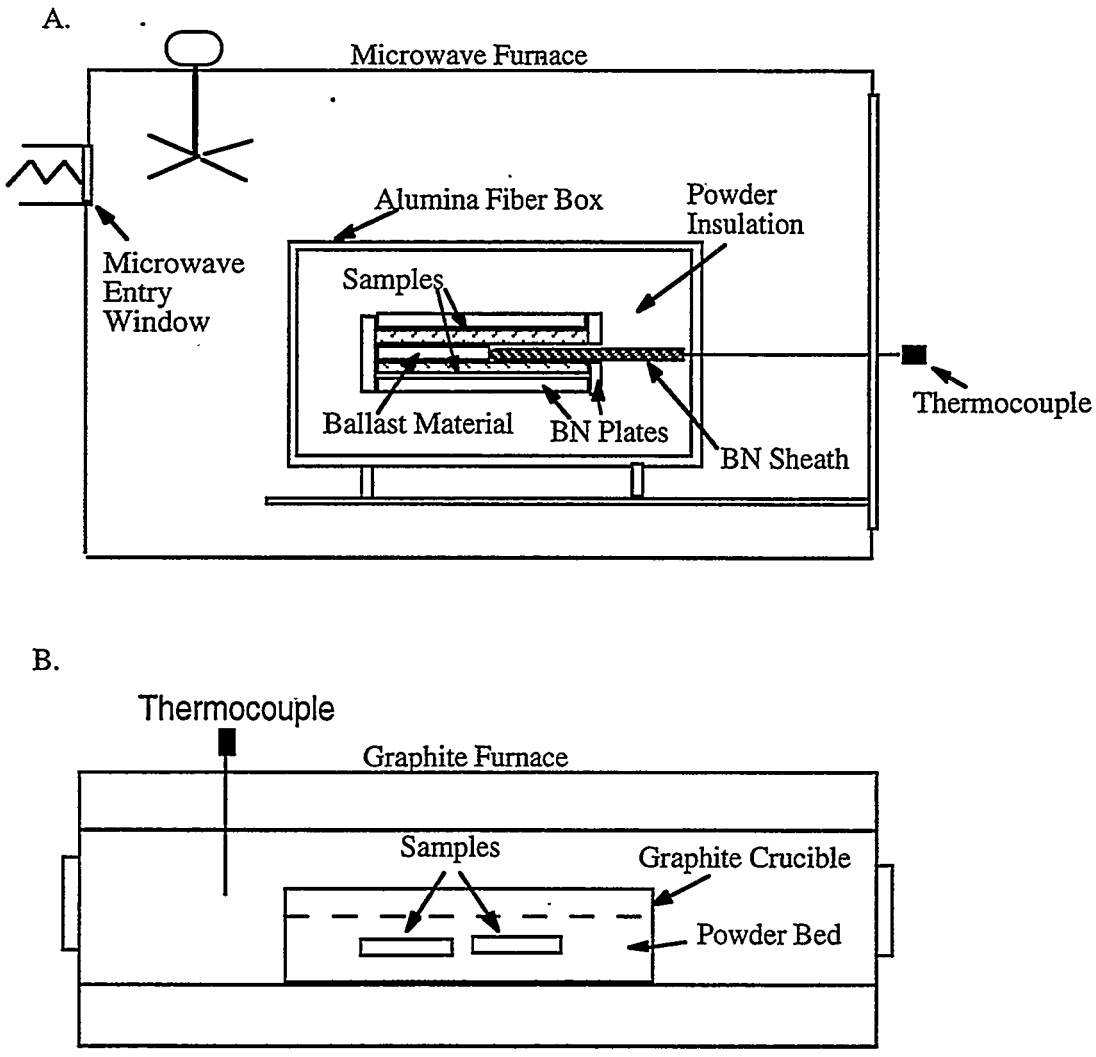

Figure 7. Schematic of sample packaging, furnace arrangement, and thermocouple placement for annealing experiments of SRB-1 and AY6 materials annealed in the a) microwave furnace and b) graphite furnace.

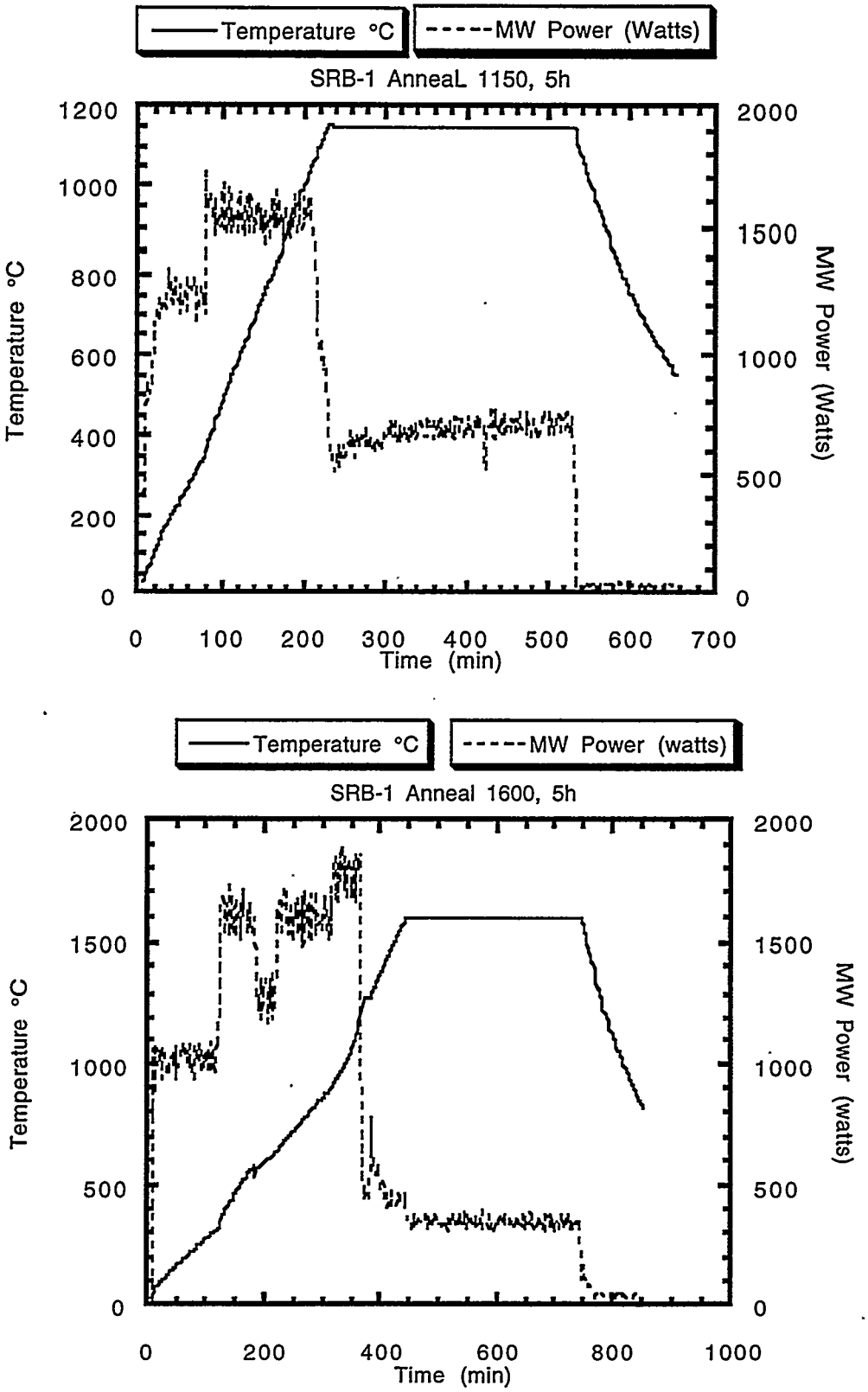

Figure 8. Temperature - microwave power plots for anneals of SRB-1, SRBSN materials performed at a) 1150°C for 5h, and b) 1600°C for 5h.

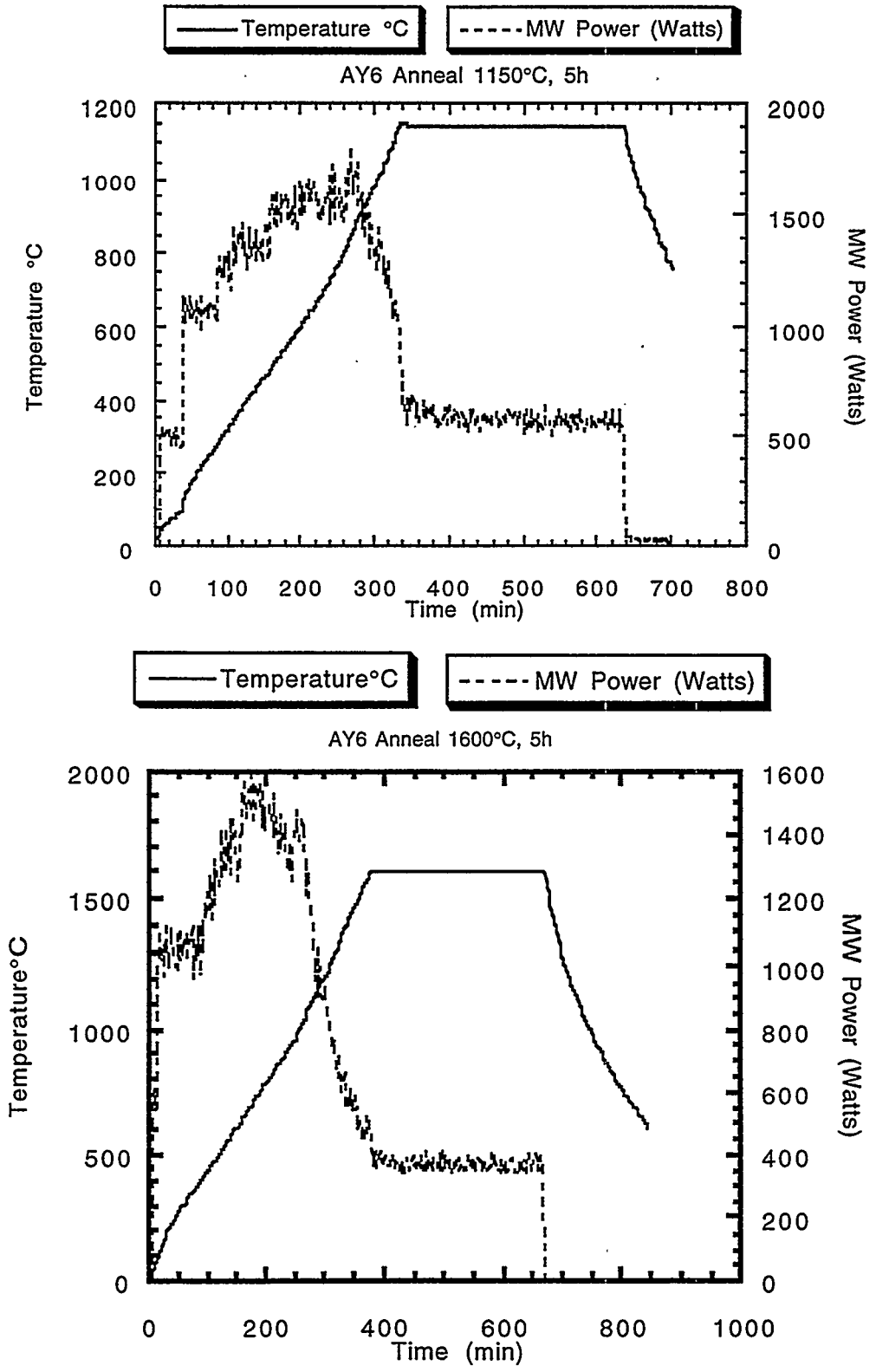

Figure 9. Temperature - microwave power graph for anneals of AY6 materials performed at a) 1150°C for 5h, and b) 1600°C for 5h.

a

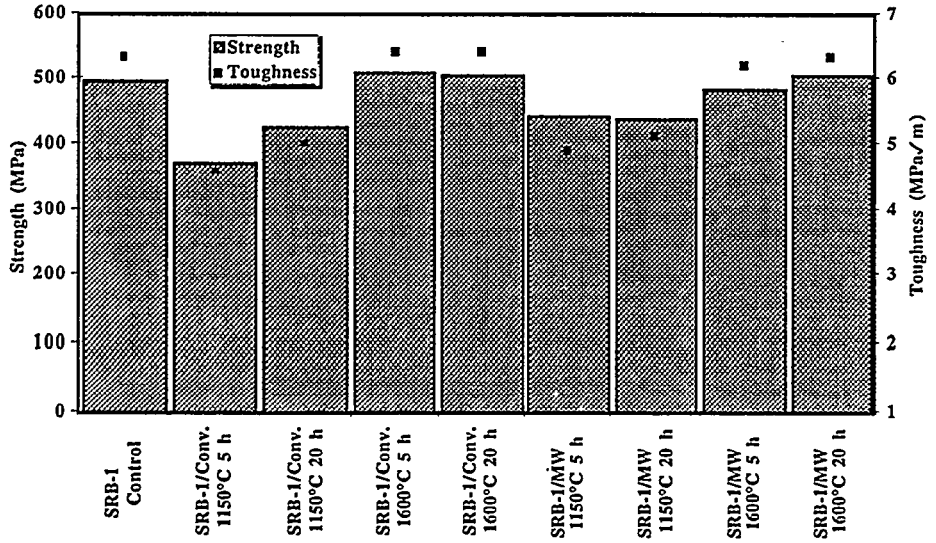

b

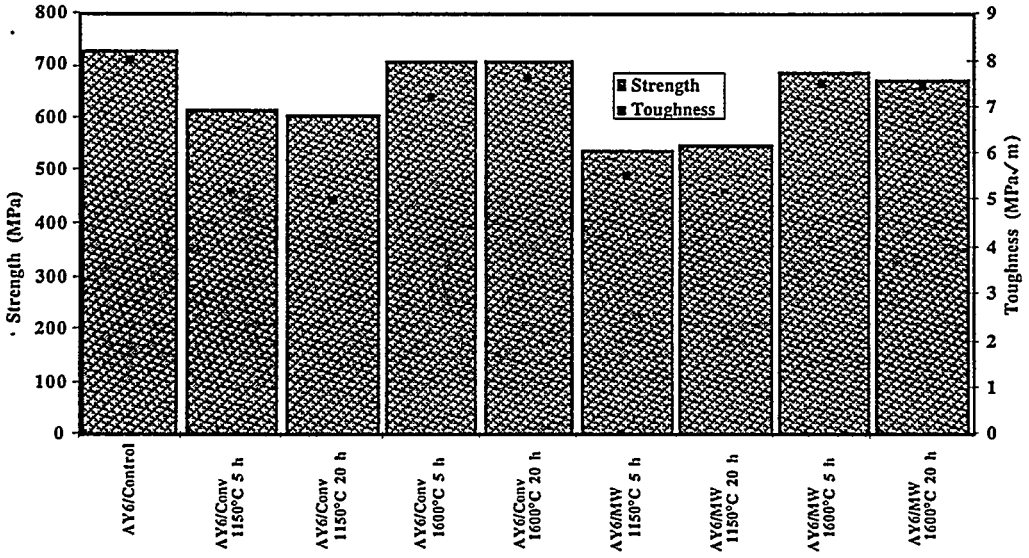

Figure 10. Room temperature strength and toughness values for a) SRB-1 and b) AY6 materials annealed by conventional and microwave heating.

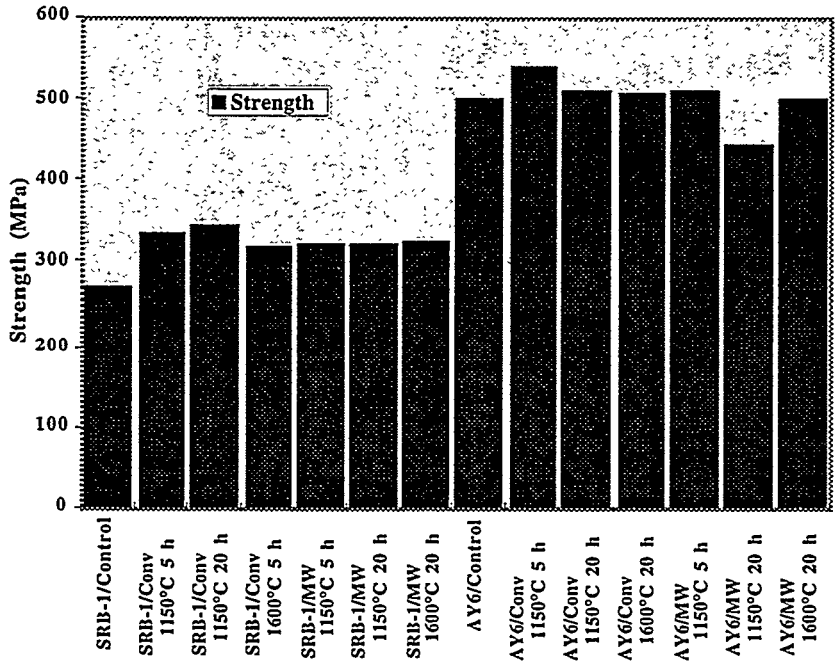

Figure 11. High temperature fast fracture strength measurements (1200°C in air) for SRB-1 and AY6 materials which were annealed by conventional and microwave heating.

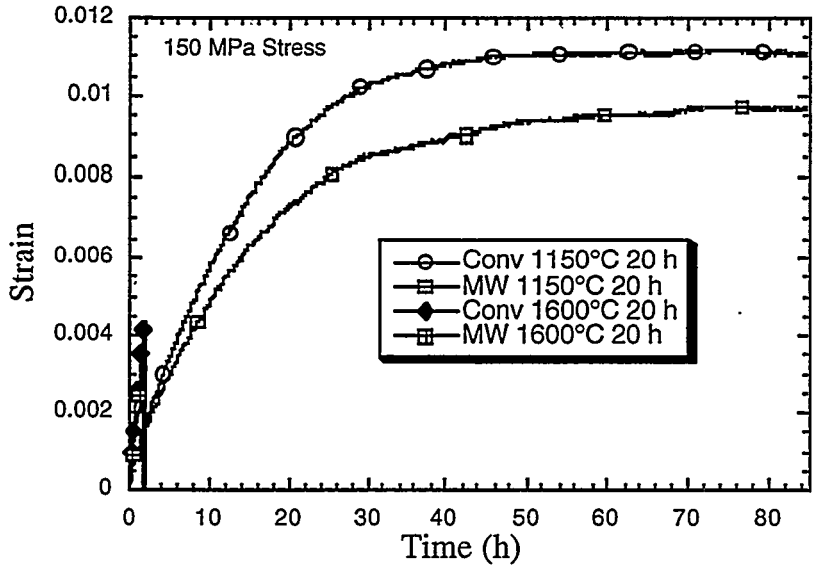

Figure 12. Creep strain versus time curves for SRB-1 materials annealed by conventional and microwave heating and tested at 1200° C in air under a stress of 150 MPa.

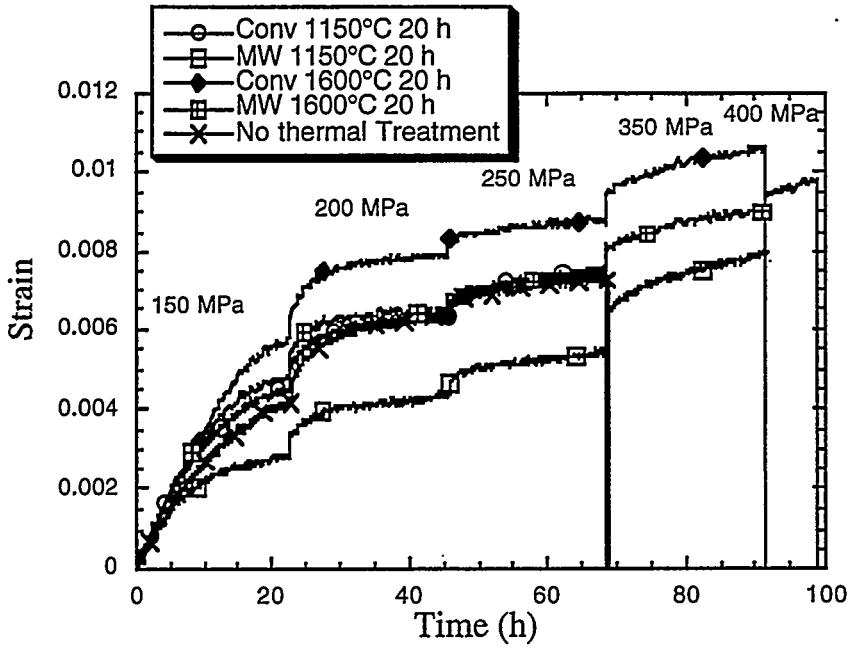

Figure 13. Creep strain versus time graph for AY6 materials annealed by conventional or microwave heating and held under the stresses shown.

COST-EFFECTIVE HIGH TOUGHNESS SILICON NITRIDE

T. N. Tiegs, F. C. Montgomery, P. A. Menchhofer, D. L. Barker and J. Schroeder
Oak Ridge National Laboratory
Oak Ridge, TN 37831

Objective/Scope

Significant improvement in the reliability of structural ceramics for advanced engine applications could be attained if the critical fracture toughness (K_{Ic}) were increased without strength degradation. Early results from ORNL research showed that significant increases in fracture toughness could be achieved by manipulating the microstructure to promote toughening mechanisms such as crack bridging. Excellent properties were obtained in this manner for the alumina and mullite matrix systems reinforced with SiC whiskers. In silicon nitride, acicular or elongated grains can be generated by in-situ growth and these can provide significant toughening on the same order as the whisker reinforced materials. Microstructural development to promote this type of growth in silicon nitride is the current emphasis of the project.

Technical Highlights

In-Situ Toughening of Silicon Nitride by Microstructure Development

ß-Si_3N_4 Nucleation and Initial Stage Microstructure Development - As reported previously, a study was initiated to determine the inter-relationships between the raw silicon nitride powders, the sintering additives as the liquid phase forms, ß-phase nucleation and the kinetics of the α-to-ß transformation. This is an area where there is a large body of fragmented data and observations, however, there is no systematic examination of the system. The work has been examining the effects of the silicon nitride powders, the type of sintering additive and the effect of ß-Si_3N_4 seeds on the initial microstructure development.

Transformation Kinetics - The effects of different sintering additive types on the transformation rate at temperatures of 1500°C and 1600°C are summarized in Figs. 1 and 2. Like the examples shown above, linear rate kinetics were observed for the various additives. The Y_2O_3-Al_2O_3 and Y_2O_3-MgO based materials had the highest transformation rates, which is not surprising since these additives also typically would have the lowest liquid phase viscosities during sintering which would enhance the transformation rate. The Y_2O_3-SiO_2 additive system would have the highest liquid phase viscosity and indeed, the slowest transformation rate is observed with these materials. The Y_2O_3-La_2O_3-SrO (La-Yb-Sr) system was intermediate in transformation kinetics compared to the other systems.

The results have established that the α-to-ß transformation kinetics for a particular sintering additive type are related to the initial ß content and the powder surface area. However, these factors alone do not explain all the differences in transformation behavior between the powders. In particular, the powder fabricated by carbothermal reduction (Dow EXP) displays a slower transformation rate than would be predicted based on the initial ß content and surface area. The difference is believed to be associated with the dissolution or melting behavior of the starting α-phase powder in the liquid phase upon which the transformation kinetics are directly dependent.

Possible influences on the dissolution behavior would include impurities (such as metallic cations, carbon and oxygen) and the bond strength in the crystal structure. In examining the data, the lower purity Si_3N_4 powders did exhibit the lower transformation rates, however, impurities, such as Ca and Fe would tend to increase the melting rate, not decrease it. Figure 3 shows the transformation rate as a function of the carbon content. While there is a definite trend to higher rates at the low carbon contents, the relationship is indeterminate at the higher carbon contents. This is probably due to which form the carbon is present in. At the low carbon contents (<0.2 wt. %), the carbon is associated within the α-Si_3N_4 structure and consequently would have a direct effect on the dissolution rate. However, at the high carbon contents of the carbothermally produced powders, the carbon may be present as SiC or even free carbon which would not directly affect the α-to-ß transformation. The relationship between the lattice oxygen content and the transformation rate is shown in Fig. 4. As indicated, the transformation rate is observed to decrease with increasing lattice oxygen. Melting involves the breaking of bonds as the material enters the liquid phase. The effect of the lattice oxygen and carbon contents on the Si_3N_4 dissolution behavior may be associated with the differences in the bond strengths: Si-N of 335 kJ/mol, Si-O of 452 kJ/mol and Si-C of 318 kJ/mol.[1] The high lattice oxygen contents and the strengths of the Si-O bond could contribute to a decrease in the melting kinetics of the α-Si_3N_4 and a decrease in the overall transformation kinetics.

Quantitative Analysis of Grain Growth - The acicular nature of the ß-Si_3N_4 grain morphology and their interlocking growth makes quantitative evaluation of the grain sizes extremely difficult. Most quantitative analysis of microstructures rely on the use of metallographic polished cross-sections of the materials and a two-dimensional representation of the planar cross-section. Because of the random orientation of the of the c-axis preferential growth direction, a plane cross-section intersects the grains at all orientations. Thus, to determine the length and aspect ratio of the acicular grains from polished specimens, several studies made assumptions on orientation frequencies to determine the grain size distribution.[2-4]

An alternative method developed in recent years, chemically dissolves the intergranular phase, the collects the ß-Si_3N_4 grains and the directly measures the grains using a scanning electron microscope (SEM).[5] The intergranular phase is dissolved by reaction with NaOH to produce sodium silicates that are soluble in water. After dissolution, the ß-Si_3N_4 grains are free from the matrix and can be collected. This method eliminates the errors associated with mathematical assumptions.

Selected samples were subjected to dissolution of the intergranular phase and collected as described. These grains were analyzed for length and diameter and the aspect ratio (length/diameter) was calculated. The samples were selected to determine the effects on the initial stage ß-Si_3N_4 grain growth of the Si_3N_4 powder type, the sintering additive composition, the liquid phase volume content and time. All of the samples were high in ß-Si_3N_4 content (95-100%). This was intended to eliminate any mis-interpretations in dimensions that would be caused by the inability to distinguish between the α- and ß-phases in the SEM after dissolution into individual grains.

The effect of the powder type on the initial stage ß-Si_3N_4 grain growth (1800°C for 15 minutes) is shown in Fig. 5. The comparison indicates that the Starck M11 powder has a shorter length, but higher aspect ratio. This says that overall, the ß- grains were much thinner in diameter than those developed in the Ube E-10 powder. Such a situation is related to the high initial ß-content of the M11 powder and its higher transformation rate. Those factors would contribute to highly acicular growth of many grains during the initial grain growth stage.

The differences in the sintering additive composition on the initial stage ß-Si_3N_4 grain growth is illustrated in Fig. 6. As shown, the higher viscosity liquid phase (Yb_2O_3-La_2O_3-SrO) results in larger average diameter and aspect ratios in comparison to the lower viscosity liquid (Y_2O_3-Al_2O_3 system). It had been previously shown that the Yb_2O_3-La_2O_3-SrO system had a slower transformation rate and this apparently encouraged grain growth in the c-axis direction of fewer grains. The Y_2O_3-Al_2O_3 composition, on the other hand, exhibited a higher transformation rate and this causes grain growth of many ß-Si_3N_4 grains and impingement. The impingement of similar sized grains would tend to limit grain growth in both diameter and length. The higher viscosity liquid phase encourages acicular growth of ß-Si_3N_4 grains because it decreases diffusivity for nitrogen and silicon and consequently, growth in diameter (the [210] direction) is limited by solute deficiency.

The effect of the liquid phase volume content on the initial stage ß-Si_3N_4 grain growth is shown in Fig. 7. As indicated, increased additive volume content results in a decrease in grain dimensions both in length and aspect ratio. Previously, the larger volume content had been shown to have a slower transformation rate indicating a diffusion controlled process. The smaller grain dimensions also suggest a diffusion controlled mechanism for the grain growth. However, the increase in additive content can also contribute to a time delay in the α-to-ß transformation and decrease the grain size in that way. This is because more of the α-Si_3N_4 must be dissolved prior to the liquid phase reaching Si and N saturation. Thus, grain growth is slowed in comparison to the lower additive content materials.

Like most materials, as silicon nitrides are held at elevated temperatures, grain growth naturally occurs. The effect of the high temperature hold time on the grain development is shown in Fig. 8 for high viscosity liquid phase compositions (Yb_2O_3-La_2O_3-SrO system). As indicated, the average grain lengths and aspect ratios increase with time (up to 60 min. in this case) which is what one would expect. While these relatively short times indicate increasing aspect ratios with time, previous results have shown long hold times to result in coarsening of the microstructures and a decrease in the average aspect ratio.[1.16]

Mechanical Properties - A study has been started to determine the effects that the different nucleation conditions have on the final mechanical properties. The initial samples have been fabricated and densified under conditions to give various levels of ß-phase contents prior to sintering at elevated temperatures. The conditions for the initial materials are shown in Table 1. As shown, the nucleation conditions did not affect the densification behavior very much. The mechanical property testing is currently in progress.

Status of Milestones

On schedule.

Communications/Visits/Travel

Travel by T. N. Tiegs to the Customers' Coordination Meeting in Dearborn, MI on October 30-November 1, 1996.

Travel by T. N. Tiegs to the American Ceramic Society Conference on Advanced Ceramics and Composites, Cocoa Beach, FL, January 12-15, 1997 to present a paper entitled "Effect of Powder Characteristics on the α-to-ß Si_3N_4 Transformation Kinetics."

Travel by T. N. Tiegs to the AlliedSignal Ceramic Components, Torrance, CA, February 21, 1997 to review program on toughened silicon nitride.

Problems Encountered

None.

Publications

T. N. Tiegs, F. C. Montgomery, J. L. Schroeder, D. L. Barker and P. A. Menchhofer, "Effect of Powder Characteristics on the α-to-ß Si_3N_4 Transformation Kinetics," to be published in Ceram. Eng. Sci. Proc.

References

1. J. Lang, "Silicate Structures and Atomic Substitution," pp. 23-43 in Progress in Nitrogen Ceramics, Martinius Nijoff Pub., The Hague, Netherlands (1983).

2. G. Wötting and G. Zeigler, "Characterization of Microstructural Variables of Sintered, Hot-Pressed and Hot-Isostatically Pressed Si_3N_4 and Their Correlation to Mechanical Properties," Ceram. Internat., 10,18-22(1984).

3. F. Mücklich, J. Ohser, S. Hartmann, M. J. Hoffmann and G. Petzow, "3-D Characterization of Sintered Microstructures with Prismatic Grains," pp. 73-86 in Tailoring of Mechanical Properties of Si_3N_4 Ceramics, M. J. Hoffmann and G. Petzow (ed.), Kluwer Acad. Pub., Netherlands (1994).

4. F. Mücklich, J. Ohser, S. Hartmann, M. J. Hoffmann, G. A. Schneiderand G. Petzow, "Quantitative Description of Si_3N_4 Microstructures," pp. 89-91 in Silicon Nitride 93, Key Engineering Mater., Vol. 89-91, Trans Tech Pub., Aedermannsdorf, Switzerland (1994).

5. K.-R. Lai and T. Y. Tien, "Kinetics of ß-Si_3N_4 Grain Growth in Si_3N_4 Ceramics Sintered Under High Nitrogen Pressure," J. Am. Ceram. Soc., 76[1]91-96(1993).

Table 1. Summary of densification results on samples fabricated using different ß-phase nucleation conditions.

TRSN Sample No.	Sintering Aid Composition	Si_3N_4 Powder Type	Nominal ß-Si_3N_4 Nucleation Conditions (°C/min)	Approximate ß-Si_3N_4 Content After Nucleation	Sintered Density (% T. D.)
55-2-1	Y_2O_3-Al_2O_3	Ube E-10	1500/180	20	99.9
54-4-2	Y_2O_3-Al_2O_3	Ube E-10	1600/15	25	99.9
54-4-1	Y_2O_3-Al_2O_3	Ube E-10	1500/60	15	99.8
54-1-3	Y_2O_3-Al_2O_3	Ube E-10	1600/60	60	100.0
54-1-1	Y_2O_3-Al_2O_3	Ube E-10	1700/60	100	99.9
55-1-2	$Sr_2La_4Yb_4(SiO_4)_6O_2$	Ube E-10	1500/180	10	99.6
55-2-2	$Sr_2La_4Yb_4(SiO_4)_6O_2$	Ube E-10	1600/15	20	99.7
55-4-1	$Sr_2La_4Yb_4(SiO_4)_6O_2$	Ube E-10	1500/60	5	99.7
55-3-3	$Sr_2La_4Yb_4(SiO_4)_6O_2$	Ube E-10	1600/60	30	99.9
55-3-2	$Sr_2La_4Yb_4(SiO_4)_6O_2$	Ube E-10	1700/60	80	99.8
56p-1	Y_2O_3-Al_2O_3	Starck M11	1500/60	20	99.9
56-1-3	Y_2O_3-Al_2O_3	Starck M11	1600/60	75	99.9
57p-2	$Sr_2La_4Yb_4(SiO_4)_6O_2$	Starck M11	1500/60	20	99.4
57p-1	$Sr_2La_4Yb_4(SiO_4)_6O_2$	Starck M11	1700/60	70	99.4

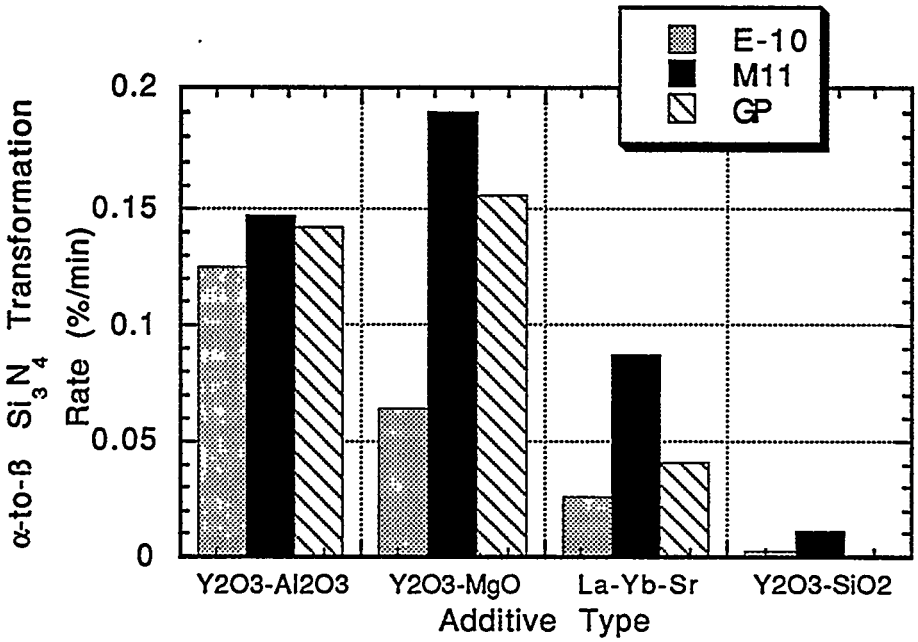

Fig. 1. α-to-ß Si_3N_4 transformation rate for the various types of sintering additives with the E-10, M11 and GP silicon nitride powders at 1500°C.

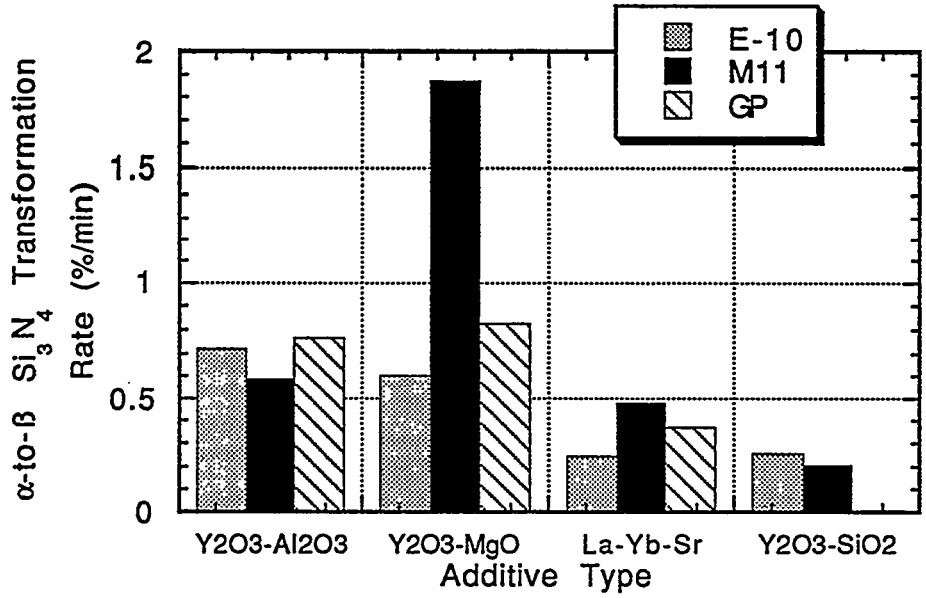

Fig. 2. α-to-ß Si_3N_4 transformation rate for the various types of sintering additives with the E-10, M11 and GP silicon nitride powders at 1600°C.

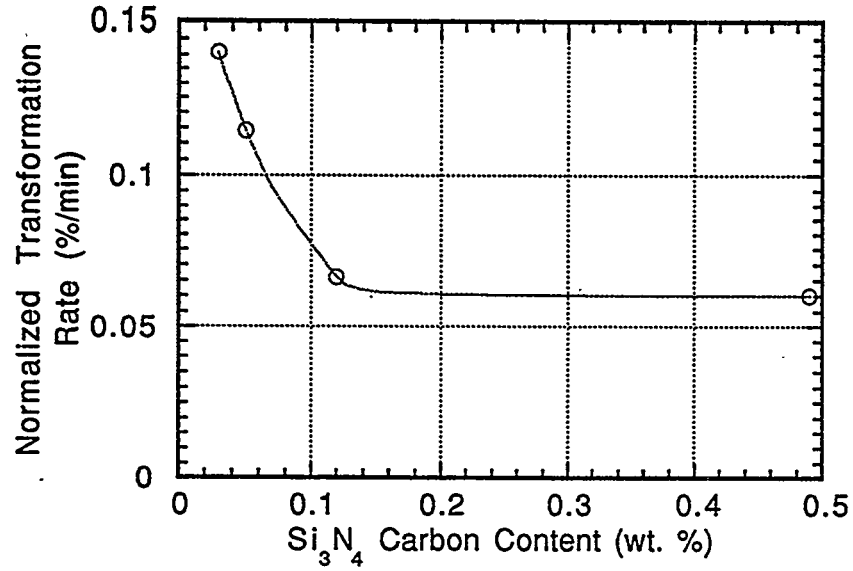

Fig. 3. Normalized α-to-ß Si_3N_4 transformation rate as a function of starting silicon nitride carbon content at 1500°C. The sintering additive was 6% Y_2O_3-2% Al_2O_3. The transformation rates were normalized to a powder surface area of 11 m^2/g and an initial ß-phase content of 2.5 %.

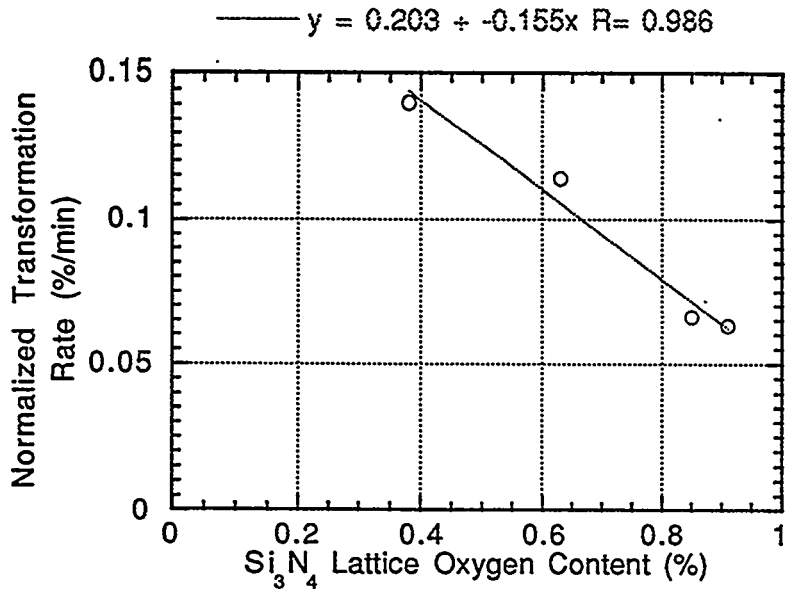

Fig. 4. Normalized α-to-ß Si_3N_4 transformation rate as a function of starting silicon nitride lattice oxygen content at 1500°C. The sintering additive was 6% Y_2O_3-2% Al_2O_3. The transformation rates were normalized to a powder surface area of 11 m^2/g and an initial ß-phase content of 2.5 %.

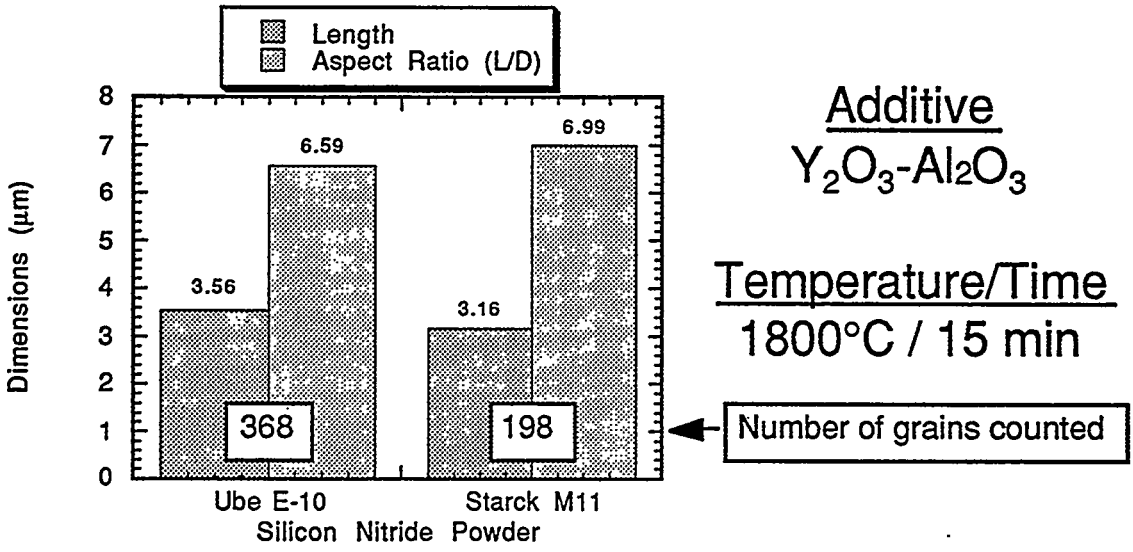

Fig. 5. Effect of silicon nitride powder type on initial stage ß-Si_3N_4 grain growth. Powders were either Ube E-10 or Starck M11 as indicated. Heating time was 1800°C for 15 minutes. Sintering additive composition was 6% Y_2O_3-2% Al_2O_3.

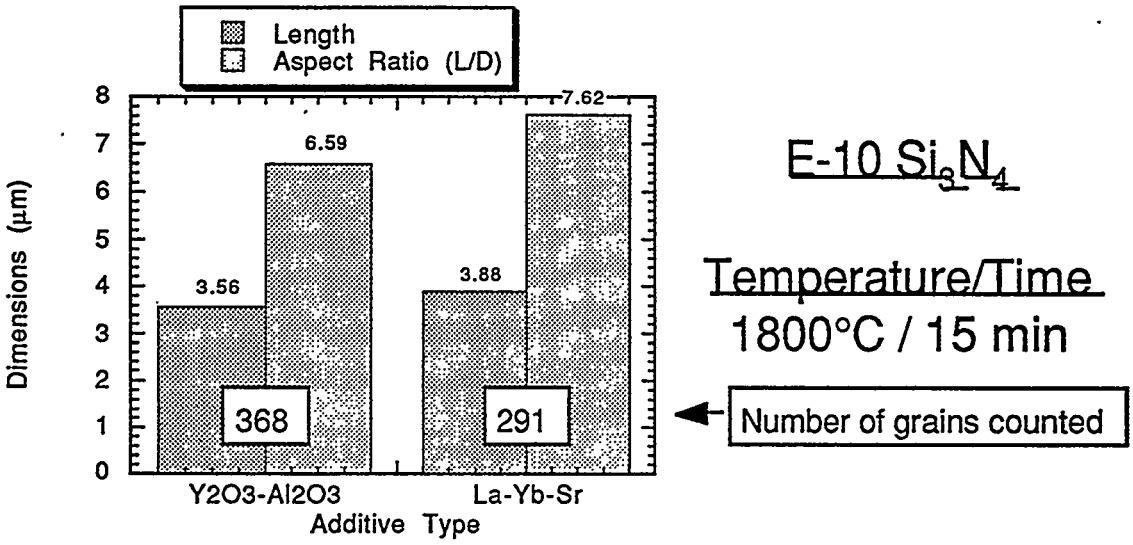

Fig. 6. Effect of sintering additive composition on initial stage ß-Si_3N_4 grain growth. Powder was Ube E-10. Heating time was 1800°C for 15 minutes. Sintering additive composition was either 6% Y_2O_3-2% Al_2O_3 or $Sr_2La_4Yb_4(SiO_4)_6O_2$.

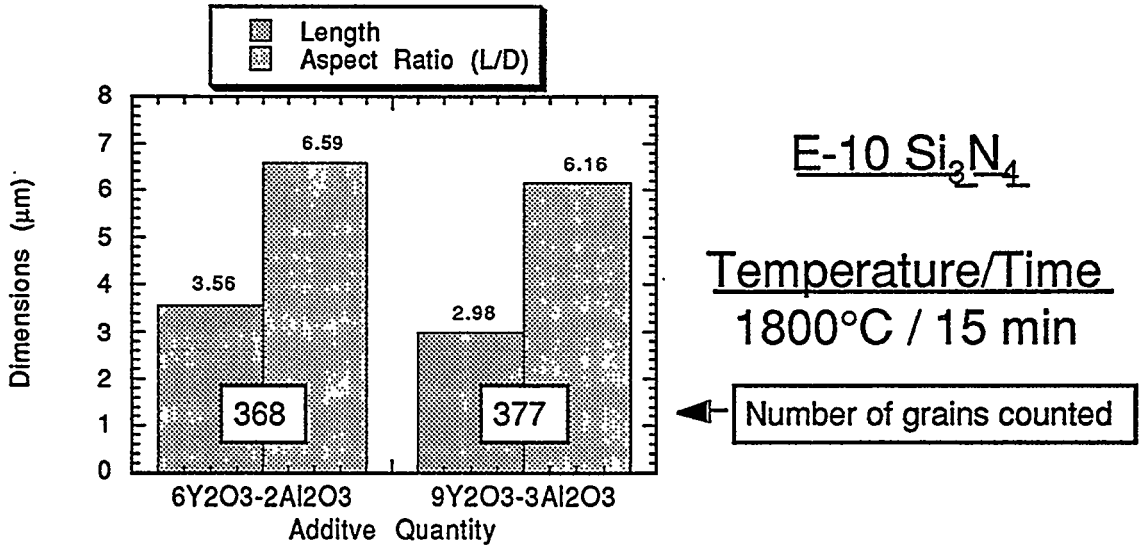

Fig. 7. Effect of sintering additive volume content on initial stage ß-Si_3N_4 grain growth. Powder was Ube E-10. Heating time was 1800°C for 15 minutes. Sintering additive composition was either 6% Y_2O_3-2% Al_2O_3 or 9% Y_2O_3-3% Al_2O_3.

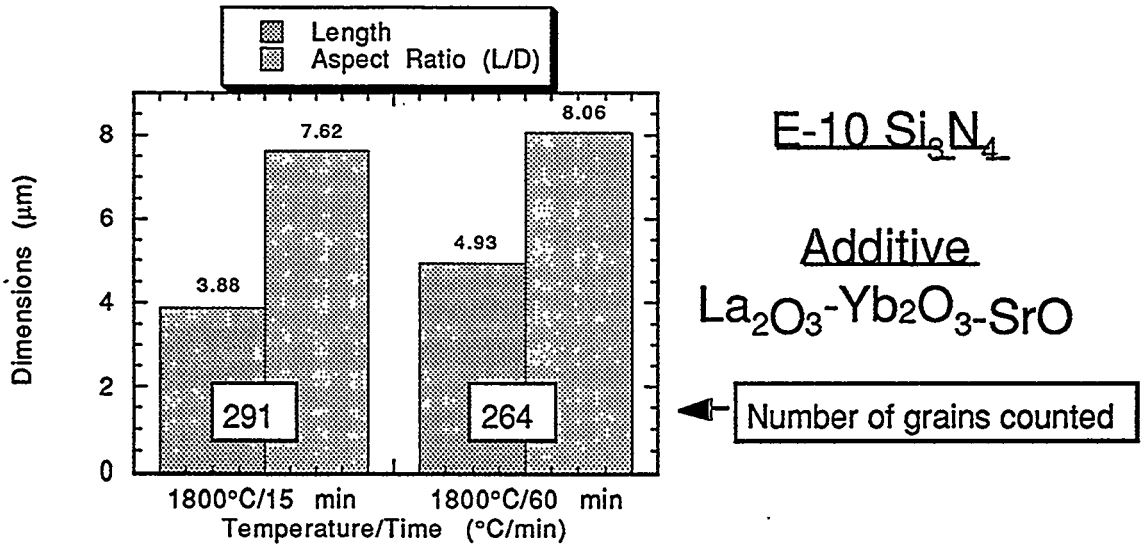

Fig. 8. Effect of sintering time on initial stage ß-Si_3N_4 grain growth. Powder was Ube E-10. Heating was at 1800°C for either 15 or 60 minutes. Sintering additive composition was $Sr_2La_4Yb_4(SiO_4)_6O_2$.

Cost Effective Sintering of Silicon Nitride Ceramics (SIU-C)-
D. E. Wittmer, Southern Illinois University, Carbondale, IL 62901

Objective/Scope

The purpose of this work is to investigate the potential of cost effective sintering of Si_3N_4 through the development of continuous sintering techniques and the use of lower cost Si_3N_4 powders and sintering aids.

Technical Highlights

Task 1. Refine Economic Model and Design for Chosen Furnace Configuration

This task was completed as reported in a previous semiannual report.

Task 2. Continue evaluation of sintering parameters on properties of selected Si_3N_4 compositions

Prototype Belt Furnace

The Model 44-BF belt furnace has been operating with the tungsten hot zone installed for over 2 years (>1500 hours) of high-temperature operation without any major problems with the furnace. Advanced ceramics compositions successfully sintered included: many silicon nitride formulations, SiAlON, AlN, and some mixed oxides. Specific furnace modifications have been suggested to Centorr Vacuum Industries to improve the operation of the next generation furnace. Also, the addition of a debinding chamber is being investigated.

Industrial Collaboration/Affiliation

Eaton Corporation

A master's thesis, "Continuous Sintering of SRBSN", was completed the results of this work (given in Tables 1 and 2), the following conclusions were made:

- The optimum continuous sintering parameters for Eaton nitrided SRBSN, based only on density, were determined to be 1775° C for 240 min, utilizing all three hot-zones and a corresponding belt speed of 0.188"/min. These conditions produced the highest average bulk density of 3.36 gm/cc with a standard deviation of 0.01. This value was greater than 100% of the target density provided by Eaton.

- The highest average four-point flexural strength of the continuously sintered Eaton nitrided SRBSN was obtained for sintering conditions of 1750° C and 240 min, utilizing all three hot-zones and a corresponding belt speed of 0.188"/min. The average strength obtained was 584 MPa with a standard deviation of 14 MPa. This value agrees well with the data obtained by Eaton for batch sintered SRBSN.

- The highest fracture toughness for the Eaton nitrided SRBSN, 5.5 MPa-$m^{1/2}$ with a standard deviation of 0.2 MPa-$m^{1/2}$, was obtained for continuous sintering conditions of 1775° C and 240 min, utilizing all three hot-zones and a corresponding belt speed of 0.188"/min. This fracture toughness was comparable to the values obtained by ORNL for SRBSN containing alumina and yttria sintering aids.

- For dense packed and the loosely packed specimen configurations, there was no observed statistical difference in the sintered densities. The densities obtained for the high and low pack density, following sintering at 1775°C for 240 min, were 3.34 and 3.35 g/cc, respectively, with a standard deviation of 0.01 for both.

- The heating rate (produced by the number of hot zones and fixed by the temperature profile and belt speed) was found to have a secondary effect on the densification of the Eaton nitrided SRBSN. The hot zone length was found to be inproportionate to the number of hot zones employed, ie. with power to two hot zones the length of the total hot zone was longer than 67% of the total hot zone produced when power was supplied to all three hot zones. This caused the bars to be at a higher temperature marginally longer when two hot zones were used instead of three hot zones for the same "planned" sintering time..

- In all cases, the use of two hot zones produced lower as-sintered strength for the Eaton nitrided SRBSN compared to the same sintering conditions using three hot zones, even though the as-sintered densities were marginally higher when only two zones were employed.

- Microwave nitridation hold promise for improving the microstructure, strength and fracture toughness of SRBSN. Limited data showed that higher strength can be obtained at lower sintered density for the microwave nitrided SRBSN, compared to SRBSN nitrided by Eaton.

Based on the results for the continuous sintering parameter design matrix for SRBSN, the optimum sintering conditions for highest density, strength and fracture toughness was predicted to be 1790°C for 120 min. Eighty-four test bars of the Eaton nitrided SRBSN and eighty-four test bars of the Eaton SRBSN that were microwave

nitrided at ORNL were continuously sintered under these conditions, and the properties of these test bars are currently being determined.

Norton Advanced Ceramics

During this reporting period, the exhaust valve work with NAC as part of the Norton Advanced Ceramics ACMT contract was completed. Additional funds have been requested by NAC to continue investigations involving sintering warpage and consistency. All of the materials that were continuously sintered have been returned to NAC. The results are reported by NAC as part of the ACMT contract.

Allied Signal, Inc.

Some test materials have been successfully sintered and were returned to Allied Signal for evaluation.

Task 3. Continue Evaluation of Low Cost Si_3N_4 Powder

Work on the Starck M-11 and Shin-Etsu powders was initiated during this reporting period. These powders are being evaluated, along with the use of alumina, zirconia, and silicon nitride milling media. The effects of turbomilling time and milling media on the sinterability, powder surface area and average particle size are being determined for the A2Y8 formulation.

Eighteen turbomilling runs in the A2Y8 formulation have been completed using Starck M-11 and Shin-Etsu powders. Alumina, zirconia, and silicon nitride milling media were used in the turbomilling for 2 and 4 hour milling times. The effect on the viscosity of the slurry and media weight loss were determined for each run, with the hopes of correlating these values with the sinterability of the disks that were pressure cast from these slurries. Samples were also taken from each turbomilling run for particle size analyses and possible oxygen analyses.

Some of the condensed data from the turbomilling runs are given in Table 3. From this data it can be observed that the viscosity decreased with increased turbomilling time for the Starck M-11 formulation, while the viscosity increased with increased milling time for the Shin-Etsu formulation. The reason for this behavior may be related to the use of pH control for the M-11 powder for dispersion, while organics provided by Shin-Etsu were used for the Shin-Etsu powder. The Shin-Etsu had a tendency to gel with longer milling times and was more affected by the turbomilling temperature. This could be a combined effect due to chemical reaction of the powder with the water, coupled with the affects of milling on the organic dispersants. Additional runs are planned with the Shin-Etsu powder at higher turbomilling temperature to see if that aids in lowering the slurry viscosity.

The data in Table 3 also show that for the Starck M-11 formulation the silicon nitride milling media had (in general) the highest media wear rate, while the yttria toughened zirconia had the lowest wear rate. The wear rate of the alumina media was between that of the other two media types. This behavior was similar for the Shin-Etsu formulations but is somewhat altered by the high viscosity encountered during the 4 hour turbomilling runs.

Disks from all twelve of the A2Y8 batches representing the test matrix and six additional batches of A2Y8 investigating repeatability, using Starck M-11 and Shin-Etsu powders, were continuously sintered in the Centorr Model 44-BF belt furnace at 1790°C or 120 min. The data in Table II gives the data for the continuously sintered disks. This data shows that the highest densities were obtained for the batches milled with the alumina media, followed by the zirconia media, and lastly the silicon nitride media. The reasons for this behavior are being further explored.

Machined test bars have recently been received for the A2Y8 formulations using the M-11 and the Shin-Etsu powders. The flexural strength and fracture toughness values will be determined during the next reporting period.

Task 4. Design and Construct Prototype Belt Furnace

This task has been completed.

Status of Milestones

1.	Refine Economic Model and Design for Chosen Furnace Configuration	Completed
2.	Continue Evaluation of Sintering Parameters on Properties of Selected Si_3N_4 Compositions	On Schedule Continuing
3.	Continue Evaluation of Low Cost Si_3N_4 Powders	On Schedule Continuing
4.	Design and construct prototype belt furnace	Completed

Communications/Visits/Travel

S. P. Etherton and M. Hoglesson to the CCM meeting at Cocoa Beach, FL, Jan. 97.

D. E. Wittmer to ORNL to discuss results with program monitor, April 97..

D. E. Wittmer to ANL to discuss potential for using synchrotron analyses for silicon nitride research, April 97.

Problems Encountered

None

Publications

S. P. Etherton, "The Effects of Continuous Sintering Parameters on the Properties of Sintered, Reaction-Bonded Silicon Nitride," M.S. Thesis at Southern Illinois University at Carbondale, accepted for May 1997 graduation.

D. E. Wittmer, S. P. Etherton, and J. P. Edler, "The Effects of Continuous Sintering Parameters on the Properties of Sintered, Reaction-Bonded Silicon Nitride," (To be published in the Composites Engineering)

Presentations

None

Table 1. Physical properties for as-sintered Eaton SRBSN.

Sintering Time (min)	Sintering Temperature					
	1725°C			1750°C		
	Bulk ρ (g/cc)	Weight Loss (%)	4-Pt. Flex. (MPa)	Bulk ρ (g/cc)	Weight Loss (%)	4-Pt. Flex. (MPa)
60	---	---	---	3.11	2.16 ± .31	424 ± 47
90	3.03	1.77 ± .37	392 ± 54	3.22	2.50 ± .27	456 ± 34
120	3.18	2.35 ± .42	380 ± 29	3.25	2.67 ± .19	450 ± 28
240	3.29	2.97 ± .40	440 ± 24	3.34	3.83 ± .36	432 ± 19
	Sintering Temperature					
	1775°C			1800°C		
	Bulk ρ (g/cc)	Weight Loss (%)	4-Pt. Flex. (MPa)	Bulk ρ (g/cc)	Weight Loss (%)	4-Pt. Flex. (MPa)
60	3.19	3.36 ± .37	420 ± 50	3.26	5.25 ± .52	380 ± 44
90	3.29	3.84 ± .32	485 ± 40	---	---	---
120	3.30	4.01 ± .26	435 ± 46	---	---	---
240	3.35	4.54 ± .44	390 ± 49	---	---	---

Table 2. The physical properties for machined test bars of Eaton nitrided SRBSN.

Sintering Time (min)	Sintering Temperature					
	1725°C			1750°C		
	Bulk ρ (g/cc)	Fracture Toughness (MPa-$m^{1/2}$)	4-Pt. Flex. (MPa)	Bulk ρ (g/cc)	Fracture Toughness (MPa-$m^{1/2}$)	4-Pt. Flex. (MPa)
60	---	---	---	3.12 ± .02	4.1 ± 0.2	418 ± 32
90	3.12 ± .02	4.1 ± 0.1	437 ± 48	3.21 ± .03	4.5 ± 0.2	513 ± 52
120	3.19 ± .02	4.3 ± 0.0	472 ± 62	3.26 ± .02	4.6 ± 0.1	562 ± 31
240	3.28 ± .01	4.6 ± 0.1	503 ± 85	3.34 ± .01	4.9 ± 0.2	584 ± 14
	Sintering Temperature					
	1775°C			1800°C		
	Bulk ρ (g/cc)	Fracture Toughness (MPa-$m^{1/2}$)	4-Pt. Flex. (MPa)	Bulk ρ (g/cc)	Fracture Toughness (MPa-$m^{1/2}$)	4-Pt. Flex. (MPa)
60	3.20 ± .02	4.4 ± 0.1	416 ± 21	3.26 ± .01	5.1 ± 0.1	434 ± 51
90	3.29 ± .02	4.9 ± 0.1	485 ± 32	---	---	---
120	3.31 ± .01	5.1 ± 0.1	523 ± 45	---	---	---
240	3.36 ± .01	5.5 ± 0.1	529 ± 45	---	---	---

Table 3. The effect of boat loading on the physical properties of as-sintered SRBSN test bars, following continuously sintering at 1775°C for 240 min.

Packing Layer (From Bottom)	Low Density Packing		High Density Packing	
	Bulk ρ (g/cc)	Weight Loss (%)	Bulk ρ (g/cc)	Weight Loss (%)
1	3.36 ± .01	2.58 ± .21	3.34 ± .01	2.3 ± .19
2	3.36 ± .01	2.52 ± .25	3.34 ± .00	2.13 ± .16
3	3.35 ± .01	2.47 ± .22	3.33 ± .00	1.97 ± .18
4	3.35 ± .01	2.36 ± .33	3.34 ± .00	1.92 ± .11
5	3.34 ± .00	2.16 ± .17	3.35 ± .01	1.82 ± .08
6	3.34 ± .00	2.05 ± .08	3.34 ± .01	1.82 ± .11
7	3.34 ± .01	2.06 ± .15	3.34 ± .01	1.76 ± .12
8	3.35 ± .00	2.07 ± .26	3.34 ± .01	1.64 ± .15
9	3.35 ± .00	1.79 ± .2	3.34 ± .01	1.58 ± .23
Average	3.35 ± .01	2.23 ± .21	3.34 ± .01	1.88 ± .15

Table 4. Comparison of viscosity and media weight loss for two commercial silicon nitride powders in the A2Y8 formulation and three commercial milling media types as a function of turbomilling time.

Type of Milling Media	Starck M-11				Shin-Etsu			
	2 h milling		4 h milling		2 h milling		4 h milling	
	Viscosity (cp)	Media Wt. Loss (%)	Viscosity (cp)	Media Wt. Loss (%)	Viscosity (cp)	Media Wt. Loss (%)	Viscosity (cp)	Media Wt. Loss (%)
Si_3N_4	12.5	0.28	7	0.8	12	0.33	58.5	0.20
Al_2O_3	10.5	0.13	9.5	0.64	46.5	0.14	50	0.22
YT-ZrO_2	13.5	0.06	8	0.16	55	0.05	>75	0.13

Table 5. Results for A2Y8 formulation and three commercial milling media types as a function of turbomilling time. Continuous sintering conditions were 1790°C for 2 hours using all three hot-zones and a belt speed of 0.375"/min.

Type of Milling Media	Starck M-11				Shin-Etsu			
	2 h milling		4 h milling		2 h milling		4 h milling	
	Density (g/cc)	Wt. Loss (%)	Density (g/cc)	Wt. Loss (%)	Density (g/cc)	Wt. Loss (%)	Density (g/cc)	Wt. Loss (%)
Si_3N_4	2.91	1.18	3.04	0.61	2.99	5.33	2.98	2.92
Al_2O_3	2.94	0.99	3.10	0.64	3.11	4.69	3.10	1.34
YT-ZrO_2	2.91	0.86	2.98	1.14	2.97	2.50	3.02	2.99

Wt. loss for the Shin-Etsu includes the dispersants and anti-foam agents.

W. B. S. Element 1.2.4.3
CHARACTERIZATION AND TESTING OF LOW EXPANSION CERAMIC MATERIALS

S. Shanmugham, K. Breder, and D. P. Stinton

Objective/Scope

Insulated exhaust portliners are needed in advanced diesel engines to increase engine fuel efficiency by increasing the combustion temperatures and reducing the combustion heat that is lost through the head and into the water cooling system. Low expansion materials have potential for this application due to their very low thermal conductivity, extraordinary thermal shock resistance, and reduction of attachment stresses. Thermal shock resistance is critical because the shape of the portliners requires that they be cast into the metallic cylinder head. Functioning exhaust portliners are inaccessible after they are cast into cylinder heads and hence, must not require maintenance for the life of the head (~ 1 million miles). A contract has been placed with LoTEC., Inc., to develop cost effective processes for the fabrication of portliners. LoTEC is investigating $Ba_{1+x}Zr_4P_{6-2x}Si_{2x}O_{24}$ (BaZPS) and $Ca_{1-x}Sr_xZr_4P_6O_{24}$ (CSZP). ORNL is assisting with the characterization and evaluation of the above compositions.

Technical Highlights

A systematic investigation of the mechanical properties of five BaZPS compositions (x=0, 0.175, 0.25, 0.375, and 0.5) and CSZP with x=0.5 (CS50) ceramic has been initiated. Additionally, the thermal properties of the BaZPS compositions are being investigated. Five BaZPS compositions and CS50 were synthesized from stoichiometric proportions of the reagent grade oxides using a solid-state reaction method. In this semi-annual report, the results of differential scanning calorimetry (DSC) studies on BS37 and BS50 are presented. The static bend testing conditions at 800°C for CS50 are also presented. The objective of the static bend testing is to determine the creep rate in flexure for CS50 at a given stress level.

DSC runs were conducted on BaZPS with x=0.375 and 0.5 in a platinum crucible with sapphire as the reference material. The DSC furnace was ramped at 50°C/min between 25°C and 1300°C in air and the data was recorded by an automated data collection system. The DSC curve of BaZPS with x=0.375 did not show any endothermic or exothermic peaks suggesting that it did not undergo any phase transition. Whereas the BaZPS composition with x=0.5 shows an endothermic peak between 430°C and 580°C (Fig. 1).

Figure 1 summarizes the endotherm regions in the DSC curves of the BaZPS compositions. The endotherm region corresponds to a phase transition and the phase transition temperature of the BaZPS compositions decreases with increasing silicon content (x in Fig. 1). For example, BaZPS with x=0 undergoes a phase transition around 900°C, while BaZPS with x=0.25 shows a phase transition around 620°C. The high temperature X-ray diffraction study showed that the BaZPS with x=0 undergoes a phase transition from R3 to R3c on heating at 900°C. For the other BaZPS compositions, the phase transition type has not yet been determined.

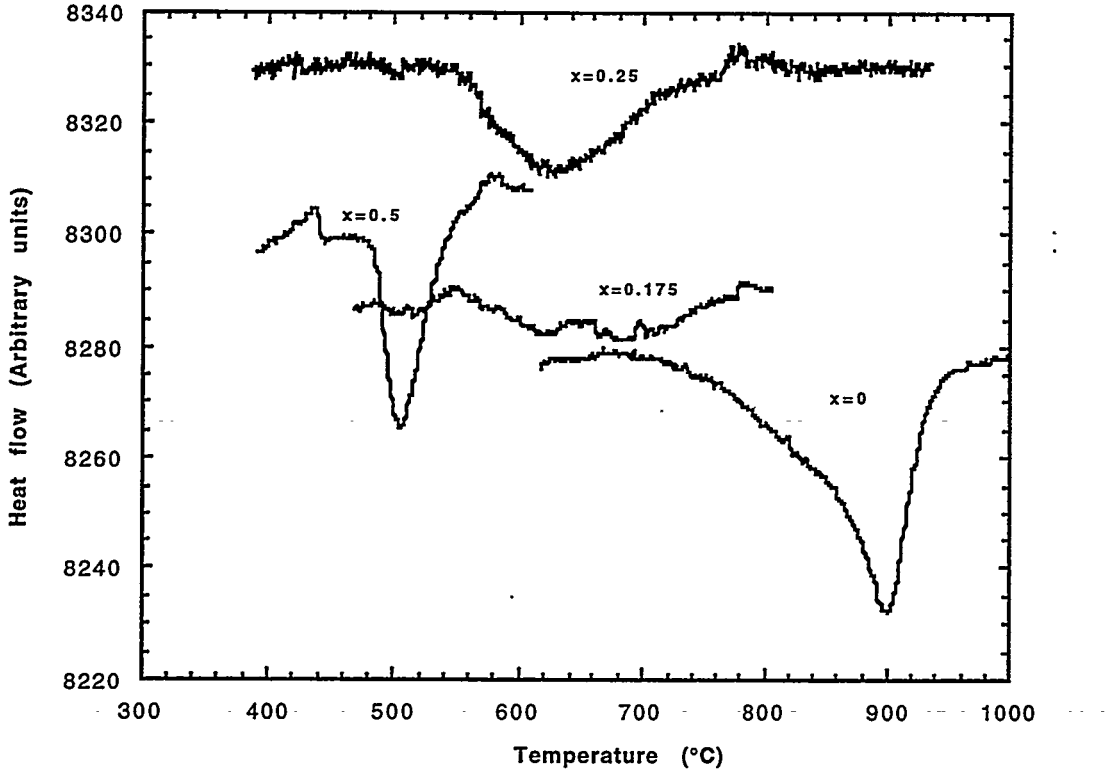

Fig. 1. The phase transition temperature of the BaZPS compositions decreases with increasing silicon content

The static bend tests of CS50 at 800°C were conducted using a specially designed flexure test system capable of separately testing up to three specimens in series in a furnace. The testing was conducted using a four-point bend fixture with 40 mm and 20 mm outer and inner spans, respectively. The specimens were pre-stressed at a low stress level, heated to 800°C, the desired stress levels were then applied and maintained for 300 h. During this period, the displacements at the load points were monitored. For each run, two specimens and an empty fixture were loaded. The empty fixture was used as a "dummy" to correct for possible variations in the fixtures themselves. As expected, the variations were negligible at these low temperatures and stress levels. After 300 h, the specimens were cooled to room temperature and removed from the furnace.

Table 1 summarizes the status of the static bend tests at 800°C for CS50 specimens along with the stress level at which the specimens were tested. The static bend testing results are being analyzed and will be presented next period.

Table 1. Static Bend Testing of CS50 at 800°C

Specimen #	Nominal Static Stress (MPa)	Status
1	40	Completed
3	40	Completed
5	60	Completed
6	60	Completed
7	70	Ongoing
8	70	Ongoing

Reference

None

Milestones

On schedule

Problems Encountered

None

Development of NZP Ceramic Based "Cast-in-Place" Diesel Engine Port Liners

Rama Nageswaran, Justin Cassell and Santosh Y. Limaye (LoTEC, Inc.)

Objective/Scope

The overall objective of this research is to develop sodium-zirconium-phosphate (NZP) ceramic based "cast-in-place" diesel engine port liners. Specific objectives are: (1) Development and optimization of the overall insulation system, (2) Refinement of the compliant layer formation process around the ceramic insulation system, (3) Development and adaptation of cost-effective powder and material fabrication processes, and (4) Creation of database of high temperature properties (stability in diesel exhaust environment, thermal cycling, thermal shock, etc.).

Technical Progress

Progress during the last six month reporting period covered the following four areas: (i) materials and processes development, (ii) solids-modeling of complex-shaped geometries, (iii) examination of compliant layer methods and (iv) evaluation of cast-in-place NZP tubes. In the following passages these four areas are discussed in more detail.

Materials and Process Development

At least one surface strengthening process for making high strength and damage tolerant BS-25 and CS-50 materials has been identified. This process(es) will be investigated in addition to the additive/second phase dispersion approach that has yielded some good results so far. Pressure slip casting (developed in Phase I) is also planned to be used to rapidly fabricate more flaw-free green NZP straight tube port liners. [High strength straight tube port liner is still a special requirement of one engine company.]

Solids Modeling of Complex-Shaped Geometries

LoTEC has acquired PT Modeler from MCAD Design Inc. for modeling complex shaped port liners. The objective behind the acquisition of PT Modeler is to conveniently and rapidly draw/design the complex shaped port liners prior to finite-element analysis. Finite element analysis will be conducted using NISA as usual.

Recently, PT Modeler was used to draw up an L-shaped port liner. Figure 1 depicts a solid-model of the L-shaped port liner that was drawn up. Other shapes such as the Y-shape and S-shape are currently being designed/modeled.

Examination of Compliant Layer Methods

The search for a new material to be used as a commercially-viable compliant layer has been conducted. A commercially available product (ceramic mat) was found, and was determined from testing to be a viable compliant layer. The advantage of the ceramic mat is that it is a high-temperature insulating ceramic mat which has favorable thermal and mechanical properties for metal casting. The favorable properties are: i) the ability to serve as a buffer between the ceramic and metal during casting, (ii) ease of application on the ceramic prior to metal casting, and (iii) greater compliance and porosity properties than LoTEC's in-house developed material.

Testing of the new compliant layer comprised metal casting of straight ceramic manifolds. A sheet of 3 mm thick compliant layer (mat) was wrapped around the ceramic tube prior to casting. After metal casting, it was found that the straight tube port liner with the new compliant layer did not display any cracks.

Evaluation of Cast-in-place Port Liner

One cast-in-place NZP port liner was stripped separate from the cast-iron surrounding it and was machined and tested for fracture strength and elastic modulus after metal casting. Comparison of properties of the previously cast-in-place BS-25 with as-sintered BS-25 revealed that there was no significant difference in properties between the two (refer Table 1). This corroborates the expectation that the properties of the NZP port liner should not deteriorate significantly after metal casting.

Future Work

In continuance with the work accomplished in Phase II, bulk and surface strengthening approaches will continue to be investigated in order to obtain high strength and high toughness NZP ceramics. It is believed that there are several combinations of mechanical properties (elastic moduli, density, strength, and toughness) and compliant layers that will yield a successfully cast-in-place exhaust port. (FEA will once again be used to guide the casting work involving the alternative materials.) In conjunction with the modifications to NZP, different types of metals will be used in casting. Casting in aluminum, in addition to cast-iron, will begin shortly.

Solids modeling of the complex-shaped port liners on PT-Modeler has been initiated with the of designing of an L-shaped port liner. In addition, work on generating the S-shaped and Y-shaped exhaust port liners is underway. The solids-modeled geometries will be imported into NISA for finite element analysis (FEA).

Status of milestones : Program on schedule.

Communications/Visits/Travel :

1) S. Y. Limaye traveled to : (i) Dearborn, Michigan to attend Annual Automotive Technology Development Contractors Coordination Meeting (AATD/CCM) in October 1996.

Problems Encountered : None.

Publications /Presentations :

1) R. Nageswaran, S. Y. Limaye, and D. Stinton, " Development of NZP Ceramic Based Cast-In-Place Port Liners for Commercial Diesel Engines," Presented at the Annual Automotive Technology Development Contractors Coordination Meeting (AATD/CCM) at Dearborn, MI in October 1996.

References : None.

Table 1. Flexural strength of BS-25 as-sintered bars versus cast-in-place BS-25 samples. (Ten samples were tested for each material type.)

Sample Type	Density (g/cm^3)	Flexural Strength (MPa)	Elastic Modulus (GPa)
BS-25 (as-sintered)	2.65-3.00	44-60	52-70
BS-25 (metal cast)	2.80	45.0	52.4

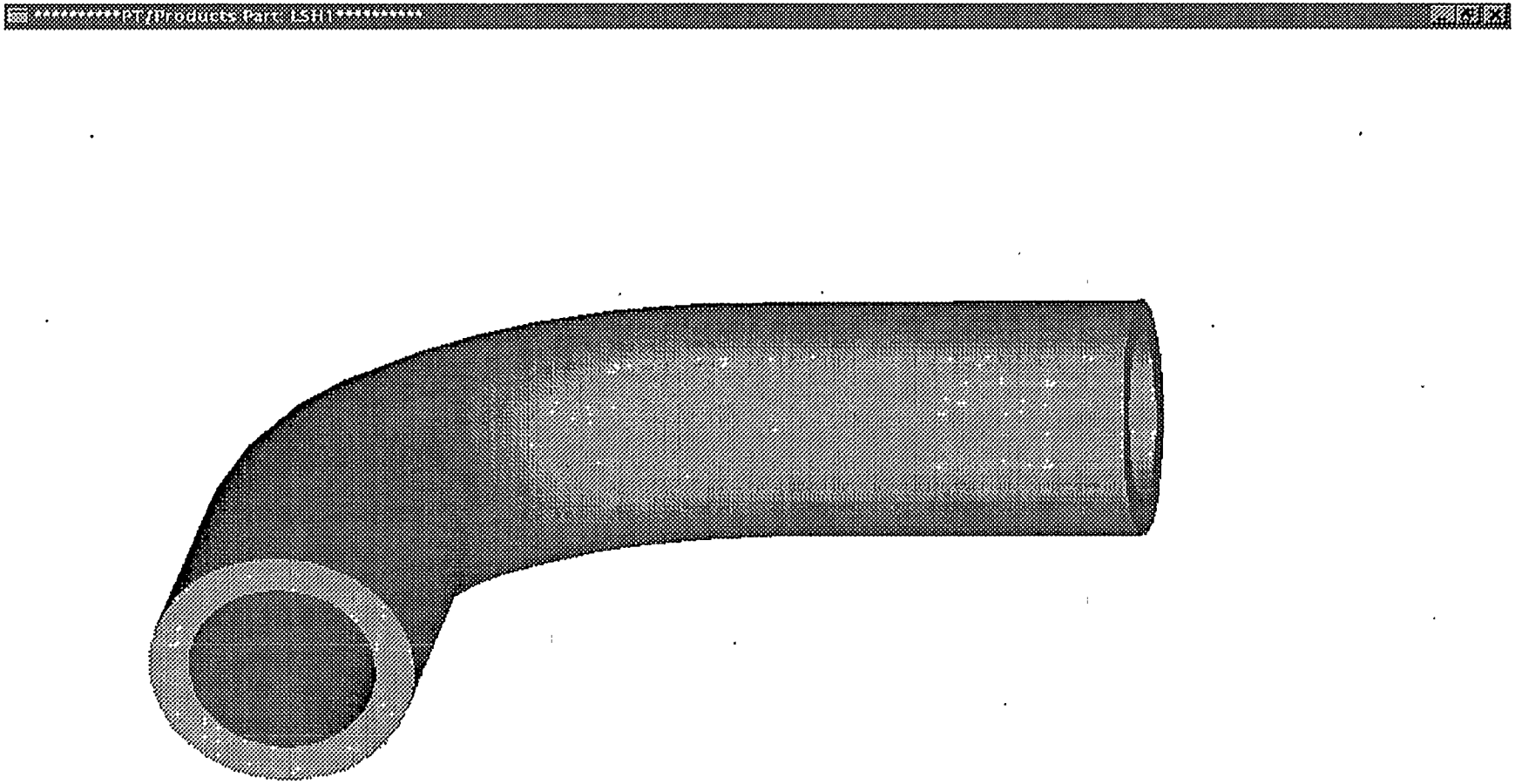

Figure 1: L-shaped port liner modeled using PT-Modeler

Development of Low Cost NZP Powder Synthesis and Processing Technology

Jay Curtis, Rama Nageswaran and Santosh Y. Limaye (LoTEC, Inc.)

Objective/Scope

The overall objective of this research is to develop a suitable technology for low cost synthesis and processing of NZP materials. The two NZP materials of primary interest are BS-25 ($Ba_{1.25}Zr_4Si_{0.5}P_{5.5}O_{24}$) and CS-50 ($Ca_{0.5}Sr_{0.5}Zr_4P_6O_{24}$). Specific objectives to be accomplished are: (1) preliminary assessment of powder techniques of specialist vendors for cost-effective NZP powder synthesis, (2) evaluation of NZP powder samples supplied by vendors for phase and impurity content, particle size and distribution, surface area, thermal stability, dispersability, flowability, sinterability after green forming, and synthesis costs, (3) selection of up to two finalist powder suppliers based on results of initial evaluation, commercial viability of the process, and scale-up costs; (4) advanced evaluation of powders supplied by two companies based on results of material properties testing such as thermal expansion, strength, elastic modulus, etc.; and (5) metal casting trials involving NZP prototype parts and testing of the prototypes for diesel-engine worthiness. A secondary objective will be to set up a hydrothermal (or other) low-cost powder synthesis facility at LoTEC as a parallel effort.

Technical Progress

Activity during the last six-month reporting period resulted in the following notable accomplishments: (i) Transfer of LoTEC's proprietary lab-scale wet chemistry processing know-how to vendors for further optimization and adaptation to large scale production, (ii) Iterative experimentation and testing to establish the most optimum powder processing routes based on techno-economic considerations, (iii) Scale up of the optimum powder processing routes and obtainment of two to three kilogram quantities of powders from the vendors for testing, (iv) Testing of the vendors' powders for powder properties (direct), (v) Preparing bulk samples from vendors' powders using LoTEC's manufacturing process and testing samples for bulk properties (indirect), and (vi) Final down-selection of the vendors' (processes) to fabricate up to 100 kgs. of BS-25 and CS-50 powders.

Direct testing of powders was done mainly at LoTEC, Inc. Indirect (bulk properties) testing was performed by LoTEC's engineer, Jay Curtis, utilizing the High Temperature Materials

Lab's (HTML, ORNL in Tennessee) facilities and technical guidance from its personnel. Analysis of all bulk testing data has been completed and will be included in the next report. (Results of direct testing of powders were provided in the last report.)

Based on detailed analyses of powder and bulk testing of the vendors' powders and on processing / scale-up capabilities of each vendor, a Stage III subcontract was decided to be awarded only to Catalytica, Inc. Although certain powder properties and projected costs (as discussed in the previous report) seemed comparable between the NexTech and Catalytica powders, noticeable differences in powder quality between the two became apparent after further analysis of the powder and bulk tests. Powders processed by Catalytica, Inc. using the microfluidization process in Stage II seemed to be superior overall. Moreover, powder production capabilities of Catalytica Inc. far exceed those of NexTech's.

Utilizing the characterization resources and experience gained during the course of this project, LoTEC has instituted a new set of powder controls based on calcined particle density and median sizes. (A brief mention of the specifics of such controls has been provided.)

Discussion

(a) Small Scale Processing and Powder Evaluation in Stage II

As described in detail in the previous report, the vendors' powders were analyzed for: particle density; sintered density; surface area; particle size distribution; phase purity; dispersibility; flowability; and pressability. Catalytica's microfluidizer based precipitation processes resulted in low surface area powders after calcination mostly due to the reactivity of the precursors selected and the need for higher calcination temperatures. On the other hand, NexTech processes which were purely hydrothermally derived had higher surface areas as compared to both Catalytica and LoTEC processes. At the end of the evaluation process, the processes were ranked in the order of their merits jointly by LoTEC and the respective vendor. (Criteria used for ranking have been outlined in the following section.)

(b) Ranking of Processes in Stage II and Scale Up

Prior to the next level of scale up (to make 5 to 10 kg. quantities of samples), it was decided to select two processes of each vendor for making both BS-25 and CS-50 compositions. Ranking of the various processes was done using a broad-based set of criteria as listed in the order of importance on the following page (Figure 1). It will be noticeable that the order of importance of these criteria (and, in fact, the criteria itself) have changed somewhat from in the past. The new

order reflects a bias toward the slip casting process (and related wet forming processes) because it is LoTEC's primary component fabrication/manufacturing route.

Of the four processes selected prior to the next scale up phase of the project (two processes for each vendor), the acid-base neutralization process developed by LoTEC (and transmitted to the vendors for their adaptation) was the first choice of both vendors. As mentioned earlier, the chemistry involved in this processing route meant that the precursor costs were lowest and environmental concerns least for this process as compared to the other processes. The second process selected from both Catalytica and NexTech's various small scale processes was the one that yielded higher surface area powders but of lower purity, at higher costs, and with associated environmental concerns.

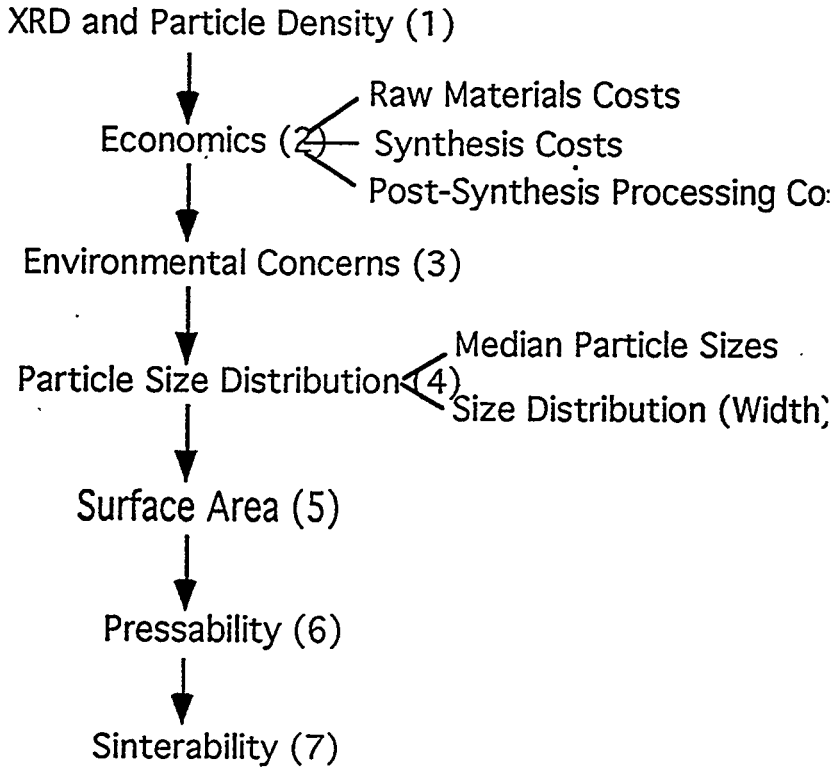

Figure 1. Listing of the criteria (in order of importance) used to rank vendor's processes.

(c) Evaluation of NZP Powders From Scaled-Up Processes

Powder Testing: As mentioned in the previous report, the precursors and approach used in the "LoTEC" route make this process the most environmentally friendly and economical of all

processes examined, thus far. Results of direct testing (except, micro analysis which is yet to be done) of all powder samples supplied by the vendors, suggested that the quality of powders resulting from the "LoTEC" wet process was more in line with that of LoTEC's solid-state processed powders. This can be noted from the property data for BS-25 and CS-50 powder samples of Catalytica and NexTech, respectively, shown in Tables 1 and 2. Also shown in the tables for comparison are LoTEC's standard powders (processed using solid-state synthesis).

XRD data, % deviation of measured particle density from theoretical for the particular composition, and dispersibility and flowability (in Tables 1 and 2) qualities of the powders served as valuable indicators for comparative analysis and drawing of other conclusions. From the tables, it is not only clear that the Catalytica BS-25 and CS-50 powders are superior overall but also the LoTEC recommended wet chemistry route resulted in more dispersible and flowable powders. In summary, it can also be stated that Catalytica powders produced using the LoTEC chemistry were most easily processable and acceptable from phase purity standards.

Bulk Sample Processing and Testing: Four batches each ~3 to 5 kg. of powders, two each for BS-25 and CS-50 corresponding to the primary synthesis route (chemistry aspects of which was recommended by LoTEC) and secondary synthesis route (developed entirely by the vendors), were obtained from the two vendors. Catalytica supplied LoTEC with 871-90-2 and 871-92-2 (BS-25s), and 871-91-2 and 871-93-2 (CS-50s). Both powders were amorphous in as received condition. Median sizes of the as-received powders are given in Table 3. Depending on their initial sizes, the powders were dry milled for a varying number of hours. All dry-milled powders were then calcined at 1050°C for 4 hrs. at the rate of 3°C/min. Median particle sizes after calcination were uniformly lower than before as can be seen from Table 3. The decrease in median sizes might be associated with renucleation of finer crystallites or breaking up of hydrated bonds of large agglomerates to form smaller ones during calcination.

NexTech's four powder batches were CZPII-10-6P and CZPII-10-13P (BS-25), and CZPII-10-9P and CZPII-10-15P (CS-50). All powders were dry milled for 18 to 24 hrs. prior to calcination (by NexTech) at 900°C. X-ray analysis of these powders showed that after 900°C calcining a common impurity phase (ZrP_2O_7) was present. Past experience, however, shows that this phase disappears if the powders are calcined at a slightly higher temperature or upon sintering. Table 4 shows the powder processing and testing/evaluation routines that were done in order to achieve a slurry of desired consistency.

All calcined powders were tested for particle density and XRD-based phase content. Once it was established that the required final phases had been achieved, slurries were made with the powders by wet ball milling with zirconia media. Based on past experience, the target median

particle size in the slurry was set to be between 1.75μm and 3.50μm in order for the slurry to have be appropriate dispersibility and viscosity characteristics. The extent of wet milling of each of these powders therefore varied (see Tables 3 and 4). In the case of NexTech powders CZPII-10-6P and CZPII-10-9P, the slurry viscosities were very high at 75w% solids loading. For these powders, the right slurry viscosity was achieved at 60 and 64w% solids loading, respectively.

These NZP powder slurries were used to pour tiles of 2"x 2" cross section. These tiles were dried, bisqued, and sintered at 1550°C for a certain length of time. Bulk samples (made from the vendor-supplied powders) of appropriate geometry and dimensions were tested (at HTML, Oak Ridge) for thermal properties such as thermal expansion, thermal diffusivity, and heat capacity, and mechanical properties (strength) as a function of temperature. All data was analyzed and compared with available standards for LoTEC BS-25 and CS-50 bulk samples. Sample geometries, test procedures, results, and inferences drawn from bulk testing will be described in detail in the forthcoming report.

Cost Analysis and Projected Costs: Analysis of the cost (shown in Table 5) of producing NZP (BS-25 and CS-50) powders as a function of the scale of production provided useful process information. In the course of scale up from Stage I, where few hundred grams of powders were synthesized, to Stage III, where a few hundred kilograms of powders will be produced, the powder costs will effectively be reduced by three orders of magnitude. This is true for both vendors' processes and powders. However, the approximate powder cost per kg. of NZP powder produced in Stage III will still be on the order of ~$80/kg in the case of both vendors. On scale up to ~10,000 kgs. powder per month, both vendors project powder costs to be between $10 and $20 per kg.

(d) Institution of Internal Controls at LoTEC

Acquisition of state-of-the-art powder testing equipment has enabled LoTEC perform extensive characterization of its in-house synthesized powders. For instance, particle density measurements made using ACCUPYC 1330 were correlated with X-ray phase analysis data in order to establish a range of acceptable densities: 3.48 to 3.55 gm/cc for BS-25 and 3.25 to 3.33 gm/cc for CS-50. Similarly, using particle size testing, the most appropriate range of median particle sizes of calcined BS-25 and CS-50 powders for quality slip preparation was determined to be between 4.5 and 6.5 μm.

Future Work :

Analysis of bulk testing data has been completed and a discussion of the results will be presented in the next report. Production of up to 100 kgs. of BS-25 and CS-50 powders under the Stage III subcontract with Catalytica is scheduled to begin after all protocols are established. Protocols will include specifications for phase purity, particle sizes of calcined powders, and stipulations for evaluation of consistency/reproducibility of the scaled up powder process. In addition, LoTEC is continuing optimization of its in-house powder synthesis process and institution of powder quality control procedures.

Status of milestones: Program on schedule.

Communications/Visits/Travel:

1 S. Y. Limaye traveled to: (i) Dearborn, Michigan to attend Annual Automotive Technology Development Contractors Coordination Meeting (AATD/CCM) in October 1996.

2. J. A. Curtis traveled to High Temperature Materials Laboratory of Oak Ridge National Lab. (ORNL) in Oak Ridge, TN, to conduct bulk property testing on samples prepared from Catalytica and NexTech powders between Nov.18th and Dec.21st, 1996.

3. R. Nageswaran traveled to Cocoa Beach, FL to make a presentation at the 21st Annual Cocoa Beach Conference and Exposition of the American Ceramic Society, held between Jan.12th and 16th, 1997.

Problems Encountered: None.

Publications:

1. J. A. Curtis, R. Nageswaran, S. Y. Limaye, and C. R. Hubbard, W. D. Porter, and S. T. Misture, "Characterization of Innovatively Synthesized Low-Cost NZP Powders "; Presented at the 21st Annual Cocoa Beach Conference and Exposition of the American Ceramic Society held at Cocoa Beach, FL, between 12th and 16th of Jan. 1997.

References: None.

Table 1. Key Results of Direct Testing of Catalytica (Stage II) Powders.

NZP Type	Lot No.	XRD Analysis	Particle Density (gm/cc)	% Deviation From Theoretical	Sintered Density (gm/cc)	Surface Area (m^2/gm)	Dispersibility (1) & Flowability (2)
BS-25	871-90-2*	Phase Pure	3.5242	+ 0.11	2.4255	3.18	1: Good; 2: Fair
BS-25	871-92-2	Small amount of $BaZrP_2O_8$	3.4345	- 2.43	2.3964	3.94	1: Fair; 2: Fair
CS-50	871-91-2*	Trace of ZrP_2O_7	3.2838	- 0.49	2.2883	1.54	1: Good; 2: Good
CS-50	871-93-2	Phase Pure	3.3054	+ 0.16	2.5377	4.06	1: Fair; 2: Good
BS-25	LoTEC #1£	Trace of ZrP_2O_7 and $BaZrP_2O_8$	3.5350	+ 0.43	2.3126	1.70	1: Good; 2: Fair
CS-50	LoTEC #2£	Trace of ZrP_2O_7	3.2676	- 0.98	2.4350	0.88	1: Good; 2: Fair

* processed using the LoTEC-recommended wet chemistry

£ typical LoTEC powder processed using the solid state reaction process

Table 2. Key Results of Direct Testing of NexTech (Stage II) Powders.

NZP Type	Lot No.	XRD Analysis	Particle Density (gm/cc)	% Deviation From Theoretical	Sintered Density (gm/cc)	Surface Area (m^2/gm)	Dispersibility (1) & Flowability (2)
BS-25	CZPII-10-6P	Traces of ZrP_2O_7 and $BaZrP_2O_8$	3.4775	- 1.21	2.2993	16.93	1: Poor; 2: Poor
BS-25	CZPII-10-13P*	Trace of $BaZrP_2O_8$	3.5147	- 0.15	3.1030	6.30	1: Good; 2: Fair
CS-50	CZPII-10-9P	Small amount of ZrP_2O_7	3.1753	- 3.78	2.3622	15.89	1: Poor; 2: Good
CS-50	CZPII-10-15P*	Small amount of ZrP_2O_7	3.1903	- 3.32	2.6859	0.52	1: Good; 2: Good
BS-25	LoTEC #1[£]	Trace of ZrP_2O_7 and $BaZrP_2O_8$	3.5350	+ 0.43	2.3126	1.70	1: Good; 2: Fair
CS-50	LoTEC #2[£]	Trace of ZrP_2O_7	3.2676	- 0.98	2.4350	0.88	1: Good; 2: Fair

* processed using the LoTEC-recommended wet chemistry

£ typical LoTEC powder processed using the solid state reaction process

Table 3. Dry and Wet Processing of Catalytica Powders to Obtain Slurries for Slip Casting.

Composition	Catalytica Lot No.	Particle Size as Received (μm)	Dry Milling Time[1] (hrs)	Size after Dry Milling (μm)	Median Size after Calcination[2] (μm)	Solids Content in Wet Milling (%)	Wet Milling Time[3] (hrs)	Median Size after Wet Milling (μm)
BS-25	871-90-2	7.16	4	5.34	4.56	75	8	2.92
CS-50	871-91-2	7.06	4	5.63	4.62	75	8	3.70
BS-25	871-92-2	15.54	12	11.27	8.20	70	12	2.29
CS-50	871-93-2	14.74	12	12.70	8.83	70	12	1.75

[1] 1:6 :: Solids: Media Ratio.

[2] Calcined at 1050°C.

[3] 1:4 Solids: Media Ratio.

Table 4. Dry and Wet Processing of NexTech Powders to Obtain Slurries for Slip Casting.

Composition	NexTech Lot No.	Particle Size as Received (μm)	Dry Milling Time[1] (hrs)	Size after Dry Milling (μm)	Solids Content in Wet Milling[2] (%)	Wet Milling Time (hrs)	Size after Wet Milling (μm)	Surface Area (m^2/g)
BS-25	CZPII-10-6P	10.00	0	-	60	20	1.93	16.89
CS-50	CZPII-10-9P	8.44	0	-	64	12	2.55	-
BS-25	CZPII-10-13P	15.00	18	10	75	12	3.22	4.75
CS-50	CZPII-10-15P	24.72	24	11	75[3]	11	2.90	-

[1] 1:6 :: Solids: Media Ratio.

[2] 1:4 :: Solids: Media Ratio, except CZPII-10-15P(1:6 Solids: Media Ratio)..

[3] 3 drops of defoamer added.

Table 5. NZP powder cost ($ per kg.) as a function of the scale of production

Vendor	Stage I (100 gm.)	Stage II (1 kg.)	Stage III (100 kgs.)	Future (10,000 kgs.)
Catalytica	$25,000	$1,500	$84	$10 to 20
NexTech	$24,300	$1,600	$83	$10 to 20

ADVANCED MANUFACTURING TECHNOLOGY

DEVELOPMENT OF ADVANCED CERAMIC MANUFACTURING TECHNOLOGY

Subcontract No.86X-SP234C

C.Burk, T.P. Leo, L.D. Lynch, B.J. McEntire - SGNICC, Norton Advanced Ceramics
Y. Kalish, R. Begin - Detroit Diesel Corporation
C. Bida, M. Hauptman, L.E. Mains - Deco Grand, Inc.
M. Tricard, D. Graham, J. Picone - Norton Compay, World Grinding Technology Center
J. Kellogg- Centorr/Vacuum Industries
V.K. Pujari, W.T. Collins - SGNICC, Northboro R&D Center
P. Parrish - BDM Federal, Inc.
T. Zahrah, S. Hollo - MATSYS, Inc.
A.E. Mascarin - IBIS Associates, Inc.
D. Wittmer - Wittmer Consultants

Report Prepared by
Vimal Pujari

Saint-Gobain/Norton Industrial Ceramics Corporation
Northboro Research and Development Center
Goddard Road
Northboro, MA 01532

Semi-annual Technical Progress Report
October 1996 - March 1997

Objective/Scope

The objectives of this program are to design, develop and demonstrate advanced manufacturing technology for the production of ceramic valves. A production manufacturing process for a ceramic exhaust valve for DDC's Series 149 diesel engine is being developed under this program. Specific objectives are: (1) To reduce manufacturing cost by at least an order of magnitude over current levels; (2) To develop and demonstrate process capability values (C_{pk}) of 0.7 or less for all critical component attributes; and (3) To validate performance, durability, and reliability of this ceramic valve in rig and engine testing.

Technical Highlights

Task 1 - Component Design and Specification

This task has been completed.

Task 2. Component Manufacturing Technology Development

2a) Environmental Safety and Health

This task has been completed.

2b) Process Cost Modeling

This task has been completed.

2c) Process Control

i.) Milling and Spray Drying Process Control

This task has been completed.

ii) Continuous Sintering

This task has been completed.

iii) Machining

During this reporting period, finish machined valves from Deco Technologies, Norton's World Grinding Technology Center (WGTC) and Chand Kare Technical Cearmics (Chand) were inspected for dimensional accuracy and subsequently proof (pull) tested as per DDC's specifications.

a) Dimensional Measurement

All key dimensional features of the machined Series 149 valve were inspected at the Northboro Research and Development Center's (NRDC) machining laboratory using state-of-the-art measurement devices such as Rank profilometer and Federal roundness equipment. Key valve dimensions measured included stem diameter and roundness, lock groove diameter and taper, and seat angle. Measured dimensions were compared with the valve print to establish the accuracy of the machining procedures. Based upon this detailed inspection, WGTC and Chand valves were found to be dimensionally superior to Deco valves. Furthermore, WGTC valves showed greater dimensional accuracy as compared to Chand machined valves.

b) Pull Test

Valve pull tests were performed using a specially designed fixture on the Instron Machine and the appropriate keepers (material and design) received from DDC. All the valves were proof tested up to a predetermined applied pull load as per DDC's specifications. Subsequently, 10 valves from each machining procedure were tested to failure. Failure load and its location on the valve were documented for each valve. Average failure stress for the three machining procedures are compared in Fig. 1. Once again, WGTC and Chand valves were found to be superior. With the exception of a few, all other valves failed at the keeper groove location, irrespective of the machining procedure employed.

Overall, 2 out of 27 WGTC valves, one out of 10 Chand valves, and 6 out of 19 Deco valves failed the proof test.

Based upon the dimensional measurement and proof testing, both the WGTC and Chand machining procedures are found to be satisfactory and acceptable for further evaluation. Currently, 30 valves are being finish machined at WGTC for the rig and engine testing.

2d) Intelligent Process Control

The development and demonstration of the Intelligent Control System (ICS) for milling and spray drying unit operations has been successfully completed at NRDC (Northboro Research and Development Center). As reported in Task 4b) the transfer of the ICS technology to the large spray dryer at the manufacturing site is currently underway.

Task 3 - Inspection and Testing

Second five hundred hour test has been cmpleted. It was run with 30° seat ceramic valves using a split set of Norton machined keepers and Milwaukee Wire soft keeps. At the end of the test, all cylinder heads were removed from the engine and disassembled. All ceramic valves are in excellent condition with no signs of wear on the seat or in the keeper groove area. Some soft deposits were found on the combustion faces of the valves, as normally expected. All keepers are in good shape, with some wear marks corresponding to the upper edges of the keeper groove on the valves. Wear marks are very similar between soft and machined keepers.

We now have fourteen ceramic valves with 1000 hours of engine testing and thrity valves with 500 hours of engine testing.

Based on the test results, the final valve design was arrived at which incorporate 30° seat angle and a keeper groove with the chamfer on the bottom side and a radius on the top side. Soft keepers will be used with ceramic valves.

Task 4 - Process Demonstration

4a) This task has been completed.

4b) Final Demonstration

Fabrication of the valves for the final demonstration set is progressing as per schedule. A total of 320 finish machined NT551 valves will now be delivered to DDC for fixture and durability testing. So far, 445 valve blanks have been densified and awaiting the final machining. Extra valves have been fabricated in the case of potential losses during machining and/or proof testing. Mechanical properties established from co-processed qualification tiles and speciments cut from densified valves are summarized in Table .1 along with the Weibull plot. These properties meet or exceed DDC's material specifications for valves.

Inherent to the final demonstration effort is the establishment of a production viable process capable of large scale fabrication of ceramic valves. Consequently, all demonstration set valves are being processed using the pre-established S.O.P. (Standard Operating Procedures) for powder milling, spray drying and densification unit operations. The milling procedure entails the use of a low cost powder processed through an efficient and reliable closed loop aqueous comminution methodology. Key to the spray drying unit operation is a high yield process monitored and controlled through the use of an Intelligent Control System (ICS). The ICS System successfully demonstrated in NRDC (Northboro Research and Development Center) spray dryer is currently being transferred to a large scale spray dryer at the East Granby production facility with the help of Matsys Corporation. Some modifications in the ICS hardware and software are required to render it compatible with the control electronics of the large spray dryer.

The NT551 rods and tiles to be delivered to ORNL for Life Prediction Methodology development are also currently being processed at the East Granby facility.

Status of Milestones

Milestones No's 1-5 are complete. Milestones No's 6 through 8 are on schedule.

Communications/Visits/Travel

10/15/96 - V.K. Pujari visited Norton Company's World Grinding Technology Center (WGTC) to review progress toward valve machining.

10/31/96 - Bob Schultz (DOE), Ray Johnson (ORNL), Arvid Pasto (ORNL), Guy Leedy (DOE), Yuri Kalish (DDC), and Vimal K. Pujari (NAC) met in Dearborne, MI for an informal, semi-annual program review.

10/28-11/1/96 - V.K. Pujari attended annual Customers Coordination Meeting and presented the technical progress report.

12/15/96 - Meeting was held at NRDC with Tom Payne of Chand Technical Ceramics to review measurements performed at NRDC on Chand's valves.

1/18/97 - V.K. Pujari and Larry Lynch of NAC visited Norton's WGTC and met with Dr. Subramanian and John Hagen to review and finalize their machining procedure.

2/20/97 - V.K. Pujari visited ORNL for a semi-annual review with Dr. Arvid Pasto, Technical monitor and Dr. Ray Johnson, Program Manager.

Problems Encountered

None.

Summary of Valve Proof Test Failures
(Statistics are for all failures in a batch)

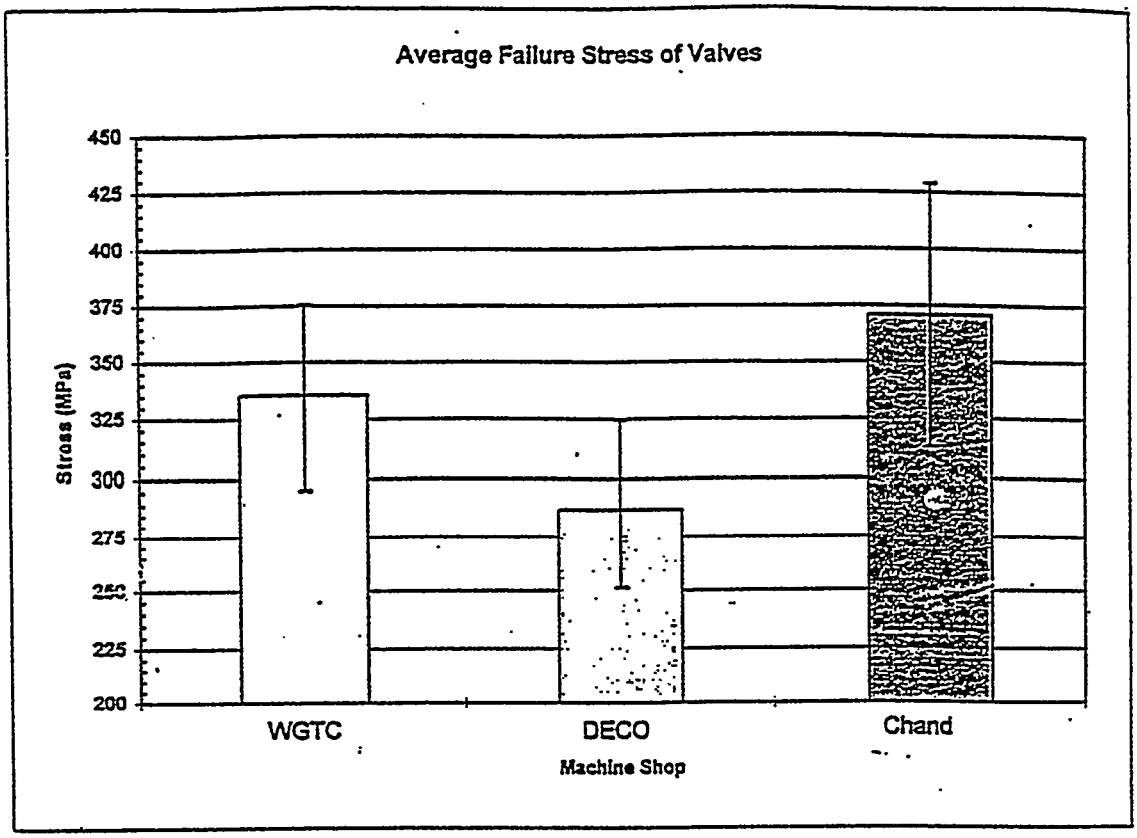

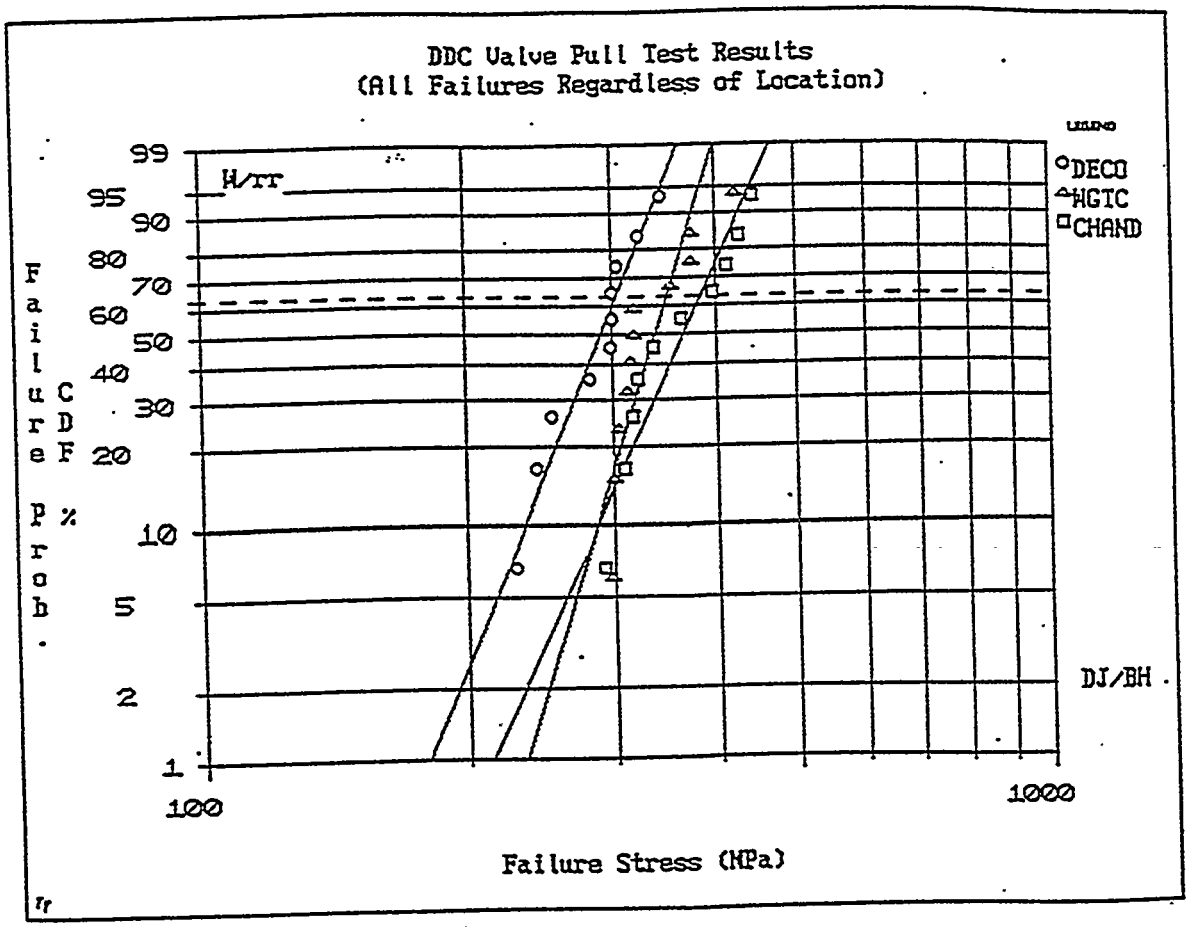

Fig. 1
Proof Testing of Machined Valves

NT 551 PHYSICAL AND MECHANICAL PROPERTIES

PROPERTIES	VALUES
Density (g/cc)	3.285 - 3.290
22°C Elastic Modulus (GPa)	302 - 310
22°C Shear Modulus (GPa)	118 - 120
22°C Poisson's Ratio	.275 - .280
22°C Hardness (GPa) at 10 kg. load	13.4 - 14.2
Porosity	< 20 μm
22°C Mechanical Properties	
⇒ Flexural Strength (MPa)	966
⇒ Characteristics Strength (MPa)	985
⇒ Weibull Modulus	20 - 30
⇒ Fracture Toughness (MPa√m)	7.01
850°C Mechanical Properties	
⇒ Flexural Strength (MPa)	932
⇒ Weibull Modulus	> 20

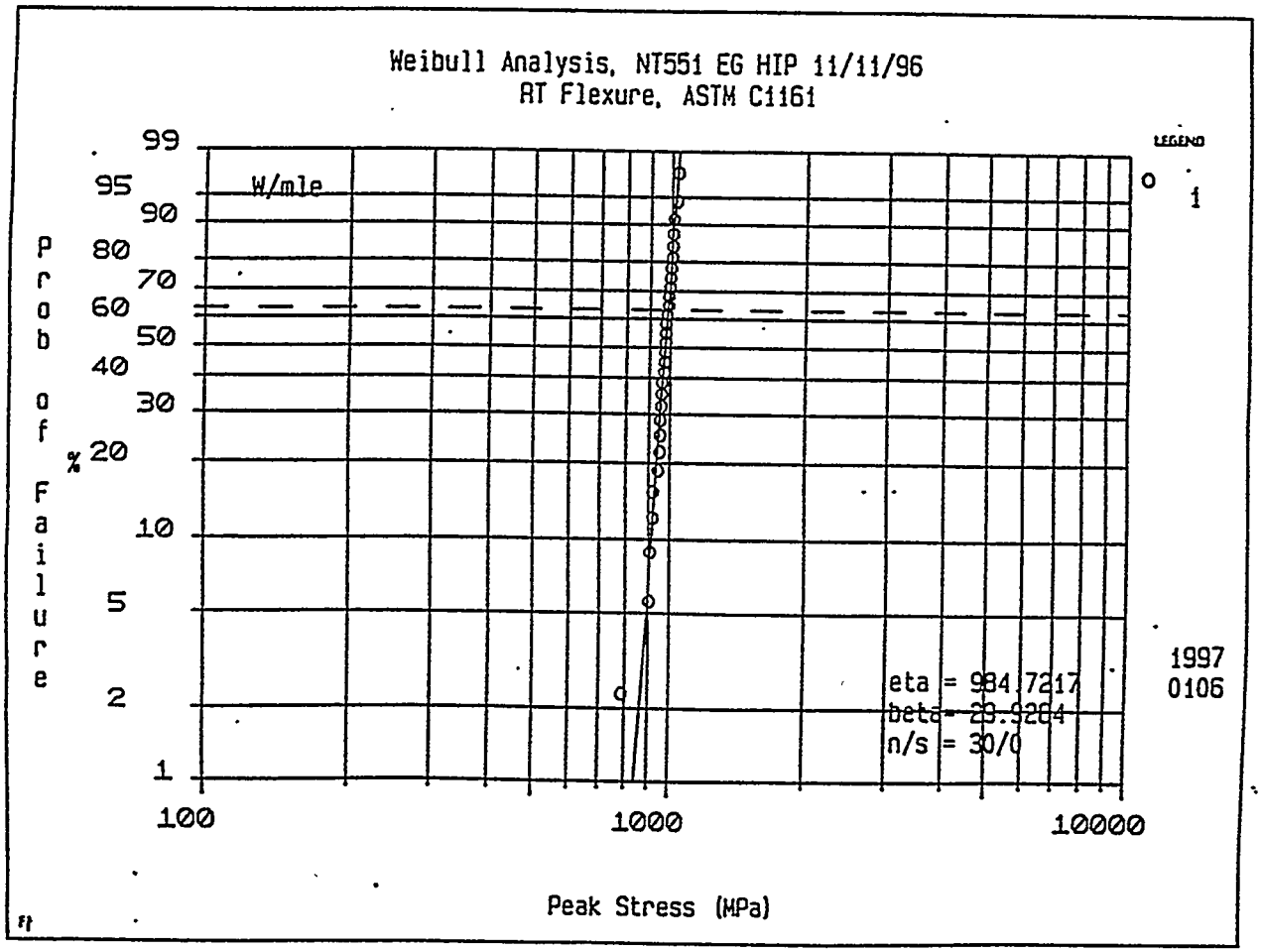

Table 1

W.B.S. Element 1.5.0.0

COST-EFFECTIVE CERAMIC MACHINING

P. J. Blau and E. S. Zanoria
Oak Ridge National Laboratory

Objective/Scope

The objective of this effort is to develop, in conjunction with U. S. industry, advanced technologies and the associated scientific and economic concepts necessary to reduce the costs associated with the machining of structural ceramics; especially, as related to the use of these materials in energy-efficient, low-emissions transportation systems. This effort consists of subcontracts to industry and in-house research at Oak Ridge National Laboratory, Argonne National Laboratory, and the National Institute of Standards and Technology. Progress reports for other than the ORNL in-house research portion of this work may be found elsewhere in this publication. The four subtasks in this effort are:

1. Technology Assessment and Future Needs
2. Advanced Machining Methods Development
3. Ceramic Machinability and Related Performance
4. Structure and Surface Quality of Machined Ceramics

ORNL in-house activities are aimed at two technical areas: (1) investigating the effects of machining practices on the durability of ceramics for valve and valve seat applications and (2) understanding and characterizing the detailed nature of machining-induced surface and sub-surface damage and their evolution in advanced ceramic materials using a range of analytical tools. The latter includes such methods as non-contact surface profiling, atomic force microscopy of ground surfaces, and scanning acoustic microscopy to detect subsurface flaws.

Technical Highlights

a. Cost-Effective Ceramic Machining Effort Featured in *Abrasives Magazine*. The CECM effort was featured in the February/March issue of *Abrasives Magazine*. The article describes the history and accomplishments of CECM since 1991. Photographs of researchers at Norton Company and Eaton Corporation accompany the article.

b. Multi-technique Analysis of Ground Ceramic Surfaces is Concluding. Two years ago, a comprehensive project was initiated to characterize the surface and subsurface features of the ground ceramic specimens using multiple techniques. The material selected for this work was GS-44 silicon nitride produced by Allied Signal Ceramic Components, Torrance CA. Two sets of surface grinding conditions were specially selected, based on previous IEA data, in order to provide specimens having relatively low and high flexural strengths.

A meeting among participants in the characterization was held on March 11, 1997 at ORNL to review all the data, and to assess which methods showed the most promise for identifying the causes for strength and performance differences between the two machining conditions. Residual stress measurements by grazing incidence x-ray diffraction were completed, and results indicated that the coarsely-ground (low flexure strength) specimens had higher residual stresses than the finely-ground specimens. These data were key to understanding the impact wear and sliding

wear results obtained on the ground surfaces. Resistance of the GS-44 to both these forms of wear benefited from the higher compressive stresses below the coarsely-ground surfaces.

J. Reintjes and his coworkers at the Naval Research Laboratory, are new volunteer participants on the surface analysis project team. Using GS-44 specimens we provided, an optical gating technique, developed by them, appears to show promise for detecting differences in the depth of subsurface damage between the two standard grinding conditions. NRL has agreed to participate in the preparation of the final report on surface damage studies, and this work will be a valuable addition to the report.

Due to a need to move the microscope to a new location, the scanning acoustic microscopy work remains to be completed. However, it is expected that the work will be finished in time to include the results in the final report, which Elmer Zanoria of ORNL is compiling for submission to an archival journal.

c. Project on Machine Stiffness Effects on Ceramic Grinding Concludes. The University of Connecticut - Storrs is completing a study of the effects of grinding machine stiffness on the quality of silicon nitride surfaces. UCONN developed special specimen fixturing to permit adjustments of the composite spindle/fixture/wheel stiffness to be made over a range which is characteristic of grinding machines. Both vitrified-bonded diamond wheels and Japanese cast iron fiber-bonded (CIFB) diamond wheels were used in these experiments. Special electrolytic in process dressing (ELID) methods were used on the CIFB wheel. ELID proved more effective in keeping the wheel dressed and running at low normal force than the conventional methods of dressing on the vitrified-bonded diamond wheel. In addition, stiffness effects on grinding were more clearly observed with the CIFB wheel under ELID conditions because the wheel dressing variability did not overcome the effects of machine stiffness to the degree that they did with the vitrified-bond wheel. A final report is being prepared.

d ORNL In-house Concluding Research on Repeated Impact. Extensive studies of the effects of tangential slip on the repetitive impact behavior of variously-ground silicon nitride surfaces are being completed. In summary, the effect of incidence angle on the rate of impact wear were different for ground and for polished silicon nitride surfaces. For ground surfaces, impact wear seemed to reach a maximum at impact incidence angles of approximately 60 - 75 degrees. For polished surfaces, the impact wear rate was minimum at 60-75 degree incidence angles. Similar effects were observed on both GS-44 and NT-154. The differences in wear behavior between polished and ground surfaces is explained in terms of the role of wear particles which form a protective layer to cushion the surfaces of the polished specimens to a greater degree than the ground surfaces.

Two papers which describe the causes of the repeated impact behavior of ground silicon nitride have been prepared and submitted for publication. One has been submitted to the *Journal of the American Ceramic Society* and the other to the International Conference on Wear of Materials, whose publisher is the archival journal *Wear*.

e. Ph.D. to be Awarded for Research on Ceramic Grinding. A Ph.D. degree in Mechanical Engineering will be awarded in May 1997 by the University of Massachusetts to Tae Wook Hwang, a graduate student of Prof. Steven Malkin. The title of his dissertation is "Grinding Energy and Mechanisms for Ceramics" and is largely the result of research conducted in conjunction with the CECM subcontract on "High-Speed, Low Damage Grinding." The research involves detailed investigations and modeling of the partition of energy and the mechanics of material removal during ceramic grinding, particularly high-speed grinding. A copy of Hwang's 205 page dissertation was presented to ORNL by Prof. Malkin during his recent visit.

Future Plans

a. Surface Quality Technique Evaluation. After scanning acoustic microscopy data have been obtained on the ground GS-44 specimens, we will include it in the comprehensive final report which compares the findings of all the surface analysis techniques used.

a. New project on Valve Guide Durability. Work is beginning on a new project to investigate the friction and durability of diesel engine valve guide materials machined from silicon nitride and other candidate materials for that application. Engineering and fabrication work is underway to reconfigure an existing wear testing machine at ORNL to hold diesel engine valve stems and candidate valve guide materials. Test specimen materials have already been received from Caterpillar Technical Center, Mossville, Illinois, and a new CRADA with that company is in the process of being established to work cooperatively in that area.

Status of Milestones

On schedule.

Communications/Visitors/Travel

Dr. Joseph Kovach and Michael Laurich, Eaton Corporation, and Prof. Steven Malkin, University of Massachusetts, visited ORNL on 3/19/97 to review progress on their subcontracts. Dr. Kovach and Prof. Malkin discussed work on High-Speed, Low Damage Grinding: Phase II. Dr. Kovach also discussed progress on the "Next Generation High-Speed Grinding Spindle" subcontract, and Prof. Malkin described the newly-initiated project to develop a "Smart Grinding Wheel" which can transmit grinding condition information to a remote computer system.

Dr. Bi Zhang and Dr. Z. Zhu, University of Connecticut - Storrs, visited ORNL on 3/24/97 to present a summary of the work performed on a subcontract dealing with the effects of machine stiffness on the quality of ground silicon nitride materials. A final report is in preparation.

Problems Encountered

We are still awaiting results of the scanning acoustic microscopy for inclusion into the final report on grinding damage in GS-44.

Publications/Presentations

1) P. J. Blau, "CECM Produces New Insights, Methods, Tools," *Ceramic Technology Newsletter*, Vol. 51 (Fall-Winter 1996).

2) C. Guo and R. H. Chand (1997) Cost-Effective Method for Determining the Grindability of Ceramics, Final Report, ORNL/SUB/93-SM036/1, 84 pp.

3) B. P. Bandyopadhyay (1997) Application of Electrolytic In-Process Dressing for High-Efficiency Grinding of Ceramic Parts, Research Activities: 1995-96, Final Report, ORNL/SUB/96-SV716/1, 72 pp.

4) P. J. Blau, R. L. Martin, and E. S. Zanoria, "Effects of Surface Grinding Conditions on the Reciprocating Friction and Wear Behavior of Silicon Nitride," accepted for the International Conference on Wear of Materials, San Diego, California, April 21-24, 1997.

5) E. S. Zanoria and P. J. Blau, "Effect of Incident Angle on the Impact Wear Behavior of

Silicon Nitride," submitted to the *Journal of the American Ceramic Society*.

6) P. J. Blau (1997) "Cost-Effective Ceramic Machining Effort Celebrates Five Years of Accomplishments," *Abrasives Magazine*, February/March, pp. pp. 10-12.

7) T. W. Hwang (1997) "Grinding Energy and Mechanisms for Ceramics," Ph.D. Dissertation, University of Massachusetts, Depart. of Mechanical and Industrial Engineering.

Innovative Grinding Wheel Design
for Cost-Effective Machining of Advanced Ceramics, Phase II

P. Kuo, R.H. Licht, S. Liu, M.R. Foley, D. Murphy, S. Ramanath (Norton Company)

Objective/Scope

The overall objectives of this Phase II program are (1) to improve or develop manufacturing technologies that enable the scale-up of Phase I, 203 mm (8 in.) diameter wheel to 356 mm to 406 mm (14 to 16 in.) diameter grinding wheels; and (2) to validate the performance of the new wheels in cylindrical grinding of advanced ceramics both in-house and at independent test sites.

In the completed Phase I, grinding test results of 76-mm (3-in.) and 203-mm (8-in.) diameter wheels indicated that a superior, next-generation grinding wheel for cylindrical grinding of ceramics had been developed[1]. Most production grinding of cylindrical ceramic parts is done on machines that use 305-mm (12-in.) to 406-mm (16-in.) diameter wheels. A Phase II program was initiated to scale-up the new Superabrasive wheel specification to these larger diameters, to make further wheel enhancements, and to perform independent validation tests.

Task 1 of Phase II will address wheel processing and wheel variable issues to achieve grinding action for the larger wheels similar to that successfully attained for the smaller Phase I wheels. Also in Task 1, Norton will develop or modify the wheel core for higher speed operation, and will determine the maximum operating speed for the new wheel system.

In Task 2, we plan to fabricate large test wheels, and to perform a cylindrical in-house grinding test at Norton's World Grinding Technology Center (WGTC) prior to independent validation testing. In Task 3, large experimental test wheels will be manufactured for independent validation at ceramic manufacturers. The following organizations are scheduled to perform validation tests: Norton Advanced Ceramics (NAC); Caterpillar Corporation; Chand Kare Technical Ceramics; and Eaton Manufacturing Technologies Center. Eaton plans to test the new wheel product under high speed grinding conditions. The NAC and WGTC wheel validation activity could complement their valve grinding development efforts currently in process under the DOE Advanced Ceramic Manufacturing Technology Program. Task 4 will include more extensive evaluation of ceramic surface integrity of ground ceramic specimens from the Tasks 2 and 3 grinding tests.

Technical Progress

Task 1: Process Scale-Up

A. Experimental Design and Definition -- Completed.

B. Strength Characterization and High Speed Core Development Completed.

C. Manufacture and Characterization of Large Wheels – Completed

The objectives of Task 1 were achieved. Scale-up of the Phase 1 wheel from 204-mm to 400-mm in diameter were successfully accomplished. Note that the original project objectives were to scale-up the wheel to a diameter of only 356 mm.

A total of seven 393-mm (15.5-in.) nominal diameter segmental wheels were made for preliminary grinding test at the Norton Company Abrasives World Grinding Technology Center (WGTC) under Task 2.

The automation of furnace cycle control was accomplished. The results showed that the product quality and consistency have been improved significantly as shown in Figures 1 and 2. Figure 1 represents the early pilot stage results and Figure 2 represents the current results from batch to batch. The entire segment manufacturing process can now be done in a production environment.

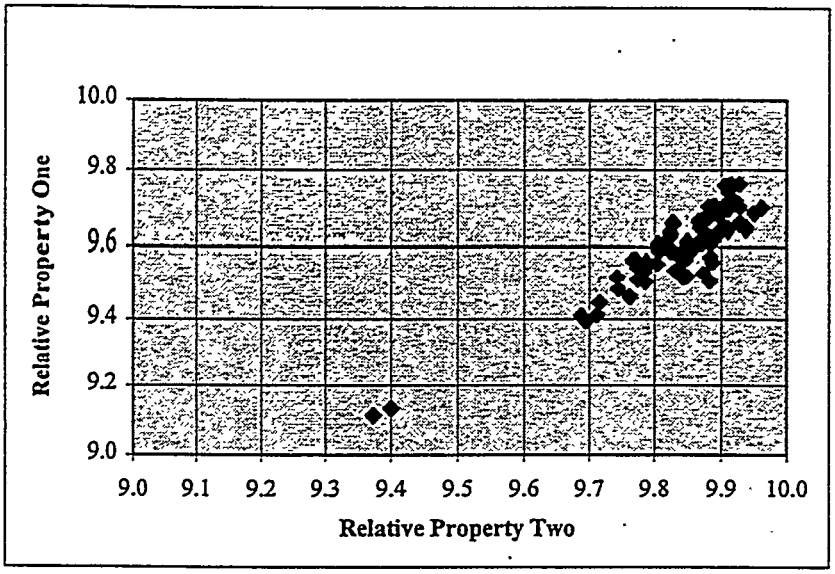

Figure 1. QC measurements on early pilot runs.

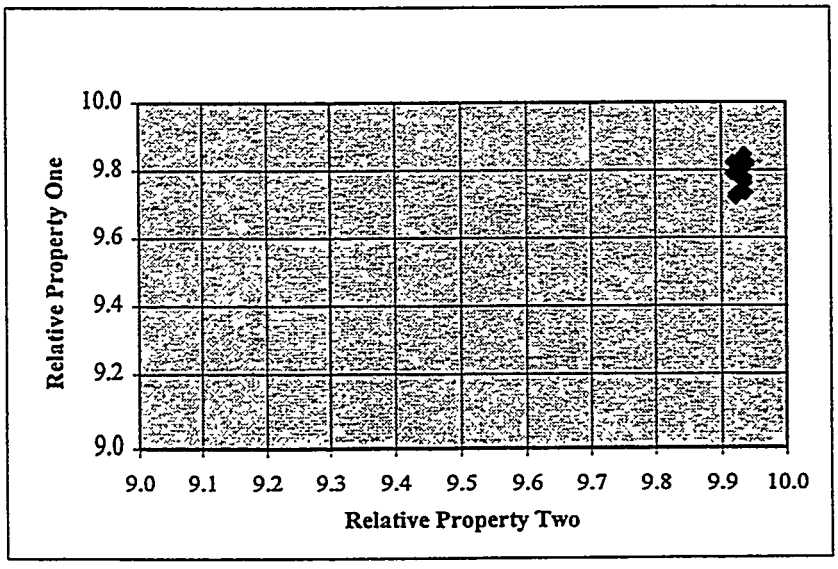

Figure 2. QC measurements on latest production runs

To characterize the maximum operating speed of this new type of wheel, full size wheels were purposely spun to destruction to determine the burst strength and rated maximum operating speed. Table 1 summarizes the burst test data for the 393-mm diameter experimental metal bonded wheels.

Table 1. Experimental Metal Bond Wheel Burst Strength Data

Wheel #	Wheel Diameter (in.)	Burst RPM	Burst speed (m/s)	Burst speed (sfpm)	Norton Rated MOS (m/s)
4	15.449	9950	204.4	40242	115.8
5	15.472	8990	185.0	36415	104.8
7	15.463	7820	160.8	31657	91.1
9	15.459	10790	221.8	43669	125.7

According to these data, the experimental ceramic grinding wheels of this design will qualify for an operational speed up to 90 m/s (17,717 surface feet/min.). Higher operational speeds can be easily achieved by some further modifications in fabrication processes and wheel designs.

For wheels # 5 and # 7, both had one segment that flew off the wheel cores. Examination of segment and core separation traces on both wheels showed that the failures occurred at the interface between segment and cement. Both wheels # 4 and # 9 had several segments that flew off the wheel cores. The separation traces as shown in Figure 3 indicated that the ultimate metal bond strength had been reached.

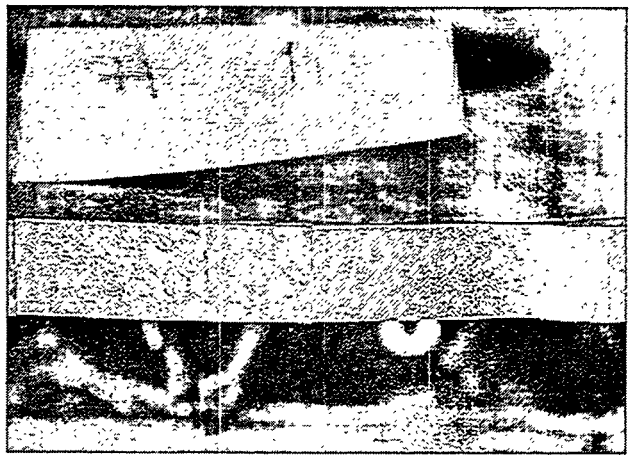

Figure 3. Fractured surface of metal bonded segments

Task 2: In-House Wheel Testing

A. Ceramic Specimen Preparation -- Completed.

The manufacture and batch characterization of over 200, NT551 silicon nitride rod specimens were completed. These specimens were used in the Task 2, in-house grinding test and were supplied to the machining subcontractors for the Task 3 validation tests.

Three separate powder batches were made of the NT551 silicon nitride powder composition. Each powder batch was characterized for surface area. Specimen rods and tiles

were cold isostatically pressed and fired to full density. The densified rod specimen dimensions are nominally 25 mm X 90 mm (1 in. x 3.5 in.). The initial densification run was done at the Northboro R&D Center and the remaining two furnace runs were done at Norton Advanced Ceramics (NAC) manufacturing plant in East Granby. We achieved theoretical density (3.29 g/cm^3) for all specimens in all three of the furnace runs. Table 2 summarizes the furnace batches and specimen quantities fabricated.

Table 2. NT551 Silicon Nitride Specimen Batch ID

Batch ID	Description	Quantity of Rod Specimens
N22	NRDC Furnace run	23
NAC1	1st NAC Furnace run	92
NAC2	2nd NAC Furnace run	96
Total		211

Rod samples from each of the three furnace batches were sliced, polished and tested to evaluate batch consistency. Table 3 is the Vickers Hardness and fracture toughness data of a rod from each batch. The fracture toughness technique used for these specimens was the Indentation Fracture Method (Anstis, et al.[2]).

Table 3. NT551 Batch Properties
Specimens Sliced and Polished From Rods, Load = 10 kg
Fracture Toughness Test Method: Indentation Fracture[2]

Batch	Specimens	Mean Vickers Hardness (GPa)	Std Dev	Mean K_{IC} MPa $m^{½}$	Std Dev
N22	5	13.29	0.05	4.47	0.18
NAC1	5	13.08	0.10	4.63	0.11
NAC2	5	13.17	0.18	4.52	0.12

Room temperature flexural strength and indentation strength fracture toughness were determined from standard ASTM C1161-B specimens machined from tiles. The tiles were from the two large NAC batches. Table 4 contains the strength and toughness data from these two tiles. The differences between fracture toughness data in Tables 3 and 4 are expected differences due to the test method.

The rod specimens for this program, as illustrated in Tables 3 and 4, show good batch to batch consistency and are typical for NT551 silicon nitride. Typical properties of NT551 silicon nitride from NAC's Advanced Ceramic Manufacturing Technology program are given in Table 5.

Table 4. NT551 Room Temperature Flexural Strength and Fracture Toughness
Test Method: ASTM C1161-B Specimens Cut From Tiles

Room Temperature Flexural Strength ASTM C1161-B			Fracture Toughness Indentation Strength, Load = 10 kg		
Sample	Batch NAC1 σ_f (MPa)	Batch NAC2 σ_f (MPa)	Sample	Batch NAC1 K_{IC} (MPa $m^{1/2}$)	Batch NAC2 K_{IC} (MPa $m^{1/2}$)
1	1092.0	786.4	1	6.45	6.58
2	840.4	934.7	2	6.37	6.70
3	1104.4	970.9			
4	982.0	1035.9			
5	930.5	919.8			
Mean	989.8	929.5		6.41	6.64
Std Dev	99.478	82.017		0.04	0.06

Table 5. Typical Properties of Norton Advanced Ceramics NT551 Silicon Nitride

Properties	NT551 Sinter/HIP
Young's modulus GPa)	310
Hardness* Vickers (GPa)	13.4
Flexural strength RT (MPa) 850°C (MPa)	 890-970 850
Fracture toughness* (Indentation Strength Method) (MPa·$m^{1/2}$)	6.5-6.9
Density (g/cm^3)	3.29

Task 2.B. Preliminary Grinding Tests in WGTC -- Completed.

The extensive in-house grinding test of the experimental metal bond vs. standard wheels was completed. Grinding was done on NT551 Si_3N_4 rods using a Studer CNC OD/ID grinder at Norton's World Grinding Technology Center (WGTC). Figure 4 shows the grinding test arrangement and the new metal bond wheel's capability to plunge grind a Si_3N_4 rod of 25.4-mm diameter into a fine needle form (approx. 1.1 mm in diameter). Figure 5 shows the various specimen produced by the metal bond wheel during Task 2 performance evaluation.

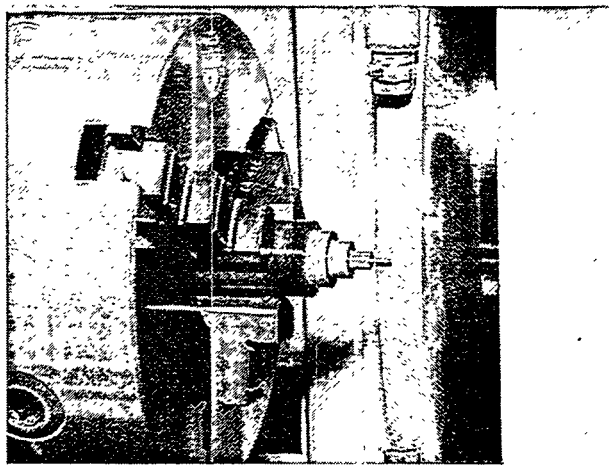

Figure 4. In-House Test Set Up

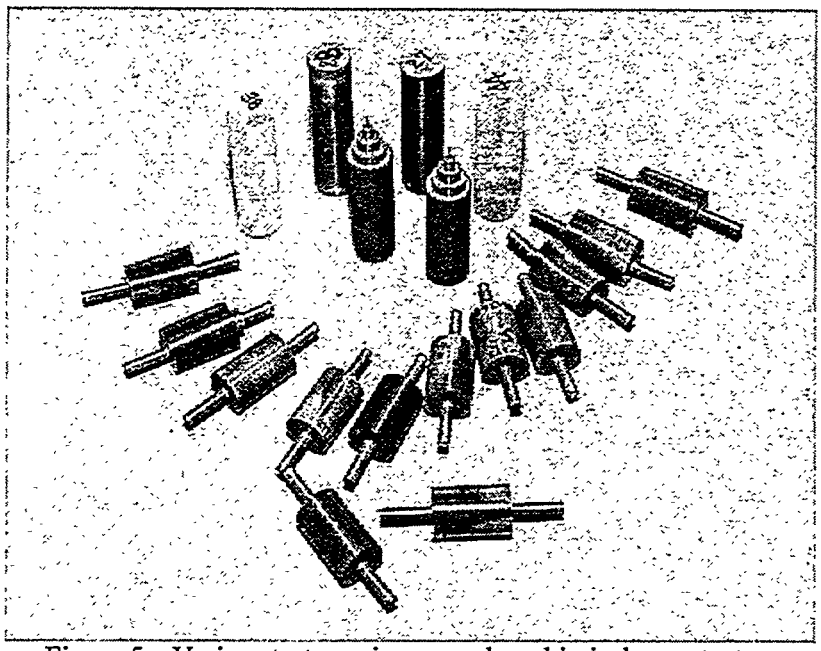

Figure 5. Various test specimen produced in in-house tests.

In-House Performance Evaluation:

A total of three, 393-mm diameter experimental metal bonded segmental wheels (#4, #5 and #6) were tested. The #6 wheel was the target grade while the other wheels were with slight grade variations. Most of the wheel tests were done on #6 as presented below. Testing was done at three speeds: 32 m/s (6252 sfpm), 56 m/s (11,000 sfpm), and 80 m/s (15,750 sfpm). One vitrified bonded diamond wheel and one resin bonded diamond wheel were included in the test matrix for comparison. The resin wheel was tested at all three speeds. The vitrified wheel was tested at 32 m/s (6252 sfpm) only. The original statement of work did not include the vitrified diamond wheel in the Task 2 evaluation.

Over one thousand plunge grinds of 6.35 mm (0.25 inch) wide and 6.35 mm (0.25 inch) deep were performed. The following describes the general testing conditions.

General Grinding Test Conditions:

Machine:	Studer S40 CNC	
Wheel Specifications:	AD320-75MXL1994	(experimental metal bond)
	SD320-R4BX619C	(resin bond)
	SD320-N6V10	(vitrified bond)
Wheel Speed:	32, 56, and 80 m/s (6252, 11000, and 15750 sfpm)	
Coolant:	Inversol 22 @60% oil and 40% water	
Coolant Pressure:	270 psi	
Material Removal Rate:	Vary, starting at 3.2 $mm^3/s/mm$ (0.3 $in^3/min/in$)	
Work Material:	NT551 Si_3N_4, 25.4 mm (1 in.) diameter X 88.9 mm (3.5 in.) long	
Work Speed:	0.21 m/s (42 sfpm), constant	
Work Starting diameter:	25.4 mm (1 inch)	
Work finish diameter:	6.35 mm (0.25 inch)	

The final truing and dressing conditions established for the metal bonded wheels were as follows:

Truing Operation:

Wheel:	5SG46IVS
Wheel Size	152 mm diameter (6 inches)
Wheel Speed:	3000 rpm; at +0.8 ratio relative to the grinding wheel
Lead:	0.015 in.
Compensation:	0.0002 in.

Dressing Operation:

Stick:	37C220H-KV (SiC)
Mode:	Hand Stick Dressing

Tests were performed in a cylindrical OD plunge mode in grinding NT551 silicon nitride rods. To preserve the best stiffness of work material during grinding, the 88.9 mm (3.5 in.) samples were held in a chuck with approximately 31 mm (1-1/4 in.) exposed for grinding. Each set of plunge grind tests started from the far end of each rod. First, the wheel made a 6.35 mm (1/4 in.) wide and 3.18 mm (1/8 in.) radial depth of plunge to complete one test. The work rpm was then re-adjusted to compensate for the loss of work speed due to reduced work diameter. Two more similar plunges were performed at the same location to reduce the work diameter from 25.4 mm (1 in.) to 6.35 mm (1/4 in.). The wheel was then laterally moved 6.35 mm (1/4 in.) closer to the chuck to perform next three plunges. Four lateral movements were performed on the same side of a sample to complete the twelve plunges on one end of a sample. The sample was then reversed to expose the other end for another twelve grounds. A total of 24 plunge grinds was done on each sample.

Grinding Performance at 32 m/s (6,252 sfpm) peripheral speed – The initial comparison tests for the metal, resin, and vitrified wheels were conducted at 32 m/s peripheral speed at three material removal rates (MRR') from approximately 3.2 $mm^3/s/mm$ (0.3 $in^3/min/in$) to approximately 10.8 $mm^3/s/mm$ (1.0 $in^3/min/in$). Figure 6 shows the performance differences, as depicted by G-ratios, among the three different types of wheels after twelve plunge grinds. G-ratio is the unit-less ratio of volume material removed over volume of wheel wear. The data showed that the N grade vitrified wheel had better G ratios than the R grade resin wheel at the higher material removal rates. The experimental metal bonded wheel (IGW #6) was far superior to both of the resin wheel and vitrified wheel at all material removal rates. Since the metal bonded wheel was extremely durable, there was no measurable wheel wear after twelve grinds. In Figure 6, the G-ratio is an estimate for the metal bond at all MRR's and an estimate for the low MRR resin wheel test, because wheel wear was not measurable. Another important observation is that the metal bond wheel is a 75 diamond concentration wheel, while the resin and vitrified wheels are 100 concentration and 150 concentration, respectively, resulting in additional cost-effectiveness of the experimental wheel.

Figure 7 shows the difference in grinding power consumption at various material removal rates for the three different wheel types. The resin wheel had a slightly lower power consumption than the other two wheels; however, the experimental metal bonded wheel and vitrified wheel had comparable power consumption at the low speed.

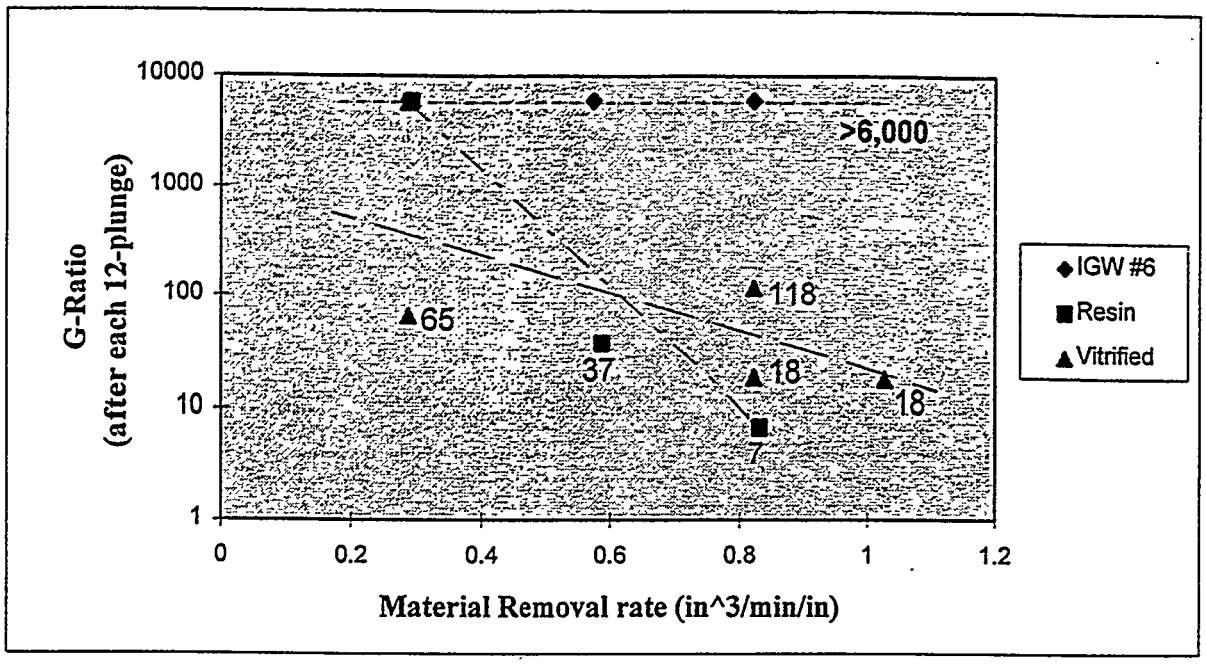

Figure 6. G-Ratio vs. material removal rate at 32 m/s grinding speed. IGW#6 is the experimental metal bond wheel.

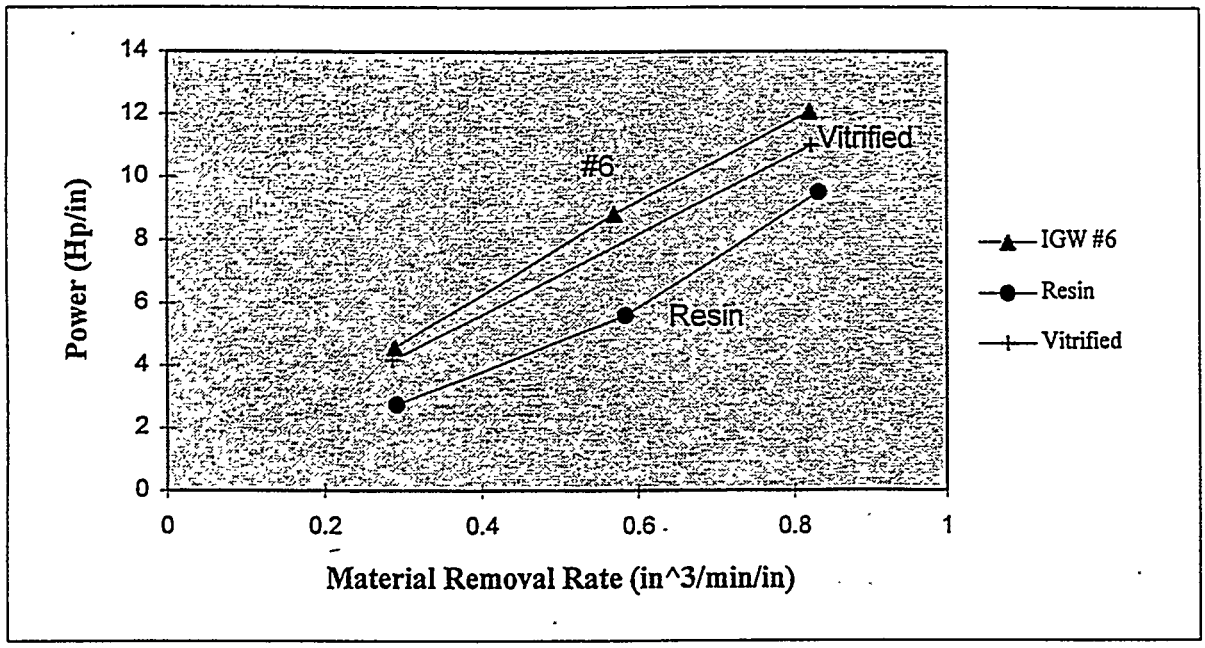

Figure 7. Power vs. MRR' of different wheels at 32 m/s grinding speed.

Figures 8 and 9 show the preliminary surface finish (Ra) and waviness (Wt) data measured on samples ground by the three wheels at the low test speed. The waviness value, Wt, is the maximum peak to valley height of the waviness profile. All surface finish data reported below were on surfaces created by cylindrical plunge grinding without spark-out. These surfaces are normally rougher than traverse grinding.

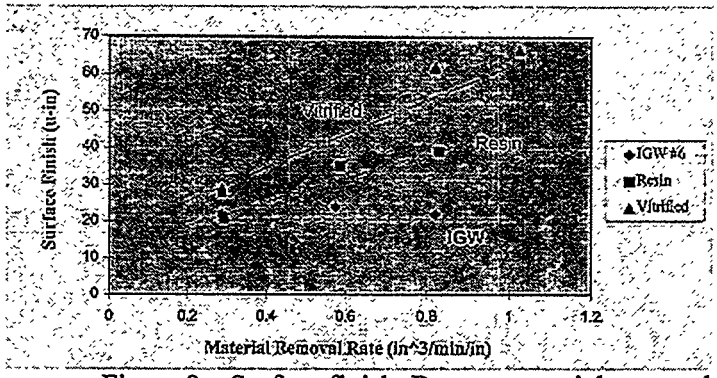

Figure 8. Surface finish, Ra, vs. material removal rate at 32 m/s grinding speed.

In general, the average surface finish and waviness of samples plunge ground by the new metal bonded wheel were in the order of 0.50 μm Ra and less than 1.0 μm Wt. The surface finish and waviness were worse for specimens ground by the resin and vitrified wheels. In addition, the roughness and waviness on the samples ground by the experimental metal bonded wheel maintained at a constant level at all material removal rates up to 10.8 $mm^3/s/mm$ (1.0 $in^3/min/in$) during this series of tests. In contrast, the samples ground by the resin and vitrified wheels showed constant deterioration in surface finish and waviness at higher material removal rates. Specimens were sent to the Northboro R&D Center for further contact, and non-contact profilomentry, as part of Task 4.

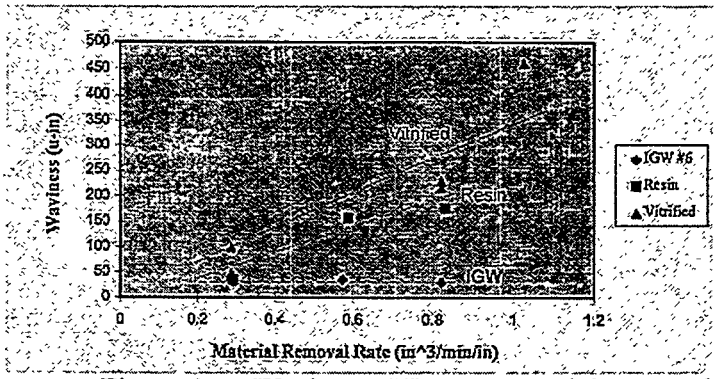

Figure 9. Waviness, Wt, vs. material removal rate at 32 m/s grinding speed.

Grinding Performance at 80 m/s (15,750 sfpm) -- Due to original design limit, the vitrified wheel did not participate in this high speed round of performance testing. Figure 10 shows the average power consumption versus material removal rate for the new metal bonded wheel and resin bonded wheel. The resin wheel and metal wheel had comparable power consumption at material removal rate of 8.6 $mm^3/s/mm$ (0.8

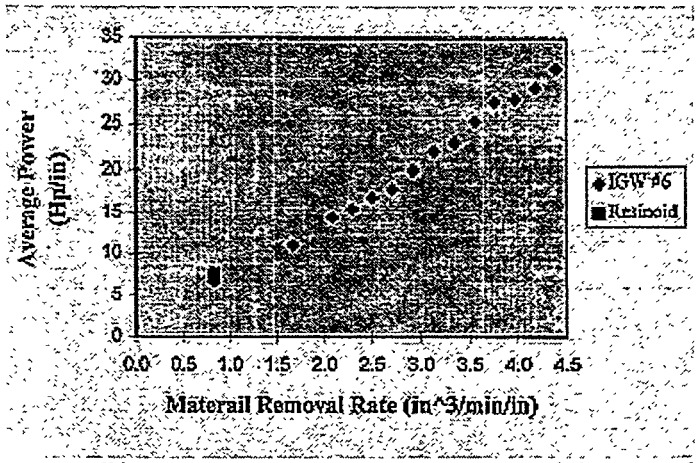

Figure 10. Average power vs. material removal rate at 80 m/s grinding speed.

in^3/min/in). For the metal bonded wheel, power appears proportional to MRR'. The highest MRR' that was conducted in this test was 47.3 mm^3/s/mm (4.4 in^3/min/in), but we believe the wheel did not reach its practicable limit. We believe the material removal rate successfully attained with the experimental wheel is not now achievable for any commercial wheel.

Figure 11 showed that the powder consumption for the experimental wheel at each material removal rate were fairly steady during the twelve grinds. This indicates that the wheel maintained its sharp cutting points during the entire length of the test at all MRR's.

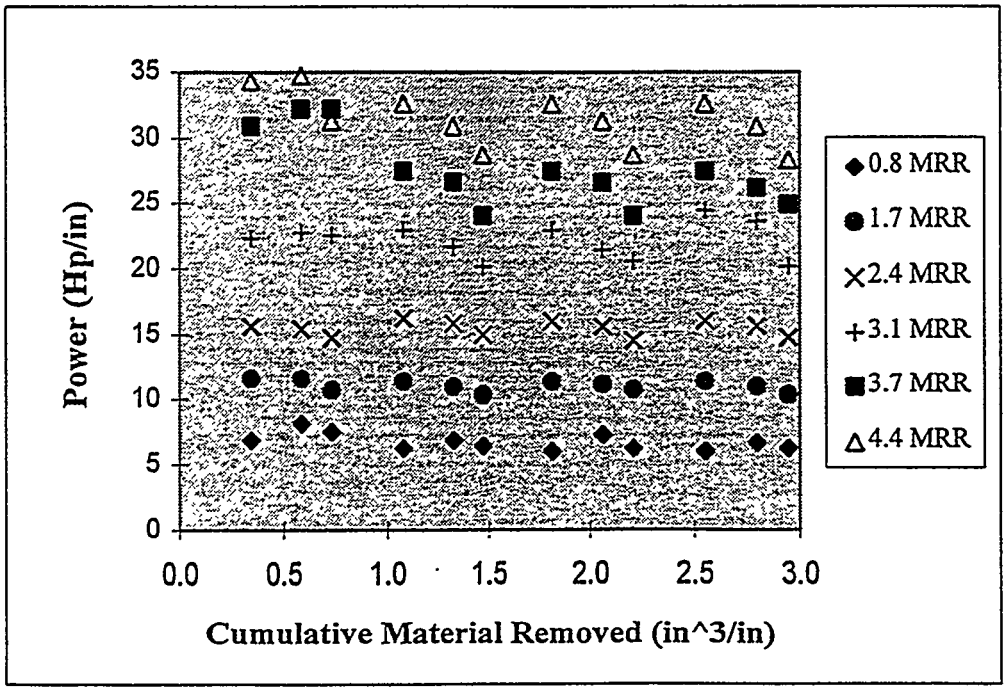

Figure 11. Grinding power vs. cumulative material removed (grinding time) of wheel #6 at 80 m/s speed.

Figure 12 shows the estimated G-ratios for the resin wheel and the new metal bonded wheel (#6) at all material removal rate conditions. Since there was no measurable wheel wear after twelve grinds at each material removal rate for the metal bonded wheel, a symbolic value of 0.01 mil (0.25 μm) radial wheel wear was given for each case. This yielded the G ratio of 6000.

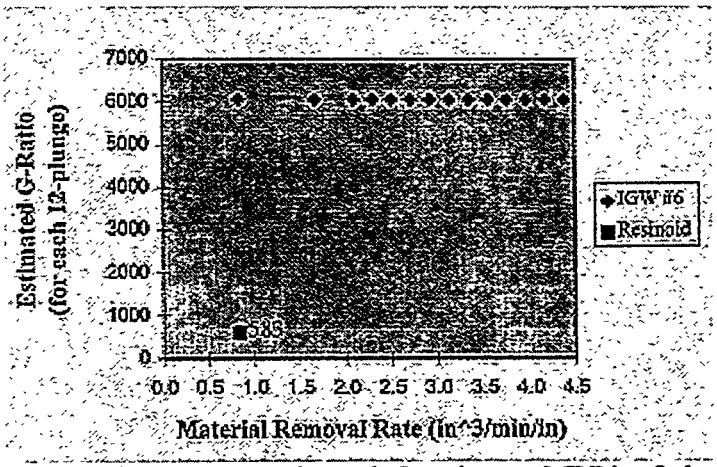

Figure 12. Estimated G-ratio vs. MRR' of the experimental metal bonded wheel at 80 m/s speed.

During the entire test, with material removal rates ranging from 8.6 $mm^3/s/mm$ (0.8 $in^3/min/in$) to 47.3 $mm^3/s/mm$ (4.4 $in^3/min/in$), the wheel was not trued or dressed. This wheel showed no measurable wheel wear after 168 plunges at 14 different material removal rates. The total amount of silicon nitride material ground was equivalent to 27,096 mm^3 per mm (42 in^3 per inch) of wheel width. By contrast, the G-ratio for the 100 concentration resin wheel at 8.6 $mm^3/s/mm$ (0.8 $in^3/min/in$) material removal rate was approximately 583 after twelve plunges. In summary, the experimental metal wheel was able to grind effectively at over 5 times the practicable MRR than the standard resin bond wheel. Also the experimental wheel had over 10 times the G-ratio compared to the resin wheel at the lower MRR, and the G-ratio difference would be much greater at higher MRRs.

According to above results, one can illustrate the potential productivity gain when using the new metal bonded diamond wheel capable of running at high material removal rates by the following example: For a hypothetical task of grinding a 25.4 mm long by 25.4 mm diameter silicon nitride rod to 6.35 mm in diameter with a 6.5 mm wide wheel, four deep plunges are required. The straight grinding time required to complete this work will be around 3.5 minutes for grinding conditions producing a MRR' of 9.0 $mm^3/s/mm$ (0.84 $in^3/min/in$), and about 10 minutes for MRR' at 3.2 $mm^3/s/mm$ (0.3 $in^3/min/in$). However, with the experimental wheel, it only requires 40 seconds to complete the task at a MRR' of 47.3 $mm^3/s/mm$ (4.4 $in^3/min/in$).

Figures 13 and 14 show that the samples ground by the experimental metal bonded wheel at all 14 material removal rates maintained constant surface finishes between 0.4 μm (16 μin.) and 0.5 μm (20 μin.), and had waviness values between 1.0 μm (38 μin.) and 1.7 μm (67 μin.). The resin wheel was not tested at these high material removal rates. At about 8.6 $mm^3/s/mm$ (0.8 $in^3/min/in$) material removal rate, the bars ground by the resin wheel had slightly better but comparable surface finishes (17 versus 20 μin.) and poorer waviness (69 versus 47 μin.). Surprisingly, there was no apparent deterioration in surface finish when the rods were ground with the new metal bonded wheel as the material removal rate increased. This is in contrast to the commonly observed surface finish deterioration with increase cut rates for standard wheels.

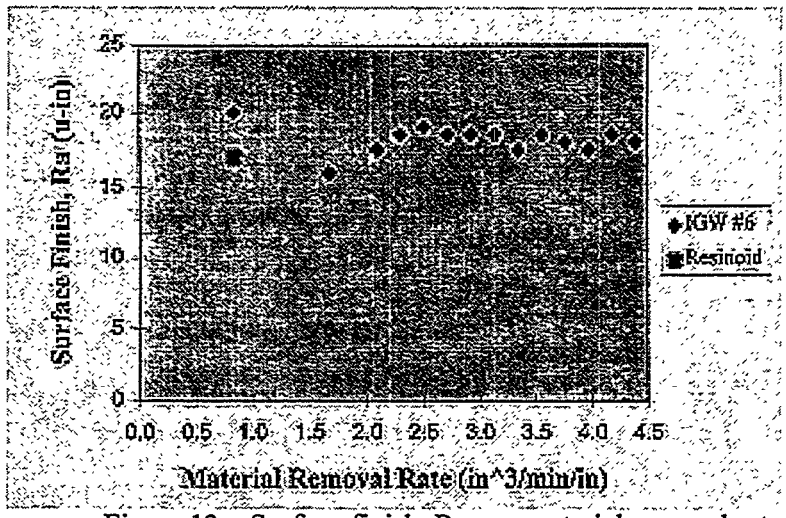

Figure 13. Surface finish, Ra, vs. material removal rate at 80 m/s grinding speed

Prior to the above test series, long duration test of 96 plunges was performed on an experimental metal wheel at 80 m/s. The material removal rate was set at 5.4 $mm^3/s/mm$ (0.5 $in^3/min/in$). The total material removed was equivalent to 15,484 mm^3 per mm (24 in^3 per inch) of wheel width. The power consumption was consistent throughout the 96 grinds. The G-ratio measured during this long duration test was about 800. No truing or dressing on the wheel was required.

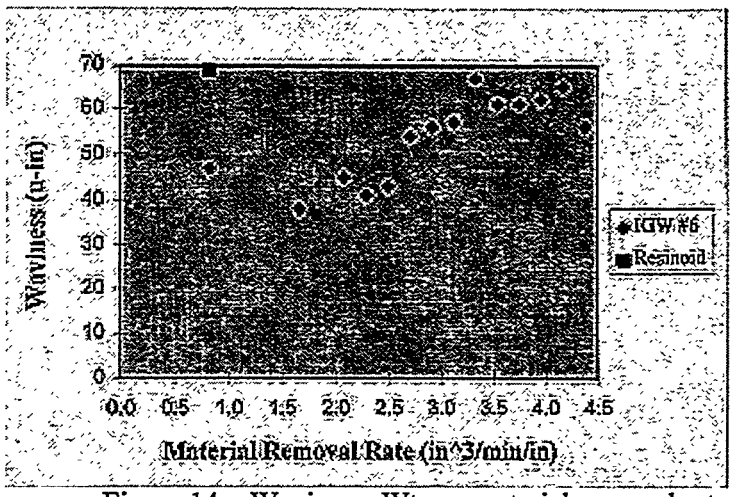

Figure 14. Waviness, Wt, vs. material removal rate at 80 m/s grinding speed

Grinding Performance as a Function of Wheel Speed: – Figure 15 shows the linear relationship between power consumption and material removal rate under various wheel speeds and types of wheel. At 32 m/s (6252 sfpm) and 56 m/s (11,000 sfpm) speeds, the power consumption for the metal bonded wheel were higher than that of resin wheel at all the material removal rates tested. However, the power consumption for the metal bonded wheel became comparable or slightly less than that of resin wheel at the high wheel speed of 80 m/s (15,750 sfpm). Overall, the trend showed that the power consumption decreased with increasing wheel speed when grinding at the same material removal rate. This is true for both the resin wheel and the experimental metal bonded wheel. This trend is probably due to the reduced chip thickness at the higher wheel speeds.

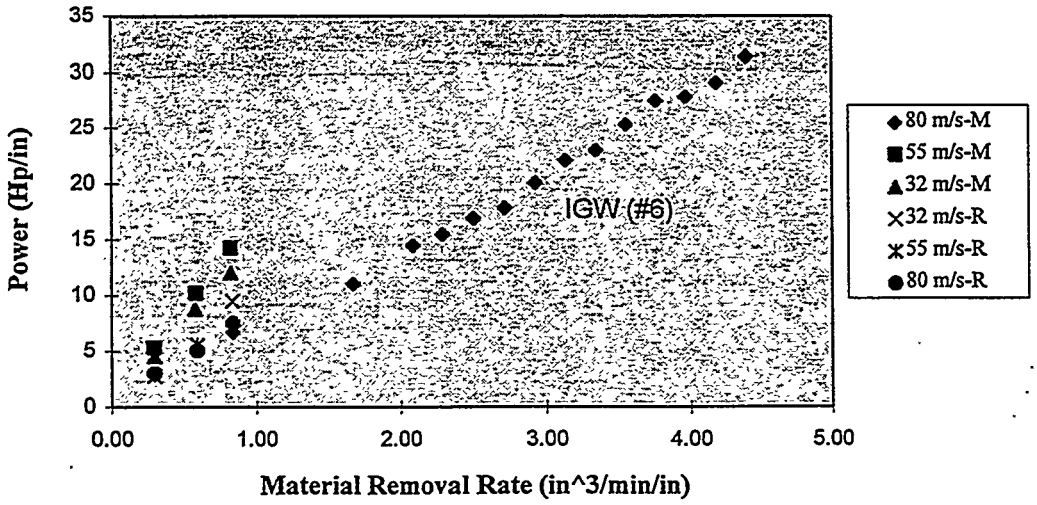

Figure 15. Power vs. MRR' of experimental metal bonded wheel #6 and the reference resin wheel at various wheel speeds.

Figure 16 shows the relationship between G-ratio and material removal rate under various wheel speeds and wheel types. Here again, due to no measurable wheel wear on the metal bonded wheel, it showed a straight horizontal line at constant G ratio of 6000 at all material removal rates and wheel speeds. For the resin wheel, the G-ratio decreases with increasing material removal rates at any constant wheel speed. G-ratio is shown to improve at higher wheel speed.

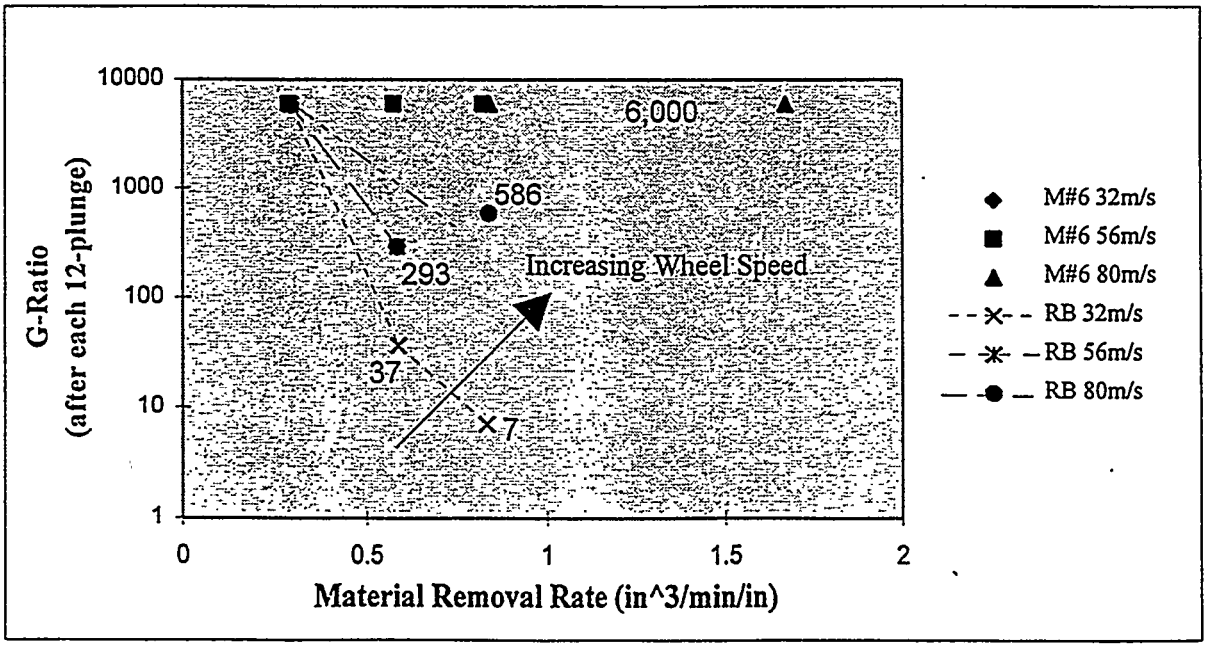

Figure 16. G-Ratio vs. material removal rate at various wheel speeds for the two types of wheel.

Figures 17 and 18 show the improvement in surface finishes and waviness on the ground bars at higher wheel speed. In addition, the samples ground by the new metal bonded wheel had the lowest measured waviness under all wheel speeds and material removal rates tested under Task 2.

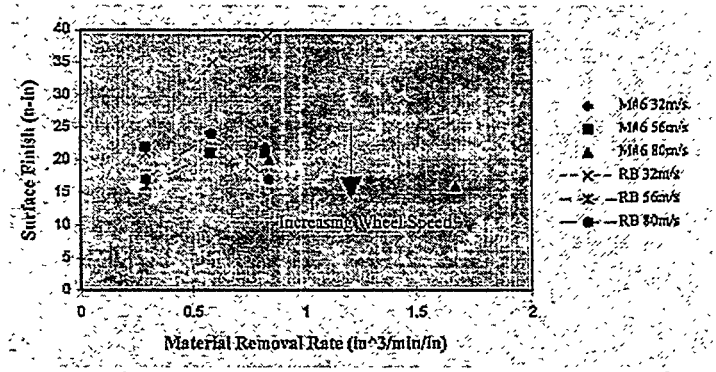

Figure 17. Surface finish, Ra, vs. MRR' at various wheel speeds for the two types of wheels.

Task 2 Grinding Test Summary -- The following are some of the key performance advantages demonstrated by the innovative metal bonded diamond wheels during the Task 2 evaluation.

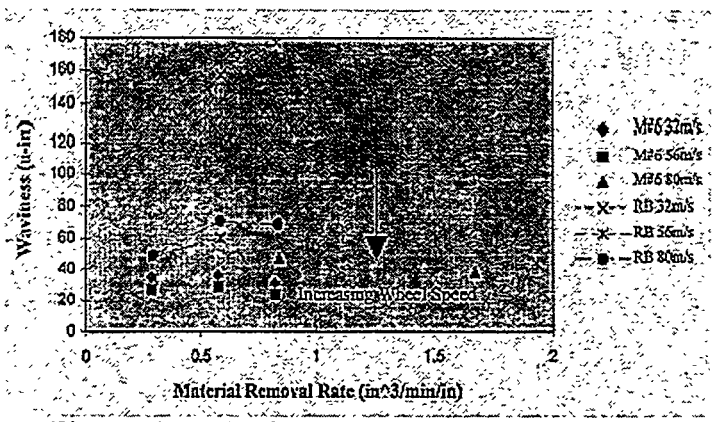

Figure 18. Waviness, Wt, vs. material removal rate at various wheel speeds for the two types of wheel.

1. The experimental metal bonded wheel reached a material removal rate of 47.3 $mm^3/s/mm$ (4.4 $in^3/min/in$) at 80 m/s wheel speed without showing wheel wear or surface finish deterioration on the ground parts. This is a significant improvement in grinding productivity and reduction of machining cost for the advanced ceramics industry.
2. At each of the material removal rates (from 8.6 $mm^3/s/mm$ to 47.3 $mm^3/s/mm$), the metal bonded wheel demonstrated consistent grinding power consumption and surface finish in grinding NT551 silicon nitride samples even after extensive plunge grinds.
3. At 32 m/s speed, the metal bonded wheel had the slightly higher power consumption than the resin wheel; but at 80 m/s the metal bonded wheel had comparable power consumption as the resin wheel.
4. The metal bonded wheel demonstrated superior wheel life compared to the resin and vitrified bonded wheels. In addition, there was no need for truing and dressing during the extended grinding tests.
5. The current experimental wheel could be operated at wheel speeds up to 90 m/s.
6. A truing and dressing method for this new metal bonded wheel was successfully developed. However, additional wheel performance benefits are expected to be realized with further improvement in truing operation.

Overall, the above results suggest that there are tremendous benefits to be realized by the ceramic industry when using this innovative metal bonded diamond wheel for cylindrical grinding. In addition, this experimental wheel does not require frequent and difficult dressing, which is characteristic of a standard metal bonded diamond wheel. This new bond demonstrated free cutting capability throughout the entire test matrix.

Task 3: Independent Validation Tests

A. Selection of Sites and Wheel Specs -- Completed.

Norton Company held preliminary meetings with both Eaton Corporation and Chand Kare Technical Ceramics to establish testing conditions and to verify details of their statements of work. AlliedSignal Ceramic Components, one of the four Independent validation test sites planned for in Task 3, withdrew their proposal. We reviewed a list of potential replacement test sites with the ORNL Program Monitor. Caterpillar Corporation submitted a proposal to

become the fourth independent validation test site, to replace AlliedSignal Ceramic Components. After review with the ORNL Program Monitor, Caterpillar was selected.

We consulted with Eaton, Chand and Caterpillar on their Statements of Work and proposed test conditions and made mutually agreed upon modifications based on the internal grinding results of Task 2. For all test sites, the experimental wheel will contain 320 grit diamond, which we concluded is the best all-purpose grit size for testing the wheel in both rough and finish grinding conditions.

The initial NAC grinding evaluation plan was finalized with NAC and the World Grinding Technology Center. The experimental metal bond wheel will be evaluated as a finishing wheel by traverse grinding diesel valve profiles (stem and base) on the Studer grinder. The experimental wheel will be compared to the finishing operation done by WGTC on NAC's valves under the ACMT program. Finish profile grinding represents one of the most time consuming valve grinding operations. Therefore, this proposed test will be the an effective method to demonstrate significant cost-effective improvements. Surface finish and power at various grinding conditions will be the main interests of this test. The test will determine maximum cut rate that can be used while still achieving the 8 μin. Ra finish requirement. The required truing and dressing frequency/characteristics of the XL metal bond and wear characteristics will also be assessed.

Purchase orders for Eaton, Chand and Caterpillar were issued. The following are the wheel specification selected for each independent grinding test subcontractor.

Chand Kare:	(400 mm diameter) 15.75 in. x 0.5 in. x 5.0002 in. 1A1SA Wheel of AD320-75MXL1994
NAC:	(400 mm diameter) 15.75 in. x 0.5 in. x 5.0002 in. 1A1SA Wheel of AD320-75MXL1994
Eaton:	(400 mm diameter) 15.75 in. x 0.5 in. x 5.0002 in. 1A1SA Wheel of AD320-75MXL1994 on customer hub
Caterpillar:	(400 mm diameter) 15.75 in. x 0.5 in. x 9.0002 in. 1A1SA Wheel of AD320-75MXL1994 on customer hub

B. Wheel Fabrication and Delivery -- Several improvements were implemented for manufacturing control and cost reduction considerations during the fabrication of experimental wheels for the validation tests. The status for the wheel and NT551 samples is as follows:

Chand Kare:	The experimental metal bonded diamond wheel, reference resin bonded wheel, SG truing wheels, and NT551 samples were shipped.
NAC:	The experimental metal bonded wheel was delivered to the WGTC.
Eaton:	The experimental metal bonded wheel, SG truing wheels, and NT551 samples were shipped.
Caterpillar:	The experimental metal bonded wheel, SG truing wheels, and ceramic specimens were shipped.

C. Independent Validation Tests at Subcontractors and Test Reports -- Tests are scheduled to commence in April or May at the four test sites.

In preparation for the NAC valve grinding test, some Task 2 plunge grinding specimens were traverse ground for evaluation of retained strength of valve stem-type rods. This test is discussed below under "Flexure Testing" in Task 4.

Task 4: Ceramic Surface Integrity -- Northboro Research and Development Center

4.A. In-House Grinding Test Specimens -- Task 4.A involves the surface integrity evaluation of NT551 silicon nitride specimens ground under the Task 2 in-house test and is now in process. Task 4.B will be the evaluation of specimens returned after the Task 3 independent grinding tests. Task 4 post-grinding surface characterization is being performed by the Northboro R&D Center (NRDC) of Saint-Gobain Industrial Ceramics, Inc. (a subsidiary of Norton Company).

All surface finish data from the Task 2 grinding test, were on surfaces created by cylindrical plunge grinding without spark-out. These surfaces are normally rougher than traverse cylindrical grinding. Under Task 2, we reported preliminary surface roughness data measured by Norton Company's World Grinding Technology Center (WGTC). Specimens were sent to NRDC for additional surface finish analysis. The NRDC surface finish data presented below were on different specimens or different plunge test surfaces than were reported above. All the WGTC surface finish data was on the twelfth, and last plunge grind of each condition. The NRDC data was taken from surfaces at the sixth plunge.

Surface Finish Analysis by Contact Profilometry -- Twenty NT551 silicon nitride samples were evaluated for average surface roughness and total waviness height using the Rank Taylor Hobson S3C 2-D Contact Profilometer and a diamond stylus with a tip radius of 2.5 μm. The results are shown in Table 6. The data cutoff length was 0.8 mm and the total assessment length was 5.6 mm for all parts. The cutoff selected is a typical length for evaluating a standard grinding procedure and the assessment length was chosen to examine the waviness produced by the wheel within one plunge span.

There was a test variable for the experimental metal bond sample numbers (plunge test number) up to 336, which used an early truing procedure. During the early part of the Task 2 grinding test, the truing technique was modified and improved. Surface finish data reported above under Task 2 was entirely from plunge tests using the improved truing technique.

Average roughness ranged from 0.49 μm to 0.76 μm for the experimental metal (XL metal) bond wheel. An important observation was that surface roughness did not increase with an increase in Material Removal Rate (MRR) or surface speed. A similar trend was reported with the WGTC surface finish data. The specimen ground with the resin bond wheel at the higher MRR and lower speed conditions (#980) experienced problems during grinding. This is evident by the poor Ra and Wt.

Lower speed, 32 m/s, data analysis -- Figures 19 and 20 show surface and waviness information versus MRR at a surface speed of 32 m/s for the vitrified, resin and XL metal bonded wheel. Data in Figure 19 indicates that the resin bonded wheel gives a finer surface finish at low speed than either the experimental wheel #6 or the vitrified wheel. Results from Figure 20 show that the experimental wheel had a smaller maximum peak to valley height, Wt, in its waviness profile than samples ground with either the vitrified or resin bonded wheel.

Table 6. Surface Finish of NT551 Samples

Sample Number (Plunge #)	Wheel Bond	MRR (in^3/min/in)	Surface Speed (m/s)	Contact Ra 0.8 mm cutoff (μm)	Contact Wt 0.8 mm cutoff (μm)	Non-Contact Ra (μm)
13-24	XL Metal	0.29	32	0.65	1.1789	0.66
1-12	XL Metal	0.29	32	0.60	1.2679	
145-156	XL Metal	0.59	32	0.70	1.2807	
157-168	XL Metal	0.59	32	0.76	1.6447	
241-252	XL Metal	0.59	56	0.52	0.7957	
253-264	XL Metal	0.59	56	0.52	0.7895	
313-324	XL Metal	0.59	80	0.49	1.1532	
325-336	XL Metal	0.59	80	0.50	0.8253	
(improved truing procedure was used for the remaining plunge specimens)						
709	XL Metal	1.05	80	0.63	0.8904	
721	XL Metal	1.26	80	0.60	1.0031	0.57
781	XL Metal	2.31	80	0.60	1.1963	
793	XL Metal	2.52	80	0.58	1.4071	0.54
949	XL Metal	4.20	80	0.51	1.0076	
961	XL Metal	4.41	80	0.49	1.4591	0.58
643	Vitrified	0.29	32	0.79	2.7131	0.80
655	Vitrified	0.84	32	0.77	9.9003	
973	Resin	0.29	32	0.45	0.7211	0.37
992	Resin	0.29	80	0.42	1.6577	
980	Resin	0.84	32	0.64	12.9327	
1004	Resin	0.84	80	0.43	1.9387	

These results do not exactly match the trends reported by WGTC for Ra. At low speed the vitrified bond again had the poorest finish but the Ra values for the experimental metal bond were poorer than the resin bond. Under Task 2, we reported that for all tests at low speed, and using the same truing conditions, the experimental metal bond wheel was superior to both vitrified and resin bond wheels. The use of the improved truing technique should improve the Ra finish of the metal bond at these low speed conditions. Figure 20 shows the experimental metal bond wheel results in better waviness, Wt, at low speed conditions vs. the vitrified and resin wheels, which is consistent with the data reported previously.

Higher speed, 80 m/s, data analysis -- Roughness and waviness information for the resin bond and experimental metal bond wheel are shown in Figures 21 and 22 for a wheel surface speed of 80 m/s. The XL metal bond wheel maintained a fairly constant surface finish and waviness even at higher material removal rates. The surface finish produced with the resin bond wheel at the lower MRR was slightly better while the waviness factor, Wt, was slightly worse than the experimental metal bond wheel. These results are similar to those trends reported above under Task 2. Again, the data shows remarkable consistency in surface finish of the experimental bond along a very wide range of cut rates.

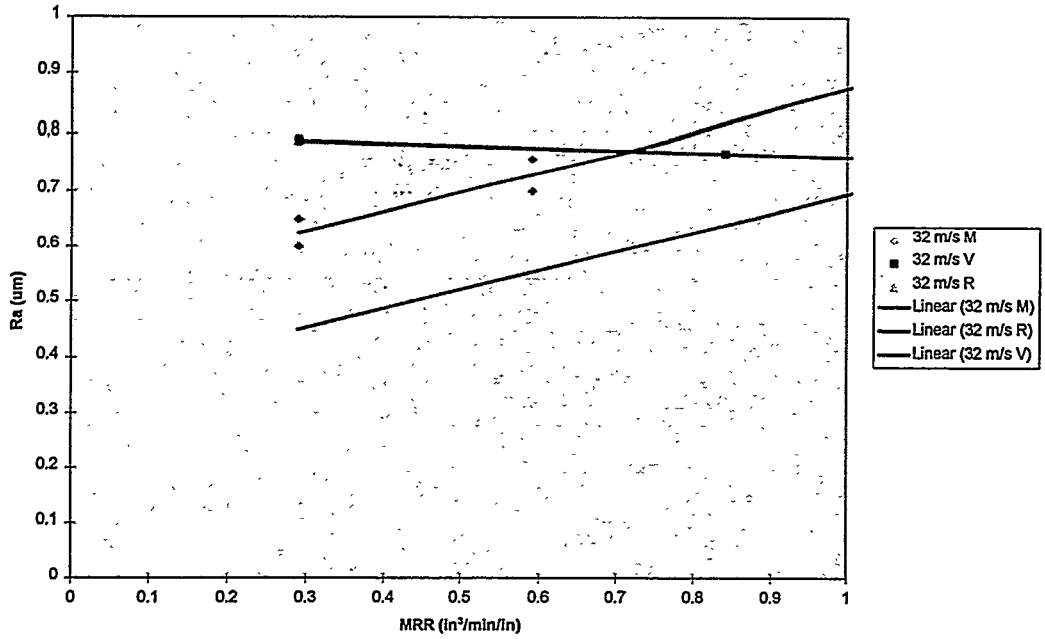

Figure 19. Surface Finish vs. Material Removal Rate (MRR) at a Surface Speed of 32 m/s. All surfaces created by plunge grinding with no spark-out. Legend Key: M = XL Metal, V = Vitrified, R = Resin.

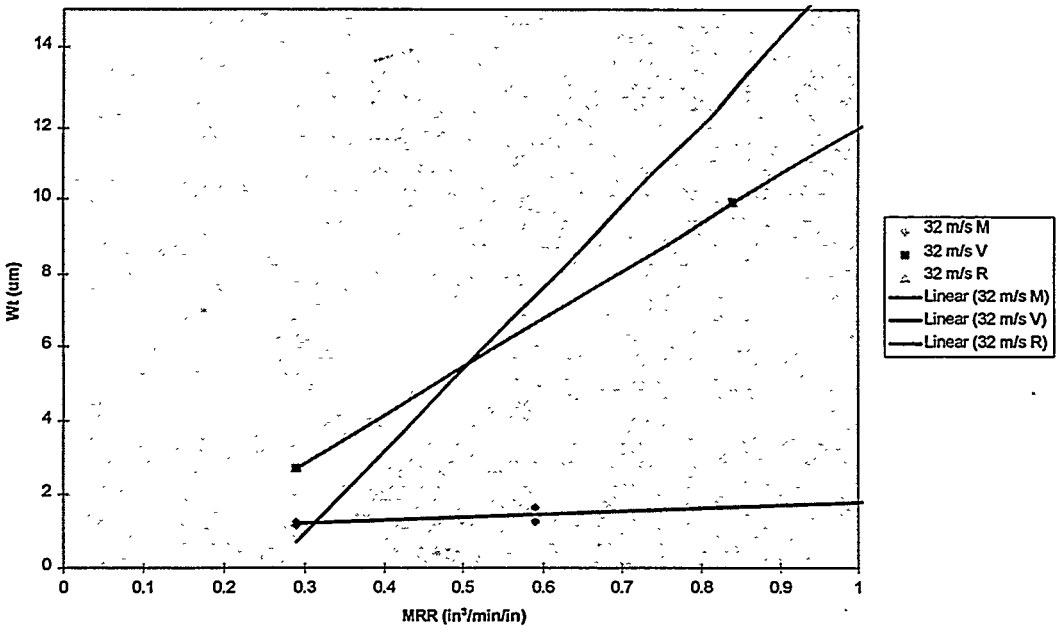

Figure 20. Waviness vs. Material Removal Rate at a Surface Speed of 32 m/s.

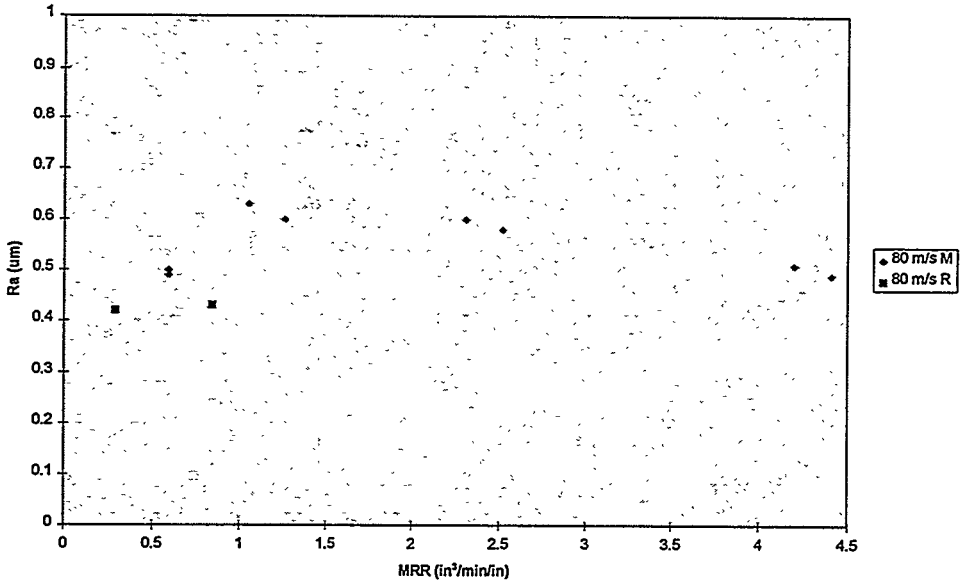

Figure 21. Surface Finish vs. Material Removal Rate at Grinding Surface Speed of 80 m/s. Legend Key: M = XL Metal, R = Resin.

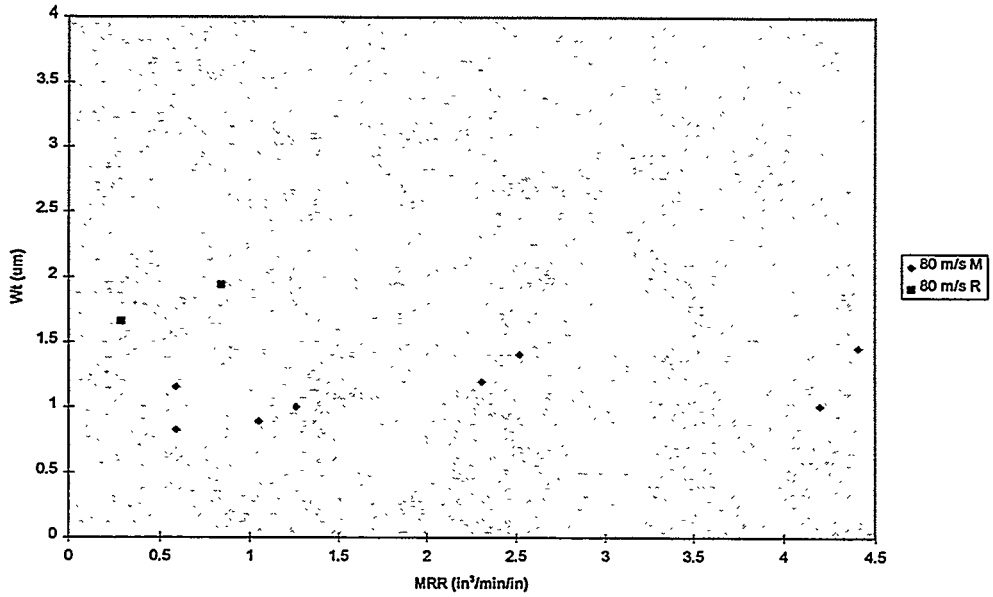

Figure 22. Waviness vs. Material Removal Rate at a Surface Speed of 80 m/s.

Figure 23 demonstrates how the surface finish improved with an increase in surface speed at a constant MRR for the metal bond wheel, as expected. Figure 24 displays the surface roughness data for all the samples for comparison purposes.

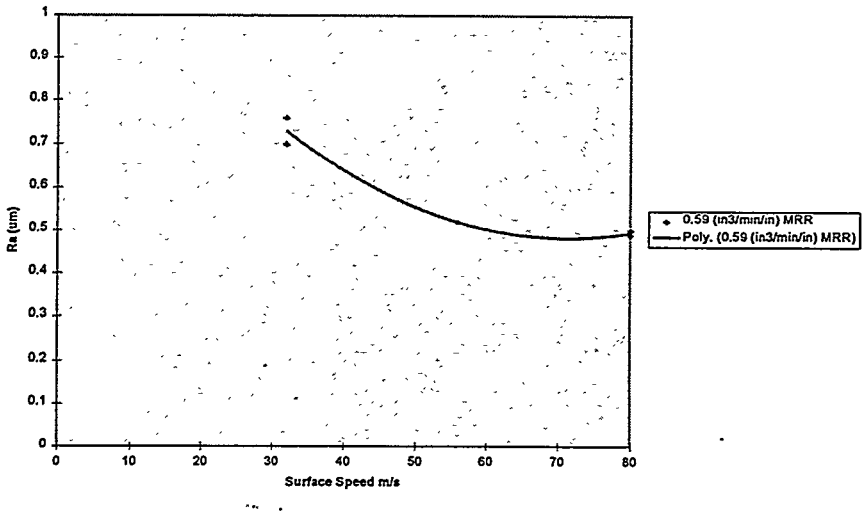

Figure 23. Surface Finish vs. Material Removal Rate for XL Metal Bond Wheel at Constant MRR.

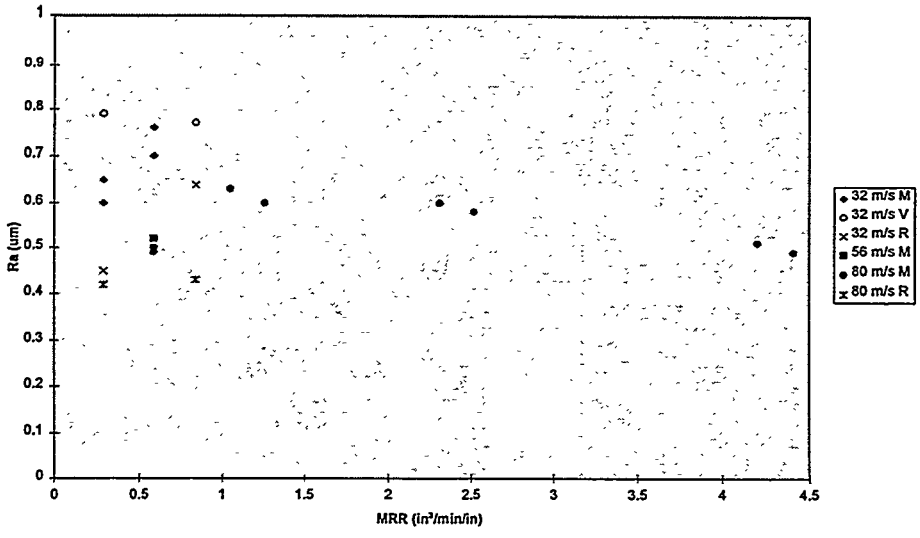

Figure 24. Surface Finish vs. Material Removal Rate for XL Metal, Vitrified and Resin Bond Wheel at 32, 56 and 80 m/s.

Surface Finish Analysis by Non-contact Interferometry -- Six of the NT551 samples were analyzed using the Zygo NewView 100 Non-contact Scanning White Light Interferometer to confirm measurements made using the Rank Taylor Hobson instrument. A 40x objective with a 1x image zoom was used, which views an area of 0.13 mm x 0.17 mm. A cylinder was removed from the image for evaluation purposes. The non-contact interferometry Ra data is listed above in Table 6. All of the measurements corresponded well with those taken with the contact profilometer.

Surface Analysis by Atomic Force Microscopy -- Three silicon nitride samples were selected for evaluation using Atomic Force Microscopy (AFM). Samples 13-24, 643, and 973 (from Table 6) were machined with a surface speed of 32 m/s and an MRR of 0.29 in^3/min/in using an experimental metal, vitrified and resin bond wheel, respectively. An area of size 25 x 25 μm and an area of size 5 x 5 μm were measured on each sample and multiple readings were taken on sample 13-24 and 973. Table 7 summarizes Rq (root mean square value), Ra (average roughness) and Rmax (lowest-valley-to-highest-peak roughness) values for all three samples.

Table 7. Roughness Values Measured By Atomic Force Microscope

Sample	25 x 25 μm Image			5 x 5 μm Image		
	Rq(μm)	Ra(μm)	Rmax(μm)	Rq(μm)	Ra(μm)	Rmax(μm)
13-24	0.44	0.36	2.18	0.25	0.11	0.78
13-24	0.26	0.20	1.75	0.17	0.18	1.13
973	0.23	0.19	1.46	0.14	0.08	0.59
973	0.69	0.57	3.30	0.20	0.12	0.82
643	0.51	0.43	3.61	0.16	0.14	0.81

Figure 25 is a typical AFM image, which shows peaks and valleys on its surface. The center valley is approximately 8 μm wide and 2.5 μm lower than its neighboring peaks. The area imaged by the AFM was smaller than the contact length of the wheel and all the valleys observed were less than one third of the abrasive grain size; therefore, it is likely that the peaks and valleys pictured are those produced by a single grit on the wheel. As shown in Table 7, there was a large amount of variability in roughness readings within each sample; therefore no further analysis was done using the atomic force microscope.

Flexure Testing -- The Task 2 WGTC grinding test evaluated the wheels in cylindrical plunge grinding mode. The specimen profile consisted of approximately 12 separate plunges on each end. This resulted in specimens with ground ends approximately 6.3 mm diameter X 25 mm long. This geometry was impractical for flexural testing to evaluate retained strength. Additionally, NAC and WGTC propose to evaluate the experimental metal bond wheel in finish traverse grinding of diesel valve stems and profiles under Task 3. For component qualification, it is considered more important to evaluate retained strength characteristics after traverse finish grinding than after rough plunge grinding operations.

After the Task 2 plunge grinding test, some silicon nitride specimens were machined in the traverse grinding mode using both the experimental metal and resin bond wheel. The wheel was fed at a depth of 0.005 in. to form a shoulder and then traversed to the end of the rod at a

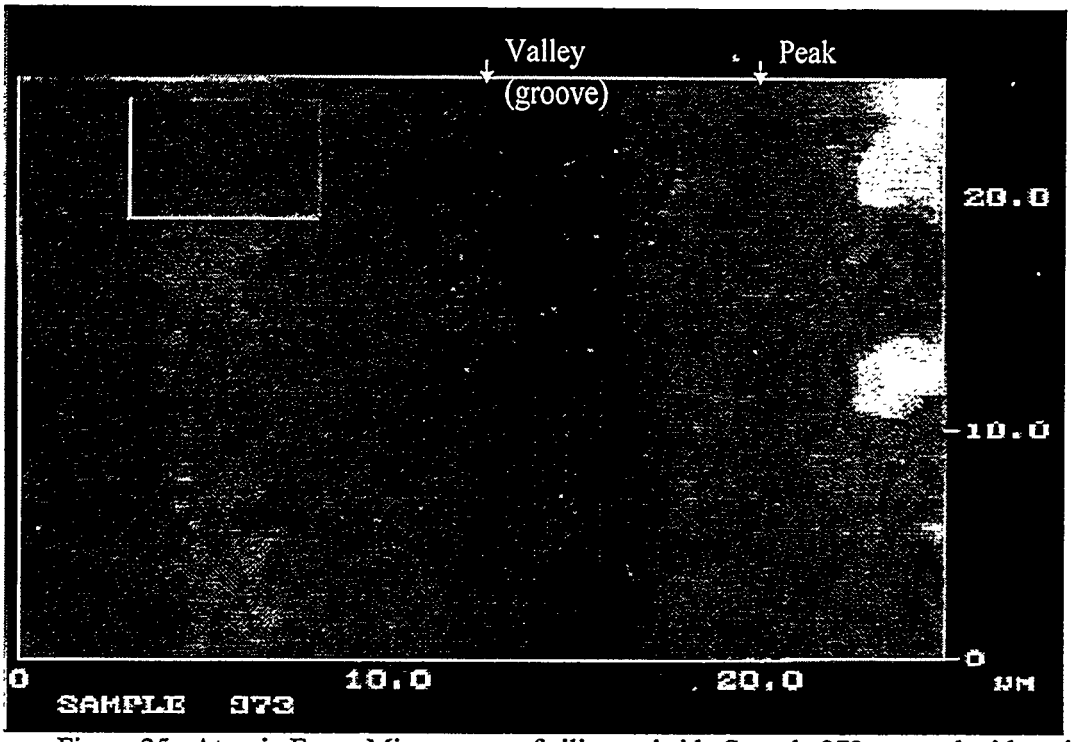

Figure 25. Atomic Force Microscopy of silicon nitride Sample 973, ground with resin-bond wheel at 32 m/s and 0.29 in^3/min/in.

rate of 16 in/min. This process was repeated until the diameter of the rod was reduced to approximately 5.8 mm. The total stock removed on each specimen in the traverse mode was approximately 0.25 mm (0.01 in.), which would be more than enough to remove damage from the previous plunge grind. The surface speed of the wheel was 80 m/s and the workpiece was rotated at 750 rpm resulting in a material removal rate of 2.9 in^3/min/in.

Preliminary 3-point bend flexure testing was performed on 9 samples machined by the metal bond wheel and 10 samples ground with the resin bond wheel. The span between outer pins was 20 mm. For this preliminary data the average flexural strength was 827 MPa +/- 76 MPa standard deviation for the specimens ground with the resin bond wheel vs. 785 MPa +/- 34 for specimens ground with the XL metal wheel. The specimens ground with the resin bond had only 5% higher average flexural strength, which is probably not significant considering the limited data points and variation. Further analysis of this data, including systematic failure origin analysis is ongoing.

These preliminary flexural strengths appear good, considering they were 5.8 mm diameter specimens with transverse, not longitudinal, grind lines.. Flexural strengths of ASTM C1161-B Specimens in 4-point bend for this material, including tiles from the same batch, are typically between a mean of 890 to 990 MPa. Lower strengths were expected from the rods due to the direction of the grind lines, which results in the orientation of the crack plane to be perpendicular to the principal stress direction initiating crack opening.

Weibull analysis is ongoing and will be presented next reporting period. We are assuming that all the failures were due to machining flaws based upon preliminary optical examination, but further SEM analysis will be done.

Fractography -- Preliminary fractography was performed using optical microscopy. As expected, the failure origin was located on or near the tensile surface of the rod. To date, only one failure has been positively identified as originating at an obvious machining flaw. SEM analysis is now in progress for the remainder of the samples and will be presented in a future report.

We intend to do additional surface characterization on selected specimens that may include liquid dye penetrant in conjunction with microfocus X-radiography (MFX), and residual stress by the X-ray Diffraction technique.

Status of Milestones - On Schedule

1.A. Experimental Design and Definition -- Completed

1.B. Strength Characterization and High Speed Core Development -- Completed

1.C. Manufacture and Characterization of Large Wheels -- Completed

2.A. Ceramic Specimen Preparation -- Completed

2.B. Preliminary Grinding Tests at WGTC -- Completed

3.A. Independent Validation Tests, Selection of sites and wheel specs -- Completed

3.B. Independent Validation Tests, Wheel Fabrication and Delivery -- Completed

3.C. Independent Validation Tests at Subcontractors and Test Reports -- In-Process

4.A. Ceramic Surface Integrity of In-House Specimens -- In-Process

4.B. Ceramic Surface Integrity of Independent Validation Test Specimens --

Communications/Visits/Travel

Michael A. Laurich, Eaton Corp. Manufacturing Technologies Center, during a visit to Norton Company Superabrasives, Worcester MA, reviewed Eaton's planned independent validation test with Norton project personnel, October 23, 1996.

R.H. Licht, P. Kuo and L.A. Broderick to Chand Kare Technical Ceramics, November 8, 1996.

Notification of Milestone 2 completion to P.J. Blau, January 15, 1997.

A meeting with NAC and WGTC was held on March 28 at the WGTC to finalize plans for conducting the NAC valve grinding experiment for the experimental metal bond.

Publications/Presentations

None

References

1. R.H. Licht, S. Ramanath, M. Simpson, E. Lilley, Innovative Grinding Wheel Design for Cost-Effective Machining of Advanced Ceramics, Phase I Final Report, Subcontract No. 87X-SM037V, published by Oak Ridge National Laboratory Ceramic Technology Project, Report Number ORNL/Sub/93-SM037/1, Publication date, Feb. 1996.

2. G. R. Anstis, P. Chantikul, B. R. Lawn and D. B. Marshall, "A Critical Evaluation of Indentation Techniques for Measuring Fracture Toughness: I, Direct Crack Measurements," *J. Am. Cer. Soc.*, **64**, 533-538, (1981).

HIGH-SPEED, LOW-DAMAGE GRINDING OF ADVANCED CERAMICS

Joseph A. Kovach
Michael A. Laurich
Eaton Manufacturing Technologies Center
Willoughby Hills, Ohio 44094

Stephen Malkin
University of Massachusetts
Amherst, Mass. 01003

Objective/Scope

The overall objective of the **H**igh **S**peed **L**ow **D**amage (HSLD) grinding project is to develop a single step, roughing-finishing process suitable for producing high-quality advanced ceramic components at high material removal rates and at substantially lower cost than traditional, multi-stage grinding processes. Initial implications from Phase I have suggested that HSLD grinding of Si_3N_4 is technically feasible. Accordingly, to achieve the overall program objective, the Phase II effort is focused on:

1.0 Continued expansion of the HSLD science base

2.0 Further development of the enabling HSLD technologies required for successful implementation, and

3.0 Economic analysis of the HSLD production cost drivers.

Technical Progress

This semi-annual report summarizes technical progress achieved during the period from October 1, 1996 to March 31, 1997. The report describes activities at the Eaton Manufacturing Technologies Center. A technical overview is presented in the following areas:

1. Effect of dressing on surface quality of S/RBSN
2. Effect of step-over on surface quality of S/RBSN
3. Grinding of S/RBSN to determine effects on MOR strength

1.0 Effect of dressing on surface quality

The condition of the grinding wheel can directly affect the resultant strength of the ceramic MOR specimen. To eliminate any "noise" in the data due to wheel dressing variations, a repeatable dressing and truing process that results in a uniform wheel surface is required. While it may be nearly impossible to generate the exact same wheel surface for each test, the dressing procedure should yield a surface that will allow the best chance of the effects of other process parameters (i.e. feeds and speeds) to be realized.

A comparison of two dressing procedures is presented. The first process dresses the wheel with a titanium roll dresser followed by sticking with a 220 grit Al_2O_3 stick. The second method again starts with titanium roll dressing but is then followed by a cup-truing process. Cup truing involves feeding the grinding wheel across a horizontal cup wheel (320 grit green carborundum abrasive) mounted on a Read Diamond Products RS-60 dresser

Figures 1 and 2 show surface finish traces of the S/RBSN surface ground with a 180 grit resin bonded wheel (D180-100-UI841) after the titanium/sticking and titanium/cup truing processes respectively. (Note that the vertical scale in Figure 1 is 50 μinch/div while it is 25 μinch/div in Figure 2). For the titanium/sticking process, the Rt value was 219 μinch while for the titanium/cup truing process, the Rt value was reduced to 94.1 μinch. A similar trend in Ra values was seen (22.0 for titanium/sticking versus 10.8 μinch for titanium/cup truing).

2.0 Effect of step-over on surface quality

Much discussion has taken place on the accuracy of longitudinal versus transverse grinding to determine MOR strength as a function of grinding conditions. With longitudinal grinding, the grinding scratches are parallel to the primary stress direction. Typically, transverse grinding is desired so that the grinding scratches are perpendicular to the primary stress direction. It is felt by many that longitudinally ground MOR bars do not give a true indication of MOR strength as a function of grinding parameters.

A typical MOR bar is 3 x 4 x 45 mm while the wheel is on the order of 12 to 25 mm wide. As such, to generate transverse grinding scratches, the wheel must be crossfed or "stepped over" across the bar. This stepping over routinely results in a deep scratch or high ridge being left at each step over. Using a half inch wide 180 grit resin bond wheel (D180-100-UI841) at 5,000 ft/min, the effect of step over distance was investigated. The depth of cut was 0.010 inches and the workpiece velocity was 100 in/min. Figures 3 through 5 show the resultant surface due to step-overs of 0.070, 0.400 and 0.015 inches respectively. Notice that as the step over distance is increased, the magnitude of the generated ridge increases.

3.0 Grinding of S/RBSN to determine effects on MOR strength

S/RBSN tile grinding was performed over this reporting period. A total of nine tiles have been ground to date in an attempt to quantify the effects on resultant modulus of rupture strength in grinding S/RBSN using different grit sizes, bond types and wheel speeds.

Four wheels were selected to be run at three wheel speeds. The following matrix indicates grinding progress to date:

	180 resin D180-100UI841	240 resin D240-100UI841	180 vitrified D91KZ125VFR	240 vitrified D64KZ125VFR
6,000 ft/min	Completed	Completed	Pending	Completed
12,000 ft/min	Completed	Completed	Pending	Completed
18,000 ft/min	Completed	Completed	Pending	Completed

Prior to each test, the grinding wheel was prepared using the titanium dressing/cup truing process. Table 1 summarizes the force, power, specific energy and surface finish data for the three wheels run. Material removal rate was held constant at 1.0 in^3/min/in under the following conditions:

- Workpiece velocity = 100 in/min
- Depth of cut = 0.010 inch/pass
- Total depth of cut = 0.030 inch
- Step-over = 0.015 inch
- Up-Grind

Figures 6 through 11 show plots of normal force, tangential force, power, specific energy and surface finish (Ra and Rt) versus wheel speed for the three wheels. Figure 6 shows that normal force for the two resin wheels increases with increasing wheel speed, while the 240 grit vitrified wheel remains fairly constant.

From Figure 7, increasing wheel speed allows the 240 resin wheel to cut more freely by reducing the tangential force. With the 180 resin, however, the tangential force increases, somewhat contrary to what would be expected. Once again, the vitrified wheel remains fairly consistent across all wheel speeds. From both the normal and tangential forces, it appears as though the 240 grit vitrified bonded wheel cuts with lower forces than either the 180 or 240 grit resin wheels.

Figures 8 and 9 respectively show that power and specific energy generally increase with increasing wheel speed. The two finer grit wheels (240 resin and 240 vitrified) require a lower specific energy than the coarser 180 resin.

It is interesting to note in Figure 10 that approximately the same surface finish (6 or 7 μinch Ra) was achieved regardless of grit size, bond type or wheel speed. The overall range of Rt values (Figure 11) was between 59 and 97 μinch with an average of 69 μinch for all wheels and speeds.

Status of Milestones

Program is back on schedule based on a no-cost extension through the end of September, 1997.

Milestone	Description	Completion Date
153203	Develop a two-color precision pyrometry system to accurately measure ceramic grinding zone temperatures.	Completed
153204	Using grinding zone temperature data, determine the thermal balance between the wheel and the workpiece under HSLD grinding conditions.	Completed
153205	Develop and report methods for dressing and conditioning of grinding wheels specifically intended for use in the HSLD grinding process.	Completed
153206	Conduct economic sensitivity analyses of the HSLD production cost drivers. Assess tradeoffs between cost and resulting quality under a wide range of operating conditions.	Sept. 1997

Communications/Visits/Travel

1) J. Kovach, M. Laurich and S. Malkin visited Oak Ridge for a program update on March 19, 1997.

Problems Encountered - None

Publications - None

Wheel Type	Wheel Speed (ft/min)	Normal Force (lb)	Tangential Force (lb)	Power (hp)	Specific Energy (in-lb/in³)	Surface Finish Ra (μinch)	Surface Finish Rt (μinch)
180 grit resin bond	6,000	23	1.0	0.18	4,857,600	6	60
	12,000	32	1.2	0.45	11,932,800	7	97
	18,000	42	1.4	0.88	20,160,000	7	66
240 grit resin bond	6,000	26	1.7	0.26	8,160,000	7	74
	12,000	30	0.8	0.45	7,680,000	7	63
	18,000	54	0.7	0.92	10,080,000	7	59
240 grit vitrified bond	6,000	22	0.7	0.21	3,360,000	7	64
	12,000	25	0.9	0.50	8,160,000	7	74
	18,000	24	0.9	0.97	12,240,000	7	66

Workpiece velocity = 100 in/min
Depth of cut = 0.010
Step-over = 0.015 inch

Table 1. Grinding data summary for S/RBSN tiles

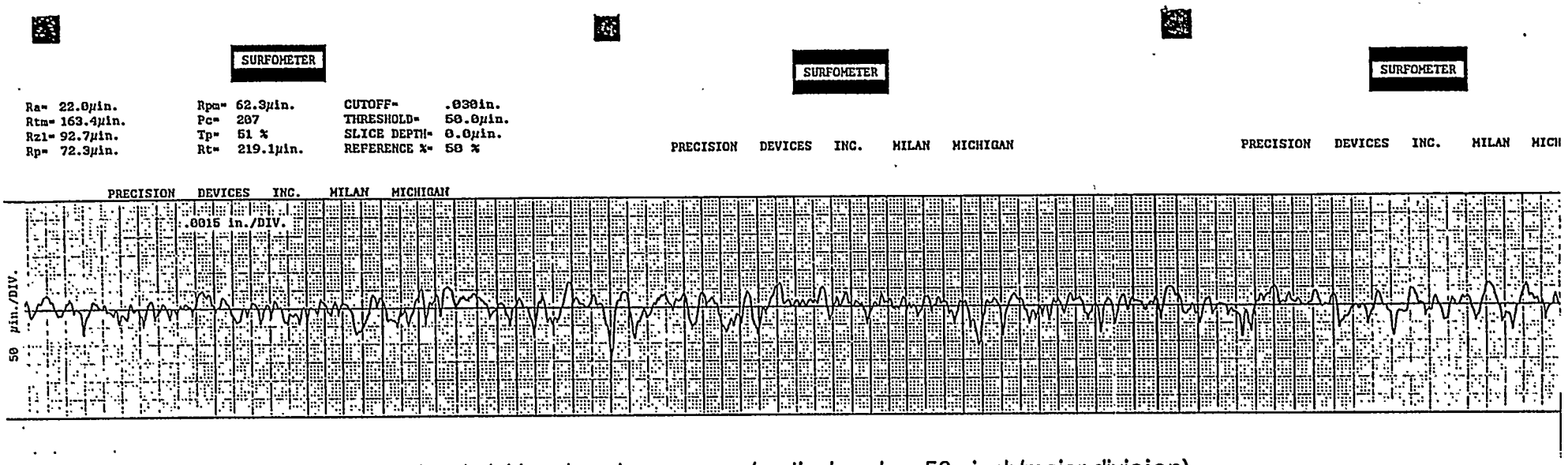

Figure 1. Part surface after titanium/sticking dressing process (vertical scale = 50 µinch/major division).

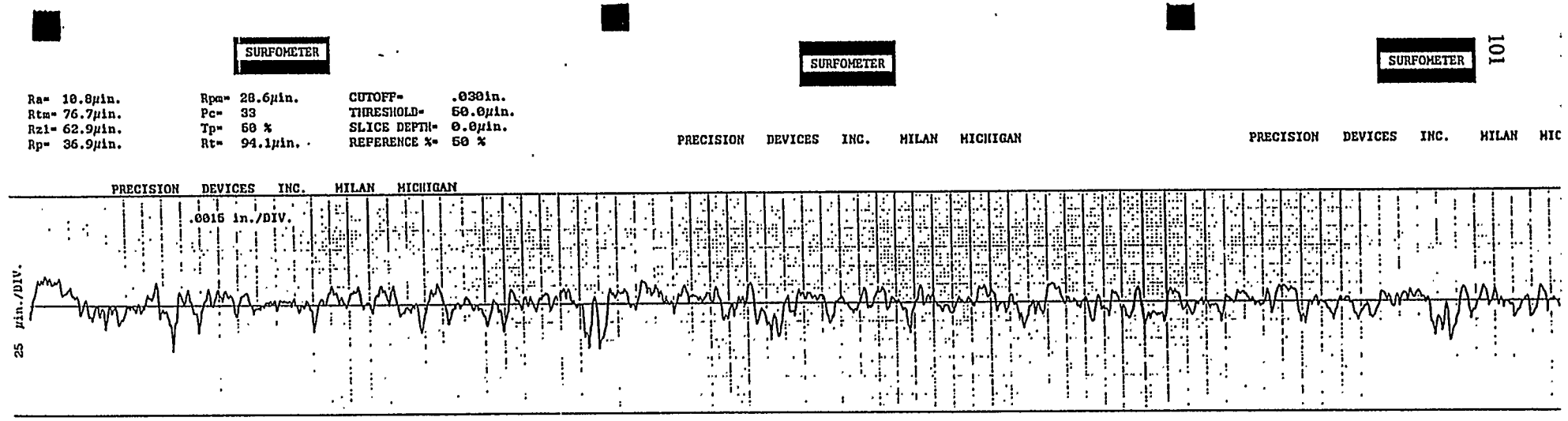

Figure 2. Part surface after titanium/cup truing process (vertical scale = 25 µinch/major division).

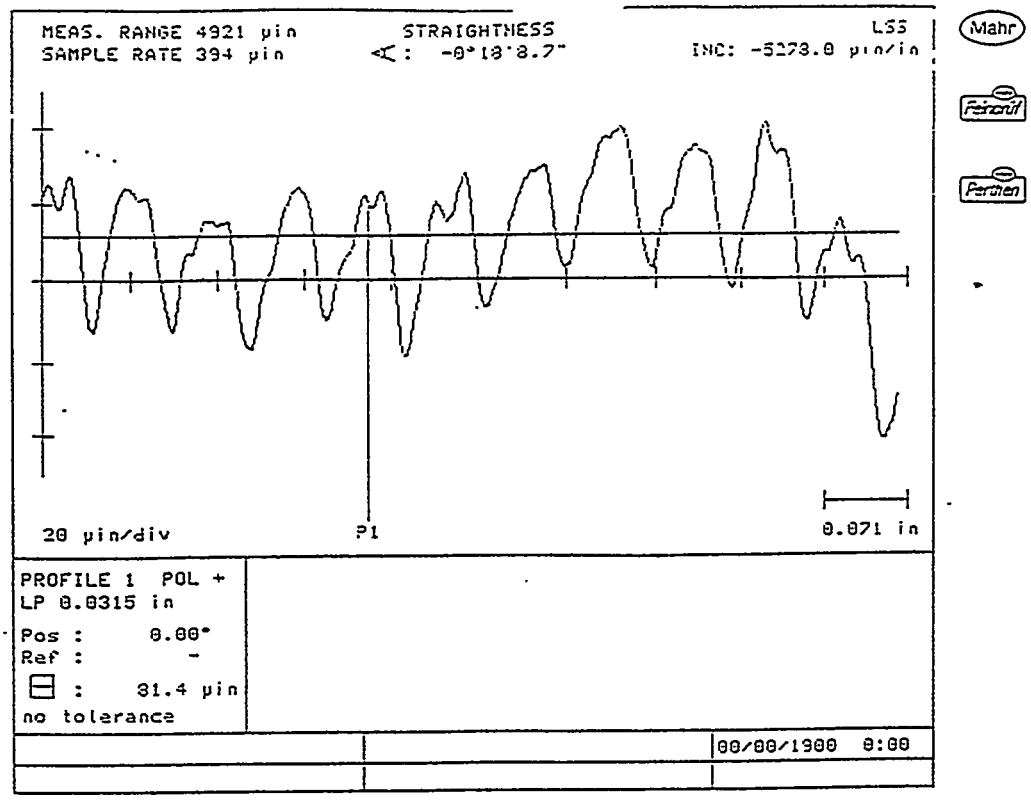

Figure 3. Effect of 0.070 inch step-over on S/RBSN surface (V_s = 5,000 ft/min).

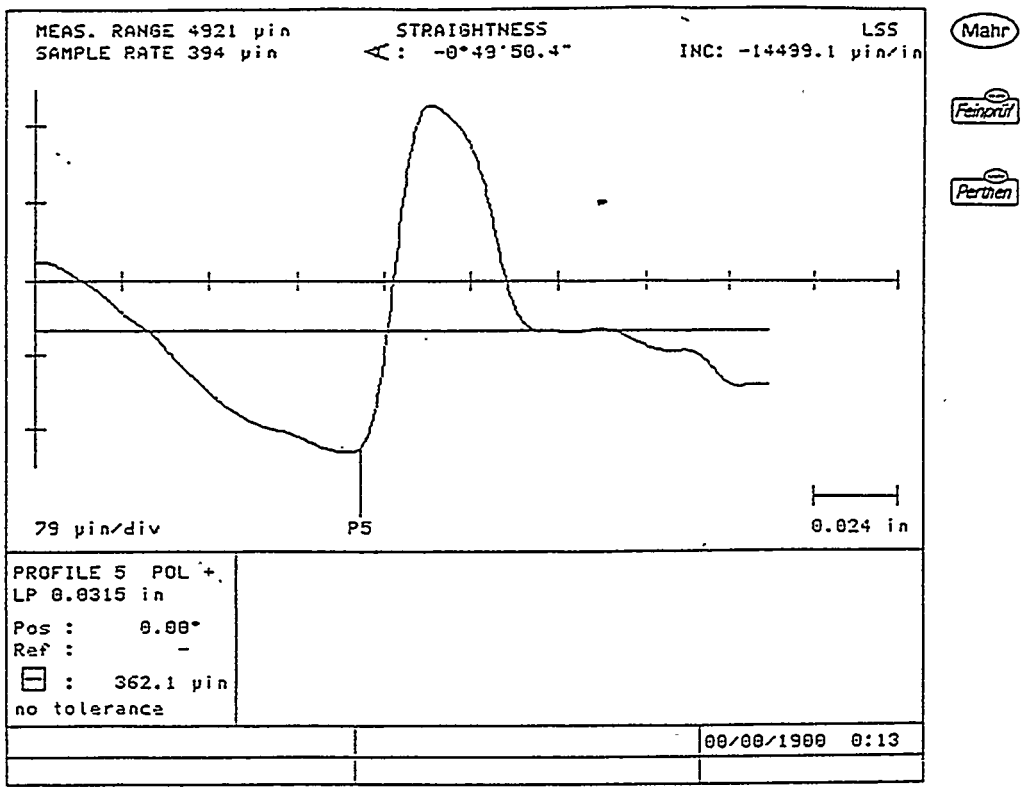

Figure 4. Effect of 0.400 inch step-over on S/RBSN surface (V_s = 5,000 ft/min).

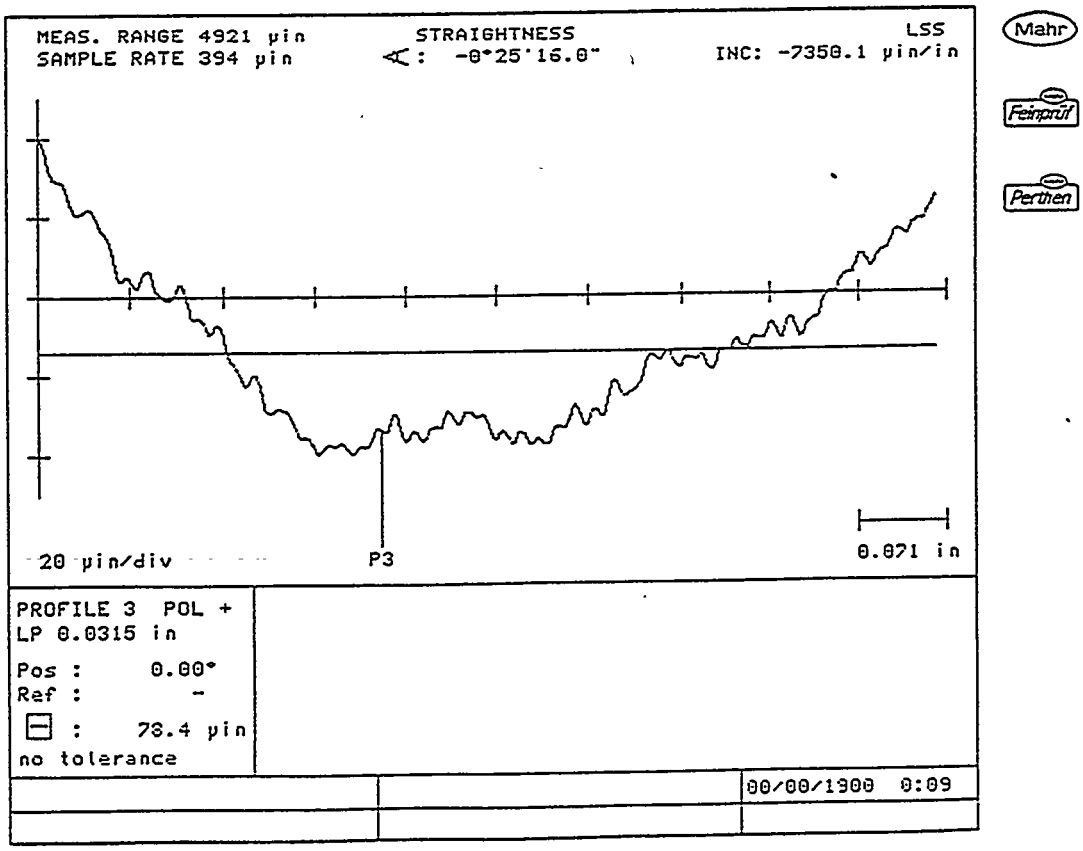

Figure 5. Effect of 0.015 inch step-over on S/RBSN surface (V_s = 5,000 ft/min).

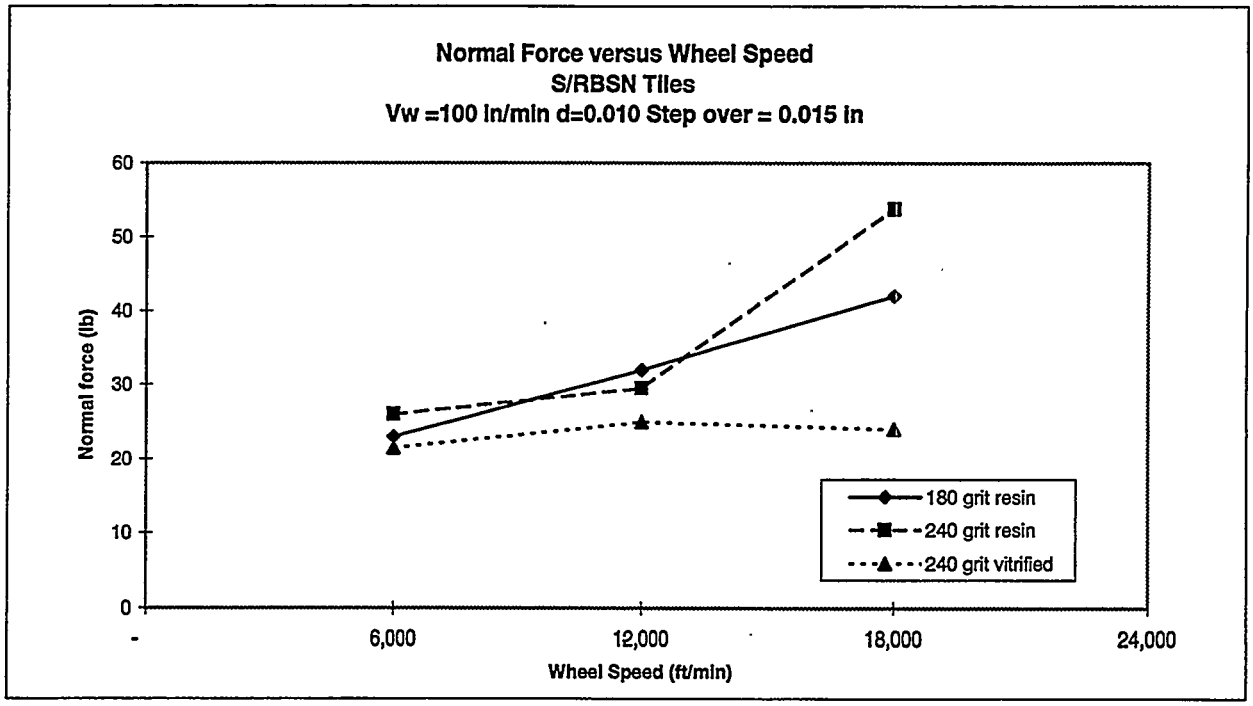

Figure 6. Normal force versus wheel speed

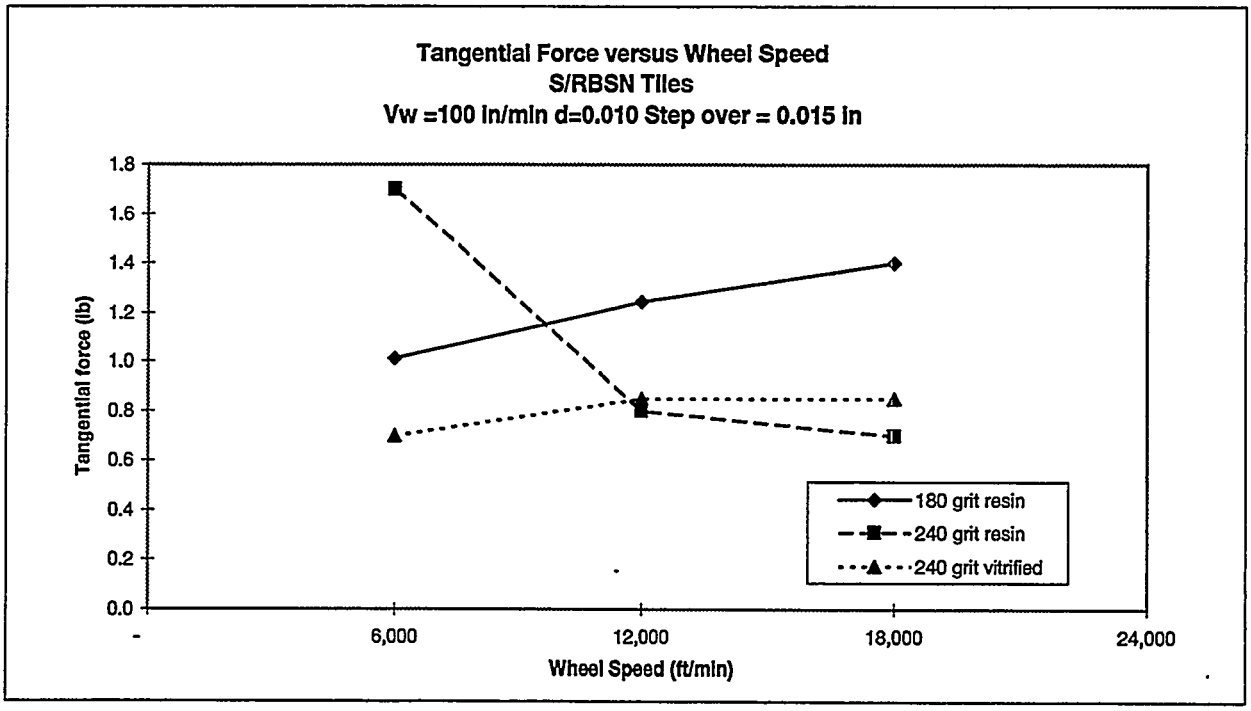

Figure 7. Tangential force versus wheel speed

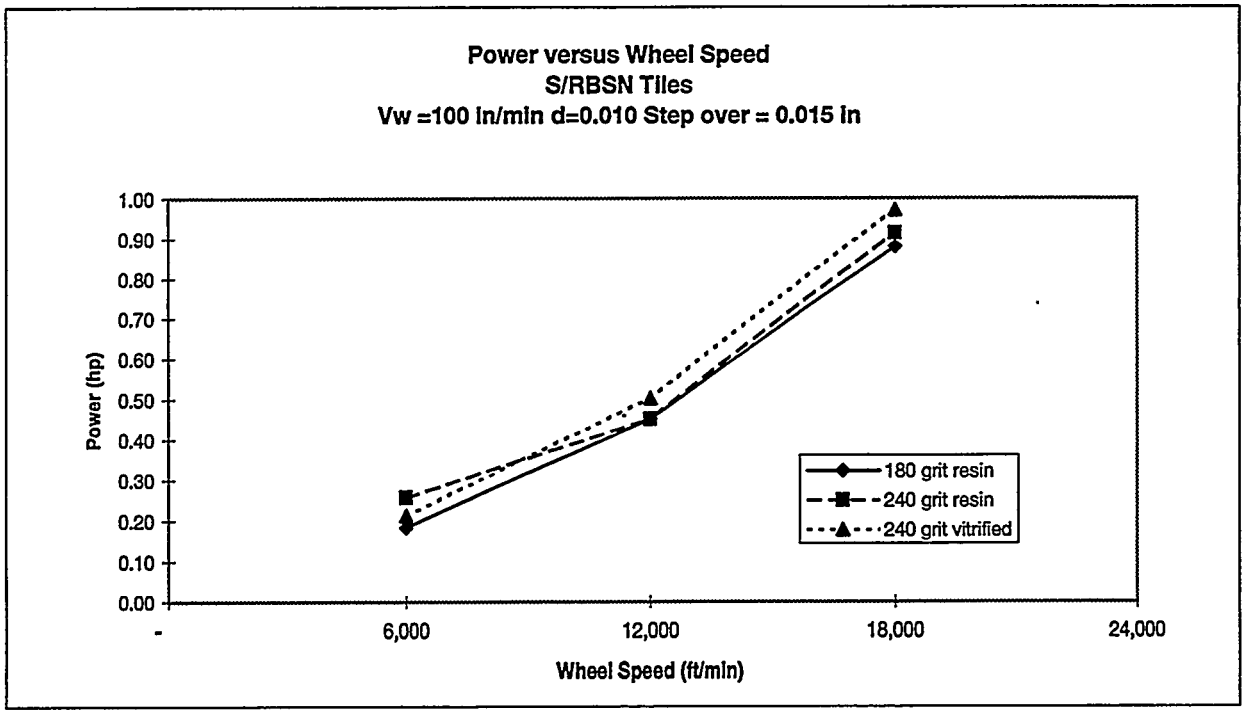

Figure 8. Power versus wheel speed

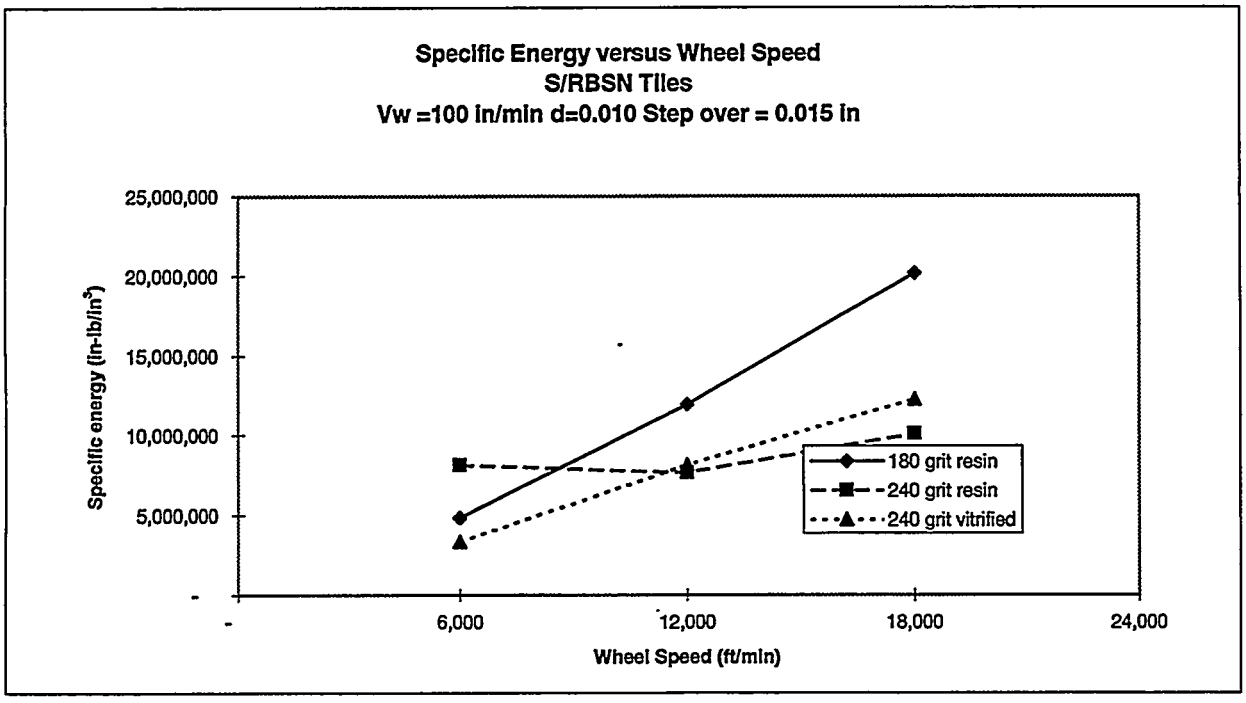

Figure 9. Specific energy versus wheel speed

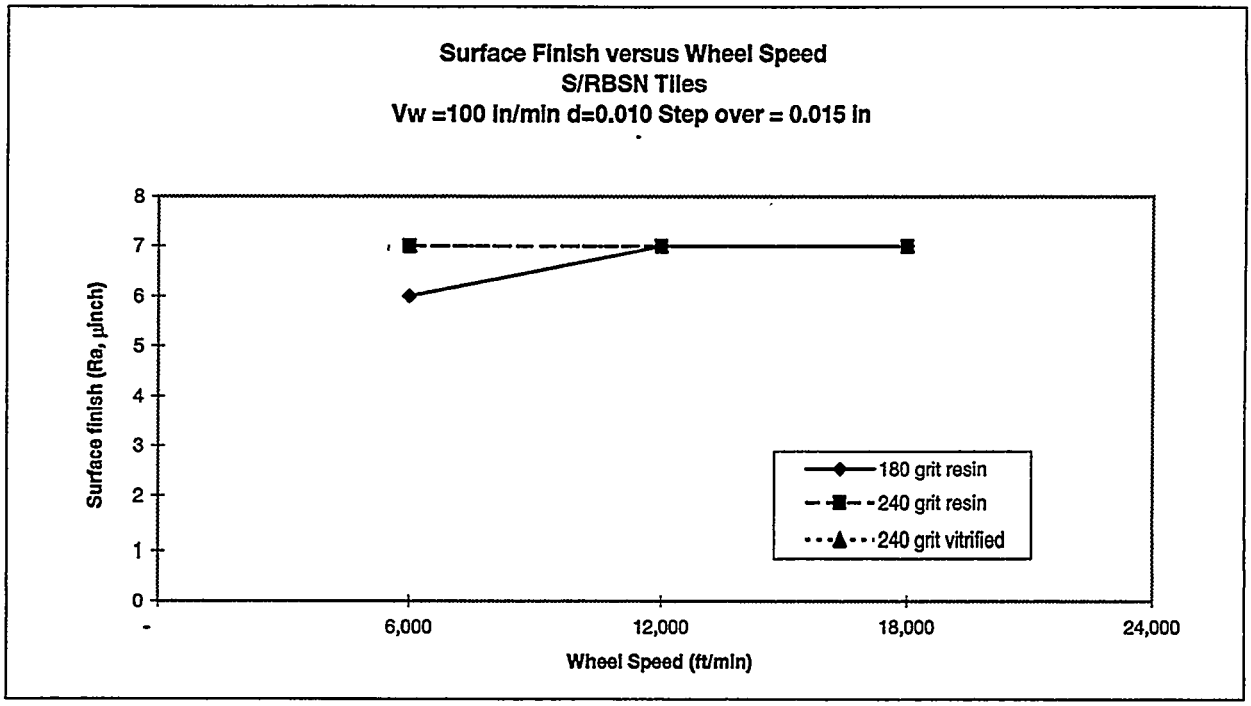

Figure 10. Surface finish (Ra) versus wheel speed

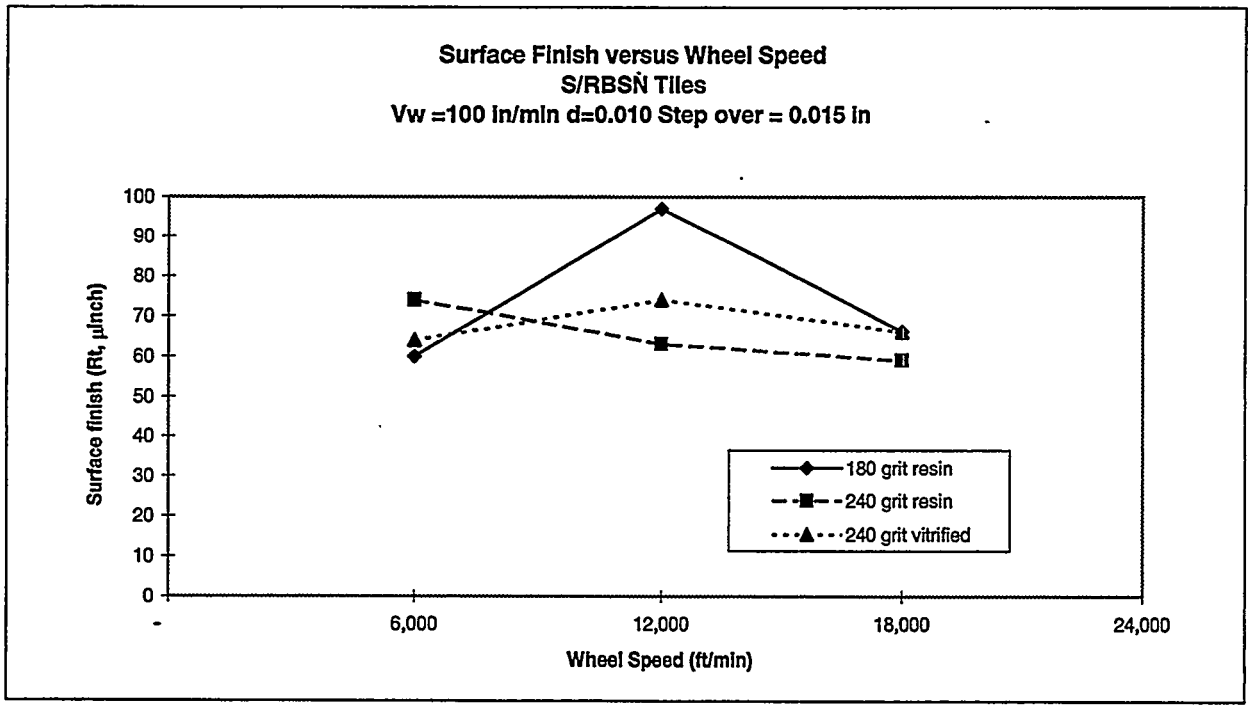

Figure 11. Surface finish (Rt) versus wheel speed

NEXT GENERATION GRINDING SPINDLE FOR COST-EFFECTIVE MANUFACTURE OF ADVANCED CERAMIC COMPONENTS

Joseph A. Kovach, Michael A. Laurich
Eaton Manufacturing Technologies Center
Willoughby Hills, Ohio 44094

Objective/Scope

The overall objective of the Next Generation Grinding Spindle (NGS) program is to design, develop, test and demonstrate the operation of a next-generation, high-stiffness spindle to be used for centerless grinding of ceramic components. More specifically, the goals lead to the demonstration of a 50 hp, twin-grip, centerless grinding spindle capable of using 12-14" diameter by 8-12" wide grinding wheels with at least 7,000 rpm capability in a through-feed or in-feed grinding mode. The spindle stiffness is to be at least 2,000,000 lb/in. Program activities involve the development of a spindle bearing arrangement as well as an integral spindle/motor package. Accordingly, to achieve the overall program objective, this Phase I effort is comprised of the following six (6) major Tasks:

1.0 Spindle Design and Verification Testing
2.0 Motor Development
3.0 Wheel Hub Development
4.0 Wheel Balancer Development
5.0 Sensors, Sealing and Support Hardware Development
6.0 Final Assembly, Testing, and Demonstration

Technical Highlights

This first NGS Phase I semi-annual report summarizes progress achieved between October 1 ,1996 and March 31, 1997 in the following technical areas:

1.0 Spindle Design and Verification Testing

The overall spindle package design has been completed. As anticipated, the final design uses an "inside-out" bearing configuration which allows for the grinding wheel/hub to rotate about a fixed shaft (e.g. wheel/axle configuration). Initially, the spindle was going to be developed for below-center centerless grinding using a Modler centerless grinder for demonstration. Recently, however, Eaton/MTC has acquired a new Cincinnati Milacron Viking centerless grinder. Since this machine is now commercially available, it was decided to alter the spindle configuration for use in the new smaller Viking machine rather than build a spindle for a one-of-a-kind custom centerless grinder. In this regard, the motor was

moved from an outboard position to a location between the bearings. This was necessary since the Viking has only 12" between the spindle saddles whereas the larger Modler has nearly 20 inches. In any event, the new design still allows for utilization of 14" diameter by 10" wide grinding wheel.

As of consequence of the new smaller packaging, the effective bearing width was also reduced. This tends to limit the choices for alternative bearing options. However, after considerable analysis a hydrodynamic bearing arrangement was selected which is capable of meeting all program goals. The selected bearing design is based upon a pivoted-pad hydrodynamic bearing concept using 3 pads where 1 of the pads can be hydraulically actuated for controlled compliance and bore diameter compensation. As a simplified back-up, the hydraulic actuator can be replaced by a spring to maintain some level of preload.

In general, conventional "plain shell" hydrodynamic bearings provide good damping, long service life, and require a minimum of support equipment. On the downside, however, conventional hydrodynamic bearings tend to lack stiffness, high speed stability, and, to some extent, precision. To improve stability, precision, and stiffness the pivoted pad approach was selected. Unfortunately, based on hydrodynamic bearing calculations, the initial designs tended to lack stiffness at light loads. In an effort to improve stiffness at low operating loads, the concept of actively altering the bearing preload/clearance was investigated. With this approach, bearing stiffness can be controlled in real-time by changing the radial bearing clearance. This is achieved by hydraulically moving 1 pad in a radial direction. The results of this investigation indicate that a stiffness above 1,000,000 lb/in per bearing can be realistically achieved over the entire anticipated operating load. To achieve the design goal of 2,000,000 lb/in stiffness a total of 2 bearings will be utilized.

In addition, it is important to recognize that the "active pad bearing" concept also allows for automatic compensation of minute changes in bore diameter arising from thermal or mechanical growth. Based on dynamic load calculations, it was learned that the bearing bore could "grow" up to 0.006" in diameter from centrifugal loads alone. As an alternative, increased use of light weight composite materials would reduce, but not eliminate, differential centrifugal expansion rates. Consequently, the APB (active pad bearing) concept was developed. Nevertheless, in the final embodiment it is anticipated that a considerable degree of carbon fiber composite material will be utilized to improve thermal and mechanical stability of the spindle system at high speeds.

Note that initially, the pivot point design was based upon a simple EDM'ed cantilever arrangement which could provide for the required pivoting motion, but is unable to effectively compensate for misalignment. Subsequently, a detailed misalignment analysis was conducted. The results of this analysis showed that self-aligning pads would be required to avoid bearing failure under worst case misalignment conditions. Consequently, the pivot point design was changed to a conventional ball & socket arrangement to compensate for any misalignments. Aside from pivot design considerations, the thrust bearings have also been designed and incorporated into this latest iteration.

In addition to the above spindle/bearing design activities, bearing test rig development is also well underway. Currently, the Modler is being modified to

serve as a bearing test rig. Stiffness and damping coefficients will be determined over the anticipated spindle operating range. A dummy bearing test spindle, which will evaluate the pivoted-pad bearings independently of the motor, is currently being designed.

2.0 Motor Development

Motor design has also been completed. A 10 pole, 24 slot, brushless DC motor configuration has been designed. Rare earth (bonded Neodymium) magnets of 0.6 tesla will be employed. It is interesting to note that the lamination package is only 2.6" (65 mm) wide and 9.8" (250 mm) in diameter, but yet is capable of delivering over 50 hp at 7,000 rpm (and a reserve of 65 hp at 9,000 rpm). Based on Motorsoft calculations, the motor has an efficiency of nearly 97% resulting in a total I^2R loss of 1.74 hp. Typically, these calculations would imply that internal motor cooling is probably not required. However, to improve thermal stability of the motor/spindle a novel internal water cooling jacket has also been designed. Currently, the motor/spindle package is undergoing a rigorous FEA study to analyze thermal stability and associated dimensional growth effects.). Terminal connection issues are also currently being resolved.

3.0 Wheel Hub Development

Based on the dynamic analyses discussed above, it was decided to utilize a high modulus carbon fiber composite for the wheel hub. This should provide a finish ground weight of 18 to 22 lbs and a stiffness in the hoop direction of over 24 MSI. The net effect is that at operating speeds the centrifugal forces will cause the motor rotor yoke back-iron to expand slightly more than the composite wheel hub thereby causing an effective press-fit between the wheel and spindle. The use of Differential Centrifugal Expansion (DCE) to retain the wheel will eliminate the need for exotic clamping systems while reducing wheel changeover time. Several composite hub sources and quotes are currently being obtained. One vendor has provided a firm quote and is now generating a table of anticipated wheel strength properties.

4.0 Wheel Balancer Development

Given the overall small size and extensive use of composites and superabrasive technology it is anticipated that in-process dynamic wheel balancing will not be required. Since the superabrasive grit layer will be on the order of 1/8" thick, excessive changes in wheel balance are not expected as the wheel wears. However, as a back-up, the use of a Hoffman Hydrokompensator is being investigated as well as a custom system from Balance Dynamics. Note that the Hoffman system uses a coolant droplet injection system to correct wheel imbalance in real-time and can be readily incorporated in the side of the spindle assembly.

5.0 Sensors, Sealing and Support Hardware Development

From a spindle/motor operational perspective, the system will be extensively instrumented with various thermocouples to measure bearing and motor temperatures. Bentley-Nevada probes will also be used to measure system stiffness.

Sealing of the bearings is a concern to prevent oil from leaking into the motor assembly, which may result in a dynamic imbalance problem. Several seal types have been investigated. Initially, the use of labyrinth seals was considered to minimize wear and power loss. However, it was felt that a more positive seal should be incorporated. Consequently, the use of the latest brush-type seals is being investigated in addition to high-speed Turcon lip-type seals.

A quote has also been received for a 50 hp brushless DC motor drive system. An order will be placed shortly.

6.0 Final Assembly, Testing, and Demonstration

Test stand design and preparation is underway. As indicated above, the Modler is being modified to evaluate the hydrodynamic spindle bearing assembly. Motor testing will also be conducted independently of the bearings using either a motor dynamometer stand or simply driving the motor externally and running it as a generator.

Status of Milestones

Program is on schedule. The first Milestone (Overall Spindle Design) has been completed.

Communications/Visits/Travel

1) Trips were made to Dupont to investigate composite material fabrication and to UES for assistance with the FEA thermal modeling effort.

2) J. Kovach and M. Laurich visited ORNL HTML on March 19, 1997 to review program progress.

Problems Encountered

None .

Publications

None

Development of an "Intelligent Grinding Wheel" for In-Process Monitoring of Ceramic Grinding

S. Malkin, R. Gao, C. Guo, B. Varghese and S. Pathare
Department of Mechanical and Industrial Engineering
University of Massachusetts
Amherst, MA 01003-2210

U. S. Department of Energy
Identification Number: DE-FG05-96OR22524

Introduction

This is the first semi-annual report for the project "Development of an Intelligent Grinding Wheel for In-Process Monitoring of Ceramic Grinding". This report covers the period from September 1, 1996 to February 28, 1997.

The overall objective of this project is to develop sensor-integrated "intelligent" diamond wheels for grinding of ceramics. Such wheels will be "smart" enough to monitor and supervise both the wheel preparation and grinding processes without the need to instrument the machine tool. Intelligent wheels will utilize reusable cores integrated with two types of sensors: acoustic emission (AE) and dynamic force transducers. Signals from the sensors will be transmitted from a rotating wheel to a receiver by telemetry. Wheels will be "trained" to recognize distinct characteristics associated with truing, dressing and grinding.

Technical Progress

This overall project is divided into six tasks as follows:

- Development of miniaturized sensors and data transmission system
- Wheel design and sensor configuration
- Calibration of the sensor integrated wheel
- Training of the intelligent wheel
- Grinding tests
- Prototype demonstration.

The technical progress is summarized in this report according to the tasks. All the activity during this first reporting period has been concerned with the first two interrelated tasks, which need to be completed before undertaking the remaining tasks.

Task 1. Development of Miniaturized Sensors and Data Transmission System

As stated above, the overall objective of this project is to develop sensor-integrated "intelligent" wheels for grinding of ceramics. In-process measurement of the grinding forces and acoustic emission activity resulting from the interaction between the grinding wheel and the ceramic workpiece necessitate miniaturized force and acoustic emission sensors that can be mounted in the grinding wheel core. Force and acoustic emission sensors are commercially available from various suppliers (e.g. PCB, Kistler, B&K), but their relatively bulky size precludes their integration into a grinding wheel which may be only about 0.5 inch thick. In order to overcome this problem, miniaturized force and acoustic emission sensors are being developed which utilize piezoceramic chips having overall dimensions of about 5 mm x 2 mm x 2 mm.. For force measurement, these piezoceramic chips will be sandwiched between the wheel core and the

bonded abrasive wheel rim as shown in Figure 1.1. For acoustic emission measurement, such piezoceramic chips will be embedded into the wheel core away from the wheel rim.

The advantages of using miniaturized piezoceramic chips are twofold. Firstly, their small size facilitates relatively easy integration into the wheel core, without altering the functional behavior of the grinding wheel. Secondly, the high rigidity, sensitivity, and mechanical resonant frequencies of piezoceramic chips make it possible to use them for measuring both the force and acoustic emission. By using appropriate electronic filters, high frequency acoustic emission signals in the MHz range and lower frequency dynamic force signals in the ten to hundred kHz range can be conveniently separated, thereby allowing for a compact and highly efficient system.

One proposed configuration of sensors to be tested is shown in Figure 1.2. An aluminum disk has been fabricated which contains five identical piezoceramic chips mounted in slots on the wheel core periphery within one quadrant of the disk. The piezoceramic chips held in slots at the wheel periphery have wires soldered on both sides for making electrical connections. The disk will be subjected to a range of static and cyclically varying forces. The output of all the five piezoceramic chips will be measured simultaneously by a data acquisition system. The optimal location of the sensors will be determined by comparing the output signals in terms of amplitude, frequency composition and phase relationships. More details about the evolution of the disk geometry and testing procedure are presented in the next section (Task 2).

The configuration of the data processing and transmission circuitry is shown in Figure 1.3. The charge amplifiers convert the electrical charge from the sensors to a voltage signal proportional to either the

amplitude of the applied forces or the acoustic emission. Signals from the charge amplifiers are filtered to limit their bandwidths to a known range and remove the irrelevant noise. The Analog/Digital conversion module, operating at a sampling rate of about 2 MHz, will log the data into the Digital Signal Processor (DSP). After analyzing the data, the DSP will send out only the relevant part of the signal through its serial output port to a data transmitter which operates in the 900 MHz range. Since this is an ISM band, no special license for RF operation is required for systems whose power output is below 1 W. The transmitted signal is received and fed through interface module to a PC data logging and processing.

Task 2. Wheel Design and Sensor Configuration

As stated above, the "intelligent" grinding wheel will consist of a disk-shaped wheel core with abrasives in a resin bond on its periphery. The wheel core houses the piezoceramic sensors and the associated electronics necessary for data conditioning and transmission.

Two approaches were considered for mounting the sensors. The initial design concept was to utilize sensors mounted in a number of cavities milled in the disk-shaped core and firmly held in place by a wedge arrangement (Figure 2.1). The deformation of each cavity under an applied grinding force causes an electrical charge on the surface of the piezoceramic sensor. The electrical charge is fed to the charge amplifier and converted to a voltage signal. The magnitude of the voltage signal is proportional to the force.

The response of the sensors is highly dependent on the system compliance, which in turn depends on the dimensions of the cavity and its location. The influence these parameters on the sensor response was analytically investigated by using a finite element (FEM) analysis. A finite element model of the

wheel with six force sensors, mounted 60 degrees apart, was developed using ANSYS in order to determine the sensor response and optimize the cavity location (Figure 2.2). The specification of the wheel and the corresponding material properties of the core and the abrasive are listed in Table 2.1. Only half of the wheel was modeled in order to keep the computation within reasonable limits without loss of accuracy. The grinding action was simulated by applying a concentrated line force across the width of the wheel at its periphery. Separate static analyses were conducted at different angular locations of the wheel in order to simulate the effect of wheel rotation. The sensor response was determined by calculating the deformation of the cavity walls under the influence of an applied load.

The first set of numerical simulations was performed to investigate the response of the force sensors to a rotating load at a fixed radial location (0.19 inch from the wheel surface) of the cavity. At first, the force was applied directly under the cavity and the static response of the all the sensors (deformation of the cavity) was determined by using the finite element method. The load was then moved to a different angular location and the static solution was repeated. Figure 2.3 and 2.4 show some of the typical results obtained from the finite element analysis. As seen in Figures 2.5, the response of the sensor rapidly diminishes as the load moves away from the sensor location. Virtually no response was visible for most of the angular locations of the load. This result indicates that the arrangement of the sensors on the wheel is critical, especially when the roundness and waviness of the wheel during the grinding process are to be monitored.

One possible way to enlarge the region of sensor response is to relocate the sensors radially inward away from the grinding wheel periphery. However, this will lead to a reduction in sensitivity. To investigate the relationship between the radial location of the sensors and their response, numerical

studies were conducted by FEM simulation of the structural response of the wheel at various locations. The results are shown in Figures 2.6 and 2.7. The sensitivity showed a rapid decrease (Figure 2.6) as the sensor was moved radially inward with no appreciable increase in the region of sensor response (Figure 2.7).

The results from this finite element analysis suggest the need for more sensors. The second design concept is based upon increasing the number of sensors. In order to increase the number of sensors, the sensor cavity was modified into a narrow slot located at the periphery of the disk (wheel core). Such an arrangement permits a large number of slots and sensors around the periphery of the wheel as seen in Figure 2.8. With this arrangement the piezoceramic sensors will be glued in the slots at the core periphery where the bonded abrasive rim is attached. The proximity of the sensors to the grinding wheel surface also increases the sensitivity.

A series of experiments will be conducted to test this design. Figure 2.9 shows a schematic of the proposed experimental setup. The test disk with sensors glued in the slots will be mounted on an Instron testing machine which provides static or cyclical loads. An abrasive layer will be attached to the disk periphery using a two-component epoxy. The epoxy also helps to protect the sensors. A preliminary set of tests will be conducted to evaluate the sensor arrangement. For these initial experiments, the sensors will be directly wired to the data acquisition system. This will be followed by full scale testing with telemetric data transfer.

Publications

None to date.

Trips and Meetings

Stephen Malkin attended a meeting at ORNL on September 11-12, 1996 to make a presentation describing this project.

Personnel

- Stephen Malkin, Sc.D., Professor, Principal Investigator

  Overall project management, grinding test and analysis.

- Robert Gao, Ph.D., Assistant Professor, Co-Principal Investigator

  Design of miniaturized sensors, telemetry, and microelectronics; testing, and prototype demonstration.

- Changsheng Guo, Ph.D., Senior Research Fellow, Co-Principal Investigator

  Mechanical design, setup, testing and prototyping of grinding wheel.

- Biju Varghese, Graduate Research Assistant, Ph.D. Student

  Mechanical design, calibration, training and testing of the grinding wheel prototype

- Sumukh Pathare, Graduate Research Assistant, M.S. Student

  Sensor development, electronic circuits design, implementation, and testing.

Wheel Dimensions	
Outer diameter	**12 inches**
Inner diameter	**5 inches**
Width	**0.5 inches**
Abrasive thickness	**0.125 inches**

Abrasive properties	
Elastic modulus	**2×10^{-6} N/mm^2**

Sensor holder (core) properties	
Elastic modulus	**10×10^{-6} N/mm^2**

Table 2.1 Wheel dimensions and material properties

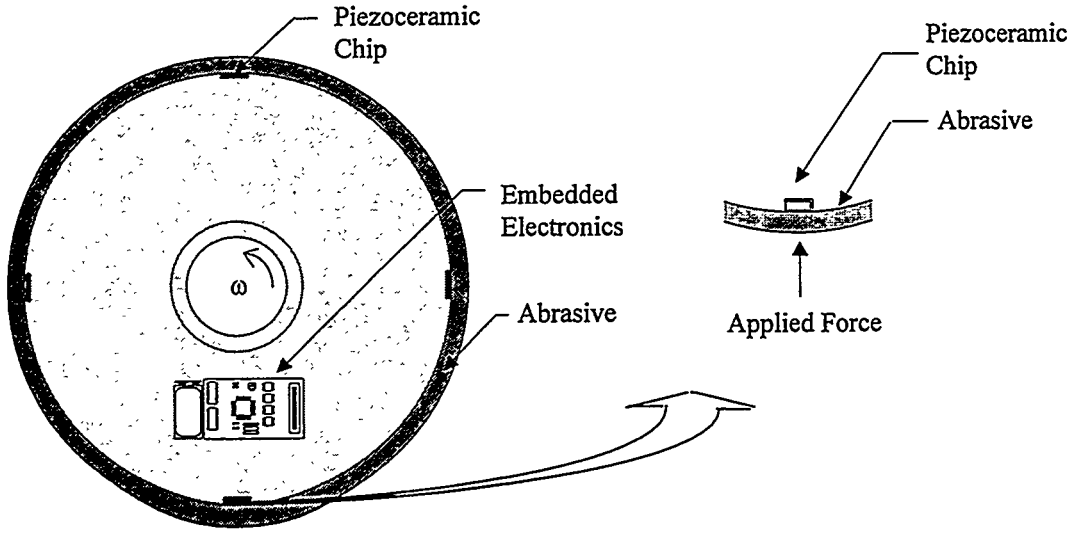

Figure 1.1 Schematic view of a sensor-embedded grinding wheel

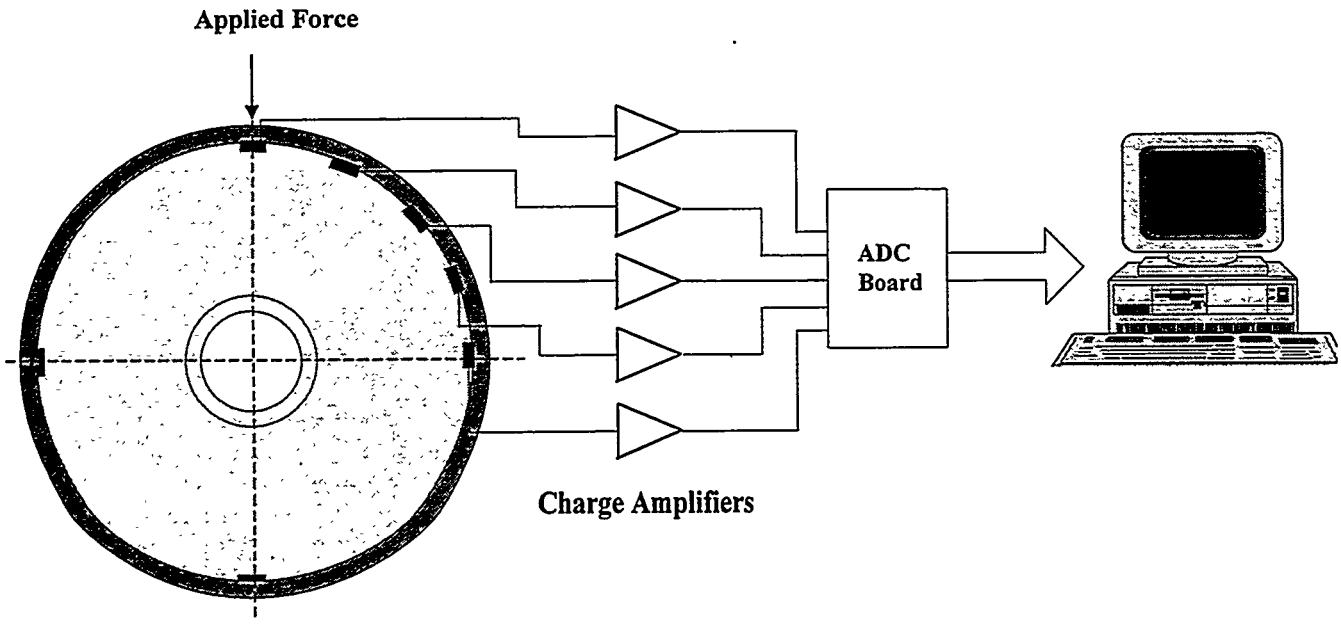

Figure 1.2 Configuration of the disk for testing the arrangement of sensors

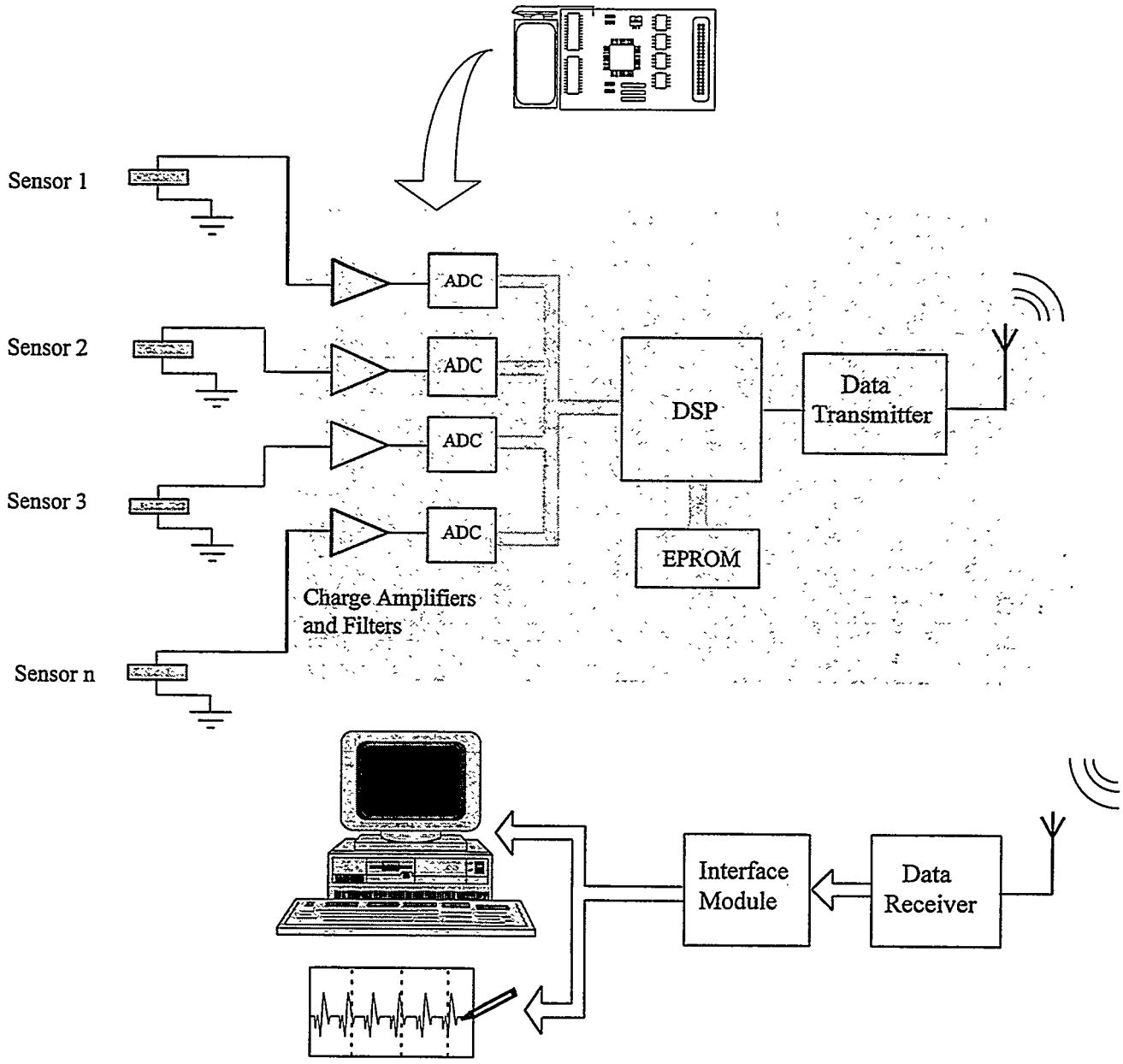

Figure 1.3 Configuration of the data processing and transmission system

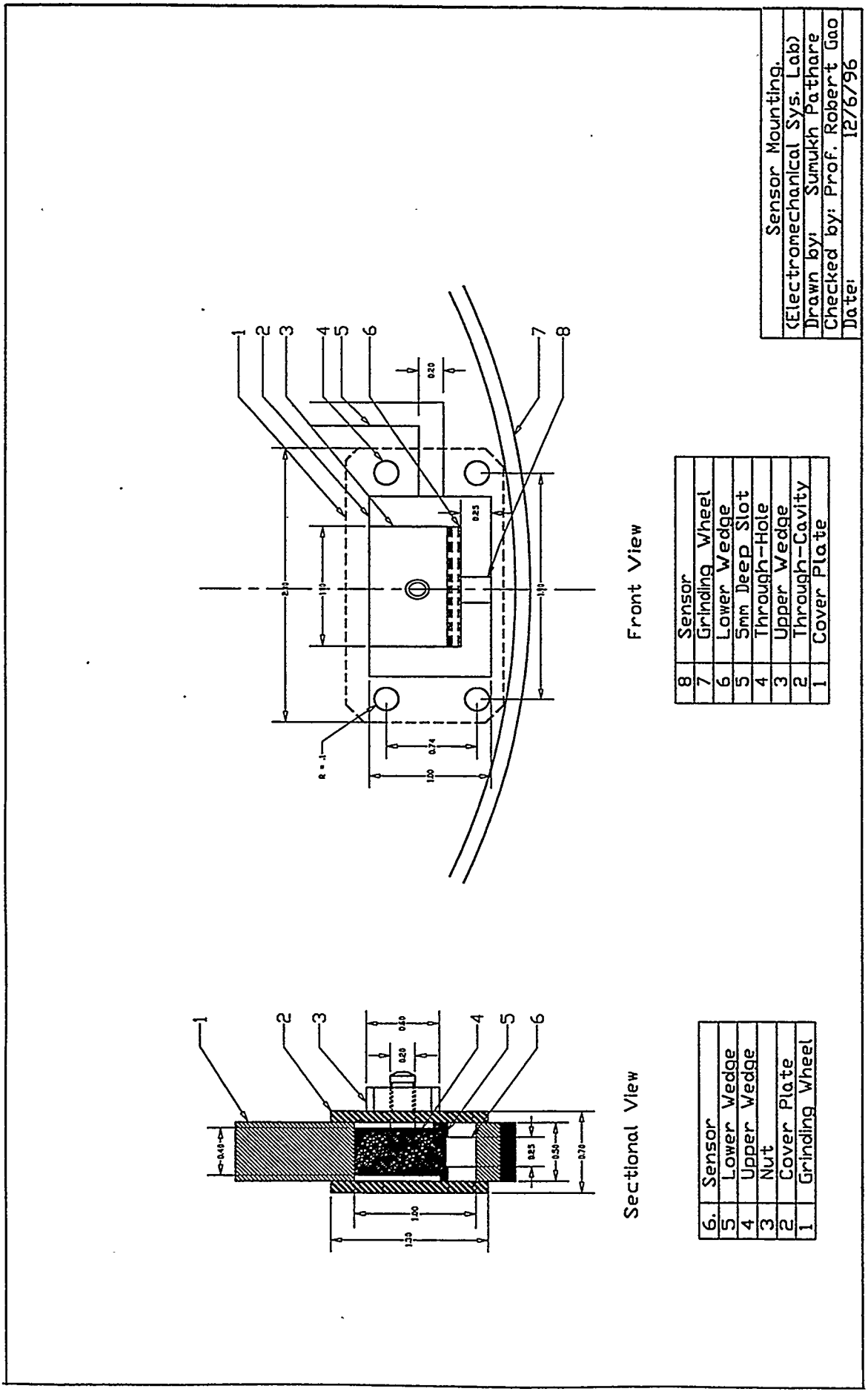

Figure 2.1 Sensor arrangement using cavities on the wheel core

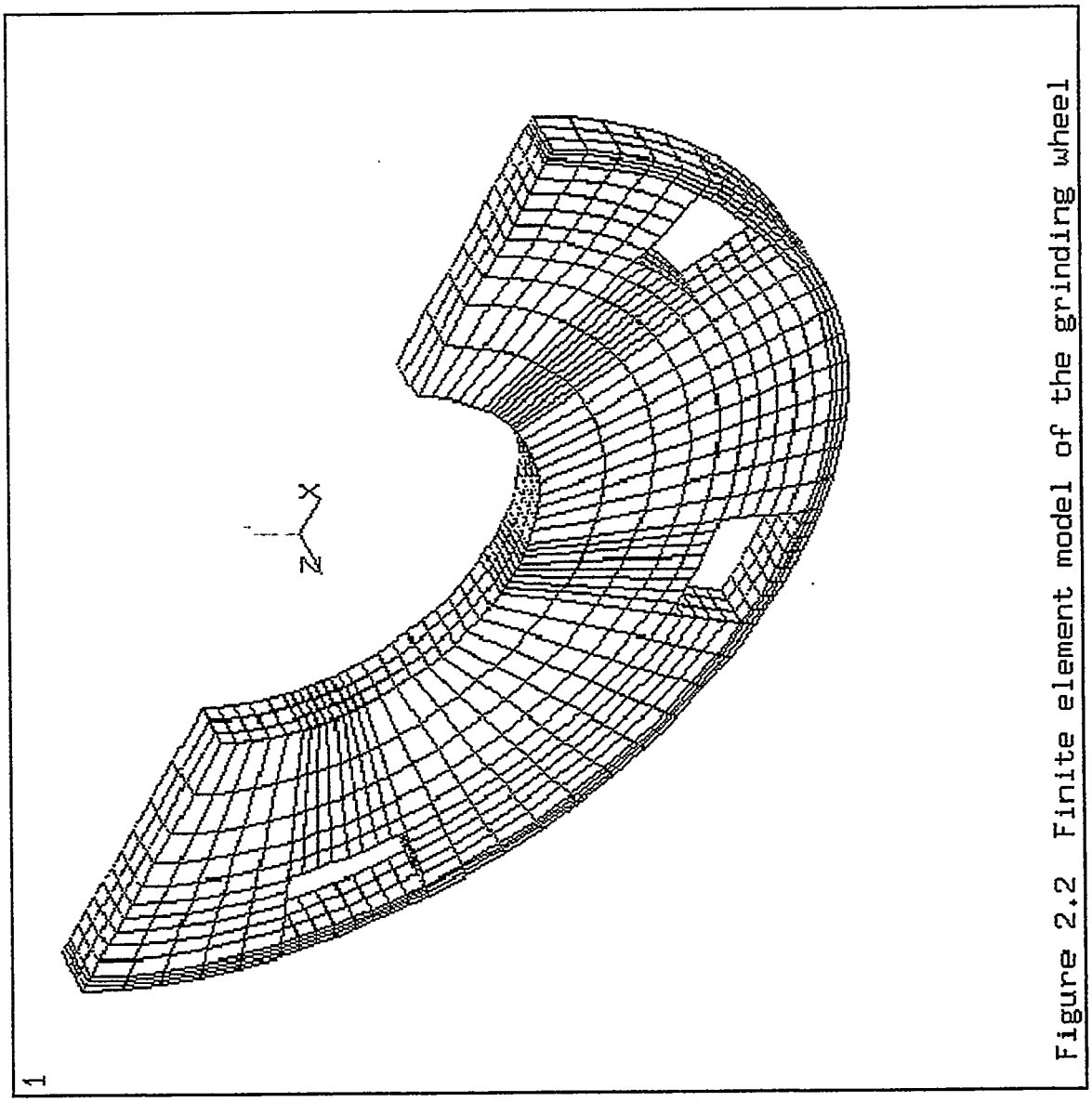

Figure 2.2 Finite element model of the grinding wheel

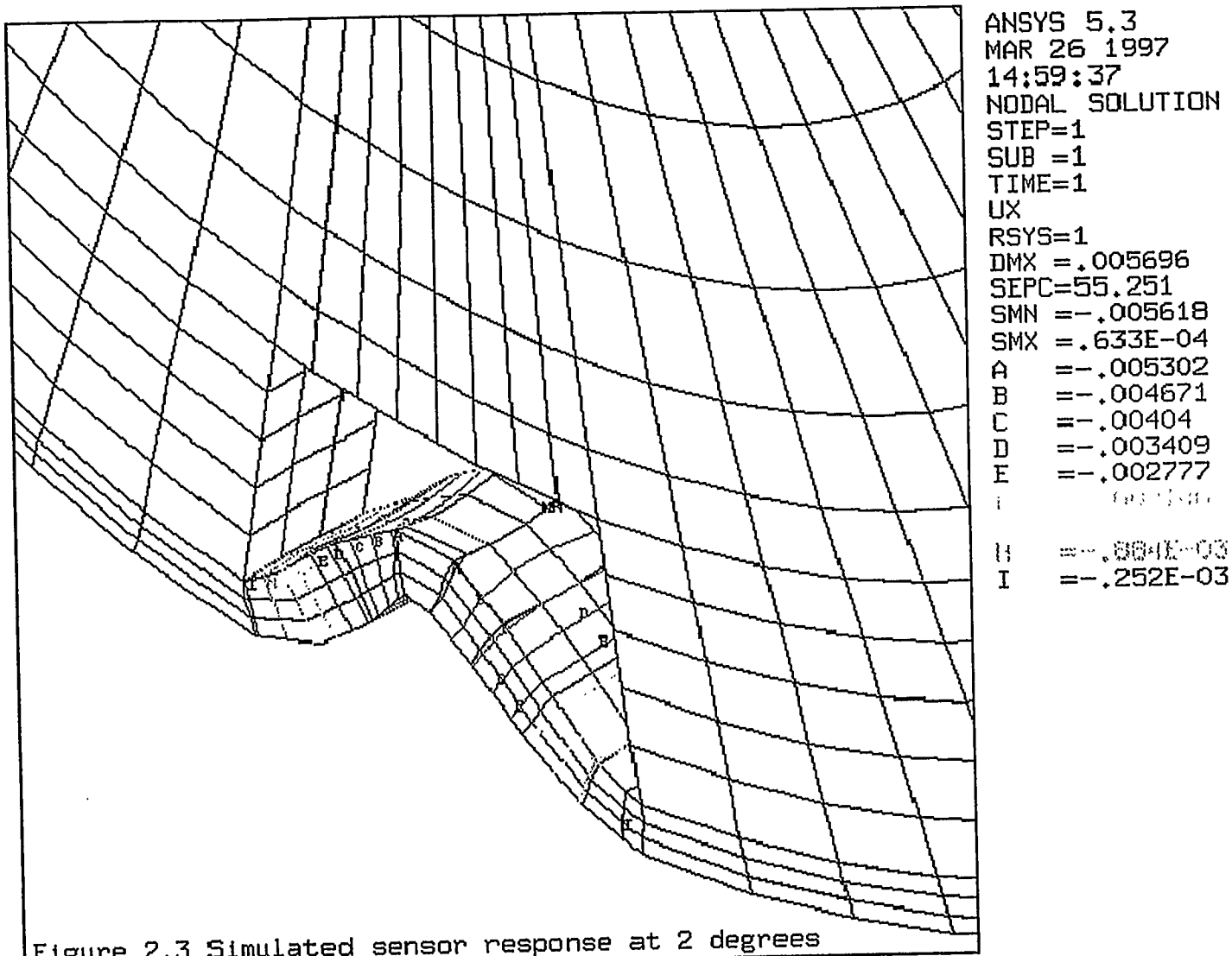

Figure 2.3 Simulated sensor response at 2 degrees

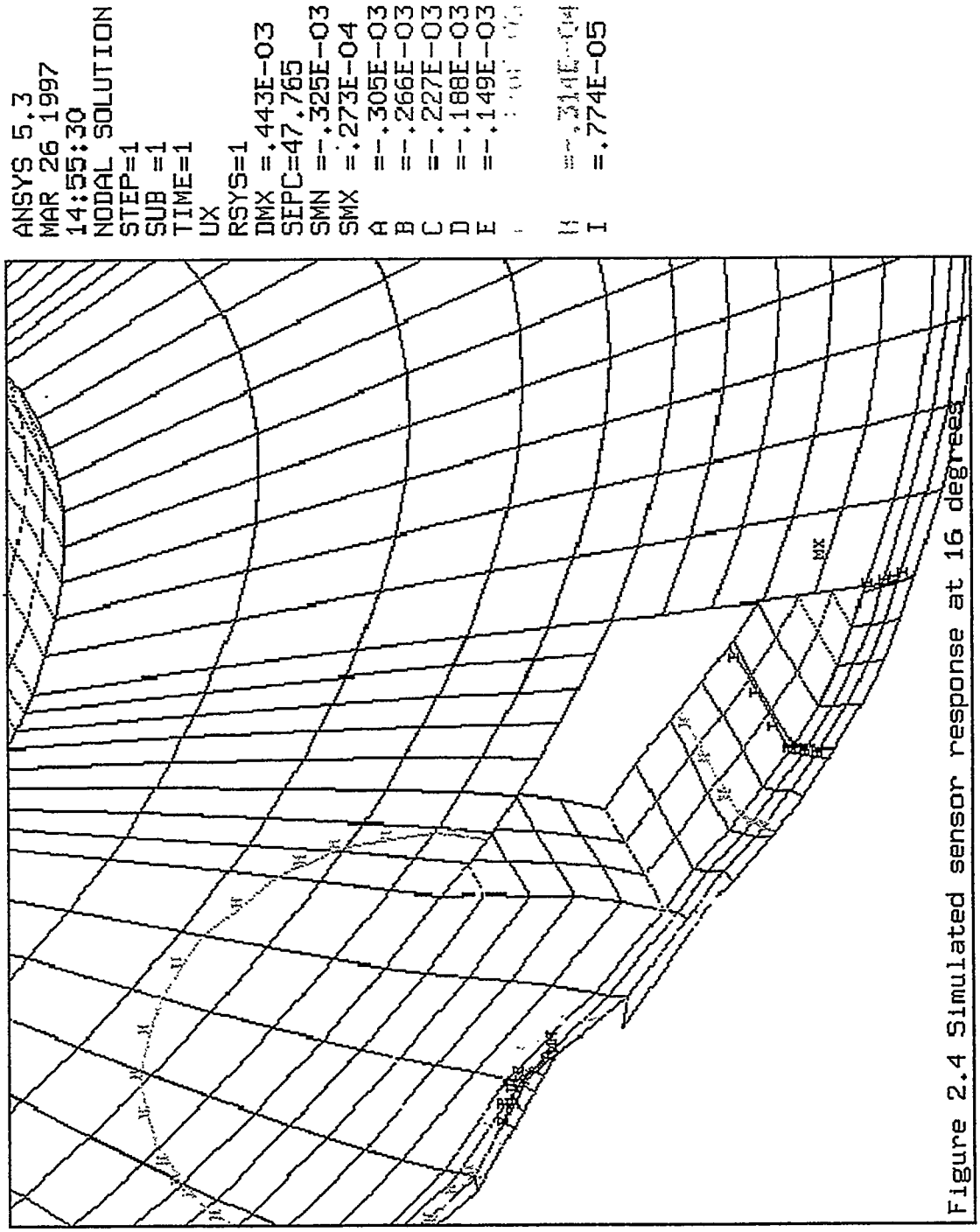

Figure 2.4 Simulated sensor response at 16 degrees

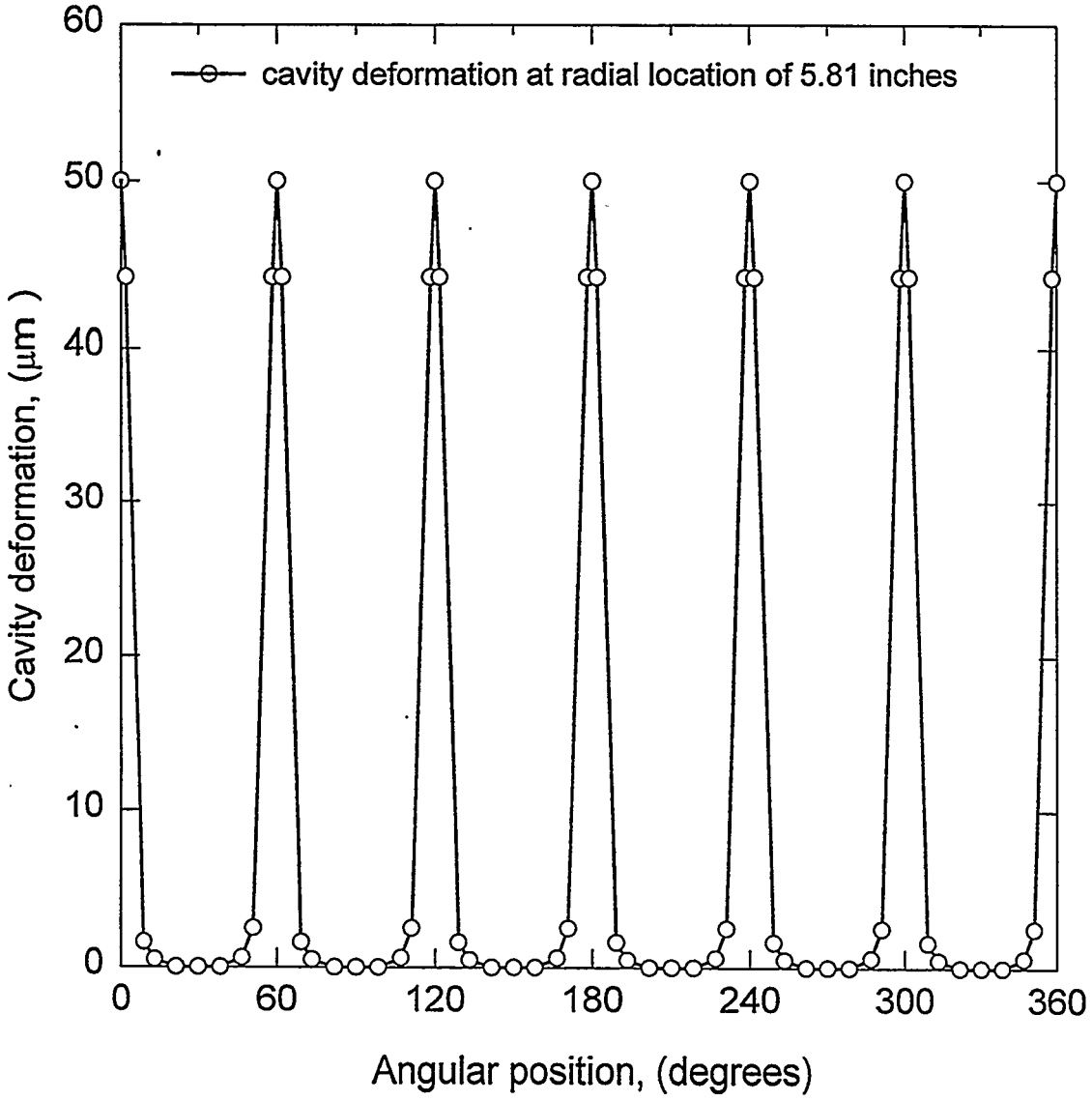

Figure 2.5 Sensor repsonse versus angular position

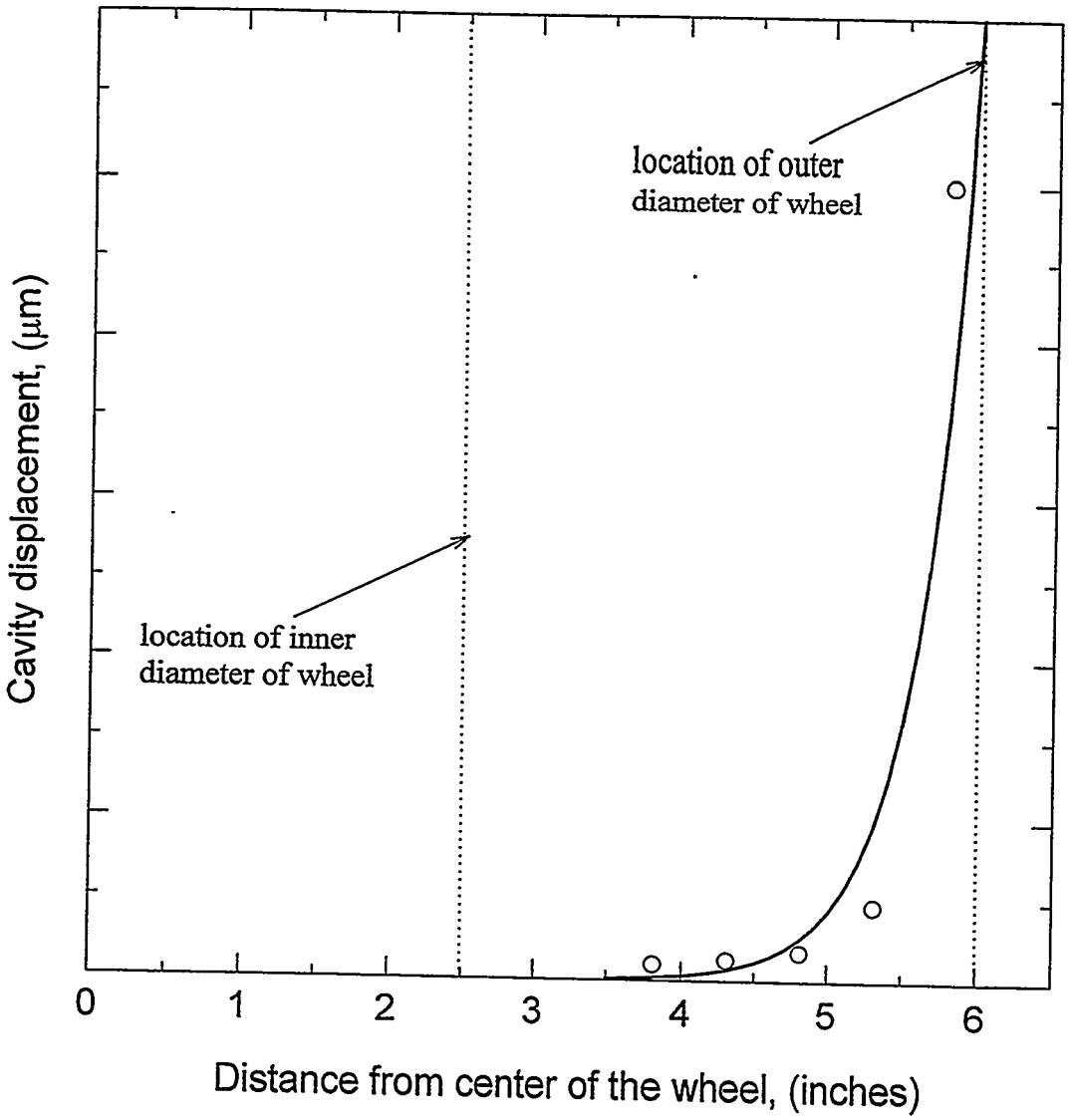

Figure 2.6 Sensor response versus radial loaction of cavity

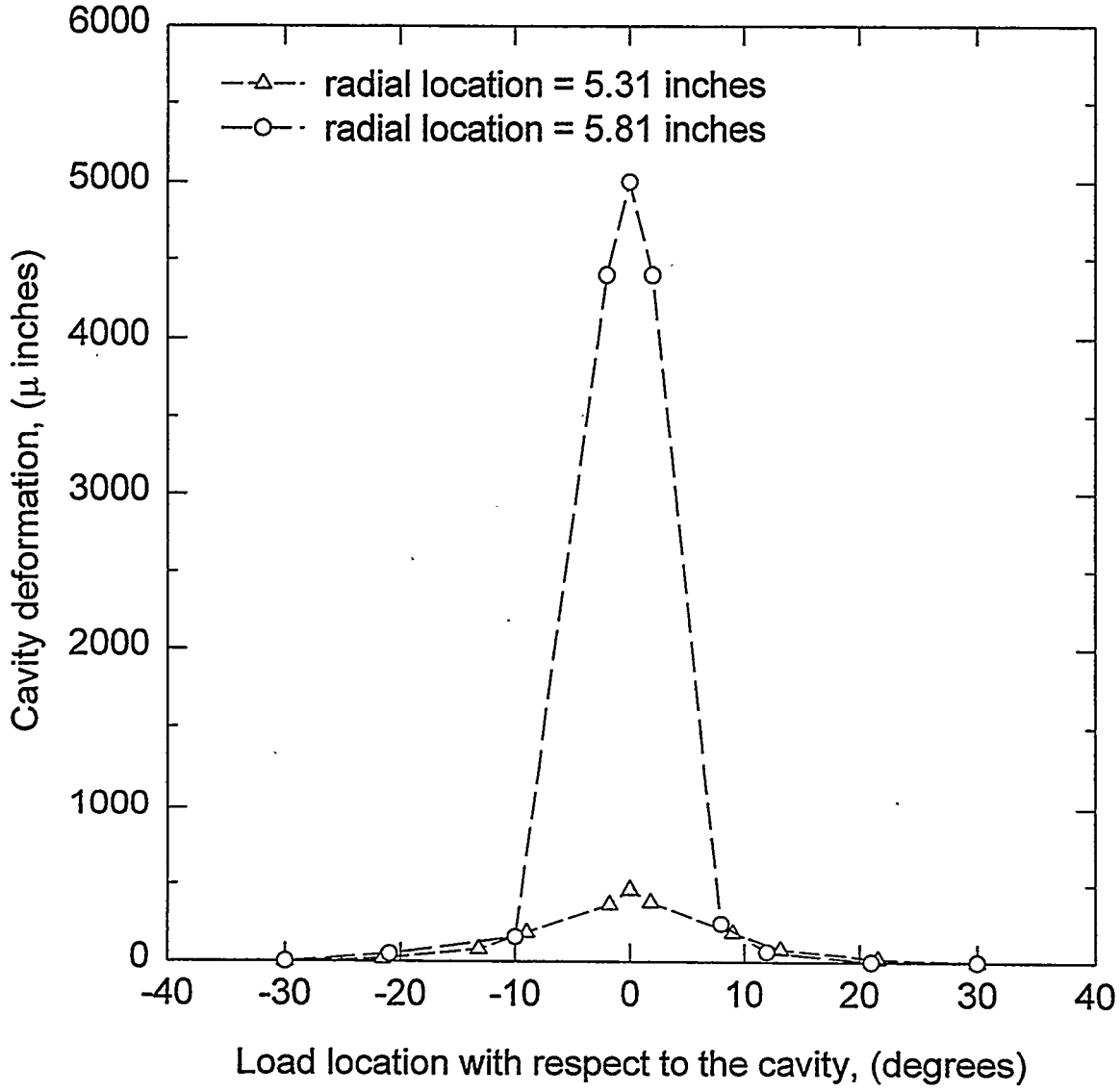

Figure 2.7 Sensor repsonse versus location of load

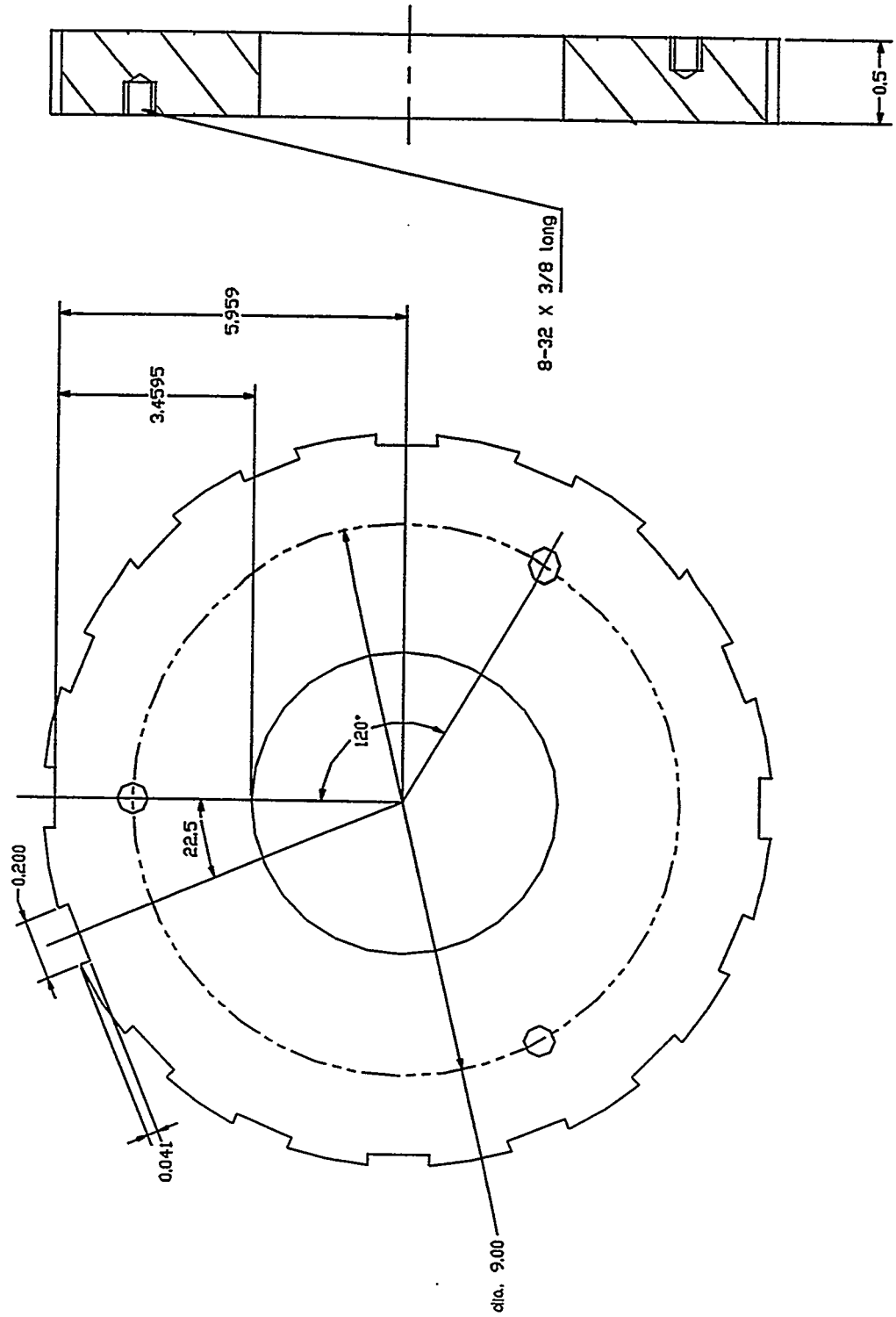

Figure 2.8 Aluminum disc (wheel core) for mounting sensors

(All Dimensions in inches)

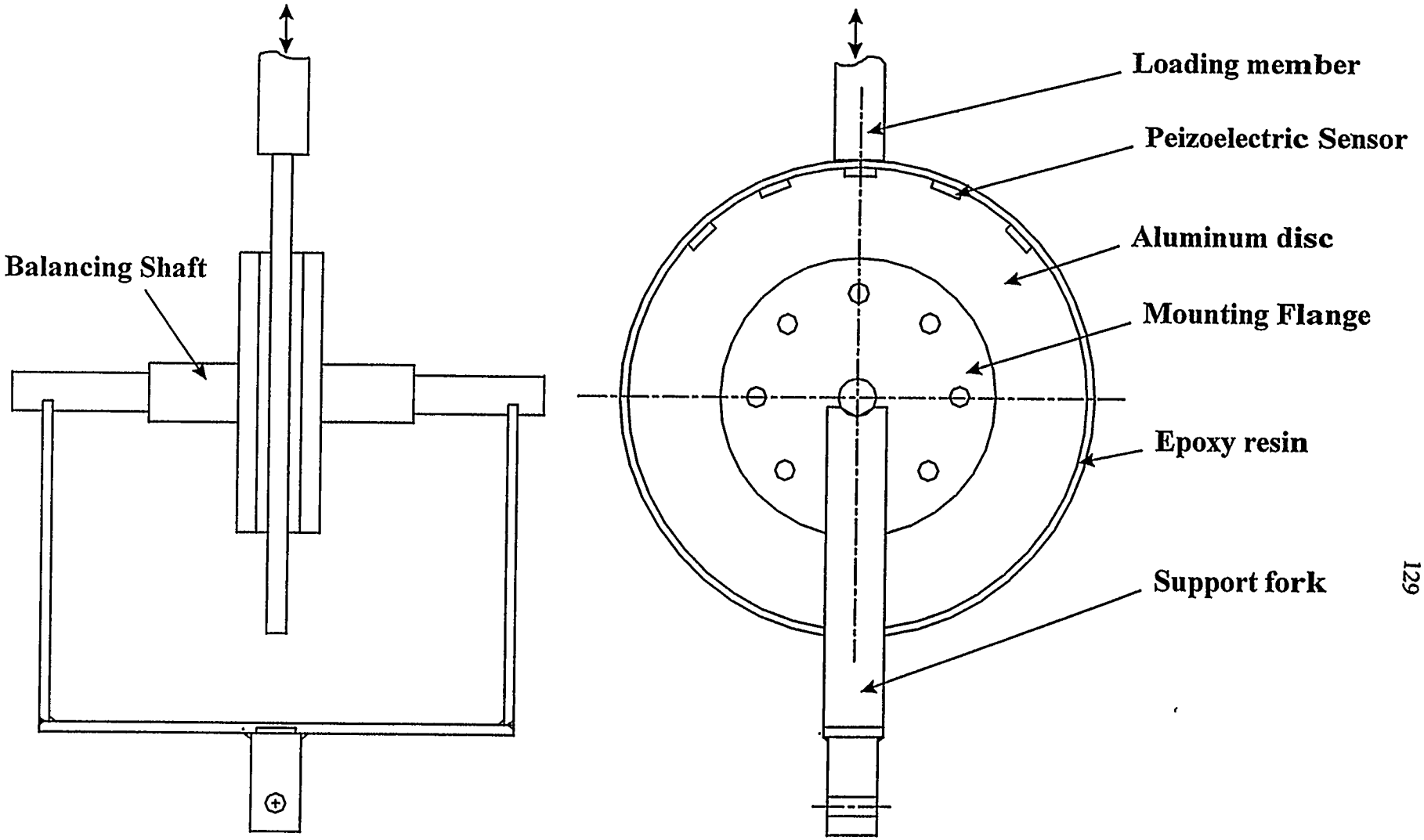

Figure 2.9 Schematic diagram of the experimental setup

Laser Scatter Methods for Detecting Subsurface Machining Damage in Ceramics – Jiangang Sun, William A. Ellingson, George A. Forster (Argonne National Laboratory), Michael H. Haselkorn, and Charles J. Anderson (Caterpillar Inc.)

Objective/scope

The primary objective of this program is to develop a laser scattering procedure that would provide a direct (near-real-time) indication of changes in the subsurface (and surface) during machining. These changes include machining-induced damage (such as median crack formation) and surface roughness. A second objective is to evaluate dye penetrant technology as an off-line indicator of surface-breaking cracks. The laser program is being executed in three steps. The first is evaluating optimization of the laser scattering procedure to examine specimens machined by innovative techniques. The second step will involve correlation of the laser scattering results with mechanical properties in "real" machined ceramic specimens. The final step will be to develop a prototype instrument to be evaluated for on-line implementation in a production environment. The investigation into dye penetrants for surface-defect detection is being conducted in three steps: review of literature, off-site visits to appropriate current users (e.g., Norton) and vendors (e.g., Sherwin, Inc.), and laboratory experiments.

Technical progress

1. Elastic Optical Scattering Results

The research for the second phase of this project has been finalized between ANL and Caterpillar. Caterpillar will be the prime contractor and ANL is to be the subcontractor. It will be focused on establishing correlations between laser scatter data with specimen microstructure and mechanical properties. Two Si_3N_4 materials will be studied: a) RBSN, Ceralloy 147-E3, and b) sintered, GS-44. A first set of 12 machined samples have been prepared by Caterpillar, and they are expected to be delivered to ANL in the next period.

We have started the effort to establish correlations between the elastic optical scattering data and the surface microstructure and machining damage. We used the rotary-ultrasonic machined sample HP38AAA in this study. This sample has been studied earlier in this project. Figures 1a-c show a photomicrograph and elastic optical scattering sum and ratio images near a corner on this sample. In the photomicrograph, Fig. 1a, it is seen that many white spots exist on the surface. These spots are correlated with the white spots on the laser scatter sum image (Fig. 1b) and black spots on the ratio image (Fig. 1c). These spots are roughly arranged in circles, and they are presumably the results of machining damage. In order to develop reliable correlations, we need to determine the sensitivity of the measured scatter data. Figure 2 shows a gray-scale profile plot along the Line AB shown in the sum image of Fig. 1b. It is evident that the intensity and shape of the various damage spots is different.

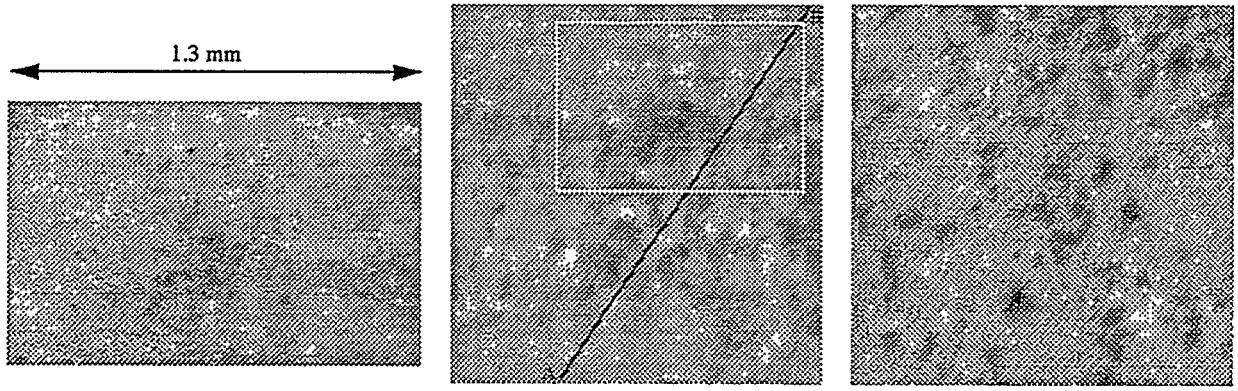

Fig. 1 Surface images for a corner of the rotary-ultrasonic machined sample HP38AAA: (a) photomicrograph, (b) elastic optical scattering sum image [the region in the white frame corresponding to the area in (a)] and, (c) elastic optical scattering ratio image

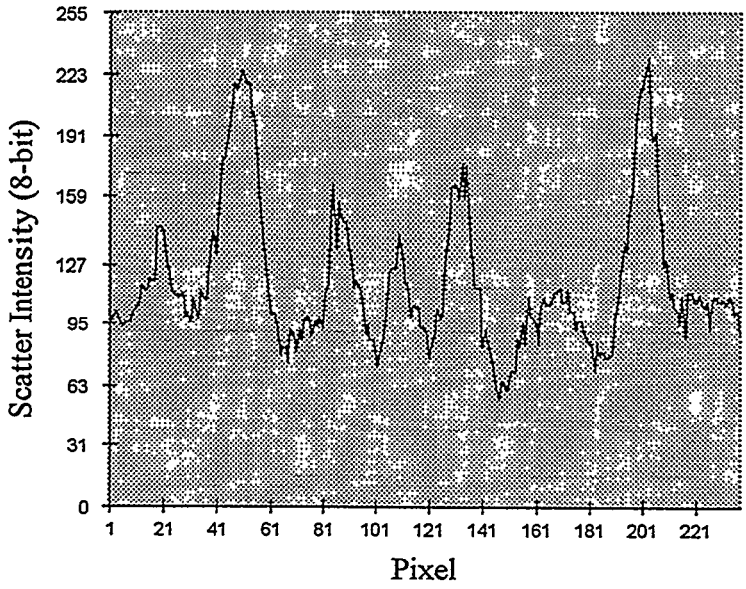

Fig. 2 Gray-scale profile plot along the AB line in the sum image shown in Fig. 1b.

2. Automation for On-Line Inspection

A demonstration of a simulated on-line inspection has been succeeded in the previous period. During this period, we have ordered and received a new Newport multi-channel optical power meter. It consists of a PC plug-in board and an amplifier box. The new PC board has a data acquisition speed up to 2000 Hz for two detectors, a significant increase from the 25 Hz speed of the older optical meter. This new meter will be installed to increase the data acquisition speed that is needed for real-time machining inspection.

Status of Milestones

All ANL milestones are on or ahead of schedule.

Communications/Visits/Travel

1. J. G. Sun presented a paper entitled "Laser-Based Optical Scattering Detection of Surface and Subsurface Defects in Machined Si_3N_4 Components" to the American Ceramic Society's 21st Annual Cocoa Beach Meeting held during January 12-16, 1997 at Cocoa Beach, FL.

2. M. Halselkorn and C. Anderson visited ANL on Dec. 10, 1996 to discuss the second phase research.

Problems Encountered

None this period.

Publications

None this period.

Milestone Schedule

Milestone:	Date	Status
1. Determine optical properties of SiAlON and GS-44 for optimum optical detection parameters (polarization, wavelength, angle of incidence, etc.).	Feb. 28, 1994	**Completed**
2. Conduct exploratory studies of dye penetrant on machined surfaces.	May 31, 1994	**Completed**
3. Submit report on dye penetrants.	Dec. 1, 1994	**Completed**
4. Correlate laser scatter analysis (ANL) of contoured specimens with mechanical properties, residual stress measurements, and mechanical surface roughness measurements (CAT).	Dec. 1, 1996	Rescheduled to Phase II
5. Correlate laser scatter results (ANL) with mechanical properties (CAT): Flat Specimens.	Dec. 1, 1996	Rescheduled to Phase II
6. Install and demonstrate prototype laser scatter device.	Aug. 31, 1996	**Completed**
Phase II: Milestone:		
7. Complete elastic optical scattering examination of first set of ground specimens.	Jun. 31, 1997	On schedule
8. Complete initial correlation of scattering data with specimen microstructure and machining-induced damage for specimen set No. 1.	Dec. 15, 1997	
9. Develop specification for laser scatter system.	May 30, 1998	
10. Complete elastic optical scattering examination of a specimen set No. 2.	Jan. 31, 1999	

TESTING AND CHARACTERIZATION

X-RAY COMPUTED TOMOGRAPHIC IMAGING

W. A. Ellingson, E. R. Koehl, H. P. Engel,
J. P. Pollinger,* and D. Twait*

Energy Technology Division
Argonne National Laboratory
Argonne, IL 600439

Objective/Scope

During this reporting period, objectives were changed to refocus the work to coincide with reorganization and restructuring of DOE's program area. The original objectives of Phase II work of this project were to (1) study the utilization of high-spatial-resolution 3-D X-ray micro-computed tomography techniques to study density distributions (X-ray densitometry) in AS-800 Si_3N_4 using special billets with final data acquisition on Series 85 nozzles; and (2) correlate destructive density analysis (to be conducted by Allied-Signal Ceramic Components) with the 3-D microtomography density data. Because rotors are no longer of technical interest, a change was made to refocus the work to study of 3-D X-ray CT densitometry reliability relative to detection of density variations in GS-44 with chopped carbon fiber. GS-44 with chopped carbon fibers is being developed as a material for valve guides as part of an effort with Caterpillar. Current processing technology is via cold isostatic pressing. Other more cost effective processing methods may be assessed and a nondestructive method to establish carbon fiber distribution would be highly desirable.

Technical Highlights

a) Correlation of Destructive to Nondestructive Density Measurements

We reported in our bi-monthly report during this period that we had obtained X-ray computed tomographic image data on the three 25 mm x 40 mm pressure slip cast AS 800 billets made for these studies. Figure 1 shows a diagram which shows where the X-ray CT (XCT) data were acquired. The individual XCT "slices" were 1 mm thick and were acquired using 424 x 424 reconstructions.

*Allied Signal Ceramic Components, Torrance, CA.

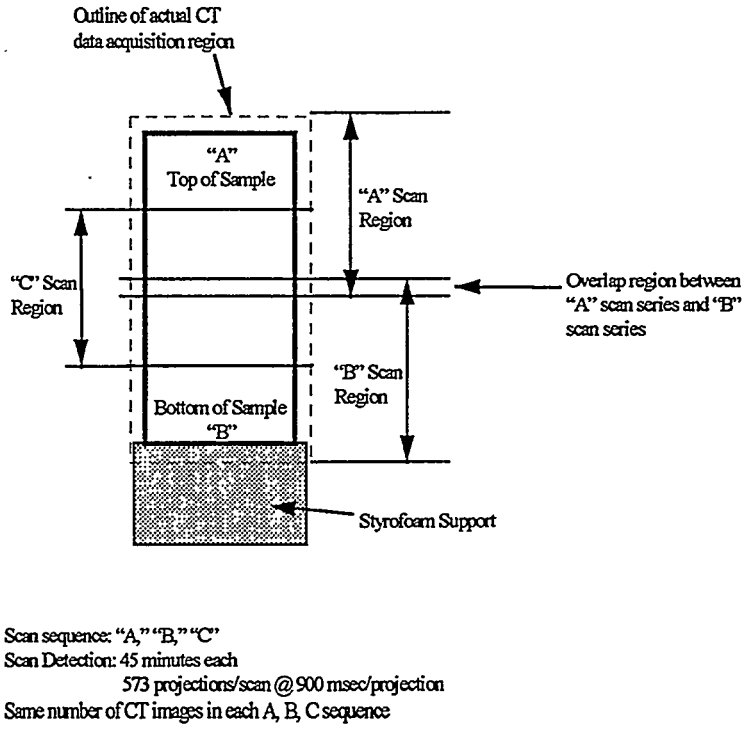

Fig. 1. Schematic diagram showing locations of A, B, C CT scan sequences

The data were then analyzed and plotted as noted in Fig. 2.

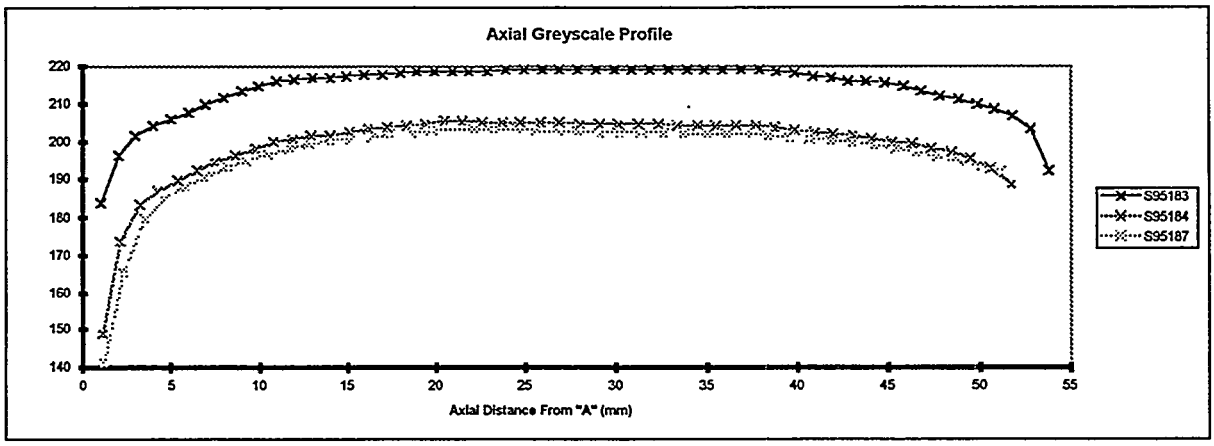

Fig. 2. Final corrected X-ray CT densitometry axial profiles used for correlation to destructive analysis.

The average % TD of the billets as sent is shown in Table 1.

Table 1. Density values of billets

Billet Number	% TD
S95183	55.84
S95184	58.44
S95187	59.03

The destructively measured density values for these three billets obtained as shown in Fig. 3, are listed in Table 2. 3-mm sections were taken off the top and bottom and the remaining 46-mm divided into 3 equal segments of about 15 mm each.

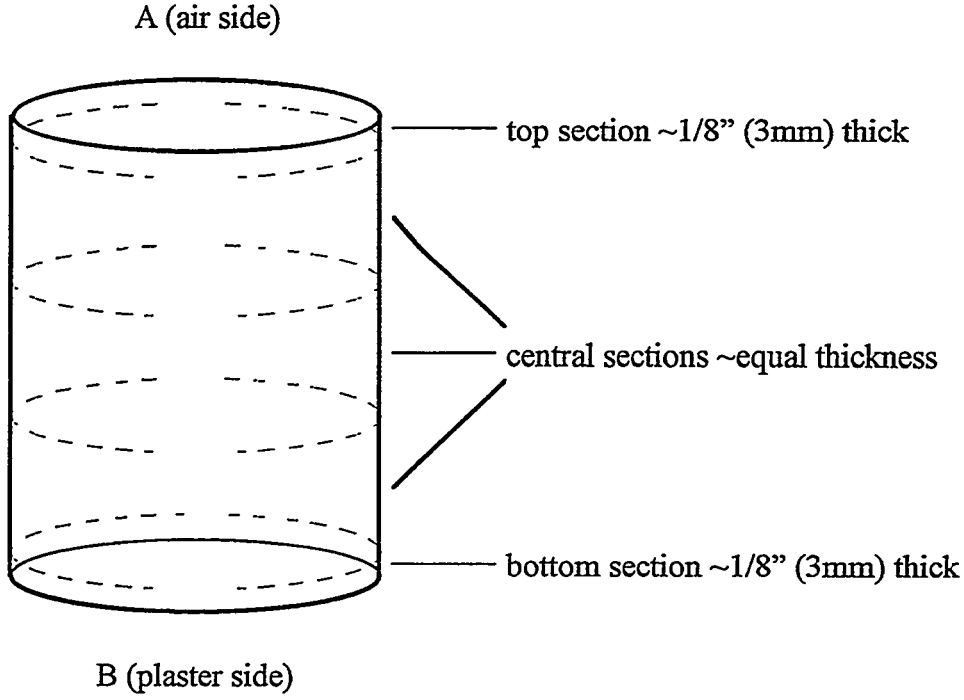

Fig. 3. Schematic diagram showing destructive sectioning.

The resulting data are listed in Table 2 and the correlation plot shown in Fig. 4.

Table 2. Destructive density measurements of AS 800 billets using Archimedes method

ID No.	Location of Section	Density (g/cc)	% Theoretical Density	Remarks
S95183	Top (air side)	1.86	56.27	The % TD of S95183 before sectioning was measured at 55.84% (refer to 4/19/96 memo from Henry Yeh). The average % TD of the S95183 sections is 56.42
S95183	Central	1.88	56.88	
S95183	Central	1.87	56.51	
S95183	Central	1.86	56.10	
S95183	Bottom (plaster side)	1.85	56.33	
S95184	Top (air side)	1.94	58.55	The % TD of S95184 before sectioning was measured at 58.44% (refer to 4/19/96 memo from Henry Yeh). The average % TD of the S95184 sections is 58.92
S95184	Central	1.95	58.81	
S95184	Central	1.95	59.02	
S95184	Central	1.96	59.35	
S95184	Bottom (plaster side)	1.95	58.86	
S95187	Top (air side)	1.96	59.32	The % TD of S95187 before sectioning was measured at 59.03% (refer to 4/19/96 memo from Henry Yeh). The average % TD of the S95187 sections is 59.54
S95187	Central	1.98	59.94	
S95187	Central	1.98	59.76	
S95187	Central	1.97	59.47	
S95187	Bottom (plaster side)	1.96	59.23	

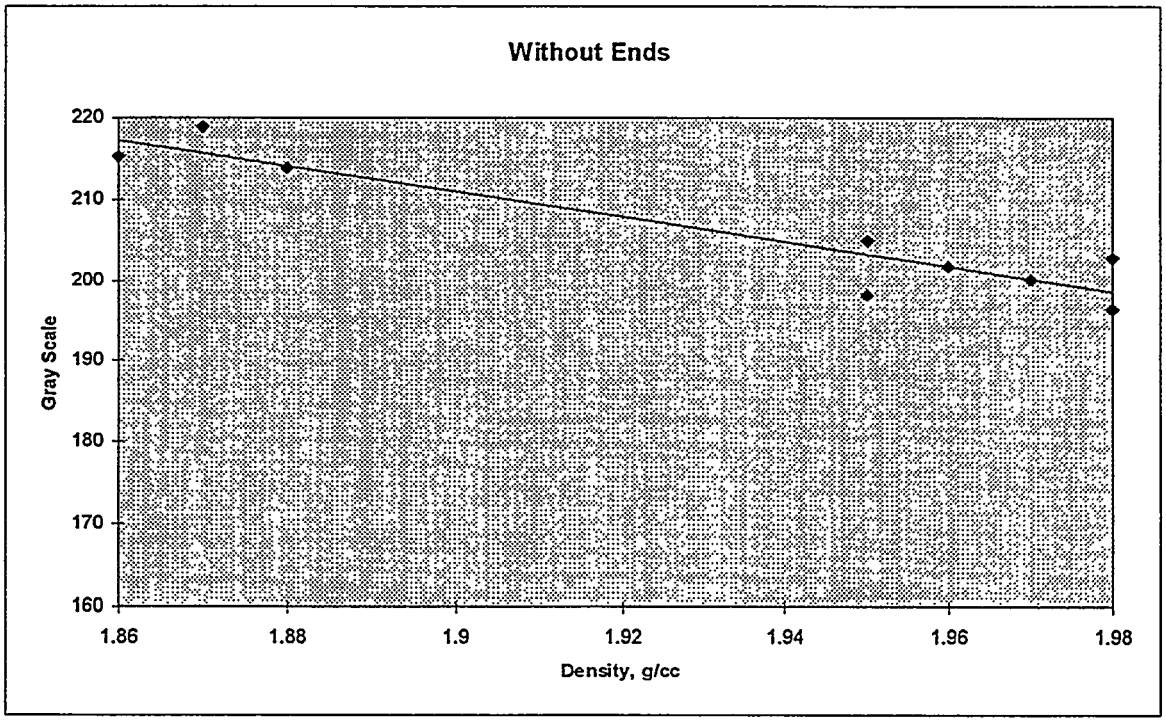

Fig. 4. Correlation between X-ray CT densitometry and destructive analysis of three AS 800 pressure slip cast billets.

b) New GS-44 chopped carbon fiber densitometry study

Our densitometry work is now focused on establishing the sensitivity of X-ray CT densitometry to distribution of chopped fiber. Specifically, the distribution of chopped carbon fiber in Allied Signal Ceramic Components GS-44 material. This is part of the Office of Heavy Vehicle Technology (OHVT) work on ceramic valve guides being developed for Caterpillar.

We received from Caterpillar, Inc., three one-half sections of valve guides which contained 0%, 10%, and 12.5 vol. % chopped carbon fiber.

These specimens were optically polished and optical photomicrographs taken. The resulting optical photomicrographs are shown in Fig. 5.

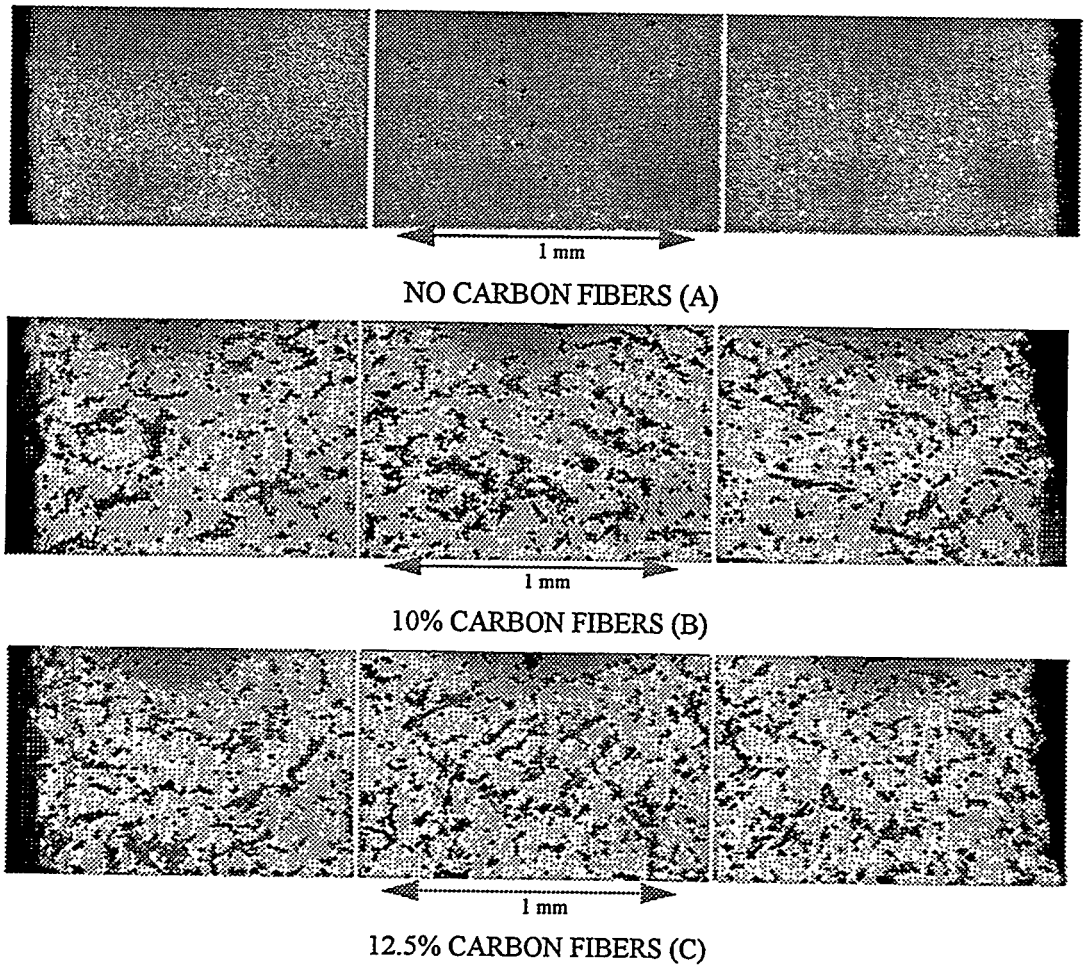

Fig. 5. Optical photomicrographs of GS-44 valve guides

Initial X-ray CT image acquisitions this period were obtained on 0% and 12.5 vol % chopped fiber. A typical CT image is shown in Fig. 6.

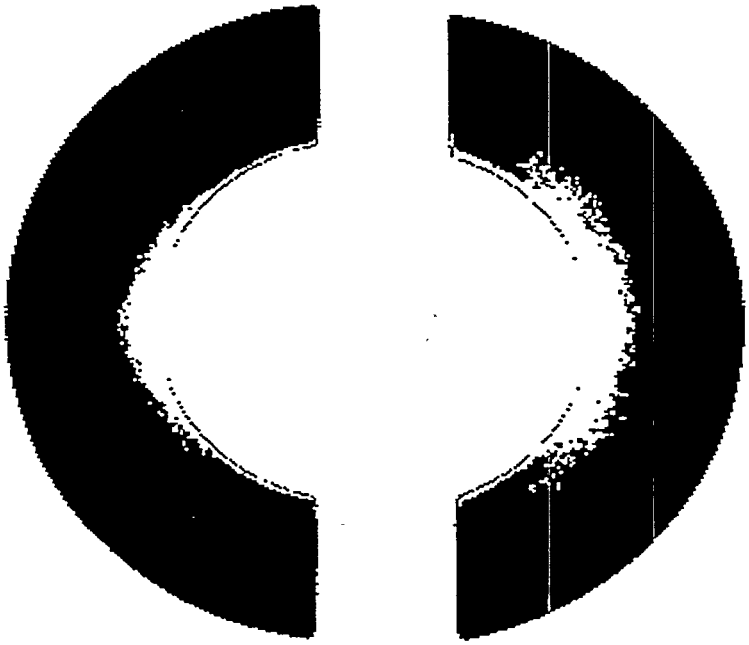

Figure: Allied Signal – Caterpillar Valve Guide Sections

Left half = 0% fiber content
Right half = 12-1/2 volume % fiber content

Fig. 6. X-ray CT reconstruction (357 x 357) with 63 μm slice thickness

TESTING AND EVALUATION OF ADVANCED CERAMICS AT HIGH TEMPERATURE

J. Sankar, A. D. Kelkar and Q.Wei (Department of Mechanical Engineering, North Carolina A & T State University, Greensboro, NC 27406).

Objective/Scope

The objective of this research is to test and evaluate the long-term mechanical reliability of a Si_3N_4 at temperatures up to 1300°C.

The required research includes four (4) major tasks:

Task 1. Cyclic Fatigue Testing of PY6

Cyclic fatigue of GTE-PY6 silicon nitride shall be performed at lower temperatures to investigate 500° -1100°C characteristics of the material at this temperature range. At these lower temperatures, there may be a true cyclic fatigue effect which enhances failure compared with the static load case.

Task 2. Stress - Rupture Study of PY6

Stress-rupture testing of GTE PY6 silicon nitride shall be performed at a lower temperature range of 500° - 1100°C. Since there is little information about the time dependent behavior of this material is available at this temperature regime, this task should provide some valuable data.

Task 3. Tensile Testing of GS 44

Pure Uniaxial tensile testing of GS 44 silicon nitride will be carried out at both room and elevated temperature up to 1200°C. The obtained data will be compared with other silicon nitride materials.

Task 4. Stress - Rupture Study of GS 44

Stress-rupture testing of GS 44 silicon nitride will be performed at various temperatures and stresses.

Technical Highlights

During this reporting period, we have used microhardness testing, high temperature thermal soaking, analytical and high resolution transmission electron microscopy(ATEM and HRTEM), field emission scanning electron microscopy(FESEM) and x-ray energy dispersive spectroscopy(EDS) to study the evolution of microstructure and composition of a sintered silicon nitride, GS44 that is considered to be a candidate for hot turbine engine application. The purpose of the study is to understand the behavior of the material under corrosive atmosphere and at high temperatures, since these conditions are typical of the service conditions for which the material has been designed. GS 44 is commercial grade sintered silicon nitride which was developed for temperature applications below 1100°C. However, for basic science research and study, this exploratory study was conducted. We started with the virgin(as received) samples(materials provided by AlliedSignal). We found that there is a considerable amount of amorphous phase in the virgin sample existing as grain boundary phase and triple junction phase. The amorphous phase was added as additives to help the densification process during sintering. It consists of alumina, magnesia and yttria. We also observed dislocation networks that are typical of sintered silicon nitride. The samples were thermally soaked in air at 1275°C for various periods of time from 12 hours to 42 hours to study the behavior of the material under corrosive condition at high temperatures. We found that the soaked samples have serious surface deterioration. Microhardness tests showed that there is a significant hardness drop with the distance from the center of the specimen towards the edge of the specimen. High resolution TEM studies showed that the grain boundary or triple junction phases have either been expanded or devitrified during the thermal soaking process at high temperatures. The following summarizes the research work:

1. We observed a considerable amount of amorphous grain boundary and triple junction phases in the virgin sample of GS44(AlliedSignal) which consist of alumina, magnesia and yttria that were incorporated during the sintering process to help densification of the ceramics. We also observed dislocation networks that are typical of sintered silicon nitride.

2. TEM studies on the thermally soaked samples showed that the grain boundary or triple junction phases have either been expanded or devitrified during the thermal soaking process at high temperatures.

3. SEM and EDS results showed that the depletion of Si and Mg occurred during the soaking process, indicating chemical encroachment of the samples.

4. Microhardness test results showed that the mechanical strength of the soaked sample degraded due to the above mentioned reasonings. However, it has been reported that the devitrification of the amorphous grain boundary or triple junction phases are beneficial to high temperature creep behavior of the material.

Results and Discussion

Fig.1 shows some TEM micrographs of the virgin GS44 sample. Fig.1a is a bright field general view of the sample, showing Si_3N_4 grains of varied grain sizes. Fig. 1b is an electron micrograph showing the triple junction phase. The insert is a selected area diffraction pattern taken from the junction phase. The diffuse ring in the pattern indicates that the triple junction phase is amorphous. It is also seen here that the triple junction phase is of distinct shape. EDS analysis was conducted on the virgin sample. Fig.1c is the EDS spectrum showing that the additives of GS44 presumably consist of alumina, magnesia and yttria.

Fig.1d is a bright field micrograph of the dislocation networks typically observed in sintered Si_3N_4. Fig.1e is the corresponding dark field image and the attached diffraction pattern shows the imaging condition of the graph. Probably because it has been considered that dislocation has little effect on the deformation and fracture mechanism in Si_3N_4 at high temperatures, there is a great paucity in the literature regarding the natures and morphologies of the dislocation in it. An early investigation showed that the Burgers vector of dislocation in β-Si_3N_4 is c[0001] and the dislocations lie on {1010}. The same investigation also indicated that the Burgers vector of the dislocation comprising the low angle boundary could not be determined due to lack of visibility conditions. The diffraction pattern of Fig.1e agrees with the visibility criteria developed and employed in the reference(E. Butler, Phil. Mag., 24(1971)829-834).

Fig.2 is the microhardness profile as a function of radial distance of a sample thermally soaked at 1200°C and 1275°C. It shows significant microhardness, or in other words, strength drop towards the surface of the specimen. In order to understand this strength drop in terms of microstructure and composition changes, we did EDS and TEM on different regions of the soaked samples. Fig.3a is an energy dispersive spectrum from the center of the sample. It shows a huge peak of Si and some Al , Mg, oxygen due to the presence of the sintering aids. The peak of nitrogen is small because of the serious absorption of the characteristic lines from nitrogen. Fig.3b is the energy dispersive spectrum from the edge, *viz.* the surface scales of the sample. The depletion of Si and Mg elements in the scales is obvious. It is then clear that material loss occurred during thermal soaking in air. The surface deterioration of the sample will decrease its effective cross sectional area and may raise the stress intensity level, and even initiate cracks with time. Fig.4 shows HRTEM micrographs taken from different regions of the soaked sample. We observed that the grain boundary phase of the specimen were either expanded considerably, as shown in Fig.4a, where the width of the grain boundary phase is measured to be roughly 5nm, while in the virgin sample, the average width of grain boundary phase is about 1.5nm, or devitrified, as shown in Fig.4b. The atomic level interface irregularity because of oxygen attack is seen in Fig.4c. We have even observed that in the region very close to the surface, the grain boundary phase has been expanded to a width around 10nm.

Status of Milestones

On schedule

Communications/Visitors/Travel

None

Publications

Q.Wei, J.Sankar, J.Narayan and A.D.Kelkar, "Morphology changes accompanying creep of sintered Si3N4 for hot turbine engine application", Proceedings of 38th Structures, Structural Dynamics, and Materials Conference, pp.978-987, AIAA, April 7-10, Kissimmee, FL.

Problems Encountered:

None

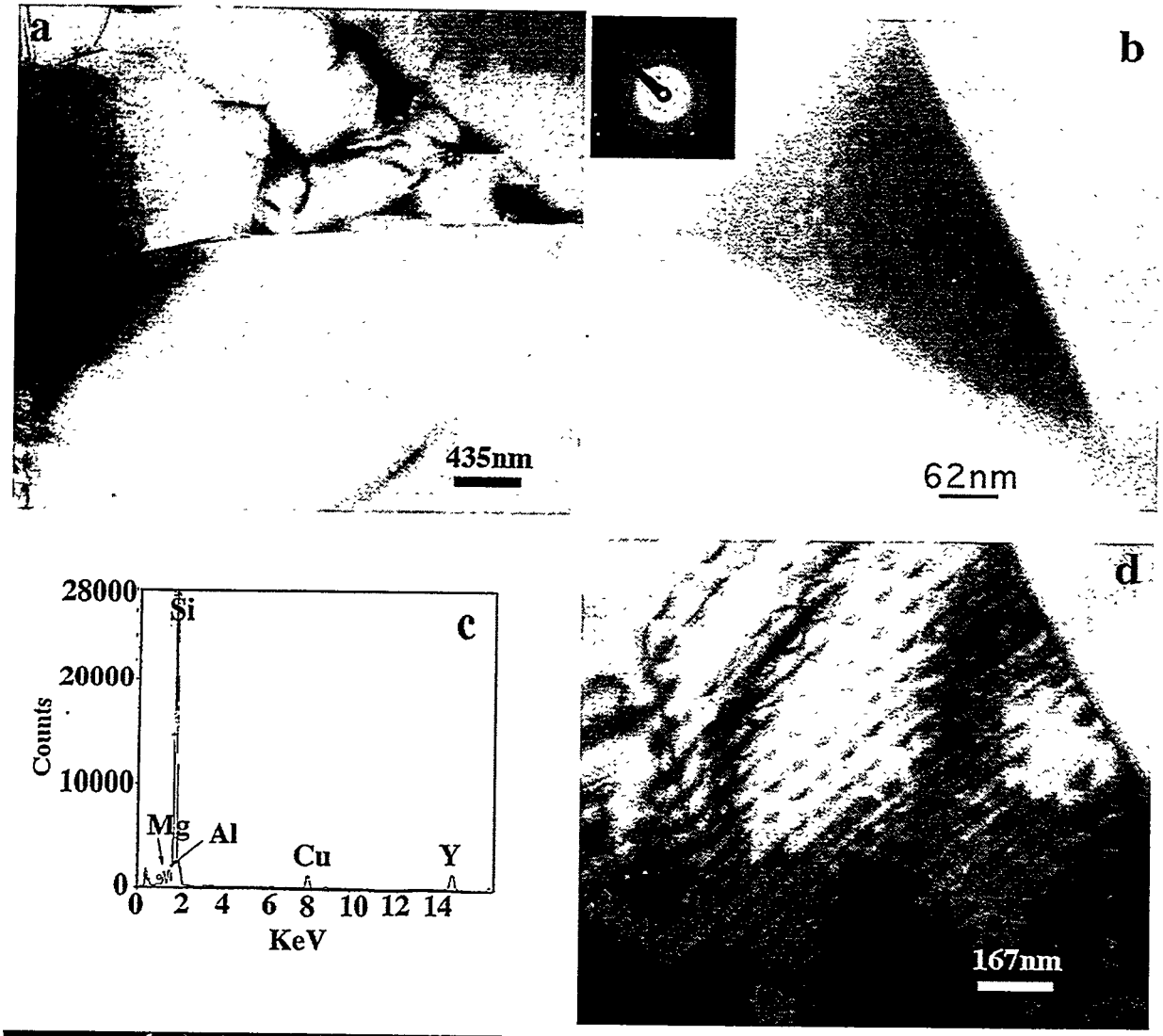

Fig.1.(a) Bright field general view of the virgin GS44; (b) triple junction phase with the insert being the SAD pattern to show the amorphousness;(c) The EDS of the virgin sample; (d) is the bright field image of the dislocation network and (e) is the corresponding dark field image. The attached SAD shows the imaging condition.

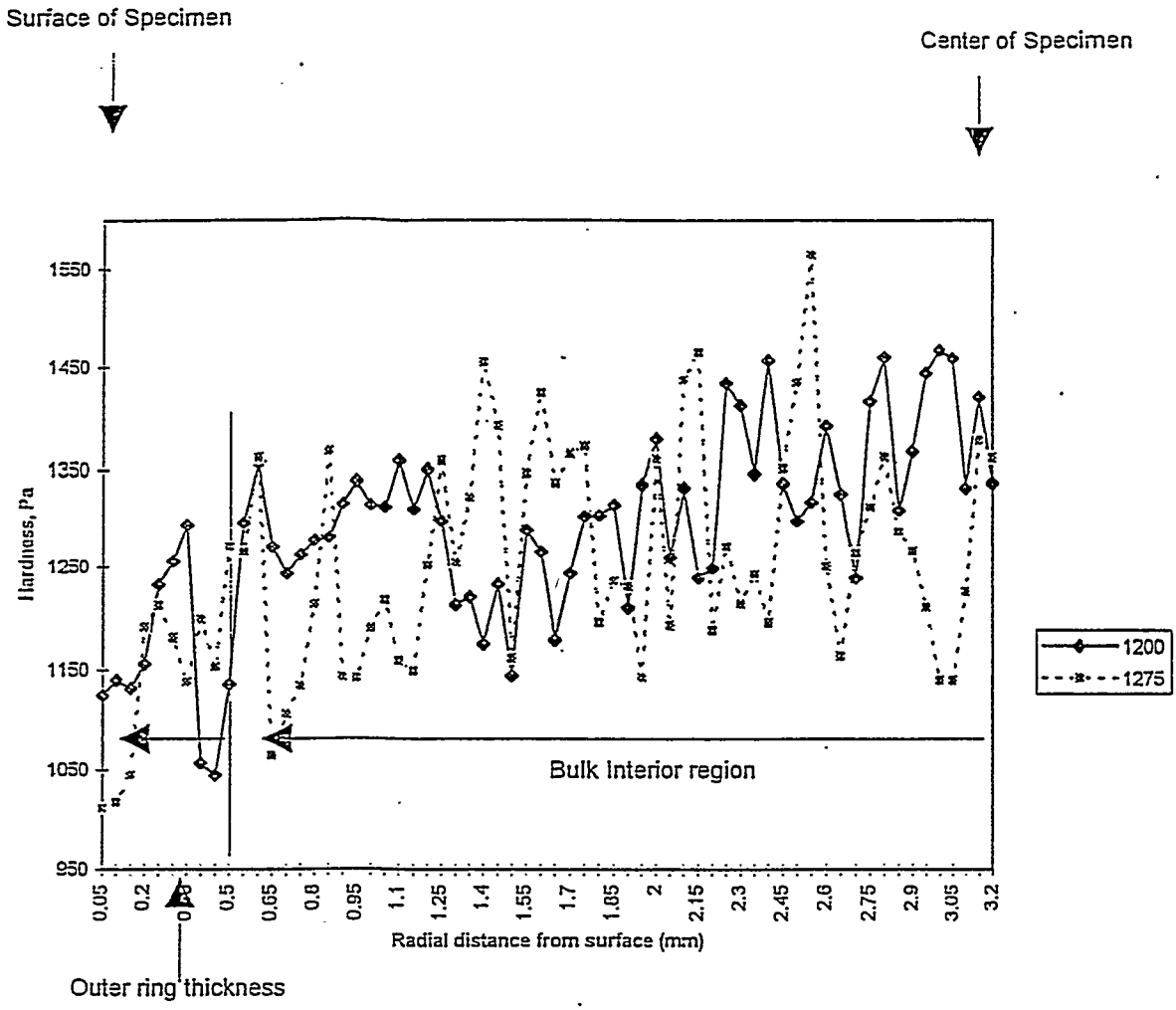

Fig 2. Microhardness as a function of radial distance for GS44-Si_3N_4 (Sintered silicon nitride) tested at 1200 °C and 1275 °C

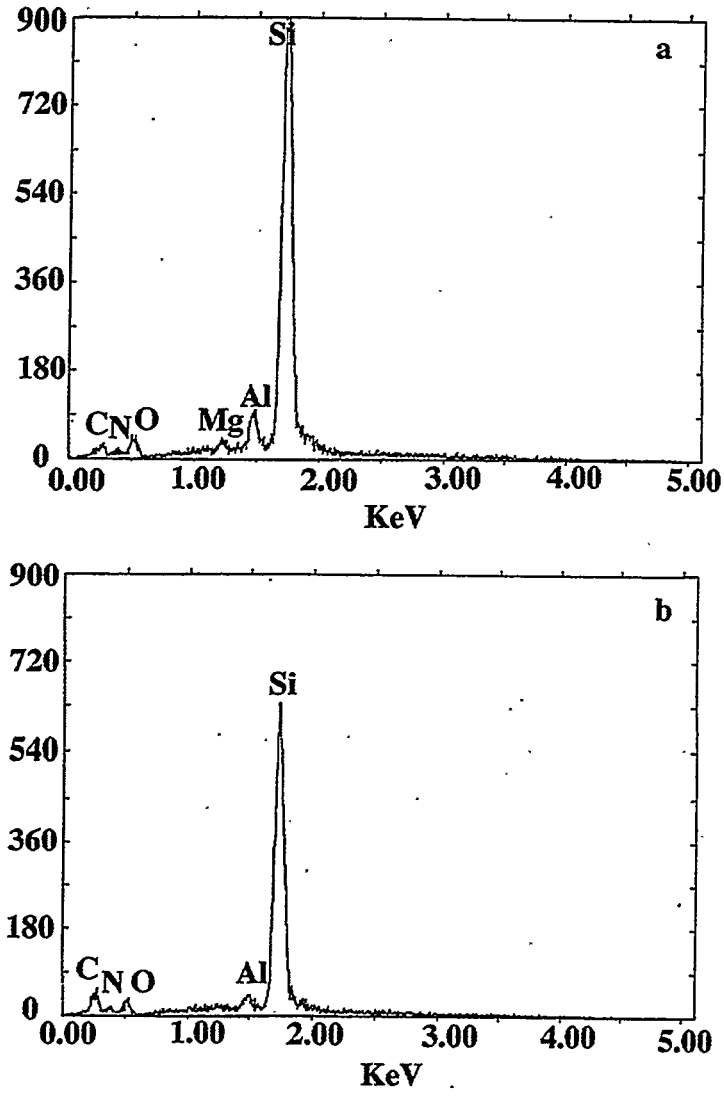

Fig. 3. Energy dispersive spectroscopy on the central area (a) and at the edge(b) of a soaked GS44 sample.

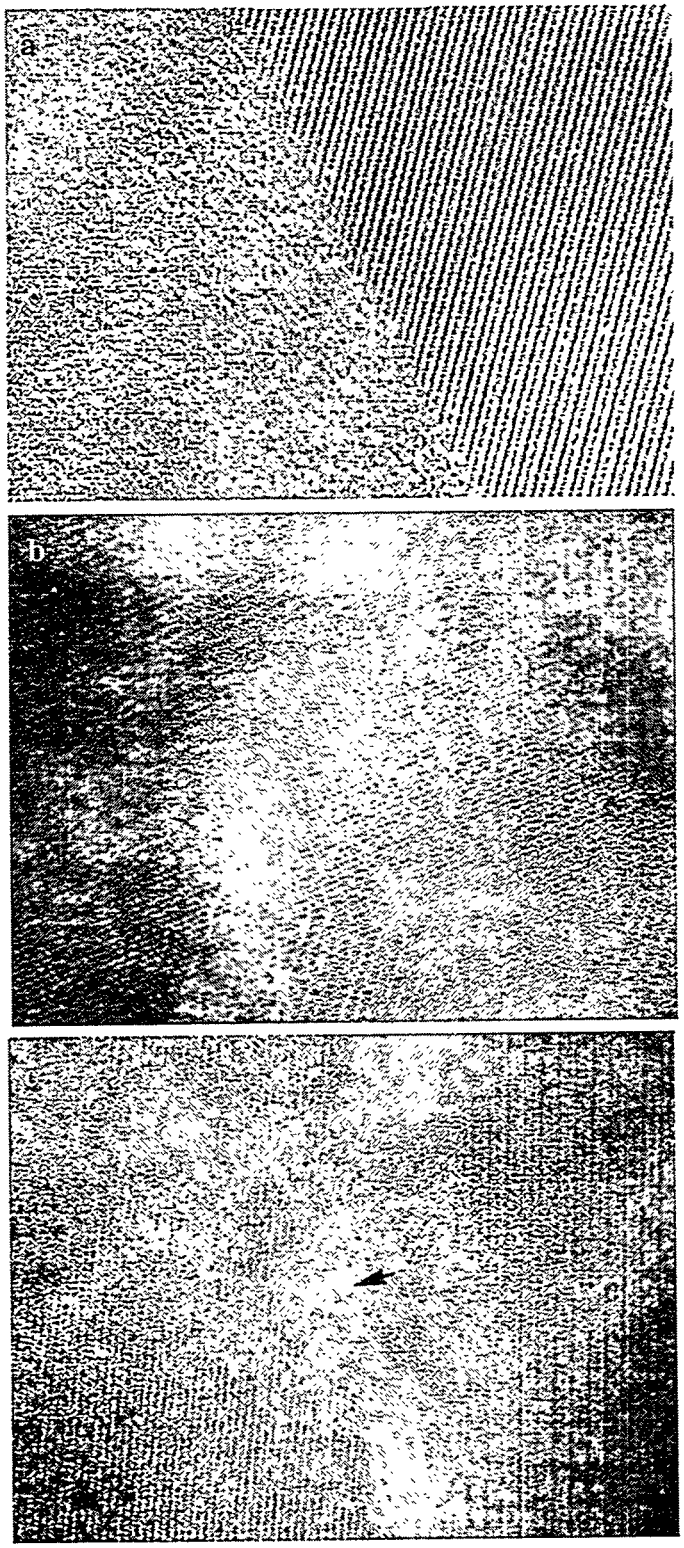

Fig.4 HRTEM of the soaked samples taken from different regions showing growth of the grain boundary phase(a), devitrified grain boundary phase(b) and irregular interface due to oxygen attact(c).

3.2.1.6 *Life Prediction Verification*

A. A. Wereszczak, M. J. Andrews, M. K. Ferber, and T. P. Kirkland (ORNL)

Objective/Scope

There are three central goals of the proposed research program: the generation of engineering data from ambient to high temperature mechanical testing; microstructural characterization of failure phenomena; and the implementation and verification of life prediction methods involving structural ceramics. Ultimately, the prediction of the high temperature mechanical performance and service life is information that is critical for the progress towards implementation of structural ceramics as components in internal combustion and automotive gas turbine engines.

The systematic study of the mechanical performance of a silicon nitride and a SiAlON is undertaken as a function of temperature and time. Studies on both SiAlON and silicon nitride will be conducted at temperatures $\approx$ <1000°C, while studies with only silicon nitride will be at temperatures $\approx$ >1000°C; these are likely operating temperature thresholds for internal combustion and automotive gas turbine engines, respectively. For the lower temperature regime, properties such as strength and fatigue life will be measured in the SiAlON and silicon nitride material as a function of temperature. For the higher temperature regime, tensile stress-rupture data of silicon nitride will be analyzed through the consideration of both fatigue and creep.

The second goal of the program is to characterize the evolution and role of damage mechanisms. The damage will be examined using metallography, SEM, and TEM. Several microstructural aspects of high-temperature failure will be examined:

(1) the nature of slow crack growth;
(2) the evolution of cavitation-induced damage and fracture;
(3) the transition between brittle crack extension and cavitation-induced growth;
(4) crack blunting; and
(5) the evolution and role of oxidation-assisted damage.

Lastly, available analytical and numerical models will be utilized to predict the life of complex-shaped components and prototype engine parts (e.g., valves). The applicability of analytical models such as the Monkman-Grant and the Sherby-Dorn models to structural ceramics will be examined, and modifications will be made where necessary to refine the models and improve their predictive capabilities. Numerical models (i.e., life prediction codes) will also be used in conjunction with generated strength and fatigue data from standard test specimens to predict the failure probability and reliability of complex-shaped components subjected to mechanical loading, such as a SiAlON or silicon nitride diesel engine valve. As a consequence of these efforts, the data generated in this program will not only provide a critically needed base for component utilization in internal combustion and automotive gas turbine engines, but also facilitate the development of a design methodology for structural ceramics subjected to mechanical loading in general.

Technical Progress

During the present reporting period, NT551 bend bars were prepared and flexure testing was initiated to generate a database on strength and fatigue for this material. NT551 is manufactured by Saint-Gobain / Norton Industrial Ceramics (SGNIC), Northboro, MA, and it is a material that the Detroit Diesel Corporation (and other internal combustion engine manufacturers as well) has interest in fabricating diesel exhaust valves from. The flexure strength of NT551 was characterized as a function of grinding direction and temperature. ASTM C1161-B bend bars

(dimensions: 3 x 4 x 50 mm) were either longitudinally or transversely machined using a 320 grit finish grinding procedure. SGNIC has interest in using 320-grit diamond machining to transversely machine NT551 Series S149 diesel exhaust valves, so this provided the rationale to machine bend bars in a similar fashion. Grinding direction was explored as an independent parameter because (1) NT551 valves are to be transversely ground, and (2) ASTM C1161 grinding procedures for structural monolithic ceramics call for longitudinally grinding, and interest existed to characterize any difference between these grinding directions. All bend bar edges were beveled longitudinally to minimize the likelihood of corner-induced failures. After machining, specimens were cleaned in isopropyl alcohol, and then subjected to an isothermal anneal at 850°C for 14 hours in ambient air (in like fashion to machined NT551 valves). Four-point flexure testing was performed at 25°C and 850°C on both longitudinally and transversely machined specimens. The test fixture consisted of a 20 and 40 mm inner and outer loading span, respectively. Most specimens were tested in a "fast-fracture" mode at 30 MPa/s, with "fast-fracture" constituting a rapid enough loading rate where any possible slow crack growth and its effects are deemed insignificant. However, some specimens were tested at 25°C at 0.3 and 0.003 MPa/s to examine slow crack growth susceptibility in NT551. Temperature was explored as an independent parameter because 850°C has been identified as a representative service temperature for the Series S149 diesel exhaust valve-face, and interest existed to characterize how NT551's flexure strength at 850°C compared with its reference flexure strength at 25°C. A resistance-heated furnace was used for the 850°C tests, and thermal stability was attained (≈ 15 minute soak) prior to specimen loading. The maximum sustained load was used to calculate flexure strength using classical beam theory (ASTM C1161).

Uncensored flexure strengths were inputted in AlliedSignal's CERAMIC code to calculate the two-parameter Weibull distribution values. Weibull Modulus (m) and characteristic strength (σ_θ) were determined for (1) longitudinally machined specimens tested at 30 MPa/s and 25°C, (2) longitudinally machined specimens tested 30 MPa/s and 850°C, (3) transversely machined specimens tested at 30 MPa/s and 25°C, (4) transversely machined specimens tested at 30 MPa/s and 850°C, (5) transversely machined specimens tested at 0.3 MPa/s and 25°C, and (6) transversely machined specimens tested at 0.003 MPa/s and 25°C. Confidence estimate bands (± 95%) were also determined to aid in the interpretation or identification of statistical significant differences (if any) existing among the sets. The uncensored probability of failure was analyzed as a function of failure stress for all six sets to assist in this interpretation. The resulting characteristic strengths and Weibull Moduli for all six sets, and their 95% confidence estimates, are listed in Table. I.

The probability of failure as a function of failure stress at 25°C differed according to whether specimens were longitudinally or transversely machined, see Fig. 1. With 95% certainty, the longitudinally machined specimens had a higher uncensored characteristic strength than the transversely machined specimens (935 vs. 838 MPa) at 25°C. However, the Weibull Modulus was lower for the longitudinally machined specimens than the transversely machined specimens (8.7 vs. 22.0), indicating that the scatter in strength for NT551 was greater for the longitudinally machined set.

Optical fractography showed that the longitudinally machined specimens failed from optically unidentifiable flaws positioned at the bend bar corners, surfaces, or within their volumes, while the transversely machined specimens all failed from optically unidentifiable flaws positioned at the specimens' surfaces. The positioning of the discrete flaw distributions are illustrated in Fig. 2. For reasons not yet understood, corner failures were associated with the higher flexure strengths for the longitudinally machined specimens, while volume and surface failures were integrated throughout the whole distribution.

The NT551 exhibited lower uncensored characteristic strength at 25°C than SGNIC's previous NT451 material (838 vs. 947 MPa), while its Weibull Modulus was arguably larger (22.0 vs. 17.0), see Fig. 3. This larger-valued Weibull Modulus may not be conclusively larger though, as the 95% confidence estimates for the NT551 and NT451 overlap somewhat, see Table I. The grinding parameters used to machine the specimen sets, whose strength distributions are shown in Fig. 3, are identical to the grinding procedures that are to be used to machine NT551 S149 valves, or that have been previously used to machine NT451 Series S149 valves. Both valve sets involve transverse machining; however, the NT551 employs 320-grit finish grinding, while NT451 employed 700-grit finish grinding. Values representing the two-parameter Weibull distribution for NT451, and 95% confidence estimates appear in Table I.

The most pronounced change in NT551's flexure strength occurred as a result of testing at 850°C. The uncensored characteristic strength for longitudinally machined specimens significantly dropped to from 935 MPa at 850°C to 498 MPa at 25°C, see Fig. 4. The Weibull modulus dropped from 8.7 at 25°C to 6.0 from 850°C, but this change was not statistically significant judging from the overlap in their 95% confidence estimates, see Table I. Most specimens tested at 850°C failed from large, optically unidentifiable flaws which were not the cause of *any* failures at 25°C. The volume-positioned flaws for those specimens tested at 25°C were not the same as those causing failure at 850°C. The uncensored characteristic strength for the transversely machined bend bars at 850°C (592 MPa) also decreased from that at 25°C (838 MPa). The uncensored Weibull Modulus also decreased from 22.0 at 25°C to 8.6 at 850°C (as shown in Fig. 5). The uncensored Weibull Modulus value of 8.6 for the transversely machined bend bars was equivalent to the uncensored Weibull Modulus for the 850°C longitudinally machined data. Although the longitudinally machined bend bars tested at 850°C may be expected to have a higher uncensored characteristic strength than for transversely machined bend bars, this was not the case as illustrated in Fig. 6. Scanning electron microscopy was used to examine some of the original fracture surfaces of the transversely machined bend bars tested at 850°C, and they were found to fail from large (≈ 10's of microns in size) agglomerate-like flaws similarly to those that were observed on longitudinally machined specimens tested at 850°C.

Two processing irregularities are believed to have caused the 850°C strength reductions illustrated in Figs. 4-6, and have reportedly been remedied by the vendor. A slightly higher carbon content was identified in the atmosphere during hot isostatic pressing, along with incomplete pressurization at the maximum temperature [1]. These problems reportedly have been corrected, and preliminary flexure strength generated by the vendor on NT551 vintages (produced after these processing corrections) yielded: (1) 25°C strengths in excess of 950 MPa and a Weibull Modulus between 20-30, and (2) 850°C strengths in excess of 900 MPa and a Weibull Modulus greater than 20 [1]. The vendor is supplying NT551 tiles of these later vintages to the herein described subtask. With regards to this issue and nomenclature, the data presented and described above were generated from specimens from the "old vintage" of NT551. The arrival of the "new vintage" of NT551 Si_3N_4 stock material is expected in late April. The testing of this new vintage of NT551 will commence as soon as it arrives to verify the vendor-reported maintenance of room temperature strength and Weibull Modulus at 850°C. Once verified, the examination of the test matrix outlined in a previous bimonthly [2] will proceed. Cylindrical bend bars will be used to generate Weibull statistics that will be used in the life prediction analysis of the valve stems; this is relevant under the circumstance when the seat insert and valve guide axes are not concentric and a bending moment is applied to the stem. All specimens will be transversely ground using equivalent stock removal rates as those employed in the machining of the NT551 exhaust valves.

The slow crack growth susceptibility of the old vintage of NT551 was examined during the present reporting period via a series of room temperature dynamic fatigue tests. Rates spanned four decades of stressing rates ($3x10^{-3}$ to $3x10^{1}$ MPa/s), and testing was performed at 25°C. With

95% confidence, the uncensored characteristic strength decreased with a decrease in stressing rate (see Table I and Fig. 7). The Weibull Moduli at 0.3 and 0.003 MPa/s (13.2 and 10.5, respectively) were conclusively lower than the Weibull Modulus at 30 MPa/s (22.0); however, the Moduli at the two slower rates were not conclusively different (with 95% confidence) even though it appeared that the Weibull Modulus further decreased in value at the slowest rate. Lastly, the fatigue-stress exponent (N) for this data was found to equal 36 (see Fig. 8), which suggests that this material is susceptible to slow crack growth at room temperature. Empirically, $N < 60$ is considered to be representative of a material susceptible to slow crack growth [3]. These experiments will be repeated with the new vintage of NT551 upon its arrival, and if such a trend is repeated, then censoring of the data may explain the significance of the changes in σ_θ and m.

Status of Milestones

A Letter Report describing preliminary findings from flexure testing of the NT551 Si_3N_4 was submitted to the Advanced Propulsion Materials Program Manager. [completion of Milestone #321613]

All other milestones are on schedule.

Communications / Visitors / Travel

A poster entitled "Life Prediction Verification for a Ceramic Diesel Exhaust Engine Valve" was presented by A. A. Wereszczak at the Annual Automotive Technology Development Customers' Coordination Meeting, Dearborn, MI, Oct. 28 - Nov. 1, 1996.

A. A. Wereszczak attended the 21st Annual Cocoa Beach Conference and Exposition, Cocoa Beach, FL, Jan. 12-16, 1997, and gave two presentations entitled "Tensile Creep Performance of a Developmental, In-Situ Reinforced Silicon Nitride" and "Prediction of SiAlON Diesel Valve Failure Probability Using AlliedSignal's *CERAMIC* and *ERICA* Life Prediction Codes."

M. J. Andrews attended an ANSYS finite element training course offered in Pittsburgh, PA, Jan. 13-15, 1997.

Problems Encountered

The identification of the strength reduction in the old vintage of NT551, its remediation, and the delayed delivery from the vendor of the new vintage of NT551 has subsequently delayed the overall mechanical testing of NT551, as well as the subsequent life prediction and reliability estimates of NT551 valves.

Publications

"Tensile Creep Performance of a Developmental, In-Situ Reinforced Silicon Nitride," by A. A. Wereszczak, T. P. Kirkland, H. -T. Lin, M. K. Ferber, C. -W. Li, and J. A. Goldacker, submitted for publication in the *Ceramic Engineering and Science Proceedings*, 21st Annual Meeting, Cocoa Beach, FL, Jan. 1997.

"Prediction of SiAlON Diesel Valve Failure Probability Using AlliedSignal's *CERAMIC* and *ERICA* Life Prediction Codes" by A. A. Wereszczak, T. P. Kirkland, M. K. Ferber, and M. J. Andrews, submitted for publication in the *Ceramic Engineering and Science Proceedings*, 21st Annual Meeting, Cocoa Beach, FL, Jan. 1997.

An article entitled "Reverse Cyclic Fatigue of a Hot Isostatically Pressed Silicon Nitride at 1370°C" by A. A. Wereszczak, T. P. Kirkland, and M. K. Ferber was published in the *Journal of Materials Science*, Vol. 31, pp. 6541-52, 1996.

An article entitled "Failure Probability Prediction of Fast-Fractured NT451 SiAlON Diesel Exhaust Valves," by A. A. Wereszczak, T. P. Kirkland, M. K. Ferber, J. M. Corum, and A. Peralta, was accepted for publication in the *Journal of Engineering for Gas Turbines and Power, Transactions of the ASME.*

An abstract entitled "Flexure Strength and Fatigue Resistance of NT551 Silicon Nitride" by M. J. Andrews, A. A. Wereszczak, T. P. Kirkland, and M. K. Ferber, was submitted for presentation at the American Ceramic Society's 99th Annual Meeting and Exposition, Cincinnati, OH, May 4-7, 1997.

References

[1] Personal communication, Vimal Pujari, Norton Advanced Ceramics.
[2] A. A. Wereszczak, M. J. Andrews, M. K. Ferber, and T. P. Kirkland, "Life Prediction Verification," pp. 19-24 in the *Heavy Vehicle Propulsion System Materials Program Bimonthly Technical Progress Report to DOE Office of Transportation Technologies, Aug. - Sep. 1996.*
[3] Personal communication, Kristin Breder, Oak Ridge National Laboratory.

Table. 1. Specimen, testing conditions, Maximum Likelihood estimates of characteristic strength (σ_θ) and Weibull Modulus (m), and their 95% confidence estimates. Values determined using AlliedSignal's CERAMIC code for the ASTM C1161-B specimen geometry.

Material	Grinding Direction	Test Temp. & Stressing Rate	Uncensored σ_θ (MPa)	± 95% Conf. Est. of σ_θ (MPa, MPa)	Maximum Likelihood Uncensored m	± 95% Conf. Est. of m
NT551 46 specimens	Longitudinal, 320 Grit	25°C 30 MPa/s	935	902, 968	8.7	6.9, 10.6
NT551 50 specimens	Transverse, 320 Grit	25°C 30 MPa/s	838	826, 849	22.0	17.9, 26.4
NT551 31 specimens	Longitudinal, 320 Grit	850°C 30 MPa/s	498	466, 530	6.0	4.5, 7.6
NT551 30 specimens	Transverse, 320 Grit	850°C 30 MPa/s	592	565, 619	8.6	6.3, 11.3
NT551 50 specimens	Transverse, 320 Grit	25°C 0.3 MPa/s	746	729, 763	13.2	10.5, 16.1
NT551 21 specimens	Transverse, 320 Grit	25°C 0.003 MPa/s	676	646, 707	10.5	7.3, 14.2
NT451 35 specimens	Transverse, 700 Grit	25°C 30 MPa/s	947	926, 966	17.0	12.6, 22.0

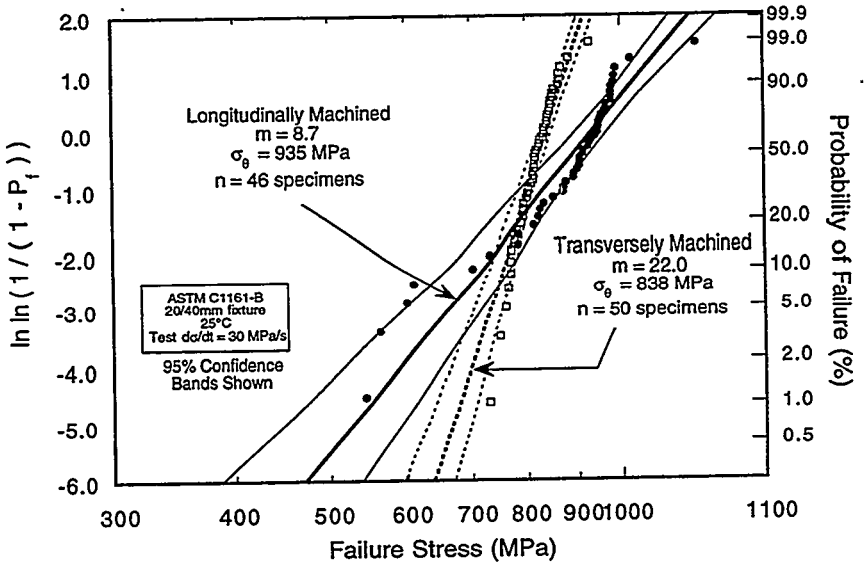

Fig. 1. The longitudinally and transversely machined NT551 specimens exhibited different uncensored strength distributions at 25°C.

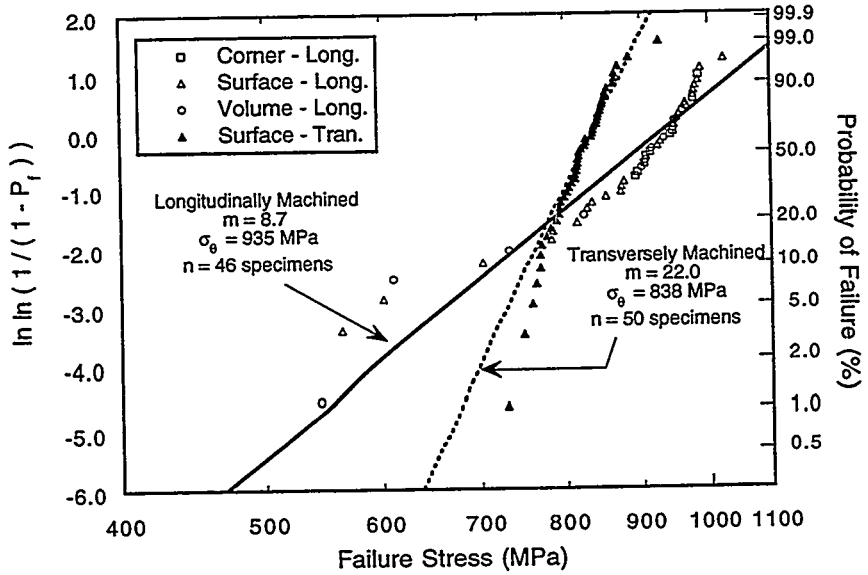

Fig. 2. Flaw location distribution for the tested longitudinally and transversely machined NT551 flexure bars.

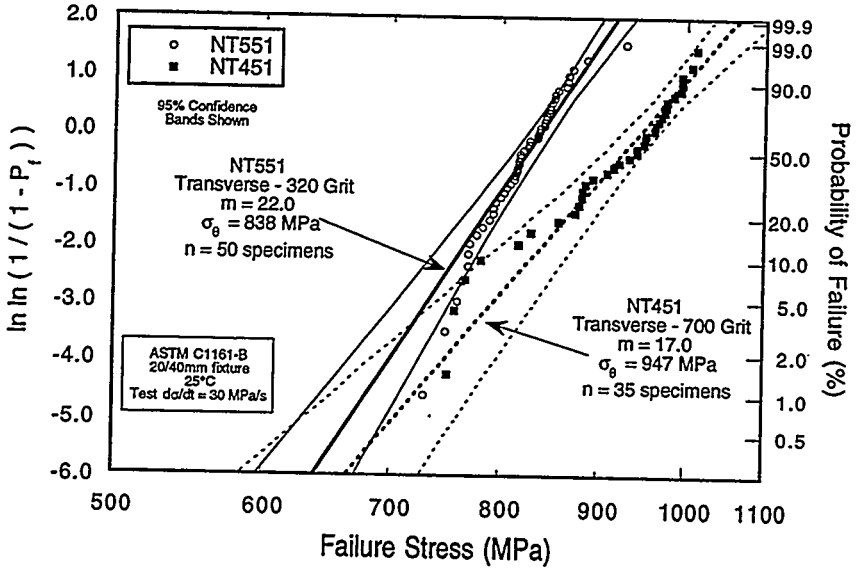

Fig. 3. Comparison of NT451 and NT551 uncensored flexure strengths. Shown specimen sets were finish ground in the same manner as respective NT451 and NT551 valves.

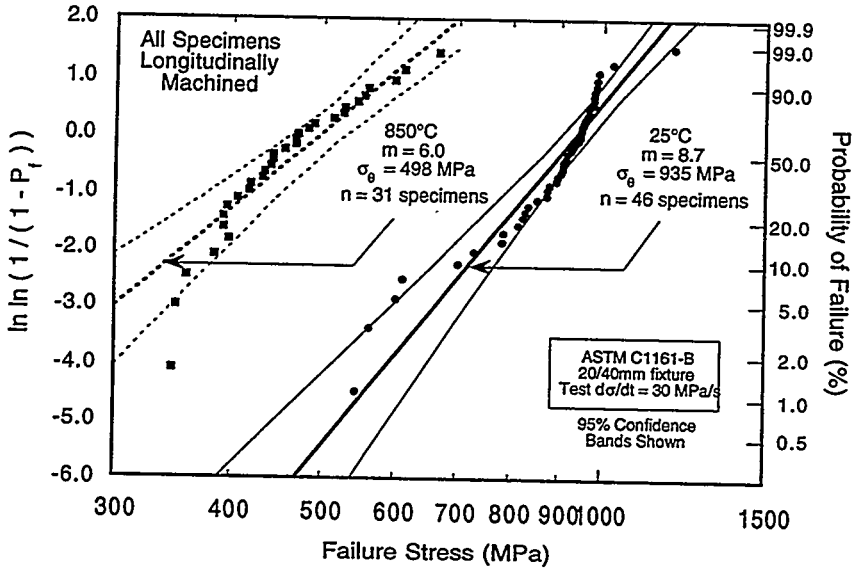

Fig. 4. Comparison of NT551 uncensored flexure strengths at 25 and 850°C for specimens that were longitudinally machined.

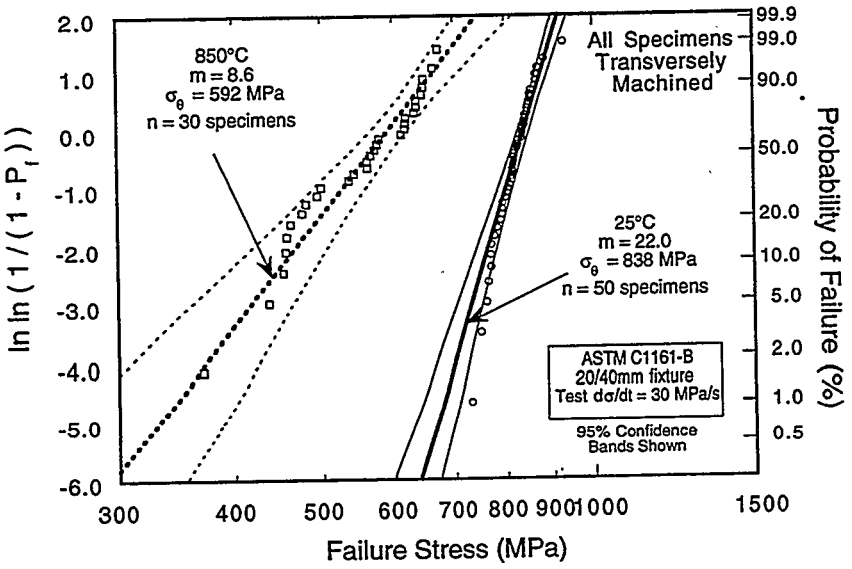

Fig. 5. Comparison of NT551 uncensored flexure strengths at 25 and 850°C for specimens that were transversely machined.

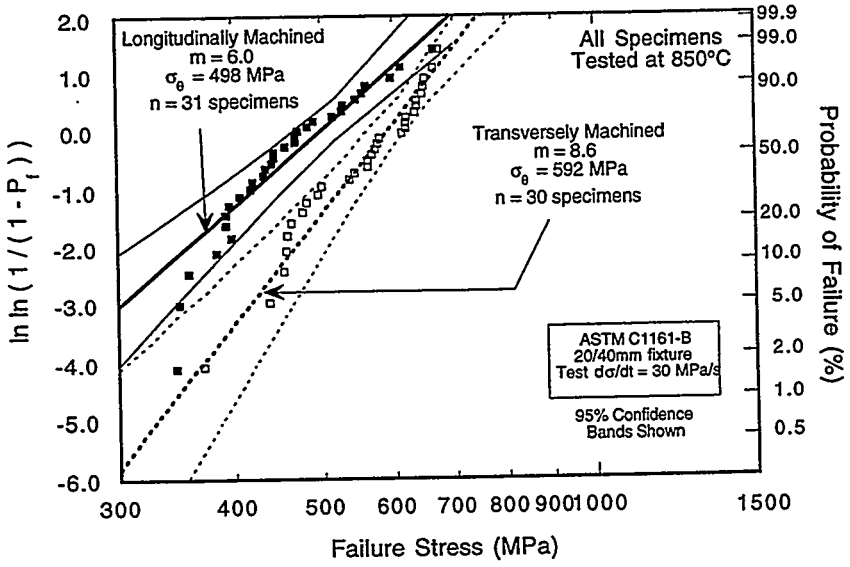

Fig. 6. The longitudinally and transversely machined NT551 specimens exhibited different uncensored strength distributions at 850°C.

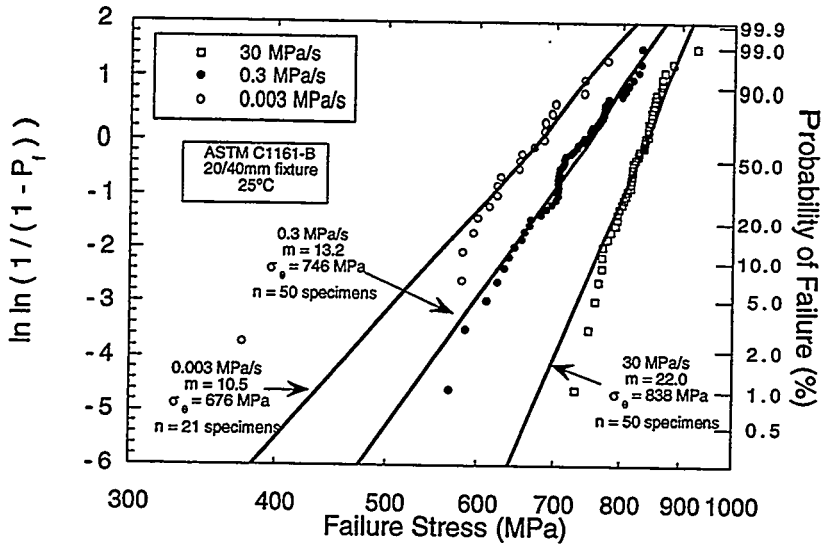

Fig. 7. Probability of failure as a function of stress and stressing rate for transversely-machined NT551 Si_3N_4. All specimens transversely machined.

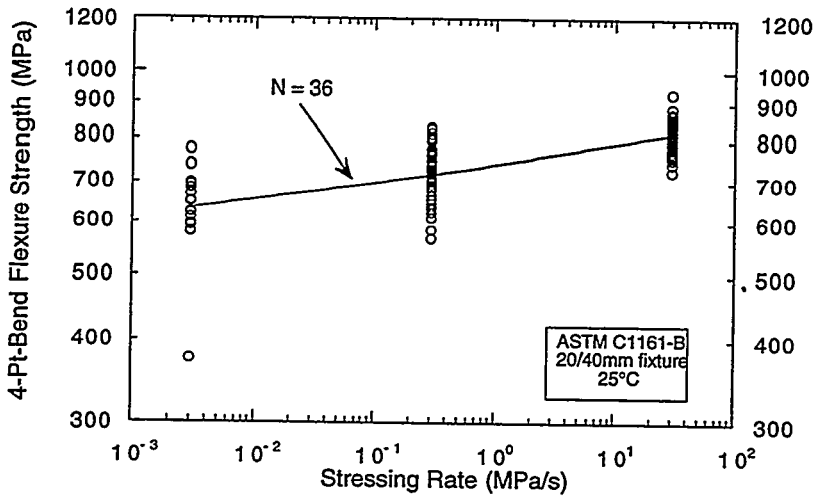

Fig. 8. A power-law fit of the flexure strength as a function of stressing rate yielded a fatigue-stress exponent equaling 36.

WBS Element 3.1.1.4

Field Emission Analytical Electron Microscopy for Characterization of Catalyst Microstructures

L. F. Allard and T. A. Nolan

OBJECTIVE/SCOPE

The objective of the research is to use analytical and high resolution electron microscopy to characterize the microstructures of emission control catalysts. Emphasis is placed on relating microstructural changes to performance of diesel oxidation catalysts. This semiannual report reviews the development of a new "collaboratory" initiative funded by DOE in which industry and national laboratories will conduct joint research on projects in materials science, including a major effort studying catalyst materials which show promise for reduction of NOx emissions from diesel engines.

TECHNICAL HIGHLIGHTS

In the Materials MicroCharacterization Collaboratory, as part of the DOE2000 initiative, we will study various lean burn catalyst systems (oxide-based, zeolite-based and others) to develop the collaboratory techniques, tools and expertise needed to support fundamental studies of these catalyst materials of interest to the Heavy Duty Vehicle Propulsion Program.

In an initial project to develop and demonstrate the collaboratory concept, we have begun the study of several NOx reduction catalyst materials which have been supplied by colleagues at Ford Research Laboratory, who will be industrial collaborators on the project. At Ford, the difference in activities of materials prepared by sol-gel processes as compared to commercial materials has been noted. For example, Ford scientists have found that Ag particles deposited on sol-gel alumina show substantial increases in the lean burn NOx conversion efficiency as compared to Ag particles deposited on a commercial alumina. It is speculated that changes in microstructure are responsible for this increase in the activty although the precise mechanism still needs to be determined. The morphology and chemistry differences between the experimental sol-gel produced materials and the commerical support materials will be studied in the collaboratory.

Initial characterizations have begun on samples of platinum-group metals (PGM) on both rare earth oxide-modified oxide supports and on alumina-titania supports, under investigation at Ford for several years, to identify the structural features common with Ag/sol-gel alumina system. For example, a number of samples derived from the metal-alkoxide $Pr_2Zr_6(\mu_4O)_2(\mu\text{-}OAc)_6(\mu\text{-}O^iPr)_{10}(O^iPr)_{10}$, prepared by a sol-gel process and calcined at various temperatures, have shown significant structural differences which may be related to ultimate performance. The base material reacted at 900°C in air, and another metal-alkoxide, $Pr(O^iPr)3 + Zr(O^iPr)4{\cdot}^iPrOH$, reacted at 400°C in air, both to yield expected PrZrOx compounds, have

been characterized by analytical electron microscopy methods. The 900°C-reacted powder comprised two distinct particle morphologies; one composed of interconnected discrete grains on the order of 0.1 μm in diameter, which showed a high volume of small internal voids, and the second comprising a dense, fine-grained aggregate structure with particles on the order of 10 nm in size. Energy dispersive x-ray spectra (EDS)from the first particle morphology showed only Zr and O, consistent with a ZrO2 composition, while the dense, fine-grained aggregates showed both Pr and Zr to be present. However, the 400°C-reacted powder showed only a single morphology; a uniform, extremely fine-grained, porous microstructure with a relative Pr/Zr composition significantly higher than the Pr-Zr aggregates of the 900°C material. The fine grain size and uniformity of composition of this latter material suggests that it might be better as a catalyst support than the base material, which has varying morphology and composition.

In similar work presently underway, which will be reported in subsequent bimonthlies, ORNL will continue to utilize the Hitachi field emission TEM to obtain basic scientific information (e.g. the changes in PGM cluster size and chemistry dependent upon reaction treatments conducted in an ex-situ reactor system) on the Pr-Zr catalyst system as well as PGM/alumina-titania materials. Partners in the DOE2000 Collaboratory will provide additonal instrumentation and expertise for the timely conduct of experiments to complement the work at ORNL. LBNL will conduct in-situ hot-stage experiments in the high voltage TEM and correlate the results to the ex-situ reactor tests. The Advanced AEM at ANL will be utilized to provide higher spatial resolution microchemistry to characterize the distribution of atomic-level clusters of heavy metals, by high-angle annular dark field techniques available only on that instrument. The results of all these studies will provide valuable information on the relationships between microstructure, microchemistry and mechanisms affecting catalyst performance and degradation in a variety of catalytic materials of interest for emission reduction applications.

MATERIALS AND TESTING STANDARDS

IEA ANNEX II Management (October 1, 1996-March 31, 1997)

M. K. Ferber and K. Breder (Oak Ridge National Laboratory)

Objective/Scope

The purpose of this task is to organize, assist, and facilitate international research cooperation on the characterization of advanced structural ceramic materials. A major objective of this research is the evolution of measurement standards. This task, which is managed in the United States by ORNL, now includes a formal IEA Annex agreement identified as Annex II between the United States, Germany, Sweden, Japan, and Belgium. The original annex included four subtasks: (1) information exchange, (2) ceramic powder characterization, (3) ceramic chemical and physical characterization, and (4) ceramic mechanical property measurements. In the United States, a total of 13 industrial and government laboratories have participated and contributed their resources to this research. The research in Subtasks 2, 3, and 4 is now complete. In 1990, research in two new subtasks was initiated, including Subtask 5, Tensile and Flexural Properties of Ceramics, and Subtask 6, Advanced Ceramic Powder Characterization. The research in Subtasks 5 and 6 was completed in 1993 and the reports were distributed. Two new tasks (Subtask 7 on Ceramic Machining and Subtask 8 on Ceramic Powder Characterization) were proposed in late FY 1993 and the research is completed (1996). Subtask 7 in the United States included eight companies and three federal laboratories. The report on the results from research performed in the United States on Subtask 7 is complete (a final report will be compiled of all the international research). Subtask 8 included six companies. The final report for Subtask 8 is complete. In 1996, research in two new subtasks was initiated, including Subtask 9 - Thermal Shock and Subtask 10 - Ceramic Powder Characterization.

Recent Developments

Summary from the Executive Committee Meeting Minutes - October 30, 1996

The meeting of the Executive committee of the IEA Annex II, IEA Cooperative Programme on Ceramics for Advanced Engines and Other Conservation Applications was held on October 30, 1996, at the Ritz Carlton Hotel, Dearborn, Michigan, U.S.A., in conjunction with the Annual Automotive Technology Development Customers' Coordination Meeting.

Each country's representative explained and distributed reports of research in their respective countries pertinent to this Annex.

Dr. Ferber gave an overview of the status of research in Subtask 7 and thanked all for their effort. Dr. K. Mörgenthaler made the comment that the IEA work has made a significant impact on the international community, good results that are being used have been produced. He stated that the main benefit is that there is a higher level of trust in data received from other countries because we have collaborated on

developing standard ways of manufacturing and testing ceramic products. Dr. Ferber brought up the fact that this project has enhanced the knowledge of what to specify in the machining of ceramics, and could foresee work on an international standard on how to specify grinding operations. All present agreed that this work is good and has benefitted the technical community.

Dr. Malghan reported on the status of Subtask 8. He thanked all for their efforts; especially Mr. Schulz, Dr. Johnson, Dr. Seitz and Dr. Pompe. He stated that Subtasks 2, 6, and 8 were unique in that all were doing the same work. No where else have procedures and data been compiled as in these reports resulting from these studies, and today we are reaping the benefits. He then presented viewgraphs about Subtask 8.

In addition, two new Subtasks (9 and 10) were discussed at the meeting (see discussion below). Although some work has been started in each country on these new subtasks, the formal approval for this research was deferred at this time, due to the ongoing effort to extend the present annex. It was the consensus of the Committee that there is enough interest in the proposed new subtasks to continue the Annex through December 1998 and the Operating Agent should proceed with requesting an extension of our current Annex through that date.

Subtask 9

Subtask 9 examines reproducibility of advanced thermal shock techniques. Dr. Ferber suggested that the international effort consist of the comparison of thermal shock data using centrally heated disk specimens. Each country would use their own system, but test the same materials, distributed from the U.S. He offered to distribute two materials, silicon nitride and one additional material. Dr. Ferber further suggested that each country would decide independently on whether to perform additional work, such as water quenching, or not. A fairly aggressive schedule was proposed with distribution of specimens from the U.S. in March of 1997.

Subtask 10

Dr. Malghan presented the proposed technical plan for Subtask 10. The objectives of Subtask 10 are to tighten and finalize procedures for characterization of secondary properties of selected powders, and to harmonize IEA efforts with JIS, ASTM and CEN leading to ISO standardization. The goal is to have a draft of a final report from Subtask 10 complete by December 1998.

Dr. Malghan then introduced Dr. George Onoda who will take over the role as Subtask 10 coordinator. The other countries representatives will remain the same, with the exception of Japan who will appoint a new Subtask 10 Coordinator in 1997. Dr. Pompe, on behalf of members in Subtask 8 and the

Executive Committee, thanked Dr. Malghan for his excellent and dedicated work in leading this effort.

Executive Committee Meeting - 1997

Japan distributed a letter of invitation for the Executive Committee Meeting to be held in Arita, Japan, during the "6th International Symposium on Ceramic Materials and Components for Engines."

Technical Highlights

Subtask 7, Machining Effects on Strength of Structural Ceramics

The report of the results from research performed in the United States (Subtask 7) was distributed March 31, 1997. The final report (Subtask 7) from Sweden was received October 1996. The final report (Subtask 7) from Japan was received March 1997.

Current Subtask 9 Technical Efforts

Each participating country was recently asked to provide details of specimen geometries used for the centrally-heated thermal shock techniques as well as the current standard for the water quench technique. Table 1 summarizes the results obtained to date. Once all of the information is received, a single specimen geometry will be chosen for each material to be distributed in the international round robin.

TABLE 1

	Germany	Japan Si_3N_4	Japan Al_2O_3	Sweden	Belgium	U.S.
Diameter (mm)	20	30+/-0.1	30+/-0.1	Same as Japan		25
Thickness (mm)	0.3	0.3	0.5	Same as Japan		0.3
Surface Condition	polished both sides (1 µm)					
No. Specimens	60					
Comments						
Water Quench Std.	CEN/TC 184	Received	Received	CEN/TC 184		(1)

(1) No standard available.

The development and verification of the thermal shock specimen used in the United States was continued. As discussed previously, the use of a resistance heating element as a source of heat flux led to a concentrated line heating across the diameter of the specimen. Finite element analysis conducted on this arrangement indicated that the largest tensile stresses were located at the edges of the specimen which experienced the highest temperatures. This result is consistent with the fracture path which was situated along the diameter running through the region of highest temperatures. In order to more closely simulate the thermal shock facility used in both Germany and Japan (centrally heated disk), the heating element shape was modified to generate spot heating. Preliminary trials using this arrangement were successful at thermal shocking a thin disk of high purity silicon carbide.

A Subtask 9 Working Group Meeting has been scheduled for May 6 in Cincinnati, Ohio, in conjunction with the 99th Annual American Ceramic Society Meeting.

Subtask 8, Characterizing Ceramic Powders

Major responsibility for this subtask in the United States is at NIST, and a detailed report of progress on this subtask is provided in the section of this report submitted by NIST. Subtask 8 report was printed at Oak Ridge National Laboratory and will be distributed by NIST.

Status of Milestones - Milestones 411520 (final report Subtask 8) and 411521 (final report Subtask 7) have been completed and will be published soon. Milestone 411522 (Executive Committee Meeting) was completed on October 30, 1996, by being held in Dearborn, Michigan. Milestone 411523 (provide report to ASTM) has been delayed until approval by DOE.

Milestone 411523 (Provide reports to ASTM) has been changed to December 1997, due to later release date of the reports listed below.

Milestone 411524 (finalize research plans on Subtasks 9 and 10) completed - December 31, 1996. Milestone 411525 (order U.S. ceramic material - Subtask 9) completed - January 31, 1997. Milestone 411526 (complete thermal shock technique development and issue letter report - Subtask 9) has been changed to July 31, 1997, due to scheduling changes to be decided at the Working Group Meeting in May in Cincinnati.

Milestone 411527 (hold working group meetings in conjunction with annual ACerS meeting (Subtasks 9 & 10) is on schedule.

Communications/Visits/Travel - Kristin Breder, Donna Conger, Matt Ferber, and Felicia Foust attended the Executive Committee Meeting of the IEA Annex II, IEA Cooperative Programme on Ceramics for Advanced Engines and Other Conservation Applications on October 30, 1996, at the Ritz Carlton Hotel, Dearborn, Michigan, U.S.A., in conjunction with the Annual Automotive Technology Development Customers' Coordination Meeting.

The following researchers visited the HTML on 10 January: Y. Nagano, A. Okada, and S. Kitaoka from Japan Fine Ceramics Center, Nagoya, Japan; H. Murata from Ishikawajima-Harima Heavy Industries Co., Ltd, Tokyo, Japan; and Y. Sanokawa from New Materials R&D Division Central Technical Research Laboratory, Nippon Oil Co., Ltd., Tokyo, Japan.

Publications and Presentations - Matt Ferber presented Subtask 7 Review and Subtask 9 Review at the Executive Committee Meeting, October 30, 1996, in Dearborn, Michigan.

"Efficient Grinding of Silicon Nitride," presented by Y. Nagano, Japan Fine Ceramics Center, Nagoya, Japan (January 1997). "Mechanical Properties of Advanced C/C Composites with Matrix Modified by SiC," presented by H. Murata, Ishikawajima-Harima Heavy Industries Co., Ltd., Tokyo, Japan (January 1997).

Kristin Breder and Mattison K. Ferber, "Effect of Machining Conditions on the Strength of Silicon Nitride - Results from Research Performed in the United States - Subtask 7," International Energy Agency - Annex II, Co-Operative Programme on Ceramics for Advanced Engines and Other Conservation Applications, High Temperature Materials Laboratory, Oak Ridge National Laboratory, Oak Ridge, Tennessee USA, December 1996.

S. G. Malghan and L. Lum (USA), M. Naito (Japan), R. Gilissen (Belgium), R. Pompe (Sweden), and G. Nietfeld and K. Meyer (Germany), "Development and Testing of Primary and Secondary Properties of Ceramic Powders - Final Report - Subtask 8," International Energy Agency - Annex II, Co-Operative Programme on Ceramics for Advanced Engines and Other Conservation Applications, Ceramics Division, National Institute of Standards and Technology, for the Heavy Vehicle Propulsion System Materials Program, Oak Ridge National Laboratory, Oak Ridge, Tennessee, December 1996.

Mineo Mizuno and Yasuo Nagano, "Report on Machining Effects on Strength of Structural Ceramics within IEA Subtask 7 - Japanese Final Report," Japan Fine Ceramics Center, Nagoya, Japan, February 1997.

"IEA Cooperative Programme on Ceramics for Advanced Engines and Other Conservation Applications. Machining Effects on Strength of Structural Ceramics (Subtask 7) - Swedish Results" - a compilation of three parts entitled: (1) L. Carlsson, "Machining Conditions for IEA Flexural Specimens Machined in Sweden," Swedish National Testing and Research Institute, Borås, Sweden, October 1996; (2) Sven Karlsson, "Mechanical Charactrisation of Foreign Materials Machined in Sweden and Fractography of AC Cerama Material Machined in the Participating Countries - IEA Annex II, Subtask 7," Swedish Ceramic Institute, Göteborg, Sweden, October 1996; and (3) Lennart Carlsson, "A Round Robin 1994 on Fractography of Silicon Nitride, Swedish Specimens - IEA Annex II, Subtask 7," Technical Note 1995:21, Swedish National Testing and Research Institute, Borås, Sweden, 1995.

NDE Standards for Advanced Ceramics

R. W. McClung

The development of standards is important for the establishment of reliability and acceptance of advanced structural materials. Committee C-28, on Advanced Ceramics, has been organized in the American Society for Testing and Materials (ASTM) to address this issue. One of the activities of the C-28 committee is nondestructive examination (NDE). The Section C-28.02.02 on NDE is reviewing existing standards on NDE (primarily developed for metals) to determine potential applicability for ceramics, as well as drafting original standards. Use of existing or modified standards, if available, is more efficient that generation of new documents and will assure the input of a large body of NDE expertise. Close liaison has been established with ASTM Committee E-7 on Nondestructive Testing, and documents are in various stages of review, recommendations for change, modification, and balloting. R. W. McClung is a subcommittee chairman in both committees and the official liaison.

Technical Highlights

Liaison and technical support have been continued between ASTM committees C-28 and E-7. To date, forty-two E-7 NDE standards identified as having potential relevance to ceramics have been reviewed in detail with recommendations made to E-7 for modifications to identified documents. Successful action is complete on 37 documents; others require action by C-28.

A new standard, C-1336 "Standard Practice for Fabricating Non-Oxide Ceramic Reference Specimens Containing Seeded Inclusions," was balloted successfully at concurrent subcommittee and committee levels and received society approval.

Standard C-1212 (on fabricating reference specimens with seeded voids) was reviewed and revised to incorporate improvements from C-1336. The revised draft was approved for a concurrent subcommittee/committee ballot which is in progress.

A limited amount of data has been identified for establishing radiographic equivalence factors for advanced ceramics. Additional specimens will be sought for experimental radiography to develop additional data. A volunteer for the radiography has been recognized. The intent of this action is to provide data for a table in an E-7 standard E-94 on the radiographic method. Other work in progress includes an amplified outline for a draft standard for reference specimens containing laser-drilled holes and a possible standard on determination of porosity in ceramics using ultrasonic velocity.

An advisory ballot was conducted within the NDE section (C-28.02.02) on six additional E-7 NDE standards that were selected as having relevance and applicability to ceramics. The six standards were E-94, Guide for RadiographicTesting; E-214, Practice for Immersed Ultrasonic Examination by the Reflection Method Using Pulsed Longitudinal Waves; E-1570, Practice for Computed Tomographic (CT) Examination; E-1647, Practice for Determining

Contrast Sensitivity in Radioscopy; E-1672, Guide to Computed Tomography (CT) System Selection; and E-1695, Test Method for Measurement of Computed Tomography (CT) System Performance. As a result of the ballot (and the section meeting in January 1997), five of the standards were determined to be directly applicable and were incorporated into a revision of C-1175, the guide to existing NDE standards applicable to advanced ceramics. E-214 was determined to require modification for ceramic applicability and has been discussed with the parent committee E-7 with request and coordination for revision. The revision to C-1175 was successfully balloted at the subcommittee level. Letters were prepared and transmitted to the E-7 subcommittee chairmen for ultrasonics and radiology requesting technical and editorial modifications to reviewed standards.

A number of new or revised E-7 NDE standards with current or potential relevance to ceramics were reviewed on E-7 committee and subcommittee ballots. The topics included a test method for calibrating and measuring CT density, a practice for calibration of transmission densitometers, a guide for ultrasonic time-of-flight sizing techniques, a guide to radiographic testing, a guide for storage of radiographic films, a guide for radioscopy, a guide for storage of media containing radioscopic data, a test method for measuring focal spots of X-ray tubes, a test method for measuring contrast discrimination visual acuity, a method for measuring brightness of fluorescent penetrants, a guide for evaluating ultrasonic search units, terminology related to radiography and visual examination, and a guide for ultrasonic detection and evaluation of discontinuities. In addition, four draft international standards on liquid penetrants were reviewed and balloted as part of the U.S. Technical Advisory Group for the International Standards Organization (ISO) TC-135 on NDE.

During meetings of Committee E-7 in January, participation by McClung as C-28 liaison included meetings of the subcommittees on radiology and ultrasonics. Significant activity is ongoing in both subcommittees that will result in standards of interest and value for advanced ceramics. Radiographic standards in progress include a standard on low-energy X-ray focal spots and several standards in various stages of development or balloting on radiographic film including image quality response at low X-ray energy, film processing control, and storage of film. Radioscopic standards being planned include digital imaging based on medical technology. New CT standards in progress include calibration and measurement of density by CT. Expansion of the radiological glossary includes adding terms on back-scatter imaging and review of European terms.

Subcommittee E7.06 on Ultrasonic Methods has many standards in different stages of preparation or ballot. Ultrasonic standards in process include procedures for contact testing, detection and evaluation of discontinuities, resonance methods, search unit evaluation, electronic characterization of instruments, and international standards on ultrasonic beam characterization.

Ceramic Characterization and Standards for Heat Engines

IEA Subtask 10
George Onoda and Lin-Sien Lum
National Institute of Standards and Technology
Bldg 223, Room A256, Div. 852
Gaithersburg, MD 20899

Objective/Scope

The objective of Subtask 10 is to tighten and finalize procedures for the characterization of secondary properties of powders. There are four focus areas relating to the secondary properties: dispersion of powders for slurry preparation, slurry preparation, spray dried powders and green body evaluation.

Subtask 10 will involve participants from Belgium, Germany, Japan, Sweden (Norway through Sweden), and the United States.

Technical Progress

The plans for Subtask 10 were drafted at a technical leader's meeting in September 1996 at Paris and presented at the IEA Executive Committee meeting at Dearborn, MI in October 1996. A questionnaire was prepared and send out in January to the participants regarding their role in the round robin studies. Most of the questionnaires were received and are presently being analyzed. The procedure for the round robin are completed. NIST will compile the procedures and distribute to the technical leaders for review before the technical leader's meeting in May. The procedures will be finalized at the meeting. An abstract has been submitted to present a paper on the Physical Characterization of Powders, with results from Subtask 2 and 6 summarized, at the symposium of "Powder Characterization for Advanced Materials Materials," at Gijon, Spain, June 16-20 1997. The final report for Subtask 8 has been completed and is being distributed to the technical leaders and the participating laboratories.

Status of Milestones

1. Technical leaders will complete improvements and tightening of procedure for the round robin studies during April 1997.
2. The next Subtask 10 technical leader's meeting will be in Cincinnati, Ohio, on May 4 at the annual meeting of the American Ceramics Society.
3. The procedures for the round robin will be finalized at the meeting in May.
4. Finalized procedures will be sent out to all participants for round robin studies after the technical leader's meeting.

Communications/Visits/Travel

The Technical Leaders meeting for Subtask 8 and 10 was held in Paris, France, on September 5-6, 1996. A report of Subtask 8 and plans for Subtask 10 were presented to the Executive Committee of the IEA at Dearborn, MI, on October 30, 1996.

Publications/Presentations

Development and Testing of Primary and Secondary Properties of Ceramic Powders: Final Report Subtask 8.

References

None

Problems Encountered

None

Ceramic Mechanical Property Test Method Development

George D. Quinn
(National Institute of Standards and Technology)

Objective/Scope

This task is to develop mechanical test method standards in support of the Propulsion Systems Materials Program. Test method development should meet the needs of the DOE engine community but should also consider the general USA structural ceramics community as well as foreign laboratories and companies.

Draft recommendations for practices or procedures shall be developed based upon the needs identified above and circulated within the DOE ceramics engine community for review and modification. Round-robins will be conducted as necessary, but shall be well-focussed, limited in scope, and complementary to IEA round-robins. Procedures developed in this program will be standardized by ASTM.

Technical Highlights and Results

Summary

The SCF fracture toughness test procedures have been refined with the goal of improving the draft ASTM fracture toughness standard. The draft standard was balloted as a Provisional standard ballot in March 1997. A review of diametral compression strength testing was completed in this semiannual period. Work on hardness and fractography has wound down following the adoption of the two hardness standards C 1326 and C 1327 and the fractography standard C 1322. Time permitting, we will prepare a comprehensive paper on hardness measurement methodology.

Earlier work in this project has contributed to the following completed standards:

1. ASTM C 1161-90 "Standard Test Method for Flexural Strength of Advanced Ceramics at Ambient Temperature," G. Quinn, NIST.
2. ASTM C 1198-91 "Dynamic Young's Modulus, Shear Modulus, and Poisson's Ratio for Advanced Ceramics by Sonic Resonance," by S. Gonczy, Allied-Signal; G. Quinn, NIST; and J. Helfinstine, Corning.
3. ASTM C 1211-92 "Standard Test Method for Flexural Strength of Advanced Ceramic at Elevated Temperature," by G. Quinn in cooperation with Mr. M. Foley, Norton; Mr. T. Richerson, Allied-Signal; and Dr. M. Ferber, ORNL.
4. MIL HDBK 790 "Fractography and Characterization of Fracture Origins in Advanced Structural Ceramics," with J. Swab and M. Slavin, U.S. ARL.
5. ASTM C 1239-94a "Standard Practice for Reporting Strength Data and Estimating Weibull Distribution Parameters," by S. Duffy, NASA-Lewis; G. Quinn, NIST; and C. Johnson, G.E.
6. ASTM C 1322-96 "Standard Practice for Fractography and Characterization of Fracture Origins in Advanced Ceramics," in cooperation with Mr. J. Swab, U.S. ARL.
7. ASTM C 1326-96 "Standard Test Method for Knoop Indentation Hardness of Advanced Ceramics."
8. ASTM C 1327-96 "Standard Test Method for Vickers Indentation Hardness of Advanced Ceramics."

In addition, work on this task has contributed to the following draft standard:

1. ASTM C-xxxx "Standard Test Methods for the Determination of Fracture Toughness of Advanced Ceramics," in cooperation with Prof. Isa Bar-on, WPI; Prof. M. Jenkins, University of Washington, and J. Salem, NASA-Lewis.
2. ISO TC 206, "Fine (Advanced Technical) Ceramics - Test Method for Flexural Strength of Monolithic Ceramics at Room Temperature"

Fracture Toughness

Work in this element was devoted to preparing the draft ASTM fracture toughness standard and analyzing new surface crack in flexure (SCF) results to refine this test method.

The last ballot for the draft ASTM standard was in October 1996 at which time five negative ballots and several strong affirmative with comment ballots were received. These were discussed in considerable detail at the ASTM C-28 meeting at Cocoa Beach in January, 1997. This outcome was rather disappointing since we had been optimistic that perhaps this version would be adopted. In hindsight, perhaps the task group members were a bit sanguine. The negative ballots highlighted a number of weak areas in the document. The task group decided that a rewrite was necessary and a new draft will be submitted for a concurrent ballot in the spring of 1997. In January and February, a very intensive review was this document was undertaken in order to meet a February 20th deadline. At NIST we:

a. Very carefully reviewed the stress intensity factor solutions for the SEPB method. Our earlier draft included some new solutions which were somewhat controversial. This survey led to the retention of some of the new solutions devised by Baratta and Freese, but a reversion to some of the earlier, more traditional solutions devised by Srawley and Gross and which are accepted worldwide.
b. Intensively reviewed the SEPB literature with respect to whether the Vickers indentations exert a residual effect on the main crack during the final fracture test. These indentations are used to aid the precracking process and it is usually expected that once the main crack has been popped in during bridge-anvil precracking step loading. There are 8 literature sources that report that these indentations can contaminate the results and lead to false fracture toughness outcomes, even though the cracks have propagated well beyond the indentations. A cautionary statement about this effect will be added to the C-28 draft.
c. Reviewed the data pertaining to stability effects upon apparent fracture toughness.
d. Thoroughly reedited the document.

The Task group prepared the latest rendition of this document as a Provisional ASTM standard. This is a formal standard which is not a full-consensus document and which can be adopted by a shorter, simpler procedure in ASTM. We intended to prepare virtually the same document as a full-consensus document. C-28 agreed to this dual track approach, but we later learned to our chagrin that ASTM frowns on such creative solutions. The Provisional Standard balloted in March-April 1997 and as of the writing of this semiannual report, no negatives had been received. The document therefore should be adopted as a formal Provisional Standard. As of this writing, the same draft is being balloted in Committee E-08, and we expect there will be some input. As soon as this is received, we then will prepare the next version of the full-consensus standard.

Experimental work in this task continues to refine the surface crack in flexure (SCF) method. The goals of this work are to reinforce and refine the procedures already specified in the draft ASTM standard. Specifically, in this six month interval we have:

a. Concluded our study of the halo which is visible on the fracture surface around precracks in some ceramics.
b. Concluded our experiments in dry-nitrogen to compare apparent fracture toughness values in air versus inert atmospheres.
c. Concluded our experiments on new materials to broaden the data base.
d. Conducted additional experiments on NC 132 hot-pressed silicon nitride with the goal of evaluating its suitability as a Standard Reference Material for fracture toughness.

We concluded from our fractographic and experimental studies that halos can be due to any one of several causes and that if there is any doubt about the halo being a manifestation of slow crack growth, then controlled atmosphere experiments are advisable. A paper with these findings was presented at the American Ceramic Society conference at Cocoa Beach in January 1997 and a more comprehensive version is in preparation.

Table I Fracture Toughness of BK-7 Borosilicate Crown Glass

Method	Condition	Other *	No. of Spec.	$K_{Ic} \pm 1\sigma$ MPa$\sqrt{m}$	Ref.
SCF	lab ambient	4.5 h	3	0.88 ± 0.09	This study
SCF	dry nitrogen	4.5 h	5	0.97 ± 0.09	This study
SCF	nitrogen	8.0 h	3	1.06 ± 0.04	This study
SCF⋆	water	annealed	-	~0.80, 0.90, 1.05 **	Fett at al. 1988
SCF⋆	water	annealed	20	0.78	Fett et al. 1988
SCF⋆	water	annealed or ground 4 to 5.5 h	-	0.85 ± 0.03	Fett et al. 1991
DCB†	vacuum	NA	4	0.86 ± 0.03	Wiederhorn and Roberts 1972
DCB	vacuum, preheated	NA	4	0.93 ± 0.01	Wiederhorn and Roberts 1972
SENB ‡	vacuum	NA	4	0.84 ± 0.01	Wiederhorn and Roberts 1972

⋆ K_{Ic} calculated on basis of estimated final crack dimensions after extensive SCG. - Not available
* 49 N Knoop precracks. Residual stresses removed by annealing; or grinding by hand (N h) off.
** Three batches † Double Cantilever Beam ‡ Precracked by a sharp chevron
NA Not applicable

In our last semiannual report, we discussed some puzzling results shown in Table I that we obtained on Schott BK-7 borosilicate crown glass. Specimens were tested in laboratory ambient or dry nitrogen. Our results were disappointing since a simple, clear answer for what is K_c is elusive. Is it 0.88, 0.97, or 1.06 MPa$\sqrt{m}$? Our numbers are similar to those given by other groups, but they also reported high variation. We speculated that the different methods were yielding different points on K-V curves and not true K_{Ic} estimates. This may still be true, but during this semiannual period we reexamined our SCF specimens and determined that there were two experimental factors that contributed to our scatter:

a. Some of our SCF specimens had precracks with a 2½ - 3° twist to the precrack. A twist is our term to describe a Knoop induced precrack that is slightly misaligned relative to the specimen long axis.
b. Many of the SCF specimens had lateral cracks that interfered with the assumed stress distribution.

Both these experimental factors raise apparent fracture toughness outcomes relative to correct values. The twist was a surprise and was traced to a slightly-misaligned Knoop diamond on the hardness machine that we used to make the Knoop precracks. We found the diamond misalignment during the course of an intensive review of some of our recent results in NC 132 hot-pressed silicon nitride whereupon we discerned that some of the precracks were not as well formed as in our earlier work. Fracture toughness outcomes had shifted to higher values as well. The effect on K_{Ic} was small (~5%) but this is an important error. The Knoop impression should be perpendicular to the specimen long axis. Early in our work in 1991 and 1992, we intentionally had tried some 5° twisted precracks with the expectation that the twist would make the precracks easier to discern and the twist would not induce enough Mode II or III loading to affect our K_{Ic} measurements. The experiments were unsuccessful since fracture tended to truncate the precrack, preventing a proper measurement of the precrack size. (Eventually we settled on a slight precrack "tilt" of 1/2°.) We reviewed the effect of a little twist on apparent toughness and found that there are about 6-8

papers in the literature that report the use of twisted Knoop precracks to study mixed-mode fracture phenomena. The data shows that at small angles, for each degree of twist the effect on fracture stress (and thus apparent toughness) was 1/2 -2%. Evidently, the jogs and irregularities of the Knoop precracks (they are often not flat) prevent the full transmission of stresses to the crack. The jogs and irregularities have a negligible effect when the cracks are perfectly perpendicular to the far field stresses, but are of much greater consequence of mixed-mode experiments and to fracture toughness K_{Ic} tests with unintentional twists, however, since they will interlock the crack faces and prevent full load application to the crack tip. Studies of mixed-mode fracture which utilize twisted Knoop precracks should be viewed with caution.

Thus, our misaligned diamond was causing overestimates of toughness of up to 5% in some of our recent BK-7 and NC 132 results. Fortunately, the draft ASTM standard requires that the Knoop precrack be aligned within 2° to the specimen axis. Our inadvertent misalignment problems confirm the suitability of this specification.

We had been alerted to the possible interference of lateral cracks on computed toughness by Prof. Jurgen Rödel of the University of Darmstadt. Initially, we had been skeptical since we polish away the indentation and the residual stress damage zone under Knoop indentations and it was thought that this would remove most of the lateral cracks. We fractographically reexamined the BK-7 specimens and found that indeed there were some lateral cracks that partially shielded the main median cracks which are used to evaluate toughness. Furthermore, we noticed a correlation between the amount of material removed and the apparent toughness: the more the material removed, the shallower the laterals and the lower the toughnesses. In the limit, for the specimens which had no remnant laterals, the apparent toughnesses were of the order of 0.85 -0.90 MPa$\sqrt{m}$. It is now evident that laterals can shield the main crack and this will require a higher breaking load to fracture the specimen. Fracture toughness mode I will be overestimated. The 5 kg indentation load that we had used for the BK-7 glass is too high and causes excessive lateral cracking. (This load was chosen since it was the norm for most of our polycrystalline ceramic work.) We will try one new round of experiments with 2 kg indentation load in the next six months.

So in summary, some atypical results on the BK-7 glass and NC 132 HPSN prompted us to critically review our procedures which in turn helped us realize some pitfalls in SCF testing. Recommendations to avoid these will be incorporated into the ASTM draft standard.

New test data has been collected on ten new materials as shown in Table II. These findings were presented in a paper at the American Ceramic Society conference in January, 1997 at Cocoa Beach. Unfortunately, we were unable to detect the precracks in several of the materials due to their

Table II. SCF fracture toughness results

Material	Source and/or code	Processing	ρ (Mg/m³)	E (GPa)	success rate	K_{Ic} ± 1σ† (MPa√m)
Si_3N_4	Dow, self-reinforced	Sintered	3.20*	306*	5/5	6.75 ±0.29
Si_3N_4	Ceradyne 147-3	SRBSN	3.2*	320*	0/5	-
Si_3N_4	Cercom CIW15	hot pressed?	-	335*	2/4	7.33 ±0.34
Si_3N_4	NKK toughened	sintered?	3.26 (13)	307 (13)	0/4	-
Si_3N_4	Wesgo SNW 1000	sintered	3.29	281	3/6	6.37 ±0.27 ★
SiC	Cercom PAD-B	hot pressed	3.20*	455*	3/6	4.31 ±0.16
AlN	Dow	hot pressed	3.26 (18)	323*	6/6	2.79 ±0.35
ZrO_2 TZP	Toshiba TASZIC	sintered	6.05*	180*	0/2	- ◊
ZrO_2 TZP	Ceramatec CZ203 Ceria	sintered	>5.8*	240*	0/4	- ◊
MgF_2	-	hot-pressed	3.18	-	4/4	0.98 ±0.04 ‡♦
PZT-8	Morgan	poled	7.58	140	7/10	1.08 ±0.10 ▾
PZT-8	Morgan	depoled	"	"	7/8	0.88 ±0.04 ▾
BK-7 glass	Schott, boro-silicate crown	melt	2.5*	82*	3/5	1.06 ±0.04 ♦
Glass ceramic	U.S. ARL SiNO	sintered	2.6	150	3/5	1.53 ±0.04
Glass ceramic	Pyroceram 9603	melt, heat treat	2.59 (25)	132 (25,26)	4/5	2.21 ±0.22 ♦
Glass ceramic	Pyroceram 9603	melt, heat treat	"	"	5/6	2.30 ±0.10

* Company-furnished data - Data unavailable
♦ Tested in nitrogen ♦♦ Tested in dry nitrogen (ultra high purity)
★ 98 N indentations ‡ 29.4 N indentations ▾ 16.7 N and 19.8 N indentations
◊ 196 N tilted and canted Vickers indentations
† Uncertainties are ± one standard deviation and were evaluated by statistical analysis of the data.
( ) Number in parenthesis is the reference source.

complicated microstructures. These findings point out the need to develop a simple dye-penetration procedure to highlight SCF precracks, a task we intend to commence in mid-1997. We were also handicapped in many instances in having only five or fewer specimens to test for a material. The ASTM draft recommends that ten or more be prepared, from which four valid tests should be obtained.

During this six month period we reviewed our NC 132 hot-pressed silicon nitride data very thoroughly with a view towards determining whether this material would be suitable as a Standard Reference Material (SRM) for fracture toughness. Such an SRM would be a excellent support for the ASTM draft standard and would be a giant step in improving fracture toughness testing in general. This old, hot-pressed silicon nitride has one of the largest mechanical property data bases (particularly fracture toughness) ever accumulated and it was featured in an international round robin in which superlative results were obtained. In addition, it is one of the rare structural ceramics for which complementary fracture toughness data exists by the three ASTM methods (SCF, SEPB, CN) and which are in excellent agreement. We now have found 38 data sets in the literature (by reputable fracture toughness test methods) which converge to 4.3 - 4.7 MPa$\sqrt{m}$. This includes the 20 laboratory VAMAS international round robin that featured the SCF method and which gave a grand mean toughness of 4.59 MPa$\sqrt{m}$. Closer examination of the VAMAS data caused us to delete several suspect entries so that our best grand mean is now 4.52 MPa$\sqrt{m}$ with a standard deviation of 0.28 MPa$\sqrt{m}$ for 98 trials. Available evidence indicates this material has little or no R-curve behavior and little or no slow crack susceptibility at room temperature. The convergence of fracture toughness results by different methods, the lack of SCG or R-curve behavior, the similarity of large and small crack specimen results, and the successful outcome of the VAMAS round robin suggest this material would be a good SRM for fracture toughness. We are studying this intensively and a new program for this purpose has been established at NIST in conjunction with this DOE program.

Table III
SCF fracture toughness data for NC 132 hot-pressed silicon nitride

Test condition	date	# Specimens	K_{Ic} MPa$\sqrt{m}$	std. dev. MPa$\sqrt{m}$
VAMAS round robin, lab ambient	1993-1994	98	4.52	.28
NIST, lab ambient, two orientations	1992	10	4.29 or 4.45	.22 or .03
NIST, lab ambient	1997	3	4.39	.39
NIST, dry N_2	1997	5	4.32	.29

During this semiannual period, Jeff Swab and I carefully reviewed our NC 132 results, particularly the fracture surfaces and some parallel experiments with inert-atmosphere versus lab ambient test results to ascertain whether SCG was a statistically significant factor at room temperature. Initially we concluded that it might, but we noticed that some of our data had been thrown off by the twisted Knoop precracks as described above. When these experiments were duplicated, but with greater care to align the diamond properly, it became apparent that we could not detect SCG in specimens tested 26 N Knoop indentation with the indentation subsequently polished or ground away. Table III shows that there was no statistically significant difference between specimens tested in lab ambient or dry nitrogen conditions. The fracture surfaces of the all NC 132 specimens that we have tested since 1992 were reexamined for evidence of stable

crack extension from slow crack growth (SCG) at room temperature. Optical fractographs suggested that there might have been some SCG, but careful SEM scrutiny suggested that most of the halos were crack reorientation effects. There was a suggestion that tungsten inclusions could have contributed in some fashion to the halo appearance, but backscattering mode examination in the SEM showed no unusual patterns. Tungsten particles permeate this material, but they are usually incidental to the bulk fracture toughness. Tungsten acts as preferential sources of creep cavitation, or if they are large enough or are in a cluster, act as strength-limiting flaws.

Hardness

The two ASTM hardness standards were adopted by ASTM in 1996. During this semiannual period, corrections and refinements to the two ASTM hardness standards were balloted in October 1996 in the ASTM C-28 main committee ballot. The revisions were: clarifications to several minor technical points, inclusion of several new references, and a major new addition to clarify the proper utilization of microscope crosshairs. The latter is one of the biggest problems in making hardness measurements. Test machine operators (novices and pros alike) often use the machine crosshairs improperly. The revisions were approved and adopted.

Fractography

"Standard Practice for Fractography and Characterization of Fracture Origins in Advanced Ceramics," was adopted by ASTM as Standard Practice C 1322-96 in January, 1996. This work is a collaboration between G. Quinn of NIST and J. Swab of U. S. Army Research Laboratory (ARL). This original goals of this fractographic element of this project is now complete. There were a few loose ends to be tidied up and some new ideas to pursue. A new activity to standardize fractographic analysis in the European Community will borrow heavily from C 1322-96, in no small part due to the success of a VAMAS fractography round robin and the success of an IEA Subtask 7 fractography exercise. ASTM C 1322 is distributed and presented as parts of fractography courses offered by the American Ceramic Society (topical course) and Alfred University (special summer course). Finally, we are undertaking a short effort to load the flaw photos in the annex to C 1322-96 into a webb site at NIST. This will make fracture origins accessible to a broad user community and will improve the fidelity of the images compared to the poor copies that are appended to the ASTM standard. We hope to link this webb site to a Weibull strength analysis site that Prof. Stephen Duffy of Cleveland State University is establishing.

Diametral Compression

The diametral compression test method, also known as the Brazilian disk method, is occasionally used to measure the strength of brittle materials. Our last semiannual report gave background information on this method which may be well-suited for determination of strength of cylindrical parts such as valves or fuel injection pins, or for small specimens cut from larger components. The highest stresses in the specimen exist both at the surface and in a large part of the volume of the specimen. The fixtures and the specimens are extremely simple and cheap. Mr. Quinn and Mr. Swab of the U. S. ARL will evaluate this method and prepare an ASTM draft standard. Our last semiannual report gave some findings from the literature review of the diametral compression test method and some preliminary observations from testing at NIST. During this six month period, we ordered some test specimens from sintered alumina AD-999 and sintered alpha silicon carbide plates.

Elastic Modulus

Two new draft standards for elastic moduli determination are being balloted by ASTM Committee E-28, Mechanical Testing. These drafts are virtually identical clones of the two standards that C-28 created, C 1198 and C 1259, with a few critical exceptions. the other ASTM committee copied the two C-28 standards but deleted the words "Advanced Ceramics" in every instance and also relaxed many of the tolerances. The former change is not of concern to C-28, but the latter is. If the tolerances are relaxed as

suggested by Committee E-28, then errors of over 1% are possible, and indeed, probable. These documents were reviewed and a negative Ballot was cast at the ASTM Society level after consultation with S. Gonczy, the C-28 task group leader for C 1198 and C 1259.

ISO Flexure Strength Standard

A new draft of the ISO flexure strength standard was prepared and distributed to the international working group members and to the ISO TC secretariat. This draft has only a few revisions and editorial refinements compared to the prior draft. More discussion is included regarding transverse grinding. Based on these revisions and ones made in late 1996, the ISO secretariat agreed to advance this document to a so called "Committee Draft" CD status. The document will be discussed in the next ISO meeting in July 1997 and probably will be advanced as a "Draft International Standard" (DIS) for formal international balloting. There was no work on the high-temperature flexure strength draft standard in this bimonthly period.

ISO Hardness Standard

An International Standards Organization Technical Committee TC 206 draft standard for Knoop and Vickers hardness has been prepared by Mr. S. Sakaguchi of NIRIN. Mr. Quinn is the USA representative in the Working Group in TC 206. Following the ISO formal meeting last summer, Mr. Sakaguchi prepared a revised draft (September 1, 1996) which incorporated nearly all the revisions requested by the United States.

Since the last report, preliminary results of a VAMAS round robin for the hardness of silicon nitride and silicon nitride reinforced with SiC whiskers are now available. We are very gratified to learn that *the best results of the exercise were obtained with Knoop 2 kg indentations as specified in the ASTM standard C 1326.* Within-lab scatter (repeatability) and between-lab scatter (reproducibility) were smallest for Knoop 2kg, as opposed to Vickers 1 kg or 10 kg or Knoop 1 kg conditions. The Knoop indentations were better able to discern whisker orientation effects as opposed to Vickers indentations. DOE contractors or subcontractors who are concerned with ISO standardization of hardness measurements are urged to contact Mr. Quinn.

Other Activities

None

Status of Milestones

A manpower shortage and many ASTM, VAMAS and ISO administrative tasks have hindered our planned progress in several topics. A postdoctoral candidate will be assigned to help with this project in June.

412123 Conduct preliminary diametral compression strength tests.
Completed October 1996.

412125 Prepare draft ISO Flexure Strength Standard.
Completed April 1996

412126 Prepare and distribute to ASTM Committee C-28 members a simple statistical analysis package for interlaboratory round robin test data.
Completed, June 1996

412127 Participate in a ceramic whisker-reinforced composite round robin *Completed May 1996.*

412130 Finish ASTM fracture toughness standard
Completed March 1996. (As a Provisional Standard.)

The following milestones are delayed:

412124 Prepare comprehensive paper on hardness testing of ceramics.
Postpone due to delays associated with preparing SRM 2831, Vickers hardness of ceramics, and also shift of work to other priorities. We also have delayed this paper due to some extraordinary new work at NIST (in an independent study) which takes an entirely new look at the interpretation of conventional ceramic hardness results.

412128 Conduct dye-penetrant experiments on SCF fracture toughness specimens
Delay to July, 1997 so that an effort can be made to finish the Vickers hardness SRM #2831.

412129 Write comprehensive report on fracture toughness evaluation by scf method March 1997
Delayed to Fall, 1997 in order to spend time on preparing revised fracture toughness ASTM draft for Spring 1997 ballot as a Provisional Standard.

412131 Complete Phase I diametral compression testing May 1997
Delayed to Fall, 1997 due to need to allocate time on fracture toughness work.

Publications/Presentations

1. "ASTM C-28: The First Decade," G. Quinn, Amer. Ceram. Soc. Bull., 75, No. 12, 45-46 (1996).
2. Fracture Toughness by the Surface Crack in Flexure (SCF) Method: New Test Results," by G. Quinn, J, Swab, and M. Hill, presented at ACS Conference, Jan. 1997, Cocoa Beach,to be publ. Ceram. Eng. and Sci. Proc.
3. "Investigation of "Halos" Associated with Fracture Toughness Precracks," by J. Swab and G. Quinn, idem.

Communications/Visits

1. Extensive communications were exchanged with Mike Jenkins, Jon Salem, and Isa Bar-On on the fracture toughness draft standard.

2. G. Quinn attended the Customers Coordination Meeting in October and helped Charles Brinkman prepare and present a poster paper: "Standardization of Mechanical Properties Tests for Advanced Ceramics."
3. Mr. Quinn attended the ASTM C-28 meeting in Cocoa Beach in January 1997.
4. Information regarding diametral compression test data and Weibull statistical analysis was sent to Andy Wereszczak at ORNL upon request.
5. A summary of contributions of the IEA program to ASTM and ISO standards development was sent to R. Johnson at ORNL.

ORNL/TM-13467

INTERNAL DISTRIBUTION

Central Research Library
Laboratory Records Department (2)
Laboratory Records - RC
L. F. Allard, Jr.
P. F. Becher
T. M. Besmann
P. J. Blau
R. A. Bradley
K. Breder
C. R. Brinkman
A. Choudhury
D. D. Conger
S. A. David
M. K. Ferber
R. L. Graves
H. W. Hayden, Jr.
C. R. Hubbard
M. A. Janney
D. R. Johnson (5)
R. R. Judkins
M. A. Karnitz
R. J. Lauf
K. C. Liu
W. D. Manly
S. B. McSpadden
T. A. Nolan
A. E. Pasto
M. H. Rawlins
M. L. Santella
A. C. Schaffhauser
D. P. Stinton
T. N. Tiegs
S. G. Winslow
R. E. Ziegler

EXTERNAL DISTRIBUTION

Jeffrey Abboud
U.S. Advanced Ceramics Assoc.
1600 Wilson Blvd., Suite 1008
Arlington VA 22209

B. P. Bandyopadhyay
University of North Dakota
Box 8359 University Station
Grand Forks ND 58202-8359

Donald F. Baxter, Jr.
Advanced Materials & Processes
ASM International
9639 Kinsman Road
Materials Park OH 44073-0002

M. Brad Beardsley
Caterpillar Inc.
Technical Center Bldg. E
P.O. Box 1875
Peoria IL 61656-1875

Bruce Boardman
Deere & Company, Technical Ctr.
3300 River Drive
Moline IL 61265-1792

Michael C. Brands
Cummins Engine Company, Inc.
P.O. Box 3005, Mail Code 50179
Columbus IN 47201

Donald J. Bray
Advanced Refractory Technologies
699 Hertel Avenue
Buffalo NY 14207

Walter Bryzik
U.S. Army Tank Automotive
Command
R&D Center, Propulsion Systems
Warren MI 48397-5000

David Carruthers
Kyocera Industrial Ceramics
5713 East Fourth Plain
Vancouver WA 98661

Ronald H. Chand
Chand Kare Technical Ceramics
2 Coppage Drive
Worcester MA 01603-1252

William J. Chmura
Torrington Company
59 Field Street, P.O. Box 1008
Torrington CT 06790-1008

William S. Coblenz
Defense Adv. Research Projects Agency
3701 N. Fairfax Drive
Arlington VA 22203-1714

Gloria M. Collins
ASTM
100 Barr Harbor Drive
West Conshohocken PA 19428-2959

Shawn Cooper
FEV Engine Technology
2285 Opdyke Road, Suite F
Auburn Hills MI 48326

Douglas Corey
AlliedSignal, Inc.
2525 West 190th Street, MS:T52
Torrance CA 90504-6099

Keith P. Costello
Chand/Kare Technical Ceramics
2 Coppage Drive
Worcester MA 01603-1252

Gary M. Crosbie
Ford Motor Company
P.O. Box 2053, 20000 Rotunda Drive
MD-3182, SRL Building
Dearborn MI 48121-2053

Pamela Cunningham
WETO Technical Library
MSE, Inc.
Industrial Park, P. O. Box 4078
Butte MT 59702

Sidney Diamond
U.S. Department of Energy
Office of Transportation Technologies
EE-33, Forrestal Building
Washington DC 28505

Barry Draskovich
AlliedSignal, Inc. Ceramic Components
2525 West 190th Street
TOR 1/5-1-27000
Torrance CA 90504

Ernest J. Duwell
3M Abrasive Systems Division
3M Center, Bldg. 251-01-34
St. Paul MN 55144

Michael Easley
AlliedSignal Engines
P. O. Box 52181
MS 551-11
Phoenix AZ 85072-2181

J. J. Eberhardt
U.S. Department of Energy
Office of Transportation Technologies
EE-33, Forrestal Building
Washington DC 20585

Jim Edler
Eaton Corporation
26201 Northwestern Highway
P.O. Box 766
Southfield MI 48037

G. A. Eisman
Dow Chemical Company
Ceramics and Advanced Materials
52 Building
Midland MI 48667

William A. Ellingson
Argonne National Laboratory
Energy Technology Division, Bldg. 212
9700 S. Cass Avenue
Argonne IL 60439-3848

John W. Fairbanks
U.S. Department of Energy
Office of Transportation Technologies
EE-33, Forrestal Building
Washington DC 20585

Ho Fang
Applied Materials
2695 Augustine Drive, MS-0962
Santa Clara CA 95054

Dan Foley
AlliedSignal Ceramic Components
MS:1/5-1, 26000
2525 West 190th Street
Torrance CA 90504

Douglas Freitag
DuPont Lanxide Composites
21150 New Hampshire Avenue
Brookeville MD 20833

Richard Gates
NIST
Bldg. 223, Rm. A-256
Rt. 270 & Quince Orchard Road
Gaithersburg MD 20899

Allan E. Goldman
U.S. Graphite, Inc.
907 W. Outer Drive
Oak Ridge TN 37830

Robert J. Gottschall
U.S. Department of Energy
Metal & Ceramic Sciences, ER-131
19901 Germantown Road
Germantown MD 20874-1290

Thomas J. Gross
U.S. Department of Energy
Office of Transportation Technologies
EE-30, Forrestal Building
Washington DC 20585

Nabil S. Hakim
Detroit Diesel Corporation
13400 Outer Drive West, A08
Detroit MI 48239-4001

Alan M. Hart
Dow Chemical Company
1776 Building
Midland MI 48674

Michael H. Haselkorn
Caterpillar Inc.
Technical Center, Building E
P.O. Box 1875
Peoria IL 61656-1875

Deborah A. Haught
U.S. Department of Energy
Ofc. of Industrial Crosscut Technologies
EE-23, Forrestal Bldg.
Washington DC 20585

John Haygarth
Wah Chang
P.O. Box 460
Albany OR 97321-0460

Gene Huber
Precision Ferrites & Ceramics
5432 Production Drive
Huntington Beach CA 92649-1525

Thomas A. Johnson
Lanxide Corporation
1300 Marrows Road
P.O. Box 6077
Newark DE 19714-6077

Yury Kalish
Detroit Diesel Corporation
Mechanical Systems
13400 Outer Drive West
Detroit MI 48239-4001

Roy Kamo
Adiabatics, Inc.
3385 Commerce Park Drive
Columbus IN 47201

W. C. King
Mack Truck, Z-41
1999 Pennsylvania Avenue
Hagerstown MD 21740

Tony Kirn
Caterpillar Inc.
Defense Products Dept., JB7
Peoria IL 61629

Joseph A. Kovach
Eaton Corporation
32500 Chardon Road
Willoughby Hills OH 44094

Edwin H. Kraft
Kyocera Industrial Ceramics
5713 E. Fourth Plain Boulevard
Vancouver WA 98661

Arthur Kranish
Trends Publishing Inc.
1079 National Press Building
Washington DC 20045

Oh-Hun Kwon
Norton Company
Saint Gobain Industrial Ceramics
1 Goddard Road
Northboro MA 01532-1545

S. K. Lau
B. F. Goodrich Aerospace R&D
9921 Brecksville Road
Brecksville OH 44141

Elaine Lentini
Saint-Gobain Industrial Ceramics
Goddard Road
Northboro MA 01532

Stan Levine
NASA Lewis Research Center
21000 Brookpark Road, MS:106/5
Cleveland OH 44135

Robert H. Licht
Norton Company
Saint Gobain Industrial Ceramics
1 Goddard Road
Northboro MA 01532-1545

E. Lilley
Norton Company
Saint Gobain Industrial Ceramics
1 Goddard Road
Northboro MA 01532-1545

B. J. McEntire
Norton Company
10 Airport Park Road
East Granby CT 06026

James McLaughlin
Sundstrand Power Systems
4400 Ruffin Road
P.O. Box 85757
San Diego CA 92186-5757

Biljana Mikijelj
Ceradyne, Inc.
3169 Red Hill Avenue
Costa Mesa CA 92626

Carl E. Miller
Delphi Energy & Engine Mgmt. Systems
4800 S. Saginaw Street, MC 485-301-150
P. O. Box 1360
Flint MI 48501-1360

Curtis V. Nakaishi
U.S. Department of Energy
Federal Energy Tech. Center
3610 Collins Ferry Rd.
P.O. Box 880
Morgantown WV 26507-0880

Malcolm Naylor
Cummins Engine Company, Inc.
P.O. Box 3005, Mail Code 50183
Columbus IN 47202-3005

Thomas J. Paglia
Coors/ACI
3315 Boone Road
Benton AR 72015

Richard Palicka
CERCOM, Inc.
1960 Watson Way
Vista CA 92083

Vijay M. Parthasarathy
Solar Turbines
2200 Pacific Highway, M.Z. R-1
San Diego CA 92186

Magan Patel
Cummins Engine Company, Inc.
Mail Code 50183
Box 3005
Columbus IN 47202-3005

James W. Patten
Cummins Engine Company, Inc.
P.O. Box 3005, Mail Code 50183
Columbus IN 47202-3005

Stephen C. Pred
Pred Materials International, Inc.
60 East 42nd Street, Suite 1456
New York NY 10165

Vimal K. Pujari
Norton Company
Saint Gobain Industrial Ceramics
1 Goddard Road
Northboro MA 01532-1545

Fred Quan
Corning Inc.
Sullivan Park, FR-2-8
Corning NY 14831

George Quinn
NIST
Quince Orchard & Clopper Road
Ceramics Division, Bldg. 223
Gaithersburg MD 20899

Harold Rechter
Chicago Fire Brick Company
7531 S. Ashland Avenue
Chicago IL 60620-4246

Jack A. Rubin
CERCOM, Inc.
1960 Watson Way
Vista CA 92083

Robert J. Russell
Riverdale Consulting, Inc.
24 Micah Hamlin Road
Centerville MA 02632-2107

J. Sankar
North Carolina A&T State Univ.
Dept. of Mechanical Engineering
Greensboro NC 27406

Maxine L. Savitz
AlliedSignal, Inc.
Ceramic Components
P.O. Box 2960, MS:T21
Torrance CA 90509-2960

Jim Schienle
AlliedSignal Aerospace
1130 West Warner Road
M/S 1231-K
Tempe AZ 85284

Gary Schnittgrund
Transfer Technology
16401 Knollwood Drive
Granada Hills CA 91344

Robert B. Schulz
U.S. Department of Energy
Office of Transportation Technologies
EE-33, Forrestal Building
Washington DC 20585

Robert S. Shane
Shane Associates
1904 NW 22nd Street
Stuart FL 34994-9270

Subu Shanmugham
MicroCoating Technologies
430 Tenth Street
Suite N-108
Atlanta GA 30318

Albert Shih
Cummins Engine Company
MC 50183
P.O. Box 3005
Columbus IN 47201

Charles Spuckler
NASA Lewis Research Center
21000 Brookpark Road, MS: 5-11
Cleveland OH 44135-3127

Gordon L. Starr
Cummins Engine Company, Inc.
P.O. Box 3005, Mail Code:50182
Columbus IN 47202-3005

Marian Swirsky
Cambridge Scientific Abstract
Commerce Park, Bldg. 4, Suite 804
23200 Chagrin Blvd.
Beachwood OH 44122

Victor J. Tennery
113 Newell Lane
Oak Ridge TN 37830

Malcolm Thomas
Allison Engine Company
P. O. Box 420 (W06)
Indianapolis IN 46206

Marc Tricard
Norton Company
Superabrasives Division
1 New Bond Street, MS-412-301
P. O. Box 15008
Worcester MA 01615-0008

Marcel H. Van De Voorde
Commission of the European Community
P.O. Box 2
1755 ZG Petten
THE NETHERLANDS

Ronald H. Walecki
Quadroid Engineering, Inc.
255 Via Linda Vista
Redondo Beach CA 90277

Michael S. Walsh
Vapor Technologies Inc.
6330 Gunpark Drive
Boulder CO 80301

Robert M. Washburn
ASMT
11203 Colima Road
Whittier CA 90604

R. W. Weeks
Argonne National Laboratory
Bldg. 362, E313
9700 S. Cass Avenue
Argonne IL 60439

Sheldon M. Wiederhorn
NIST
Building 223, Room B309
Gaithersburg MD 20899

Matthew F. Winkler
Seaworthy Systems, Inc.
P.O. Box 965
Essex CT 06426

Thomas J. Wissing
Eaton Corporation
26201 Northwestern Highway
P.O. Box 766
Southfield MI 48037

James C. Withers
MER Corporation
7960 S. Kolb Road
Tucson AZ 85706

Dale E. Wittmer
Southern Illinois University
Mechanical Engineering Dept.
Carbondale IL 62901

Egon E. Wolff
Caterpillar Inc.
Technical Center
P.O. Box 1875
Peoria IL 61656-1875

Roy Yamamoto
Ethyl Petroleum Additives, Inc.
500 Spring Street
P. O. Box 2158
Richmond VA 23218-2158

Thomas M. Yonushonis
Cummins Engine Company, Inc.
1900 McKinley Avenue
P.O. Box 3005, Mail Code 50183
Columbus IN 47202-3005

Jong Yung
Sundstrand Aerospace
Dept. 789-6
4747 Harrison Avenue
Rockford IL 61125

A. L. Zadoks
Caterpillar Inc.
Technical Center, Building L
P.O. Box 1875
Peoria IL 61656-1875

Zhenqi Zhu
University of Connecticut
Precision Manufacturing Center
Longley Building, U-119, Rt. 44
Storrs CT 06269-5119

Department of Energy
Oak Ridge Operations Office
Assistant Manager for Energy
Research and Development
P. O. Box 2001
Oak Ridge TN 37831-8600

For distribution by microfiche
as shown in DOE/OSTI-4500,
Distribution Category UC-332
(Ceramics/Advanced Materials).